Author:
Fasano, Angelo

Title:
Stability and Serviceability Driven Design for Excavations in Clays

Author:
Fasano, Angelo

Title:
Stability and Serviceability Driven Design for Excavations in Clays

Stability and Serviceability Driven Design for Excavations in Clays

by

Angelo Fasano

A dissertation submitted to the University of Bristol in accordance
with the requirements of the degree of Doctor of Philosophy
in the Faculty of Engineering, Department of Civil Engineering

April 2021

ABSTRACT

Deep excavations in clayey deposits present challenges of varying nature, depending on the characteristics and mechanical properties of the soil strata. In general, stability and/or serviceability performance aspects are the primary considerations for projects in normally consolidated and over-consolidated clayey deposits, respectively.

A series of commonly available constitutive models have been reviewed. The suitability of these models for use in routine soil-structure interaction analyses, in lieu of the popular linear elastic – perfectly plastic (Mohr-Coulomb) model, has been investigated.

The research has focussed on two case histories, namely a 20m excavation in London Clay and a 15m to 17m deep excavation in Boston Blue Clay.

For the London Clay case history, the use of a constitutive model able to capture the progressive stiffness degradation behaviour with increasing strains is considered essential, in order to provide accurate predictions of ground movements in the zone surrounding the excavation. The findings of the study presented indicate that the use of a model in which the stiffness is controlled by the mean effective stress (p') and the pre-consolidation stress (p_c) would provide reasonable results in terms of both wall deflections and overall ground movements.

Aspects of the behaviour of the Boston Blue Clay have been reviewed, based on data from a comprehensive ground investigation. Small strain stiffness, stiffness degradation with strain and undrained shear strength properties have been investigated in detail. Stability of the excavation is a key concern in these ground conditions. The findings of the study indicate that, for the case study concerned, the *DSS* undrained shear strength profile can be adopted for excavation stability assessments using limit equilibrium or finite element methods, assuming isotropic behaviour for the material. The study has also highlighted the significance of partial consolidation mechanisms occurring during the basement excavation, indicating that the undrained assumption made as part of traditional stability assessments, may not be accurate, and total stress analyses/calculations, carried out for preliminary stability assessment, should be based on relatively conservative undrained shear strength parameters.

ACKNOWLEDGEMENTS

I would like to express my gratitude to my supervisor, Dr. Andrea Diambra, for his continuous support and incitement. Without his help and commitment, I would not have been able to complete my thesis.

I wish to thank my early supervisors, Prof. David Muir Wood and the late Dr. David Nash, for the immensely fascinating soil mechanics discussions during the initial years of my study.

Special thanks to my parents, for their support, to my partner Daniela, for her constant encouragement and patience, and to my beautiful daughter Maria, for her smile.

Finally, I would like to thank Alex Nikolic, Tony Suckling and all my other colleagues at A-squared, for the help and support over the past years.

AUTHOR’S DECLARATION

I declare that the work in this dissertation was carried out in accordance with the requirements of the University's Regulations and Code of Practice for Research Degree Programmes and that it has not been submitted for any other academic award. Except where indicated by specific reference in the text, the work is the candidate's own work. Work done in collaboration with, or with the assistance of, others, is indicated as such. Any views expressed in the dissertation are those of the author.

April 2021

Angelo Fasano

TABLE OF CONTENTS

CHAPTER 6. CONCLUSIONS

CHAPTER 1

INTRODUCTION

1.1 Background

Deep excavations in clayey deposits present challenges of varying nature, depending on the characteristics and mechanical properties of the soil strata.

For excavations in soft normally consolidated deposits, the viability of the schemes and the design of the earth retention systems is often driven by considerations related to the excavation short term stability. Base and global stability failures are not uncommon in such deposits, when these aspects are not adequately addressed as part of the design process.

On the other hand, for excavations in stiff over-consolidated clays, stability is rarely a concern, as a result of the relatively high undrained shear strength of the material. In this case, particularly for projects in congested urban settings, serviceability considerations in relation to retaining wall performance and ground movements, are a key aspect of the design.

This thesis investigates critical aspects to be accounted for when designing excavations in both normally and over-consolidated clays, with particular emphasis on the appropriate selection of simple constitutive models, typically used in the day-to-day geotechnical practice, and on the account for the three-dimensional nature of the excavation. The work builds upon selected aspects of different case histories, following the author's experience on these projects.

1.2 Research Objectives

This dissertation covers aspects of the behaviour of clayey deposits associated with excavation problems. The topics presented somehow follow the author's experience on excavation projects in varying ground conditions and with different design drivers.

The research objectives comprise aspects related to three main overall topics:

- Review of the key features of various constitutive models, commonly adopted in the engineering practice to simulate the behaviour of clays.

  This part of the study (Chapter 2) examines a number of constitutive models, with increasing degree of complexity, available in the commercial finite element software Plaxis.

  Although the general features of these models are presented in the software manual (Plaxis, 2018), details of their formulation, in relation to elastic properties, yield surface, plastic potential and hardening rules, are often not provided to the user. For example, with reference to the hardening soil model family (Plaxis, 2018), the models are presented with focus on a number of input parameters, such as E_{50}^{ref}, which may have a clear physical meaning for selected load paths (i.e. drained triaxial tests on normally consolidated samples), but are not the actual internal parameters used by the models.

  Therefore, the aim of this part of the study is to investigate the above key features, by reviewing the models' formulation and carrying out selected analyses. The models are then used in finite element analyses of selected case studies in the subsequent parts of this dissertation.

  It is worth noting that numerous other constitutive models have been formulated by a number of researchers and implemented in various software packages. However, the study presented herein is limited to selected models implemented in the software Plaxis, following the author's professional experience. Particular emphasis will be given to those models commonly used in the day-to-day geotechnical practice.

- Serviceability performance assessment of excavations in stiff over-consolidated clays.

  This part of the study (Chapters 3 and 4) explore the use of a number of constitutive models for the assessment of excavation projects in stiff over-consolidated clays.

  In general, the key aspects that this part of the study tries to address are the following:

  - Importance of the clay high stiffness at very small strains and stiffness degradation behaviour with increasing strains, when simulating excavation problems.

    The study shows that, although the commonly adopted linear elastic – perfectly plastic assumption may provide a reasonable prediction of wall deflections, it is inadequate for the prediction of ground movements in the zone surrounding the excavation. The use of a model capturing the progressive stiffness degradation behaviour with increasing strains is essential for this purpose.

  - Benefits and pitfalls of the currently available stress dependent stiffness formulations in the models examined.

    The findings indicate the use of a model in which the stiffness is controlled by the mean effective stress and the pre-consolidation stress (Generalised Hardening Soil model – Petalas, 2013), provides more reasonable results in terms of both wall deflections and overall ground movements, compared to the minimum principal effective stress formulation of the Hardening Soil model with small strain stiffness.

  - Benefits of using three dimensional simulations in routine design, as opposed to two dimensional analyses, based on plane strain assumptions, which are commonly adopted within the industry.

The study shows that the use of three dimensional soil-structure interaction simulation allows a more accurate assessment of earth pressure distributions, with due account for soil arching effects, and sub-structure behaviour. A Corner Optimisation Technique is presented. The method, implemented by the author on a number of projects, allows significant optimisation of wall reinforcement and embedment requirements, in proximity to excavation corners.

- Stability assessment and time dependent behaviour of an excavation in normally-consolidated clays.

  Selected aspects of a case study involving an excavation in normally consolidated Boston Blue Clay are presented in Chapter 5, as follows:

  - Experimental investigation of the strength and stiffness properties of the Boston Blue Clay.

    Advanced in-situ and laboratory testing data have been interpreted with a view of providing new insights in the behaviour of this material. Some of the data presented, in particular in relation to small strain stiffness and stiffness degradation with strain, are relatively rare. The author is not aware of the existence of data from self boring pressuremeter testing from other sites in the Boston area.

    The author believes that the data and interpretation presented would be very useful to designers of deep excavations in the Boston area.

  - Importance of strength anisotropy in base stability calculations/analyses.

    The results demonstrate that, for the case study concerned, an accurate assessment of the excavation base stability does not necessarily require the explicit consideration of anisotropic strength properties, but can be achieved with the use of an undrained shear strength profile evaluated from direct simple shear testing, using limit equilibrium or finite element methods, assuming isotropic behaviour for the material.

- Three dimensional analysis of excavation stability.

  The findings indicate that the explicit consideration of three dimensional collapse mechanisms can lead to a more accurate prediction of the excavation stability factors of safety, with relatively significant enhancements in estimated factors of safety, compared to plane strain conditions, for excavations with relatively small ratios of plan dimensions and excavation depth.

- Observed time dependent performance of the excavation base.

  The findings highlight the importance of taking into account the appropriate construction sequence and carrying out a time dependent coupled simulation of the excavation. It is shown that this would lead to potentially significant optimisation of basement raft designs and a more accurate assessment of foundation system performance.

1.3 Thesis Structure

The content of the following chapters is briefly summarised below.

Chapter 2 presents a review of the key features of various constitutive models, commonly available in Plaxis.

Chapter 3 presents the assessment of the serviceability performance of an excavation in London Clay. Various constitutive models are adopted to simulate the behaviour of the London Clay. The benefits of using elasto-plastic models able to capture the small strain stiffness of the London Clay and its stiffness degradation behaviour, in lieu of the commonly adopted linear elastic – perfectly plastic (Mohr-Coulomb) model, are investigated. In addition, different stress dependency formulations for the stiffness parameters are reviewed and compared.

Chapter 4 reviews the advantages of using a three dimensional modelling approach, in comparison with the standard plane strain analysis method, for a number of case histories. Opportunities for retention system design optimisation using three dimensional soil-structure interaction analyses are presented, together with an insight into potential construction related savings and efficiencies.

Chapter 5 focusses on a case history of an excavation in normally consolidated Boston Blue Clay. A detailed assessment of the ground model at the site is presented, alongside considerations related to the Boston Blue Clay undrained shear strength, small strain stiffness and stiffness – strain degradation behaviour, based on advanced laboratory and in situ testing carried out at the site. The chapter subsequently focusses on aspects related to the stability and time dependent behaviour of the excavation.

Chapter 6 draws conclusions from the performed review and numerical investigation, summarising the main findings and limitations of this study, and making suggestions for further research.

CHAPTER 2

CONSTITUTIVE MODELS REVIEW

2.1 Background

The use of finite element analysis in the geotechnical engineering practice has become more and more popular in recent years. The technique is often adopted to predict the behaviour of excavations, in order to aid the design of retaining systems and foundations, and to assess likely ground movements and potential impact of the works on existing assets.

A key ingredient of a finite element analysis for a soil-structure interaction problem is the selection of suitable constitutive models to simulate the behaviour of soil strata subject to specific loading paths.

Numerous constitutive models have been developed over the past decades, trying to capture various features of soil behaviour, including non-linear stress-strain pre and post-peak behaviour, unloading-reloading, anisotropy, structure degradation, time dependent behaviour, etc. The selection of the appropriate constitutive model depends on the analysed problem, but it is also, to some extent, a matter or mathematical aesthetic and personal choice (Muir Wood, 1990).

It is indeed impossible to provide an exhaustive review of all the models proposed in the literature. However, considering the practical focus of this dissertation work, the following review will concentrate on those models which are more commonly used in the day-to-day geotechnical practice. In particular, this review focusses on a selected series of constitutive models, commonly available in finite element software Plaxis. Plaxis is a widely adopted commercial finite element software, which allows the two or three dimensional analysis of soil-structure interaction problems.

2.2 Considered constitutive models

It should be highlighted that, despite the numerous and sophisticate modelling development in the literature, the most commonly adopted constitutive model for clay by the industry, is still the so-called Mohr-Coulomb model. This model combines linear elastic pre-failure behaviour with the Mohr-Coulomb failure criterion. As such, it is called linear elastic – perfectly plastic model.

Based on the author's experience, the adoption of the Mohr-Coulomb model is very common for projects dealing with the study of excavation problems, both in terms of stability (ultimate limit state conditions) and performance (serviceability limit state conditions). The simplistic assumption, particularly in relation to the pre-failure linear behaviour, often results in poor predictions of ground movement and overall substructure behaviour (for example Simpson et al., 1979).

A step forward from the assumption of linear elasticity is the introduction of stiffness degradation functions. An example to simulate the non-linear soil behaviour is the proposal by Jardine et al. (1986) in which the material Young's Modulus and Bulk Modulus vary as a function of the strain. The model is able to reproduce the progressive stiffness degradation with strain along monotonic loading paths. However, it is not able to adequately capture the sudden increase in stiffness typically observed upon stress reversal.

A more sophisticated improvement is the inclusion of the critical state concept in the constitutive modelling framework. Indeed, in this respect the most important and famous advancement in the modelling clay soil is represented by the Cam Clay (Roscoe and Schofield, 1964) and Modified Cam Clay (Roscoe and Burland, 1968) models, which are formulated within the framework of the critical state theory. Muir Wood (2004) states that the Cam-Clay is reasonably the first hardening soil model that has become generally adopted for soils. The models simulate the soil response eventually tending towards an ultimate condition (critical state), in which plastic shearing could continue indefinitely without changes in volume or effective stresses. These models

assume isotropic hardening plasticity, with an ellipse-shaped yield locus, the size of which is a function of plastic volumetric strain.

As mentioned above, further modelling features have been progressively introduced through the years based upon the previous frameworks. Indeed, simulation of additional behavioural features comes at expense of increased model complexity and larger number of modelling parameters. This poses challenges to the industrial practice because of the necessity of full understanding of complex modelling features and behaviour as well as for the calibration of a larger number of modelling parameters, which is often carried out based upon a limited and simple set of experimental tests. As such, examples of these more sophisticated models will be provided at the end of this literature review, to provide the reader with an overview of potential developments and future trends, but, considering the industrial focus of this work, they will not be analysed in detail.

However, a detailed review is provided for selected constitutive models, with different properties and level of complexity, which are commonly available in the finite element software Plaxis. The main objective of this review is to assess their key features and review benefits and disadvantages associated with their use. Selected models from this review will then be used for the analysis of geotechnical problems in clays. These applications are presented in the next chapters.

The following constitutive models have been considered in this chapter.

[standard Plaxis models]

- Soft Soil model (Plaxis Material Models Manual, 2019)
- Hardening Soil model (Shanz et al., 1999)
- Hardening Soil model with small strain stiffness (Benz, 2007)

[user defined Plaxis models]

- Generalised Hardening Soil model (Petalas, 2013)
- NGI ani2 model (Andresen & Jostad, 2002)

The review of these models has been carried out by means of extensive parametric analyses, mainly related to triaxial testing loading conditions, aimed at capturing key aspects of the models formulation. The following sections present the features of the models and provide some details of the testing/validation study carried out.

2.3 Soft Soil model

2.3.1 General framework

Yield locus, elasticity and hardening rule

The Soft Soil (SS) model available in Plaxis is an elasto-plastic model based on the framework of isotropic hardening plasticity.

The SS model is based on the Modified Cam Clay (MMC) model. The idea at the base of the SS model is to avoid stress states characterised, in a triaxial *q-p'* plane for example, by high deviator stress *q* and low effective mean stress *p'*. In fact, unrealistically high *q* values are allowed by MCC model in the dry zone of the *q-p'* plane, as indicatively shown in Figure 2.1 (yellow hatched zone).

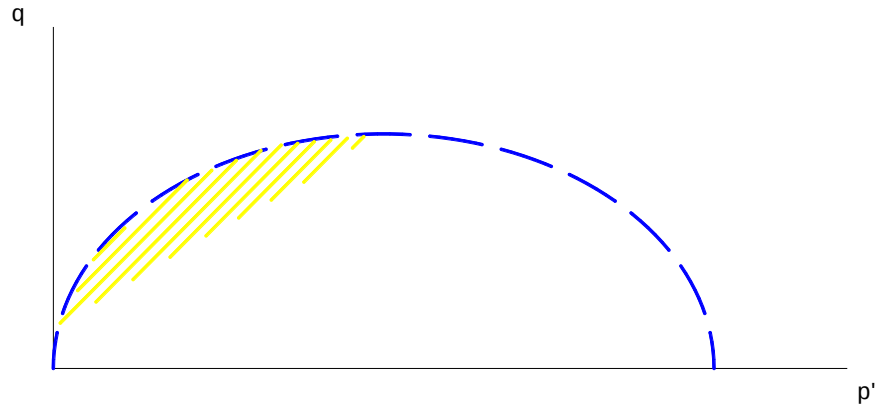

Figure 2.1 High deviator stress zone highlighted in yellow

In a *q-p'* plane, the yield locus comprises a hardening cap, which expands following primary loading, and a straight line, representing a Mohr-Coulomb failure criterion, which limits the values of the deviator stress *q*. The two curves define a global yield locus in the *q-p'* plane, as shown in Figure 2.2. As shown in Figure 2.2, the slope of the Mohr-Coulomb failure criterion is a function of the effective friction angle of the soil (φ').

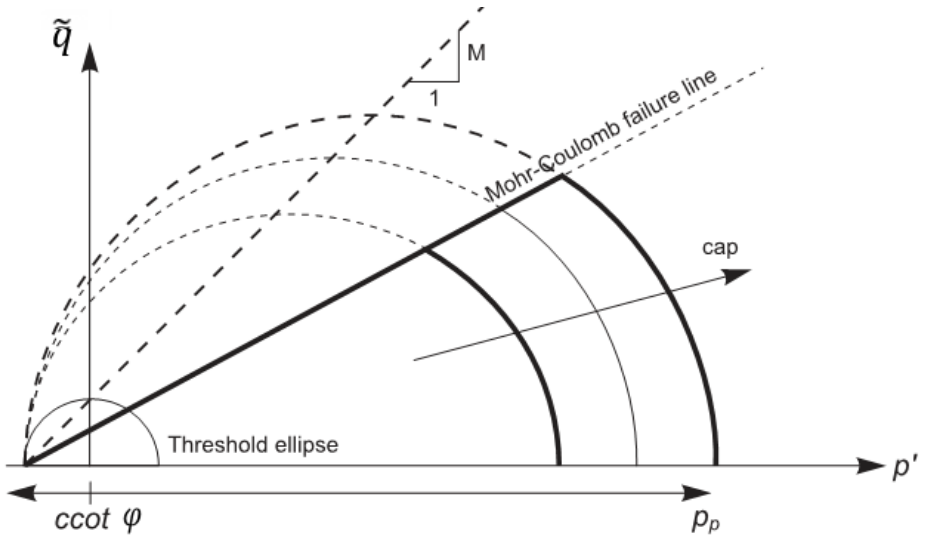

Figure 2.2 Soft Soil Model yield locus

The yield locus bounds the elastic zone. The soil behaviour within the elastic domain is described by straight lines in a ε_v *-p'* plane (see Figure 2.3), whose slope is defined by the parameter κ^*. Following this behavioural framework, the soil stiffness is dependent on the stress level.

In the *p'-q* plane, the cap of the yield locus is described by a portion of an ellipse. The cap size is defined by the isotropic pre-consolidation stress p_p, which is the intercept of the ellipse on the *p'* axis. The hardening of the cap is governed by volumetric plastic strains, ε_v^p. The evolution of the plastic volumetric strain is linked to the gradient λ^* of the virgin compression line in the volumetric plane in Figure 2.3. The shape of the ellipse is defined by the parameter *M*, ratio of the two ellipse axes (and defining the slope of the line passing through the apex of the ellipse as shown in Figure 2.2). The

parameter *M* is not a direct input. It is related to the coefficient of earth pressure at rest for normal the consolidated material (k_o^{NC}), which is required in input. In the SS model, the parameter *M* is used to define the cap shape.

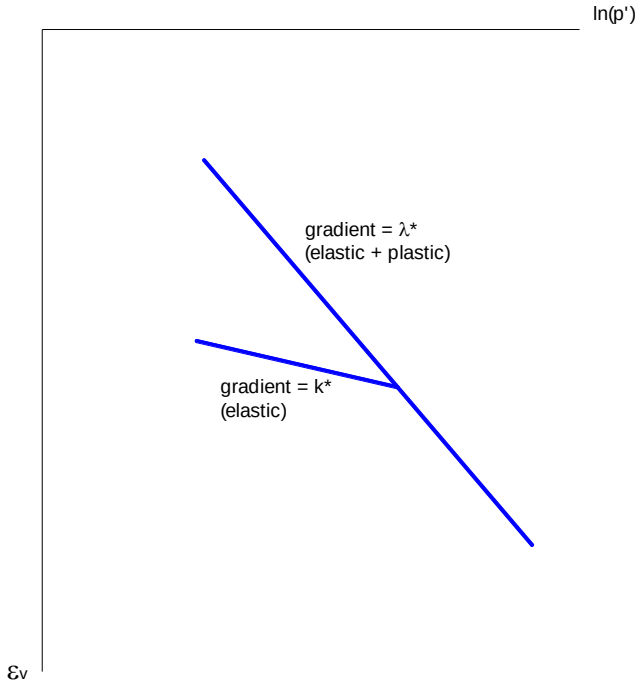

Figure 2.3 Stress-strain behaviour in the volumetric plane

The Mohr-Coulomb failure line has a different slope compared to the *M* line. It is characterised in general by a non-associated flow rule.

As explained above, the parameters *M* and *φ'* are completely independent, the first being related to the cap and the second to the Mohr-Coulomb failure line.

Plastic flow

An associated flow rule is adopted for the hardening cap. The cap hardening yield locus (*f*) is defined by the following expression:

$$\frac{q^2}{M^2(p' + c \cdot cot(\phi))} + p' - p'_0 = f \tag{2.1}$$

where *c* would be the cohesion intercept of the Mohr-Coulomb failure line with the deviatoric stress axis, while p'_0 is the pre-consolidation stress, which is a function of plastic strain.

Assuming *c =0*, the cap hardening yield locus (*f*) can be rewritten as:

$$f = \frac{q^2}{M^2 p'} + p' - p'_0 \tag{2.2}$$

In view of the associated flow rule, we can impose that the plastic potential (*g*) coincides with the yield locus (*f*). As such, we can express the plastic component of incremental isotropic and deviatoric strains ($d\varepsilon_p^p$ and $d\varepsilon_q^p$), respectively:

$$d\varepsilon_p^p = \frac{\partial g}{\partial p'} = 1 - \frac{q^2}{M^2 + p'^2} \tag{2.3}$$

$$d\varepsilon_q^p = \frac{\partial g}{\partial q} = \frac{2q}{M^2 p'} \tag{2.4}$$

Therefore, in order to evaluate the direction of the plastic flow vector (which can be defined as the ratio of the above), the previous equations can be combined to give:

$$\frac{\delta d\varepsilon_p^p}{\delta d\varepsilon_q^p} = \frac{1 - \frac{q^2}{M^2 p'^2}}{\frac{2q}{M^2 p'}} = \left(1 - \frac{q^2}{M^2 p'}\right)\frac{M^2 p'}{2q} = \frac{M^2 p'}{2q} - \frac{q}{2p'} = \frac{M^2}{2\eta} - \frac{1}{2}\eta = \frac{M^2 - \eta^2}{2\eta} \tag{2.5}$$

However, as shown in Figure 2.4, a different plastic flow is imposed for the linear portion of the yield locus (blue line in Figure 2.4), where the direction of the plastic flow

vector is vertical (parallel to the deviatoric stress axis) for any stress point. Therefore, it is clear that the point of intersection between cap and Mohr-Coulomb line is characterised by a singular behaviour. In this point, the cap gradient vector has a given inclination. Therefore, the cap plastic strain vector involves some plastic volumetric strain. On the contrary, the Mohr–Coulomb line involves plastic strain vectors parallel to the *q* axis (if the material has zero ultimate dilatancy). When a stress path travels along a cap hardening path, a sudden change in plastic strain direction takes place at this intersection point, as indicated schematically in Figure 2.4. A number of test models have been analysed in order to explore the key features of the model. Selected aspects are presented in the following.

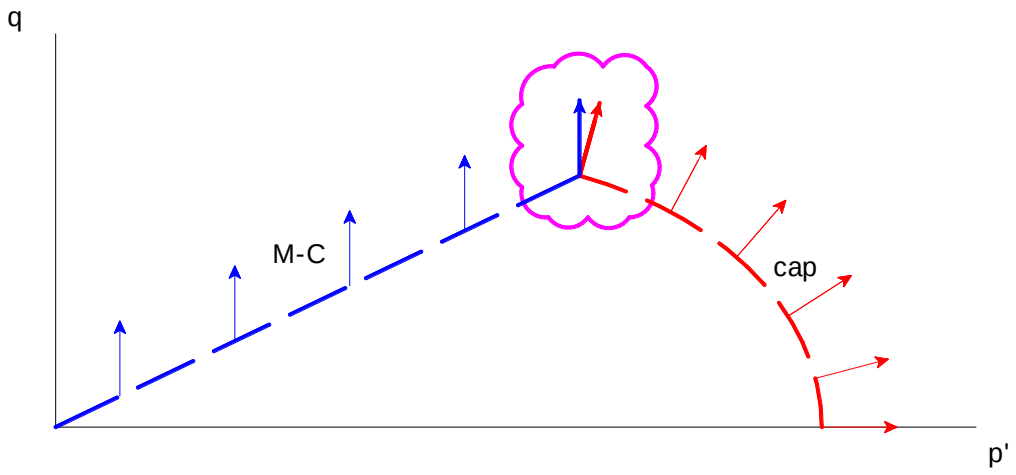

Figure 2.4 Plastic flow vectors

2.3.2 Analysis of some model aspects

Singularity of plastic flow

A number of test models have been analysed in order to verify this plastic flow relationship. The results indicate consistency between the evaluated plastic flow directions and the above expression. It is interesting to note the previously mentioned stress-strain discontinuity at the interception with the Mohr-Coulomb line, as shown in

Figure 2.5 and Figure 2.6, showing results of a triaxial compression test model, on a normally consolidated sample.

Figure 2.5 shows the stress strain relationship. The point of discontinuity is indicated in the diagram. Figure 2.6 shows the undrained stress path in a *p'-q* plane, starting from an isotropically consolidated condition. The diagram indicates the progressive expansion of the ellipse-shaped yield locus, and the evolution of the plastic flow directions, which become vertical (i.e. zero plastic volumetric strain) upon reaching the Mohr-Coulomb perfect plasticity line.

The singularity in the stress-strain behaviour can have consequences in finite element analyses, associated to the unrealistic sudden change in behaviour in areas where the Mohr-Coulomb yield locus is reached. These can potentially cause loss of accuracy of the solution.

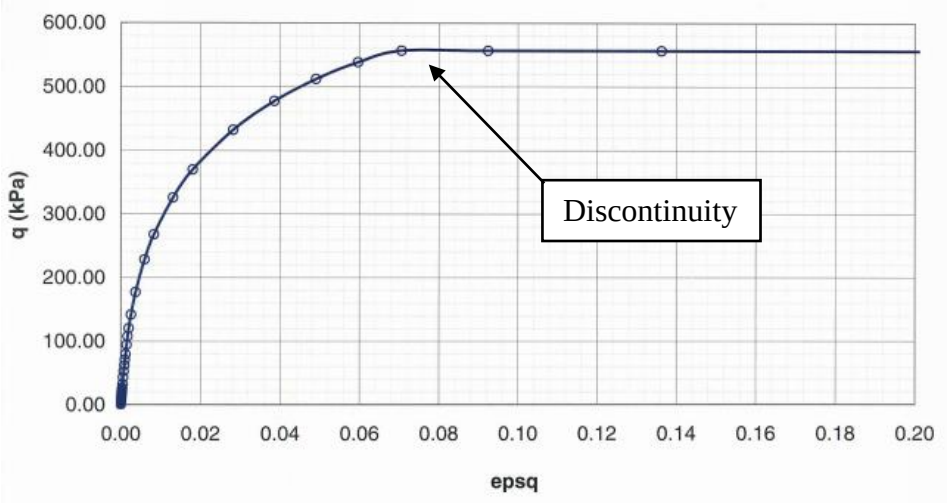

Figure 2.5 Stress-strain behaviour in undrained triaxial compression

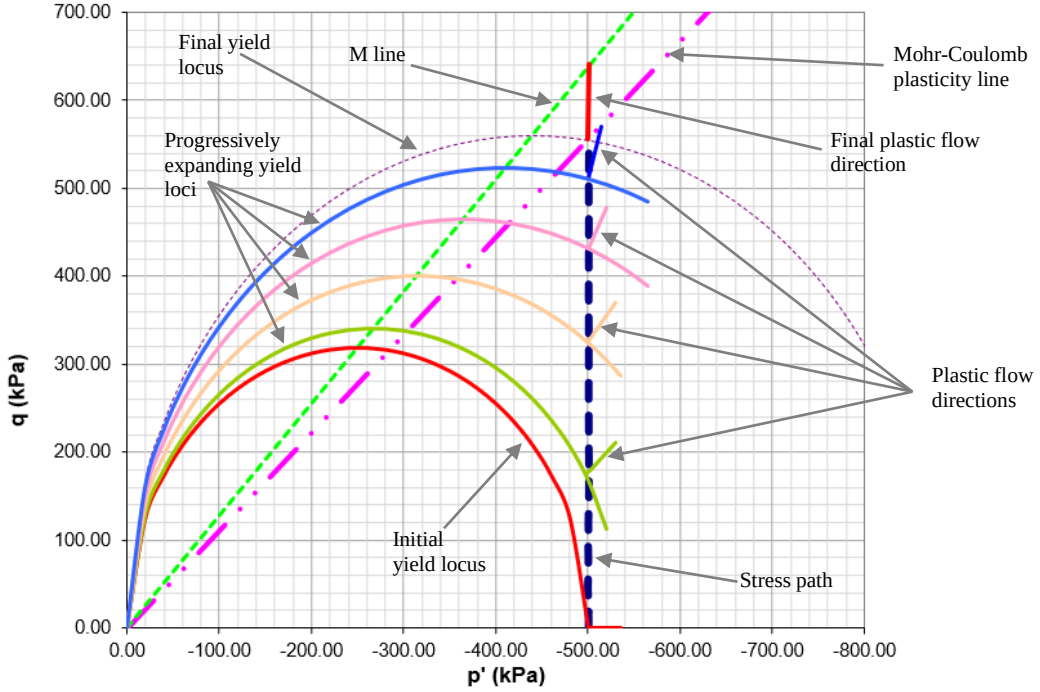

Figure 2.6 Plastic flow vectors at increasing deviatoric stress in undrained triaxial compression test (negative vales of p' refer to compressive stresses)

Undrained stress path

Clay soils are often assumed to behave in an undrained manner during loading/unloading associated with construction or excavation works. Accurately modelling the undrained behaviour of a clay is therefore a key consideration in order to predict the performance of retaining walls or foundations in these soils.

A validation exercise has been carried out, deriving the relationship describing the triaxial test stress path in undrained conditions. It is assumed that the stress state is always in contact with the yield locus, i.e. plastic strains develop throughout all the loading process. The analytical procedure is presented below.

Assuming no volume change in an undrained test, the volumetric elastic strain (ε_p^e) has to be equal and opposite to the volumetric plastic strain (ε_p^p):

$$\delta\varepsilon_p^e = -\delta\varepsilon_p^p \tag{2.6}$$

The above expression can be rewritten in terms of stress variables and slope of the recompression and virgin compression lines (κ^* and λ^*, respectively, see Figure 2.3) as follows:

$$\kappa^* \frac{\delta p'}{p'} = -(\lambda^* - \kappa^*) \frac{\delta p'_0}{p'_0} \tag{2.7}$$

By considering the following relationship for the cap of the yield locus (f):

$$f = \frac{q^2}{M^2 p'} + p' - p'_0 = 0 \tag{2.8}$$

it can be derived the following expression:

$$\frac{\eta^2}{M^2} + 1 - \frac{p'_0}{p'} = 0 \tag{2.9}$$

where η is the stress ratio q/p' which can be rewritten as follows:

$$\frac{\eta^2 + M^2}{M^2} - \frac{p'_0}{p'} = 0 \tag{2.10}$$

and expanded in incremental terms:

$$\frac{\partial p'}{p'_0} - \frac{p'\delta p'_0}{p'^2_0} + \frac{2\eta M^2 \delta\eta}{(\eta^2 + M^2)^2} = 0 \tag{2.11}$$

Introducing equation (2.10), equation (2.11) can be rewritten as

$$\frac{\partial p'}{p'} - \frac{\delta p'_0}{p'_0} + \frac{2\eta\delta\eta}{\eta^2 + M^2} = 0 \tag{2.12}$$

and further introdcuing (2.7), the following expression can be derived:

$$\frac{\delta p'_0}{p'_0} = \frac{-\kappa^*}{\lambda^* - \kappa^*}\frac{\delta p'}{p'} \tag{2.13}$$

and expanded into:

$$\frac{\delta p'}{p'}\left(\frac{\lambda^*}{\lambda^* - \kappa^*}\right) = \frac{2\eta\delta\eta}{\eta^2 + M^2} \tag{2.14}$$

Integrating between two different states, indicated by *i* and *i+1* (current state):

$$\frac{\lambda^*}{\lambda^* - \kappa^*}\int_i^{i+1}\frac{\delta p'}{p'} = -\int_i^{i+1}\frac{2\eta\delta\eta}{\eta^2 + M^2} \tag{2.15}$$

$$\frac{\lambda^*}{\lambda^* - \kappa^*} \ln\left(\frac{p'_{i+1}}{p'_i}\right) = \ln\left(\frac{\eta_{i+1}^2 + M^2}{\eta_i^2 + M^2}\right)^{-1} \tag{2.16}$$

$$\left(\frac{p'_{i+1}}{p'_i}\right)^{\frac{\lambda^*}{\lambda^* - \kappa^*}} = \frac{\eta_i^2 + M^2}{\eta_{i+1}^2 + M^2} \tag{2.17}$$

The final expression for the stress path in an undrained test can be derived:

$$\frac{p'_i}{p'_{i+1}} = \left(\frac{\eta_{i+1}^2 + M^2}{\eta_i^2 + M^2}\right)^{\frac{\lambda^* - \kappa^*}{\lambda^*}} \quad \text{(stress path in undrained test)} \tag{2.18}$$

A comparison of the analytical solution and the Plaxis output is presented in Figure 2.7. A very good correspondence is found between theoretic (curve named “theoretic”) and computed (curve named “Plaxis model”) stress paths.

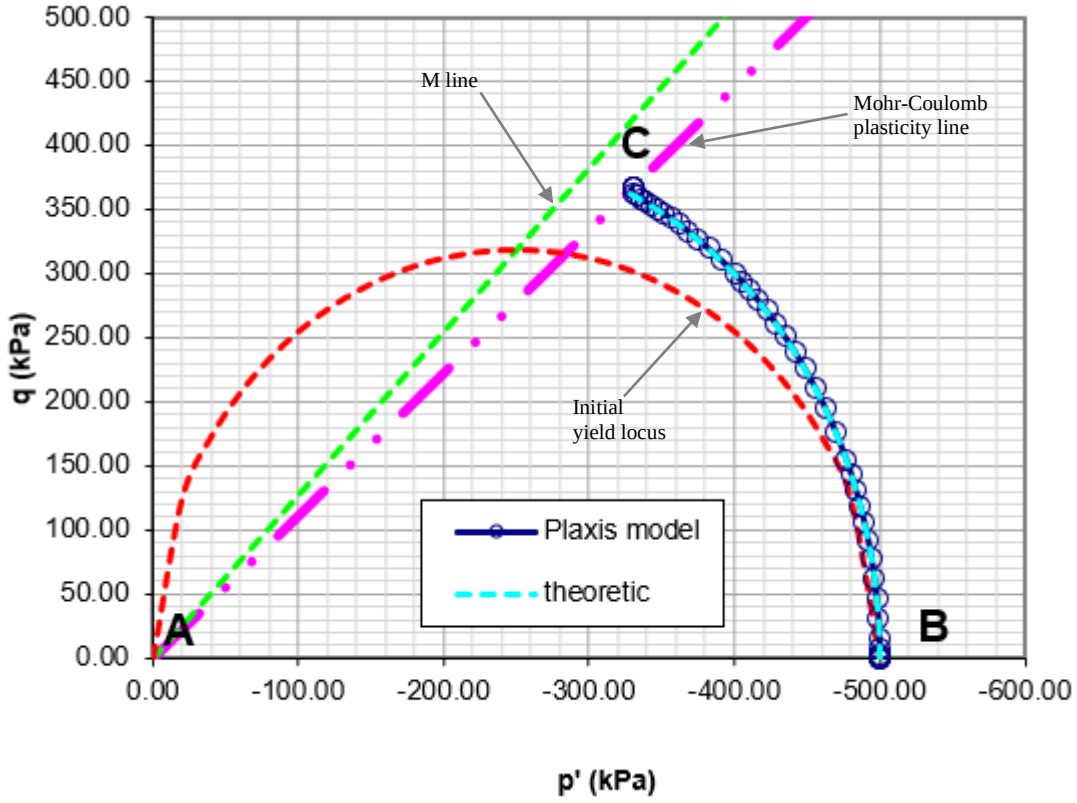

Figure 2.7 Stress path in undrained triaxial compression test – comparison of theoretic solution and Plaxis model output (negative vales of p' refer to compressive stresses)

2.4 Hardening Soil model

2.4.1 General framework

Yield locus and hardening

A key aim of the Hardening Soil (HS) model is to reproduce the hyperbolic stress-strain relationship generally observed in a triaxial compression test, using an elasto-plastic formulation with hardening plasticity rather than remaining within the elastic framework (for example Duncan & Chang, 1970, Jardine at al., 1986). Details of the model formulation are given by Benz (2007) and Shanz et al. (1999).

With reference to a triaxial p'-$\underline{q}$ plane ($\underline{q}$ being a modified deviatoric stress, $\underline{q}=\sigma'_1+(\delta-1)\sigma'_2-\delta\sigma'_3$, with $\delta=(3+\sin\phi)/(3-\sin\phi)$; $\underline{q}=q$ in triaxial compression) two independent yield loci are defined (Figure 2.8). An ellipse shaped cap yield locus, similar to the SS model cap surface, governs soil volumetric hardening. A separate surface (shear yield in Figure 2.8) controls shear hardening. A Mohr-Coulomb failure line bounds the zone of possible stress states.

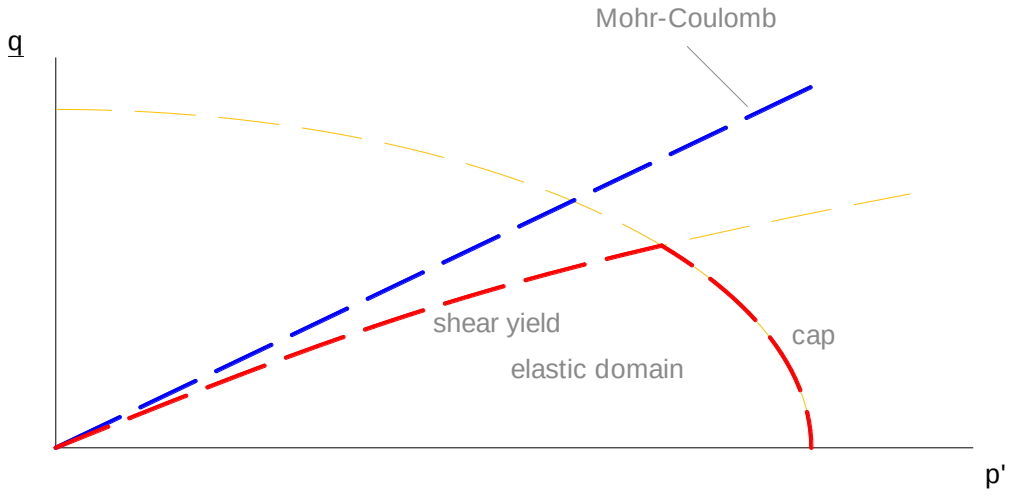

Figure 2.8 HS model yield loci

The shape of the cap curve is defined by the parameter α, ratio of the ellipse axes. α is not a direct input parameter but depends on the coefficient of earth pressure at rest for normal consolidated material (k_o^{NC}).

The cap is characterised by an associated flow rule and its hardening (indicated in Figure 2.9) is defined by a relationship between the variation of cap plastic volumetric strain ($d\varepsilon_{pc}^{v}$) and the variation of isotropic pre-consolidation stress dp_p.

$$dp_p = H\left(\frac{\sigma_3 + c\cot\varphi}{p^{ref} + c\cot\varphi}\right)^m d\varepsilon^v{}_{pc} \tag{2.19}$$

where m is a direct input parameter, defining the shape of the shear hardening curves in the p'-q plane, and H is defined by the following equation:

$$H = \frac{K_s K_c}{K_s - K_c} = \frac{1}{\frac{K_s}{K_c} - 1} K_s \tag{2.20}$$

K_s being the elastic bulk modulus, dependent on the stress level, and K_c being the elasto-plastic bulk modulus. K_c is related to the cap bulk modulus K_{cap} through the following relationship:

$$\frac{1}{K_c} = \frac{K_s + K_{cap}}{K_s K_{cap}} \tag{2.21}$$

K_{cap} is not a direct input parameter, but is related to the stress dependent input parameter E_{oed}.

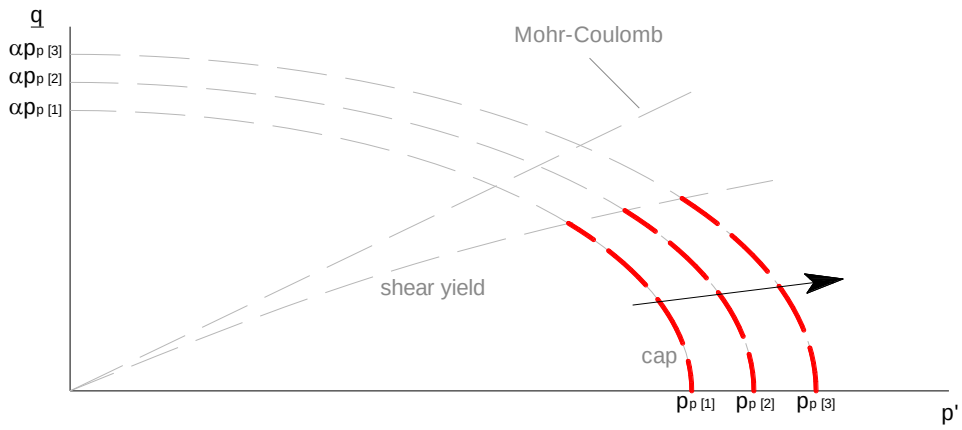

Figure 2.9 Cap hardening – progressively expanding cap yield locus

The shear yielding is related to deviatoric loading. The shear yield locus hardening is presented indicatively in Figure 2.10. A shear hardening parameter (plastic shear strain γ_p) appears in the formulation of the yield function. The shear hardening is governed by a stiffness parameter E_i. E_i is not a direct input parameter but it is related to the stress dependent stiffness E_{50}.

The shear hardening is in general characterised by non-associated plastic flow. The flow rule links plastic shear strain and plastic volumetric strain through the mobilised dilatancy angle (ψ_m). ψ_m is a function of mobilised angle of shearing resistance (φ_m), ultimate dilatancy angle (ψ) and angle of shearing resistance (φ). This relationship is based on an adaptation of the Rowe's stress-dilatancy theory. In particular, the mobilised dilatancy angle (ψ_m) is zero for $sin(\varphi_m)<3/4sin(\varphi)$. A dilatancy cut-off can be set to limit the material volumetric expansion. However, this requires the input of in situ void ratio and maximum void ratio. The plastic volumetric strain associated with the shear hardening is always zero if a zero dilatancy angle is set.

The two input parameters E_{oed} and E_{50} are completely independent since they are associated to the two separate yield loci. When a stress point lays at the intersection of the two yield loci, both the plastic mechanisms (cap and shear hardening) develop.

Within the yield loci (see Figure 2.8) the material behaves elastically. The elastic soil stiffness (E_{ur} – unloading/reloading Young's modulus) is another stress dependent parameter.

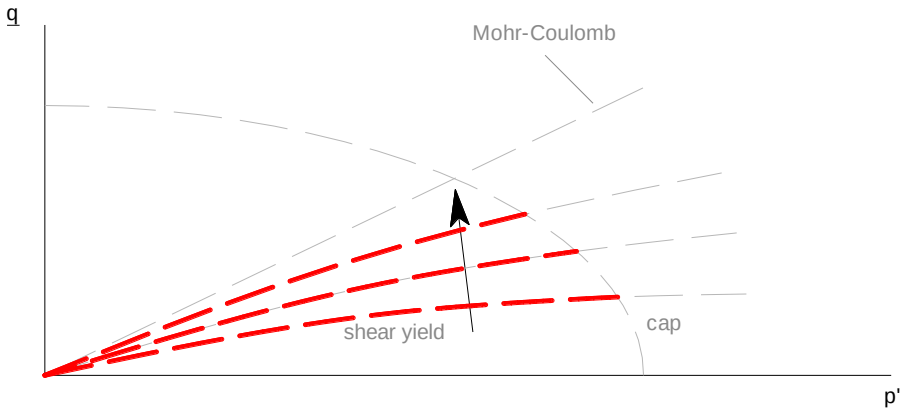

Figure 2.10 Shear hardening – progressively expanding shear yield locus

The internal parameters α, K_{cap} and E_i

The internal parameters α, K_{cap} and E_i govern the two hardening mechanisms of the HS model. As mentioned previously, they are not direct input parameters, but depend on k_0^{NC}, E_{oed} and E_{50}. Once these three parameters are defined, Plaxis carries out a triaxial compression and an oedometer test at stress point level. The three internal parameters are modified iteratively, until consistency with the input values is achieved.

If a relatively low value of E_{oed} is used as input, large volumetric strains would be generated during the stress point internal triaxial test. Due to the associated flow rule related to cap plasticity, large deviatoric strains are produced too. In order to achieve the input E_{50} secant stiffness, the internal parameter E_i must consequently be fairly high. In the case the internal procedure finds that $E_i > E_{ur}$, a paradox condition, in which elasto-plastic strains are smaller than elastic strains, would occur. In this case, Plaxis adopts a stiffness cut-off, imposing $E_{max}=E_{ur}$, and therefore cutting off the initial part of the stress-strain curve, as indicatively shown in Figure 2.11, where an example stress-strain curve is presented. At most, the curve can be cut off over the full distance between the origin and the E_{50} point (where $q = q_f/2$), in which case $E_{50}=E_{ur}$.

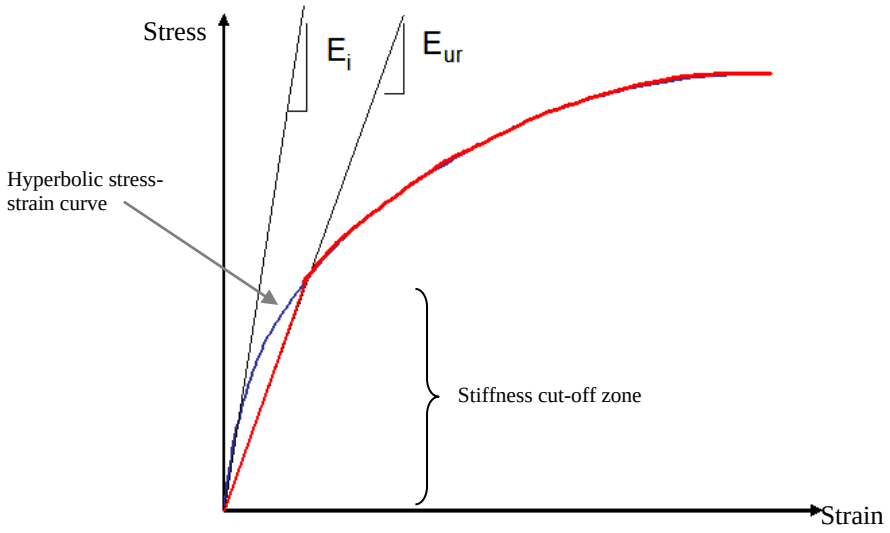

Figure 2.11 Stiffness cut-off shown in an indicative stress-strain curve

2.4.2 Analysis of some model aspects

A spreadsheet has been set up to reproduce the stress-strain behaviour of the HS model along triaxial compression stress paths, to better understand some of the model features.

Three mechanisms may be active at each point, depending on the stress state and loading direction: elasticity, cap plasticity and shear plasticity. Each one of them is examined.

Elasticity

The axial strain variation link with stress changes follows theory of elasticity:

$$\delta\varepsilon_a{}^e = \frac{1}{E}(\delta\sigma'_a - 2\upsilon \cdot \delta\sigma'_r) \tag{2.22}$$

Shear plasticity

The axial strain produced by the shear hardening mechanism is given by the following relationship (Plaxis Material Model Manual, 2018):

$$\varepsilon_a{}^{ps} = \frac{1}{E_i} \cdot \frac{q}{1-\frac{q}{q_a}} - \frac{q}{E_{ur}} \tag{2.23}$$

Differentiating it, it is possible to obtain the following incremental formulation

$$\delta\varepsilon_a{}^{ps} = \left[\frac{1}{E_i\left(1-\frac{q}{q_a}\right)^2} - \frac{1}{E_{ur}}\right]\delta q \tag{2.24}$$

Cap plasticity

The cap yield surface is defined by the equation

$$f_c = \frac{q^2}{\alpha^2} + p'^2 - {p_p}^2 \tag{2.25}$$

The cap is characterised by an associated flow rule, in view of which

$$\delta {\varepsilon_q}^{pc} = \frac{\frac{\partial f_c}{\partial q}}{\frac{\partial f_c}{\partial p'}} \cdot \delta {\varepsilon_v}^{pc} \tag{2.26}$$

Being $\frac{\partial f_c}{\partial p'} = 2p'$ and $\frac{\partial f_c}{\partial q} = \frac{2}{\alpha^2} q$, the following relationship is derived

$$\delta {\varepsilon_q}^{pc} = \frac{q}{\alpha^2 p'} \delta {\varepsilon_v}^{pc} \tag{2.27}$$

Considering that $\delta {\varepsilon_a}^{pc} = \delta {\varepsilon_q}^{pc} + \frac{1}{3} \delta {\varepsilon_v}^{pc}$, it follows

$$\delta {\varepsilon_a}^{pc} = \left(\frac{q}{\alpha^2 p'} + \frac{1}{3} \right) \delta {\varepsilon_v}^{pc} \tag{2.28}$$

Expressing $\delta\varepsilon_v^{pc}$ using equation (2.19), a stress-strain relationship is obtained, which relates variation of the axial plastic cap strain ($\delta\varepsilon_a^{pc}$) and variation of the hardening parameter p_p.

$$\delta {\varepsilon_a}^{pc} = \left(\frac{q}{\alpha^2 p'} + \frac{1}{3} \right) \cdot \frac{d p_p}{H \left(\frac{\sigma_3 + c \cot \varphi}{p^{ref} + c \cot \varphi} \right)^m} \tag{2.29}$$

From equations (2.22), (2.24) and (2.29) it is possible to evaluate the axial stress-strain behaviour for triaxial compression paths in drained conditions. The formulations of deviatoric and volumetric strain generating from the three mechanisms, easily derived from those expressions, have been implemented in a spreadsheet. Consistency between the spreadsheet and Plaxis output has been verified for a number of triaxial test conditions, involving one, two or all the deformation mechanisms.

It is worth noting that the stress-strain hyperbolic relationship in triaxial compression, that the model aims to achieve, is reproduced (in most cases) in stress paths involving elastic and shear hardening only. If cap hardening develops alongside the other two mechanisms, or if the stiffness cut off procedure described above (when $E_i > E_{ur}$) is active in elastic and shear hardening paths, strictly speaking the stress-strain curve travels along a non-hyperbolic route.

Undrained stress path

As previously mentioned, accurately modelling the clay undrained behaviour is important for the analysis of retaining walls and foundations problems in clays. A validation exercise has been carried out, comparing the theoretic undrained stress path with a Plaxis model output.

The shape of an undrained stress path is dictated by the cap hardening behaviour. With reference to a triaxial test for example, the plastic volumetric strain produced by the cap hardening associated flow rule has to be balanced by an elastic volumetric strain, in order to have zero total volumetric strain. The elastic volumetric strain is obviously directly linked to $\delta p'$, and therefore drives the stress path direction in a p' - q space. A relationship has been derived for the stress path under undrained triaxial loading, in the assumption $m=1$.

The following expression (Plaxis Material Models Manual, 2018) can be used to define the cap plastic volumetric strain. The expression includes the internal parameter β, in lieu of the cap bulk modulus (K_{cap}).

$$d\varepsilon^{v}{}_{pc} = \frac{\beta}{p_{ref}{}^{(1-m)}} p_p{}^{-m} \delta p_p \tag{2.30}$$

Assuming $m=1$,

$$d\varepsilon^{v}{}_{pc} = \frac{\beta}{p_p} \delta p_p \tag{2.31}$$

In undrained conditions, no volume change is allowed, therefore the elastic and plastic volumetric strain must counteract each other.

$$\frac{\delta p_p}{p_p} = -\frac{\delta p'}{\beta K} \tag{2.32}$$

Note that the only plastic volume strain is related to cap hardening mechanism, in the assumption of dilatancy angle set to zero.

In the case plasticity is developing, $f_c=0$ and $\delta f_c=0$ (where f_c is the cap yield locus)

$$f_c = 0 \rightarrow \frac{q^2}{\alpha^2} + p'^2 - p_p{}^2 = 0 \tag{2.33}$$

Introducing $\eta = \frac{q}{p'}$, it follows

$$\frac{p'^2}{p_p{}^2} = \frac{\alpha^2}{\eta^2 + \alpha^2} \tag{2.34}$$

$$\delta f_c = 0 \rightarrow -\frac{2p'}{{p_p}^2}\delta p' + \frac{2p_p{p'}^2}{{p_p}^4}\delta p_p - \frac{2\eta\alpha^2}{(\eta^2+\alpha^2)^2}\delta\eta = 0 \tag{2.35}$$

Combining (2.32) and (2.34) with (2.35), it follows

$$\delta p'\left(\frac{1}{p'} + \frac{1}{\beta K}\right) = -\frac{\eta}{\eta^2+\alpha^2}\delta\eta \tag{2.36}$$

This expression can be integrated between current state *i* and *i+1*.

$$\int_{p'_i}^{p'_{i+1}}\left(\frac{1}{p'} + \frac{1}{\beta K}\right)\delta p' = -\frac{1}{2}\int_{\eta_i}^{\eta_{i+1}}\frac{2\eta}{\eta^2+\alpha^2}\delta\eta \rightarrow ln\left(\frac{p'_{i+1}}{p'_i}\right) + \frac{p'_{i+1}-p'_i}{\beta K} = -\frac{1}{2}ln\left(\frac{{\eta_{i+1}}^2+\alpha^2}{{\eta_i}^2+\alpha^2}\right) \tag{2.37}$$

The (2.37) has been applied along a generic triaxial stress path and has proven consistent with the Plaxis output, as shown in Figure 2.12. The figure shows a comparison between the theoretic curve (curve named "theoretic") and the Plaxis model output (curve named "Plaxis model").

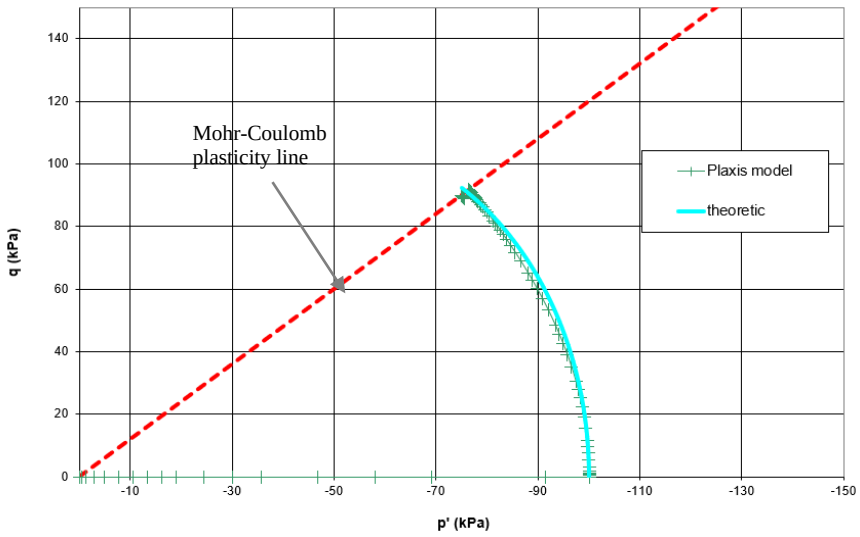

Figure 2.12 Undrained triaxial compression stress path – comparison between theoretic curve and Plaxis output (negative vales of p' refer to compressive stresses)

2.5 Hardening Soil model with small strain stiffness

2.5.1 General framework and discussion on small strain stiffness formulation

The Hardening Soil "Small" model (HSS model) available in Plaxis is an extension of the Hardening Soil model (HS model). The HS model is characterised by elastic behaviour within the yield surfaces (Figure 2.13), with stress dependent stiffness moduli. The input parameters that govern the soil behaviour inside the elastic domain are E_{ur} (Young's modulus at a reference pressure p_{ref}) and ν_{ur} (Poisson's ratio).

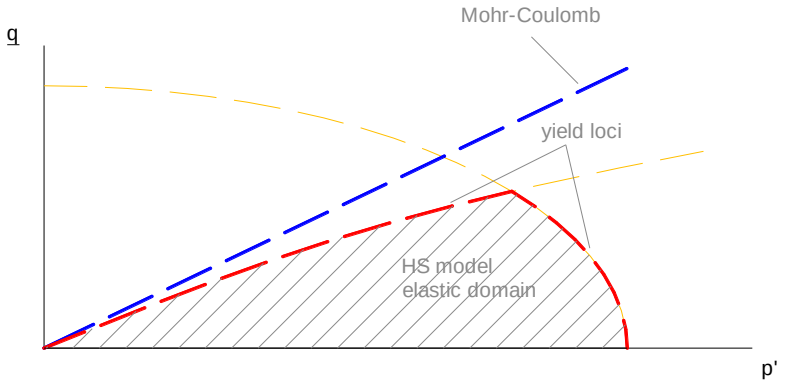

Figure 2.13 HS model yield loci and elastic domain

An S-shaped stiffness-strain *(G-γ)* relationship is adopted to model the decay in soil stiffness with strain. The *G-γ* curve is dependent on the stress level. The function is defined by the input parameters G_0^{ref}, small-strain stiffness at a reference stress level p_{ref} and $\gamma_{0.7}$, shear strain at which $G=0.7G_0$.

The stiffness degradation curve is followed both along elastic and elasto-plastic stress paths. In the case both elasticity and plasticity mechanisms are active, "primary loading" conditions apply. Unload-reload conditions are related to purely elastic deformation mechanisms. In an unload-reload case, the strain level at which $G=0.7G_0$ is $2\gamma_{0.7}$ (i.e. twice the input value). In primary loading it is $\gamma_{0.7}$. In this case, plastic deformations are responsible for the stiffness reduction from the red to the blue curve in Figure 2.14. In order to achieve this behaviour, the HS model hardening formulations are modified in the HSS (Benz, 2007).

The input parameter $\gamma_{0.7}$ is doubled in the unload-reload case to simulate the hysteretic stress-strain behaviour shown indicatively in Figure 2.15, reflecting the so-called Masing rule. The Masing rule (Masing, 1926) states that the unloading-reloading stress-strain curve has a homological ratio of two to the monotonic primary loading stress-strain curve. The monotonic primary loading curve is shown in red in Figure 2.15, while the unloading-reloading curves are shown in blue.

The stress dependent parameter G_{ur}, already present in the HS model formulation, represents here a minimum cut-off value for the elastic shear modulus. If G_0 coincides with G_{ur} the HS model behaviour is reproduced. Once the elastic stiffness reaches G_{ur}, the hardening mechanisms coincide with the ones used in the original HS model.

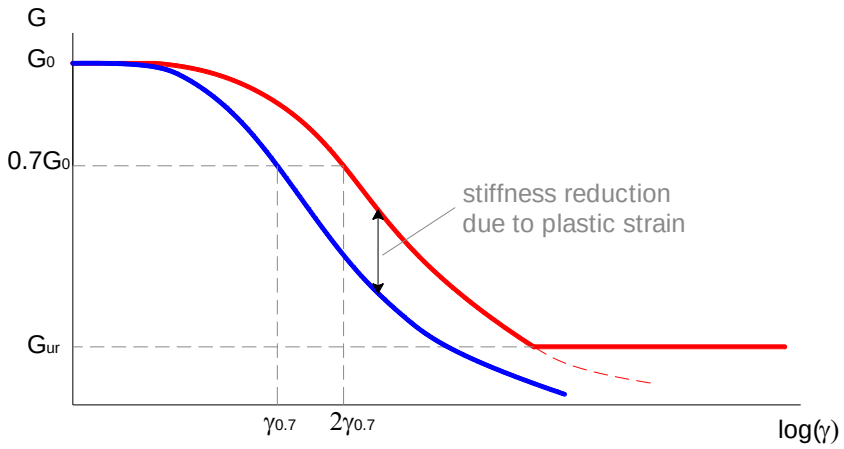

Figure 2.14 Indicative stiffness-strain degradation curve

The model formulation accounts for strain path reversals using a scalar strain parameter (γ_{hist}) dependent on the three principal deviatoric strains. In the case of strain reversal occurring, the stiffness recovers its initial small strain value and starts decaying again according to the hyperbolic formulation as the (reversed) strain increases.

γ_{hist} is the projection of the strain history on the loading direction. In the case the direction of loading γ_{hist} are inconsistent, γ_{hist} is reset to zero and the stiffness is set back to the small strain G_0 value. Details of the strain reversal algorithm are provided by Benz (2007).

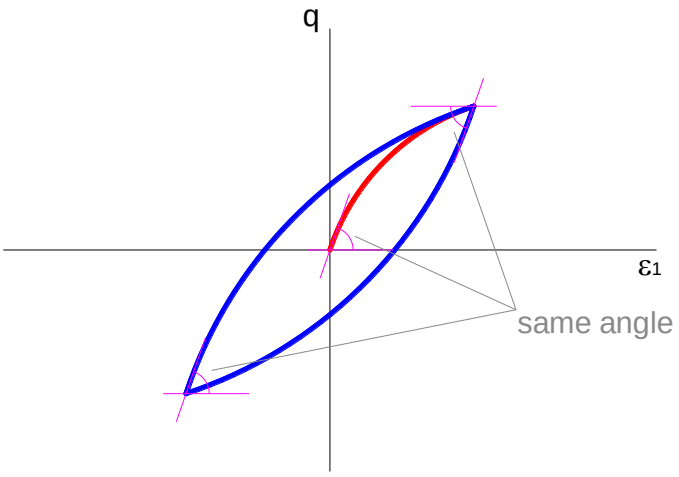

Figure 2.15 Indicative stress-strain hysteretic behaviour (showing the Masing rule concept)

2.6 Generalised Hardening Soil model

2.6.1 General framework

The Generalised Hardening Soil (GHS) model is a general version of the hardening soil models (with and without small strain stiffness) presented previously. The GHS model has a series of switches, which allow the definition of specific stress and strain dependent stiffness formulations. Particular sets of input parameters would reproduce the HS and HSS models features.

Some of the key improvements of the GHS, in comparison to the HS and HSS models, are related to the stress dependency of the stiffness parameters based on the mean effective stress (p') and pre-consolidation stress (p_c), as opposed to the minimum principal stress, σ'_3, considered in the original HS and HSS formulations.

The p' dependency is generally consistent with other models often adopted for undrained loading of stiff clays (for example the Jardine et al., 1986 model), which focus on the stiffness degradation with strain, using normalised stiffness parameters (E_u/p').

The p_c dependency prevents the excessive reduction in stiffness, and consequent over-prediction of heave displacements, occurring in the region below the base of excavations, where σ'_3 can reduce to very small values.

The model is able to consider the strain dependency of the stiffness, reproducing the HSS features in this respect.

2.6.2 Analysis of some model aspects

Discussion on stress dependency

A number of stress dependent formulations are available for the various stiffness parameters. They are based on the minimum principal stress (σ'_3) or mean effective stress (p') or a combination of one of these variables and the pre-consolidation stress (p_c), as presented by the following relationships (Petalas, 2013).

$$E = E_{ur}^{ref} \left(\frac{\sigma'_3 + c \cdot cot\,\varphi}{\sigma^{ref} + cot\,\varphi} \right)^m \tag{2.38}$$

$$E = E_{ur}^{ref} \left(\frac{\sigma'_3 + p_c}{2p^{ref}} \right)^m \tag{2.39}$$

$$E = E_{ur}^{ref} \left(\frac{p' + p_c}{2p^{ref}} \right)^m \tag{2.40}$$

It is worth noting that the first formulation coincides with the HS and HSS assumption.

The third formulation (2.40), involving p' and p_c, is particularly interesting, as it considers these parameters in lieu of the minimum principal stress, σ'_3. This formulation is adopted in the analyses presented in the next chapter.

As previously mentioned, the presence of p_c prevents unrealistically high heave ground movements from taking place at the excavation base, upon unloading. In addition, the presence of *p'* is considered appropriate for problem involving loading/unloading of stiff clays.

2.7 NGI ani2 model

2.7.1 General framework

The NGI ani2 material constitutive model (Andresen & Jostad, 2002) is a total stress material model that takes into account the strength and stiffness anisotropy of normally consolidated (or slightly over-consolidated) clays.

The model has been developed in order to study the effects of strength anisotropy on the behaviour of saturated clays, subjected to monotonic undrained loading (Andersen & Jostad, 2002). The non-linear stress-strain behaviour is a function of the major principal stress orientation.

With regards to undrained shear strength, the NGI ani2 model requires the input of three normalised undrained shear strength parameters, related to three modes of shearing, namely direct simple shear (DSS), plane strain active (PSA) and plane strain passive (PSP) loading conditions. Convenient strength normalising parameters (S_{norm}) could be the DSS undrained shear strength (S_{uDSS}) or the effective vertical stress (σ'_v). The normalised undrained shear strength can then be set as a function of depth. The model also requires the input of three strain levels at which these strengths are achieved.

2.7.2 Analysis of some model aspects

Anisotropic Stress-strain response

Example normalised stress-strain diagrams are presented in Figure 2.16.

The three curves shown are representative of compression (magenta curve), extension (blue curve) and DSS (black curve) shearing modes. The compression and extension shearing start from an anisotropically (K_0) consolidated state (initial τ_0/σ'_{v0}=0.225), while the DSS starts from a τ_0/σ'_{v0}=0 condition.

The curves are defined based on the input of i) normalised small strain stiffness (G_0/σ'_v), ii) normalised undrained shear strength S_u/σ'_v (0.28, 0.11 and 0.2, for compression, extension and DSS, respectively) and iii) shear strain levels at which the strength is achieved (0.75%, 3% and 2.5%, for compression, extension and DSS, respectively).

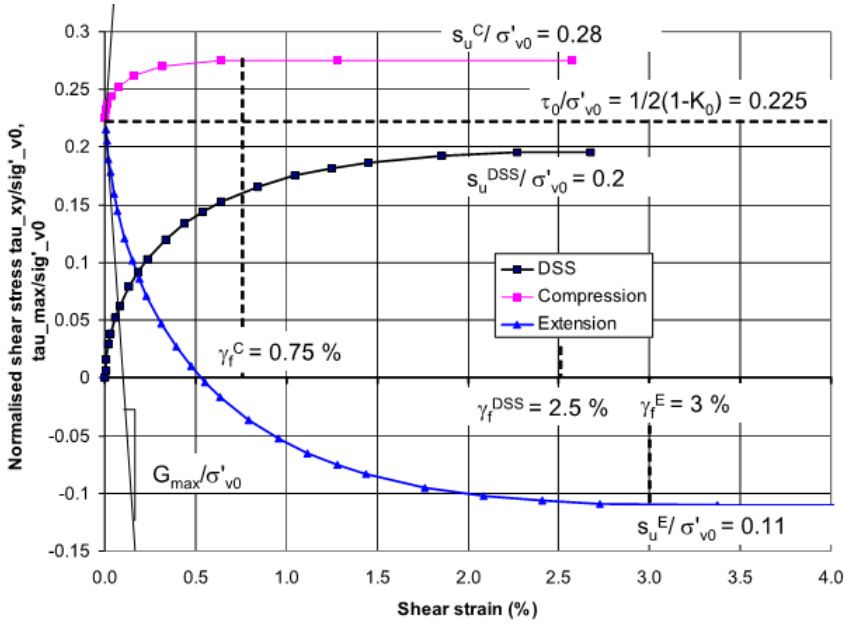

Figure 2.16 Example of normalised shear stress – shear strain curves (from NGI-ani2 material model manual)

The model has been used to assess the stability of an excavation in normally consolidated clay, presented in Chapter 5. The key aspect considered for this application has been the clay undrained shear strength anisotropy, which is explicitly considered by this model.

2.8 Further more complex models

In addition to the constitutive models examined in this chapter, numerous advanced models have been developed in the past decades to simulate the behaviour of clays. These models are generally based on the concepts introduced by the Cam Clay model. A brief description of some of these models is presented below. The models have not been examined in detail as part of this study, as the review has primarily focussed on models readily available in Plaxis.

An evolution of the Cam Clay model is represented by multiple (nested) surface plasticity and bounding surface plasticity models. These nested yield surfaces move in the stress space, "dragged" along the stress path, and an external bounding surface, representing the soil consolidation state, is able to expand during loading of normally consolidated soil. Selected examples of this type of models include the ones proposed by Mroz et al. (1981) and Al-Tabbaa and Muir Wood (1989).

Mroz et al. (1981) proposed a model which combines a bounding surface, defining the consolidation state of the soil, and a series of nested yield surfaces, able to translate during specific stress paths. A kinematic hardening behaviour is associated with each yield surface, depending on its relationship with the external bounding surface. An indicative view of the nested surfaces adopted in the Mroz et al. model is presented in Figure 2.17.

The Al-Tabbaa and Muir Wood (1989) model features a kinematic ellipse shaped surface (bubble) which travels inside a larger Cam Clay type yield surface (bounding surface). The model is able to simulate cyclic unloading-reloading paths, combining elastic behaviour inside the bubble and kinematic hardening plasticity when the bubble surface is dragged by the stress path. The model reproduces the Modified Cam Clay behaviour under monotonic loading. An indicative view of the outer yield surface and bubble yield surface is presented in Figure 2.18.

An enhancement of the Al-Tabbaa and Muir Wood (1989) model has been proposed by Rouainia and Muir Wood (2000), by modelling the bounding surface as a structure surface, the dimensions of which (in relation to a reference surface) are a function of the

degree of structure that characterises the clay. The gradual collapse of this structure surface towards the reference surface represents the progressive destructuration of the material. An indicative view of the reference surface, structure surface and bubble (yield surface) adopted in the Rouainia and Muir Wood model is presented in Figure 2.19.

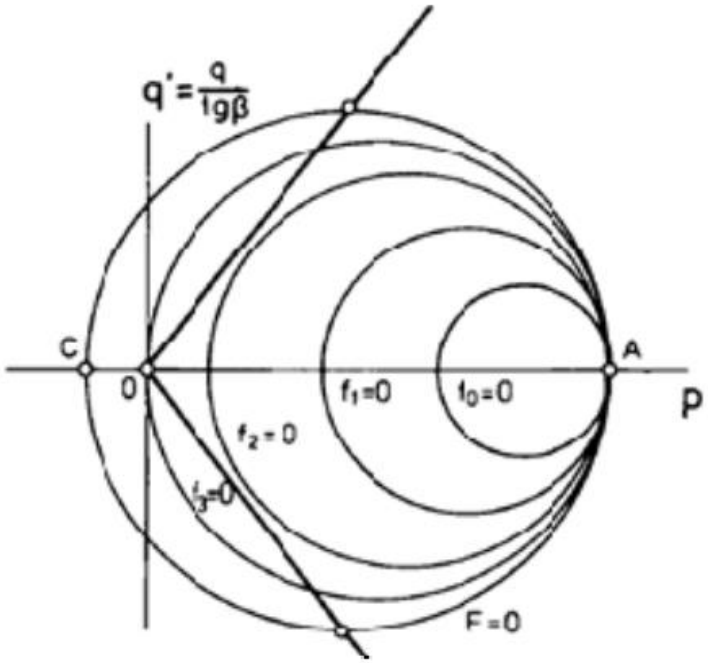

Figure 2.17 Indicative view of the nested surfaces adopted in the Mroz et al. model (after Mroz et al., 1981)

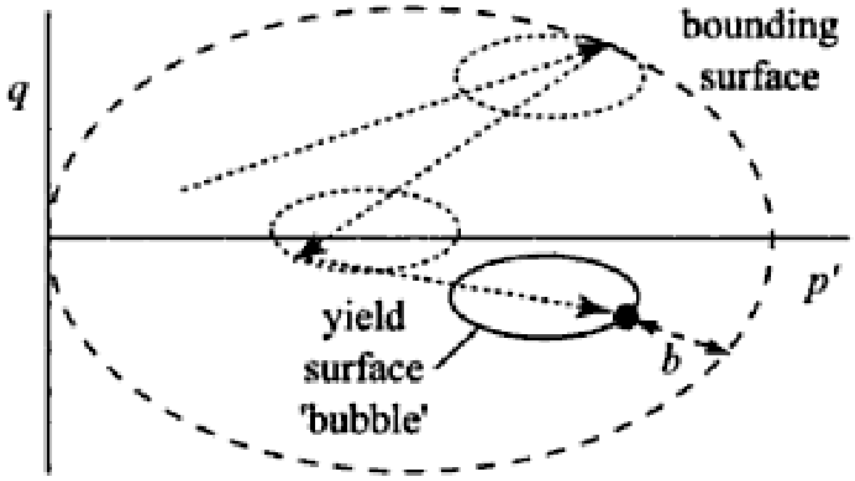

Figure 2.18 Indicative view of outer yield surface and bubble yield surface adopted in the Al-Tabbaa and Muir Wood model (after Al-Tabbaa and Muir Wood, 1989)

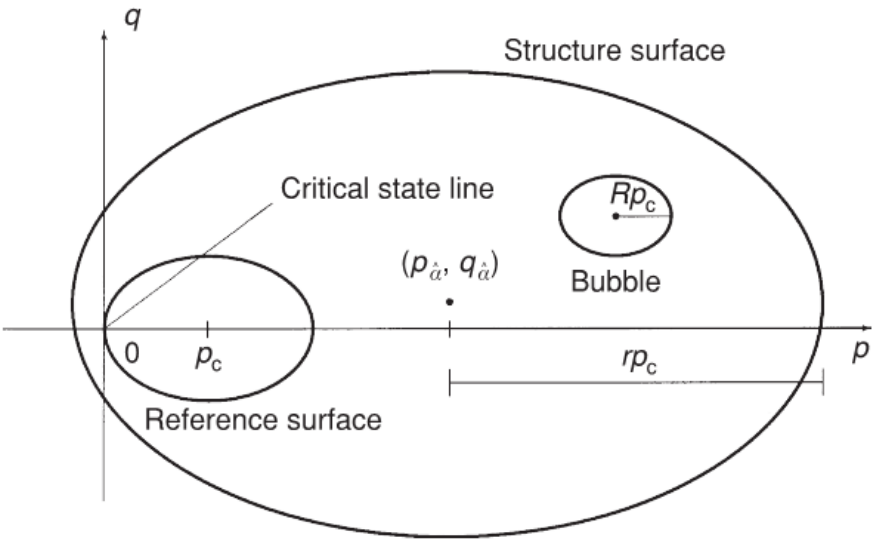

Figure 2.19 Indicative view of reference surface, structure surface and bubble yield surface adopted in the Rouainia and Muir Wood model (after Rouainia and Muir Wood, 2000)

A series of models have focussed on modelling clay strength and stiffness anisotropy.

Dafalias (1986) proposed a model generally based on the Modified Cam Clay model, with a rotated and distorted ellipse yield locus.

The S-CLAY1 model proposed by Wheeler et al. (2003) comprises an inclined yield surface of the same shape as that initially suggested by Dafalias (1986). The rotational law is a function of both plastic volumetric and deviatoric strain increments.

The MIT-S1 model proposed by Pestana and Whittle (1999) features a bounding surface, the orientation of which is related to a hardening rule based on the concept that the principal direction of anisotropy rotates towards the principal stress axes and is a function of both deviatoric and volumetric plastic strain increments.

Although the models mentioned in this section are able to capture a number of features of soil behaviour, they are characterised by relatively complex formulations and numerous input parameters, which would require relatively sophisticated testing data. This poses challenges for the day-to-day use of the models in the current engineering practice. Although the models may give an indication of potential developments and future trends, considering the industrial focus of this work, they have not been analysed in detail.

2.9 Conclusions

A number of elasto-plastic constitutive models have been examined and their key features have been reviewed. The models are available in Plaxis as standard or user defined material models.

Selected aspects of the models have been investigated, following the author's work experience, reviewing the suitability of the models for the assessment of specific geotechnical problems.

The Soft Soil model is based on the Modified Cam Clay framework, combined with Mohr-Coulomb perfectly plasticity.

The Hardening Soil model family (including the small strain and generalised versions) is based on two yield loci, namely a volumetric hardening cap type surface and a deviatoric hardening surface, combined with Mohr-Coulomb perfectly plasticity. The small strain version of the model captures the behaviour of soil at small strains, and the progressive stiffness degradation with increasing strain. The generalised version of the model provides a more general framework, within which different features can be introduced. An aspect of the Generalised Hardening Soil model formulation which is considered in the following chapter, is the stress dependency of the stiffness parameters, based on the mean effective stress p' and the pre-consolidation stress p_c.

The NGI ani2 model is a total stress model, suited for the analysis of stability problems in undrained clays.

The use of some of these constitutive models, in lieu of the popular linear elastic – perfectly plastic (Mohr-Coulomb failure criterion), is explored in the following chapters.

In addition to the constitutive models examined in this chapter, numerous more complex models have been developed in the past decades, generally based on the concepts introduced by the Cam Clay model. Selected examples of these models have been briefly described in the previous sections. The models have not been examined in detail as part of this study, as the review has primarily focussed on models readily available in Plaxis, which may be adopted for routine analyses on industry projects.

CHAPTER 3

SERVICEABILITY PERFORMANCE ASSESSMENT OF AN EXCAVATION IN LONDON CLAY

3.1. Background

This chapter focusses on a 20m deep excavation case study in Central London. The author has been involved in the design and performance assessment of the proposed earth retaining walls and in the evaluation of the ground movements induced by the excavation/construction works.

The following sections provide details of the ground model at the site and the soil strata strength and stiffness parameters, evaluated from a site-specific ground investigation. A series of parametric numerical analyses are then presented, involving different constitutive models for the key strata affecting the excavation behaviour, in terms of retaining wall deflections and ground movements in the zone surrounding the basement. Findings of the various analyses are compared between them and against case histories, in order to highlight the key features of soil behaviour which a constitutive model should capture, for excavation problems in stiff clays.

3.2. Research Objectives

The study presented in this chapter explores the performance of a series of constitutive models in simulating the behaviour of stiff clays in excavation problems. The importance of modelling soil behaviour within the small strain range and the stress and

strain dependency of the material stiffness are highlighted. In particular, the objective of the research is to investigate the use of a version of the Plaxis Generalised Hardening Soil (GHS) model, in which the stress dependency of the stiffness parameters is based on the average mean stress and pre-consolidation stress. The benefits of using this model, in lieu of the traditionally adopted Mohr-Coulomb model or the standard Hardening Soil "Small" (HSS) model, are explored.

3.3. London excavation project

The proposed Central London scheme comprises a new building with seven storeys above ground and a 3-level basement. A reinforced concrete secant pile wall will be installed along the basement perimeter, in order to allow excavation and construction works. The proposed building foundation comprises a reinforced concrete raft. A permanent underdrainage system is proposed, to prevent groundwater uplift pressures from acting at the raft underside.

An indicative view of the proposed excavation cross-section is presented in Figure 3.1.

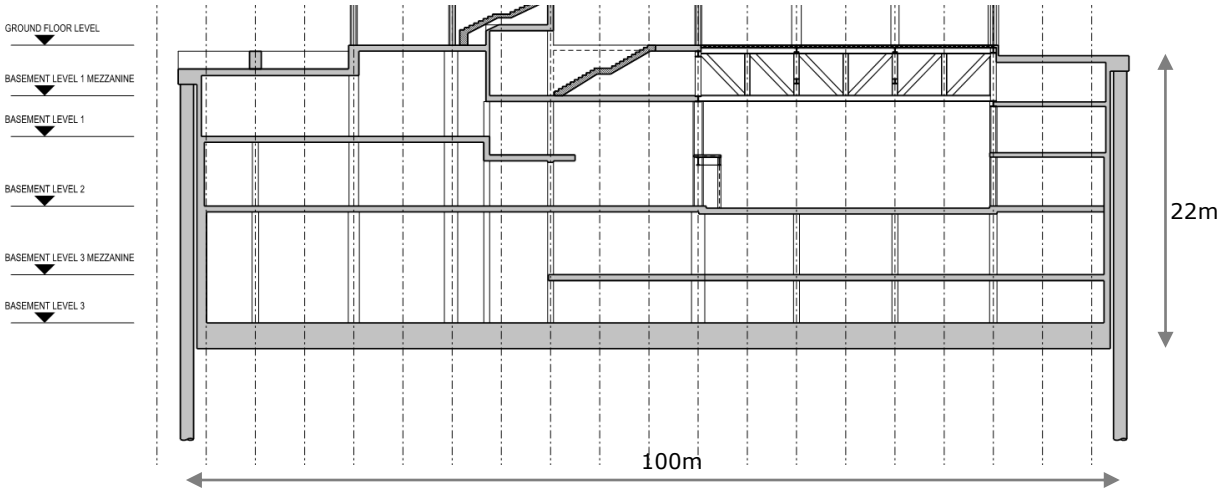

Figure 3.1 Proposed excavation indicative cross-section

The site is bound by a number of public roads along its perimeter and numerous existing buildings are located in relatively close proximity to it, thus the importance of carrying out detailed soil deformation assessment in such congested scenario.

The proposed construction sequence involves a top-down excavation, where permanent reinforced concrete slabs, acting as props for the retaining wall, are sequentially installed prior to excavation below slab level.

This chapter presents assumptions and findings of a number of numerical simulations, carried out to investigate the behaviour of the retaining system and the ground movement distribution in the zone surrounding the site.

The assessment focusses on the end of excavation stage of the proposed works. The analyses have been undertaken using the commercial software Plaxis 2d.

3.4. Ground conditions

A site-specific ground investigation has been carried out by a specialist contractor. The investigation comprised a number of boreholes, in situ and laboratory testing and groundwater monitoring. In situ testing included self-boring pressuremeter testing (SBPT), undertaken at a number of levels within the London Clay and Lambeth Group strata.

The soil stratigraphy reflects the typical geological sequence expected in the central area of London, as reported in Table 3.1. A suitable ground model and set of soil strength and stiffness parameters have been evaluated. The parameters assumed as part of the analyses carried out, are also summarised in Table 3.1.

The Made Ground, River Terrace Deposits and Thanet Sand strata comprise mainly granular material. These strata have been modelled as linear elastic – perfectly plastic materials (Mohr-Coulomb failure criterion) in the Plaxis analyses carried out.

Undrained behaviour has been assumed for the London Clay and Lambeth Group strata during basement excavation and building construction (short term loading/unloading stages).

Linear or non-linear behaviour has been assumed for the London Clay and Lambeth Group strata, as part of a series of parametric analyses. The non-linear analyses aim at capturing the stress dependent behaviour of these material within the small strain range and the stiffness degradation with strain.

As presented in Chapter 2, the stiffness degradation behaviour is often presented using the mean effective stress (*p'*) to normalise the equivalent undrained Young's Modulus ($E_u=3G$), using the expression $3G/p'$. Self-boring pressuremeter testing curves, showing $3G/p'$ as a function of shear strain (γ), are presented in Figure 3.2, alongside the profile adopted as Plaxis input (red line) for the London Clay and Lambeth Group strata, as part of the study carried out. The stiffness curve adopted (red line) has been calibrated trying to broadly follow the average of the pressuremeter stiffness curves in the strain region between 10^{-4} and 10^{-3} (0.01% and 0.1%), which is of relevance for retaining wall problems (Atkinson, 2000).

Based on the available groundwater monitoring data, a hydrostatic pore water pressure profile, with groundwater table at 19mAOD, has been assumed.

Table 3.1 Ground model and soil parameters

Soil stratum	Elevation of top of stratum (m AOD)	Bulk unit weight, γ_b (kN/m^3)	Undrained shear strength, S_u (kPa)	Angle of shearing resistance, ϕ' (°)	Effective cohesion, c' (kPa)	Drained Young's Modulus, E' (MPa)	Coefficient of earth pressure at rest, K_0
Made Ground	25.9	19	0	23	0	15	0.61
River Terrace Deposits	23.6	20	0	35	0	60	0.43
London Clay	17.6	20	85+8.2z[1]	24	0	68+6.56z[1][2] non-linear[2]	1.2
Lambeth Group	-18.5	20	85+8.2z[1]	24	0	68+6.56z[1][2] non-linear[2]	1.2
Thanet Sands	-35.8	20	0	35	0	375	1
Rigid boundary	-45						

Notes:

[1] z refers to depth below top of London Clay stratum

[2] Linear and non-linear behaviour modelled as part of different parametric Plaxis analyses

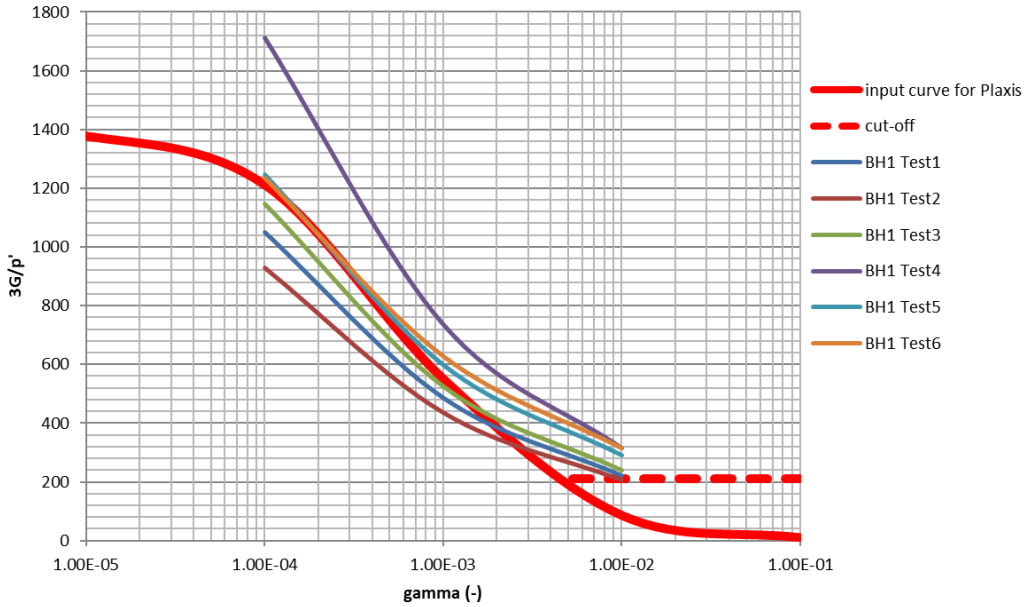

Figure 3.2 Stiffness degradation curves from pressuremeter testing – design profile adopted in Plaxis shown in red

3.5. Finite element analysis

The excavation problem has been modelled by undertaking a plane strain analysis, considering a representative cross-section through the site. Only half of the excavation width has been modelled, taking advantage of the generally symmetric geometry. A view of the Plaxis model is presented in Figure 3.3. The left vertical boundary of the model in Figure 3.3 has been defined at 100m distance from the retaining wall (approximately 4.5 times the excavation depth) in order to ensure that the boundary condition (zero horizontal displacements) does not have an impact on the wall and ground movement predictions (CIRIA C760).

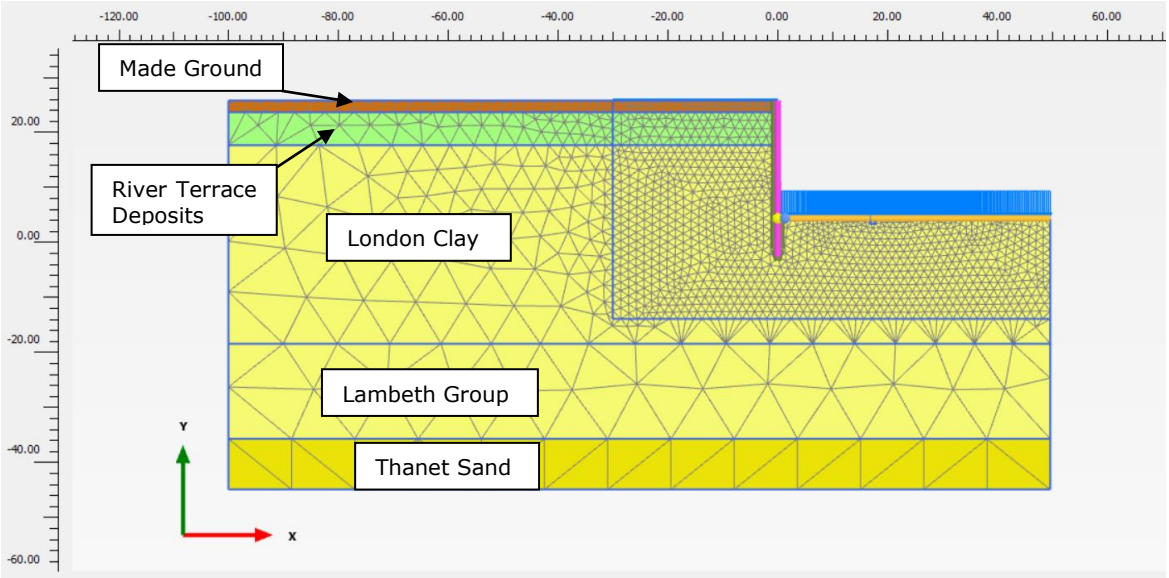

Figure 3.3 View of the Plaxis model

The following idealised construction stages have been modelled, in line with the proposed construction sequence.

1. Stress initialisation.
2. Wall installation (wall wished-into-place, i.e. no installation induced ground movements considered – Figure 3.4 (a)).
3. 10kPa surcharge applied at ground level, on the wall active side, indicatively representing traffic or alternative loading potentially present outside the site footprint.
4. Excavation to 24.15mAOD.
5. Installation of the ground floor reinforced concrete slab.
6. Excavation to 13.97mAOD (Figure 3.4 (b)).
7. Installation of Basement Level 2 and 1 (B2 and B1, respectively) reinforced concrete slabs.
8. Excavation to formation level (4.085mAOD – Figure 3.4 (c)).
9. Construction of 1.75m thick foundation raft (Figure 3.4 (d)).

10. Proposed building loading (uniform load applied at raft level).
11. Consolidation – dissipation of excess pore water pressures in order to achieve long term conditions.

A sketch schematically showing the construction sequence analysed is presented in Figure 3.4.

The proposed raft foundation scheme includes a permanent underdrainage system installed beneath the raft foundation. The system comprises a layer of compacted granular material, with slotted drainage pipes buried in it, leading to sump pits where groundwater is collected to be pumped away.

The presence of the underdrainage system influences the pore water pressure distribution in the soil volume surrounding the basement. The long term pore water pressure field modelled, considers the steady state seepage induced by the presence of the underdrainage system. A plot showing the long term groundwater head distribution is presented in Figure 3.5.

A series of assumptions have been made with regards to properties of the structural elements modelled. The slabs (acting as permanent props) have been modelled as springs, with stiffness values of 39,000 kN/m/m, 500 kN/m/m and 137,000kN/m/m for the ground floor, basement B1 and basement B2 slabs, respectively, based on the specific geometry and arrangement of these slabs.

Piled walls have been modelled using linear elastic plate elements, with a Young's Modulus of 19.6GPa (70% of 28GPa, as per CIRIA C760 guidance). A Young's Modulus of 28GPa has been used to model the 1.75m thick raft.

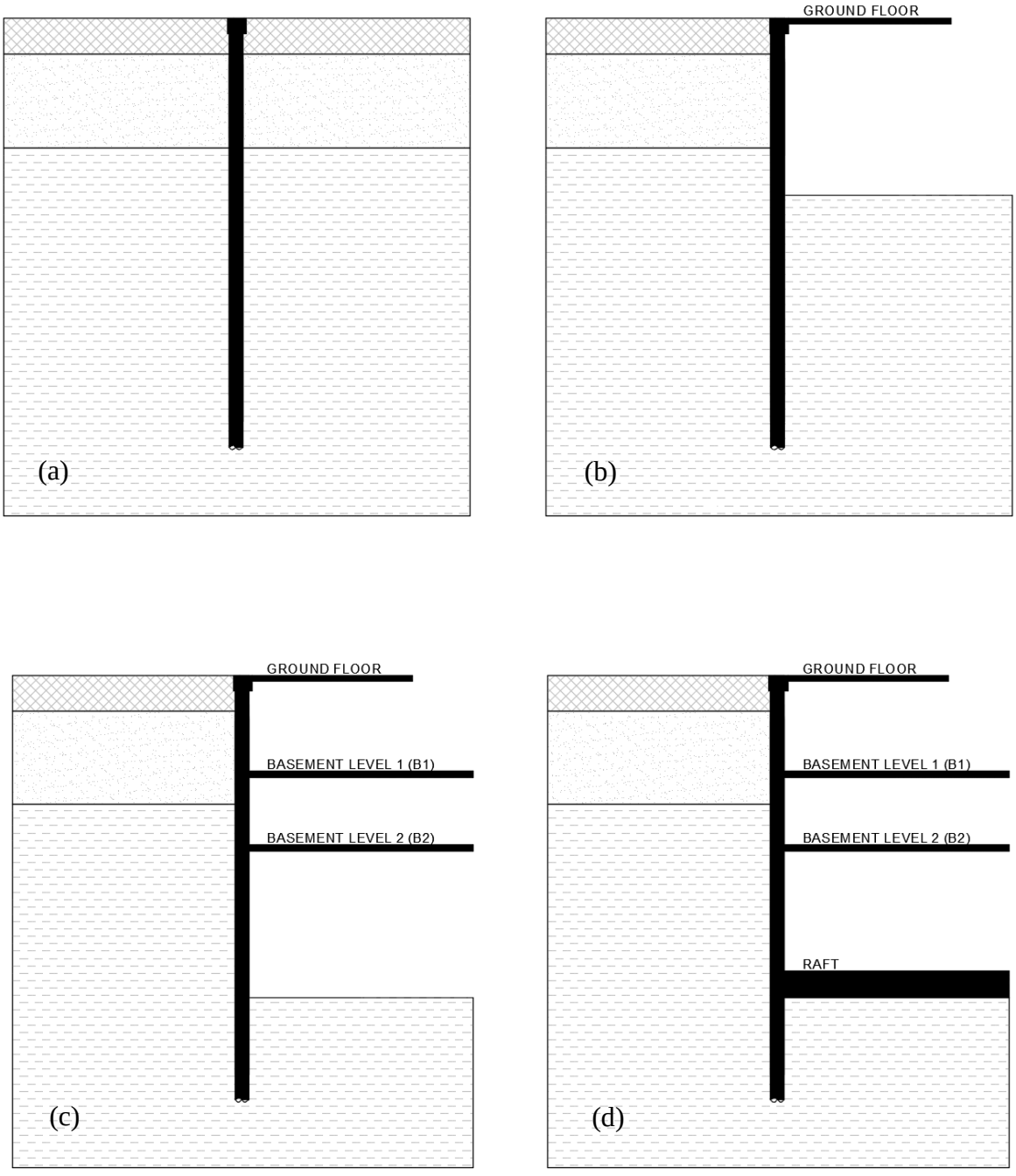

Figure 3.4 Sketches illustrating the proposed excavation/construction sequence

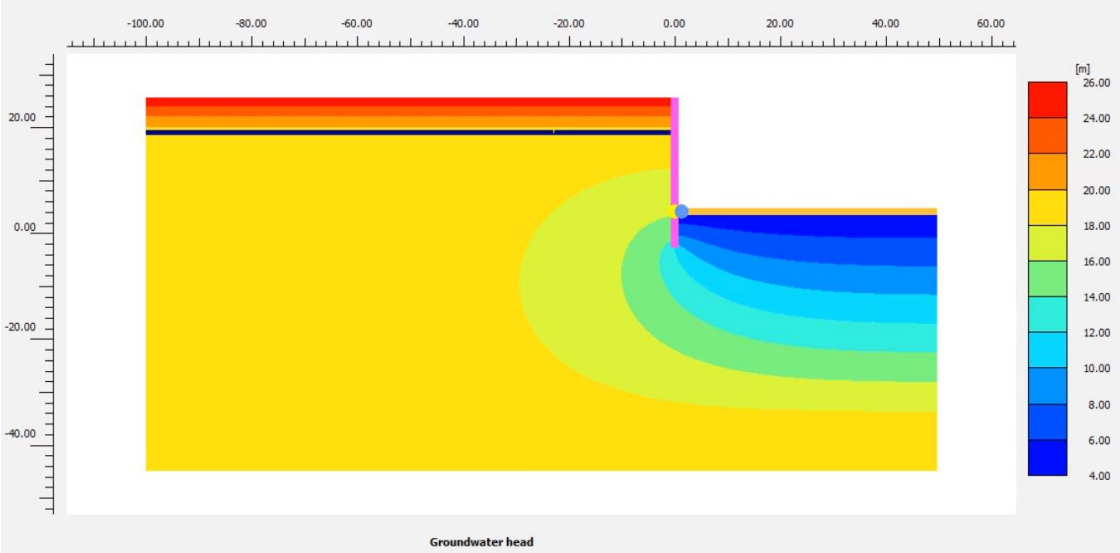

Figure 3.5 Long term groundwater head field indicating a steady state seepage condition induced by the presence of a raft underdrainage system

3.5.1 Mesh refinement sensitivity

The model mesh adopted for the analyses presented in the following sections comprises approximately 4,400, 15-node triangular elements. A relatively coarse mesh has been adopted in the left and lower zones of the model shown in Figure 3.3, while a much finer mesh has been adopted in proximity of the retaining wall and excavation base.

A sensitivity study has been undertaken, in order to establish the impact of the mesh refinement on the ground movements and wall performance evaluated. Numerous models have been analysed, varying the number of elements between approximately 300 and 10,000. Figure 3.6 shows example of the mesh refinements considered, with 310 and 4,400 elements.

The findings of the sensitivity study are indicatively presented in Figure 3.7, where the maximum wall horizontal deflection is shown as a function of the number of mesh elements considered. The maximum wall deflections are expressed as percentage of the value estimated using a very fine mesh (10,000 elements).

Approximately 5% lower wall deflections are evaluated with a very coarse mesh (approximately 300 elements), compared with a refined mesh, comprising in excess of 4,000 elements.

The maximum wall deflection is very similar (within 0.2%) for meshes with more than approximately 4,000 elements.

As mentioned above, a mesh comprising 4,400 elements has been adopted for the study presented in the following sections. The selection is considered to be a reasonable compromise, considering both accuracy of the output and analysis running time (approximately 15 minutes on a computer with Intel Core i3 2.4GHz processor and 6GB of RAM, using the GHS model).

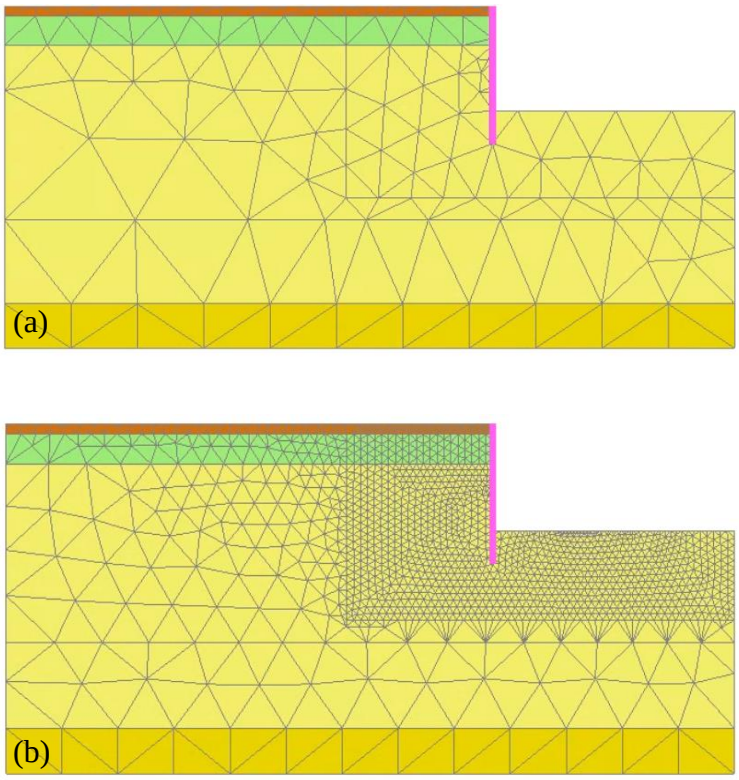

Figure 3.6 Different mesh refinements – 310 elements (a), 4400 elements (b)

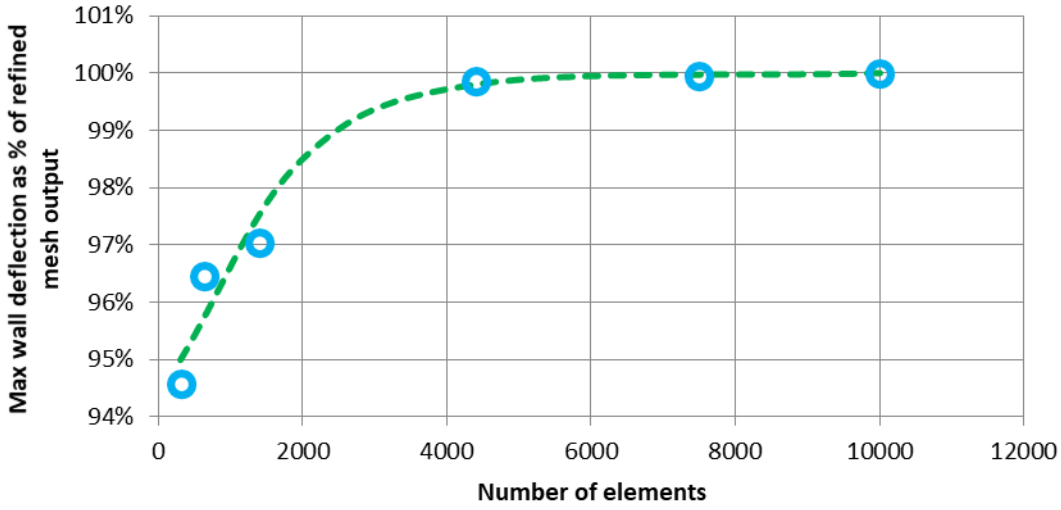

Figure 3.7 Maximum wall deflection (expressed as percentage of the value obtained using a very refined mesh with approximately 10,000 elements) as a function of the total number of mesh elements

3.5.2 Parametric study – clay modelling

A number of parametric analyses have been carried out, varying the constitutive model assumptions adopted for the London Clay and Lambeth Group strata, as follows.

- Scenario A – linear elastic – perfectly plastic behaviour (Mohr-Coulomb model). $E'=0.8E_u$, based on the theory of elasticity, assuming a drained Poisson's Ratio ν' of 0.2. Strength and stiffness parameters adopted for Scenario A are presented in Table 3.1.

- Scenario B – HSS model. Stiffness degradation profile as shown in Figure 3.2.

- Scenario C – GHS model. Stiffness degradation profile as shown in Figure 3.2.

The key input parameters for Scenarios B and C are summarised in Table 3.2 below.

Table 3.2 Stiffness degradation parameters for *Scenarios B* and *C*

	Scenario B (HSS)	Scenario C (GHS)
$G_{0\ ref}$ (MPa)	46,540	23,270
$\gamma_{0.7}$ (-)	0.00025	0.00025
$E_{50\ ref}$ (MPa)	6,000	3,000
$E_{oed\ ref}$ (MPa)	4,000	2,000
$E_{ur\ ref}$ (MPa)	16,800	8,400

Notes:

[1] Reference stress p_{ref} = 100kPa assumed.

Clay stiffness considerations

With regards to calibration of the stiffness parameters adopted as part of the different analysis scenarios, the following considerations can be made:

- Scenario A – The material stiffness has been evaluated based on the empirical relationship $E_u=1000s_u$, as commonly adopted for multi-propped excavations, in the engineering practice (ref. CIRIA C760).
- Scenarios B and C – The adopted strain – stiffness degradation curves have been based on data from self-boring pressuremeter testing, presented in Figure 3.2.

Details of the formulation of the HSS and GHS models are presented in Chapter 2. The key difference between the two models is the stress dependency formulation of the stiffness parameters, which is based on the minimum principal effective stress (σ_3') for the HSS model and on the mean effective stress (p') and pre-consolidation stress (p_c) for the GHS model.

The different formulation has significant consequences on the actual stiffness adopted by the model throughout the excavation unloading stages. In this respect, it is worth

noting the following points, in terms of variation of the key stress parameters during undrained unloading of a stiff over-consolidated clay:

- σ_3' – the minimum principal effective stress is expected to undergo significant variations (reductions) during the undrained unloading associated with the excavation process. This is expected to be of significance in proximity to the retaining wall, and in particular on the passive side, in the excavation base region.

- p' – the mean effective stress is expected to remain broadly constant during the undrained unloading, for stresses remaining within the elastic range.

- p_c – the pre-consolidation stress would also remain constant during the unloading process.

The diagrams in Figure 3.8 show stress paths during an isotropically consolidated (cell pressure 100kPa) undrained triaxial extension test model, assuming linear elastic perfectly plastic (Mohr-Coulomb) behaviour. The stress path is plotted in terms of both principal effective stress, σ_1' vs σ_3', (Figure 3.8a) and in terms of effective isotropic stress versus effective minor principal stress (Figure 3.8b). As discussed above, it is evident that while σ_3' changes considerably, p' remains broadly constant.

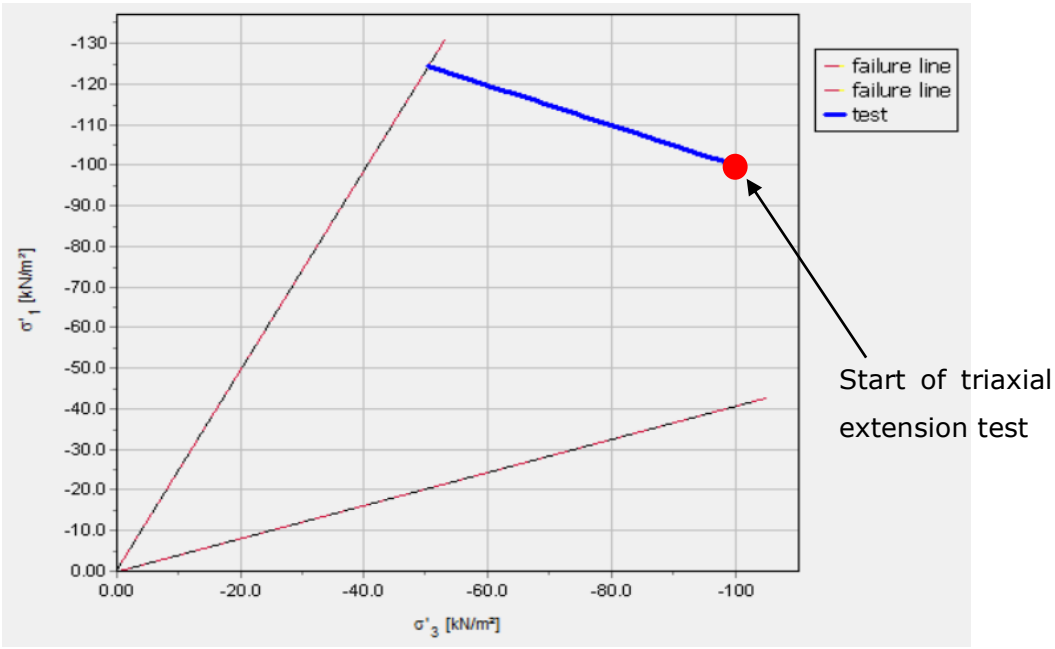

(a)

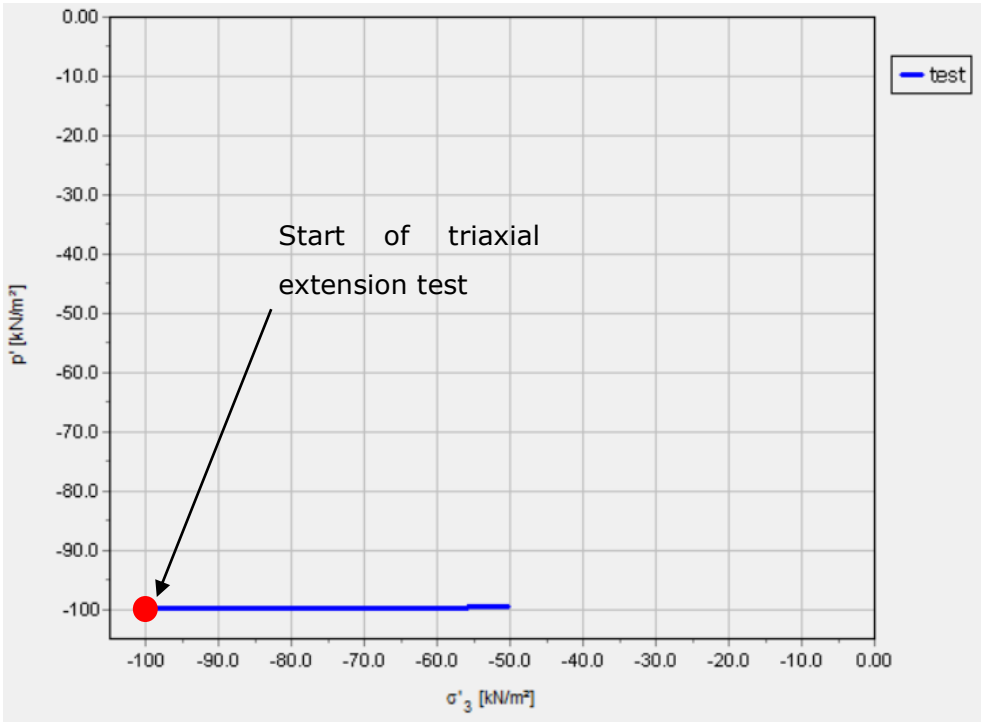

(b)

Figure 3.8 Stress paths from undrained triaxial unloading model showing constant p' (a) and varying σ_3' (b) – negative values refer to compressive stresses

A direct consequence of the reduction in σ_3' is the significant (and relatively uncontrolled) reduction in soil stiffness, when using the HSS model. The reduction in stiffness results in higher retaining wall and ground movements, as shown later by the analyses output.

On the contrary, the broadly constant p' and p_c ensure full control of the stiffness degradation curve, when using the GHS model.

The evolution of clay stiffness (Shear Modulus G) with mobilised strain, at selected points surrounding the retaining wall, has been reviewed in the modelling scenarios involving degradation of stiffness with strain. The points selected are shown in Figure 3.9.

Figure 3.10 to Figure 3.12 provide comparisons between the stiffness evolution in the two models. The Shear Modulus progressively reduces with increasing strains. The diagrams indicate a more pronounced reduction in stiffness of the HSS model, which, as anticipated, is a direct consequence of the reduction in σ_3'.

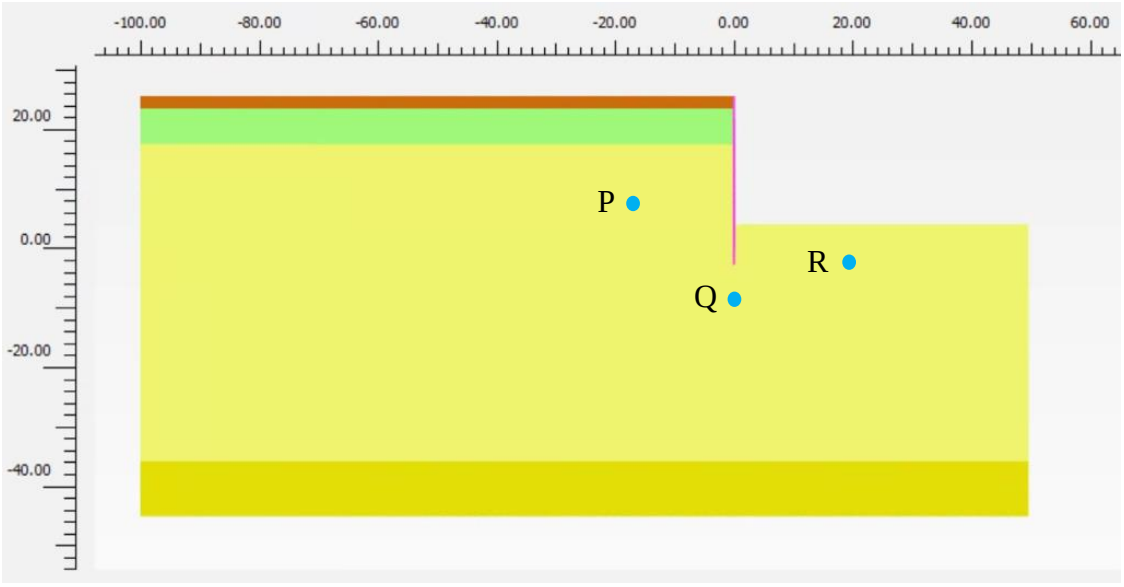

Figure 3.9 Monitoring points for stiffness evolution review

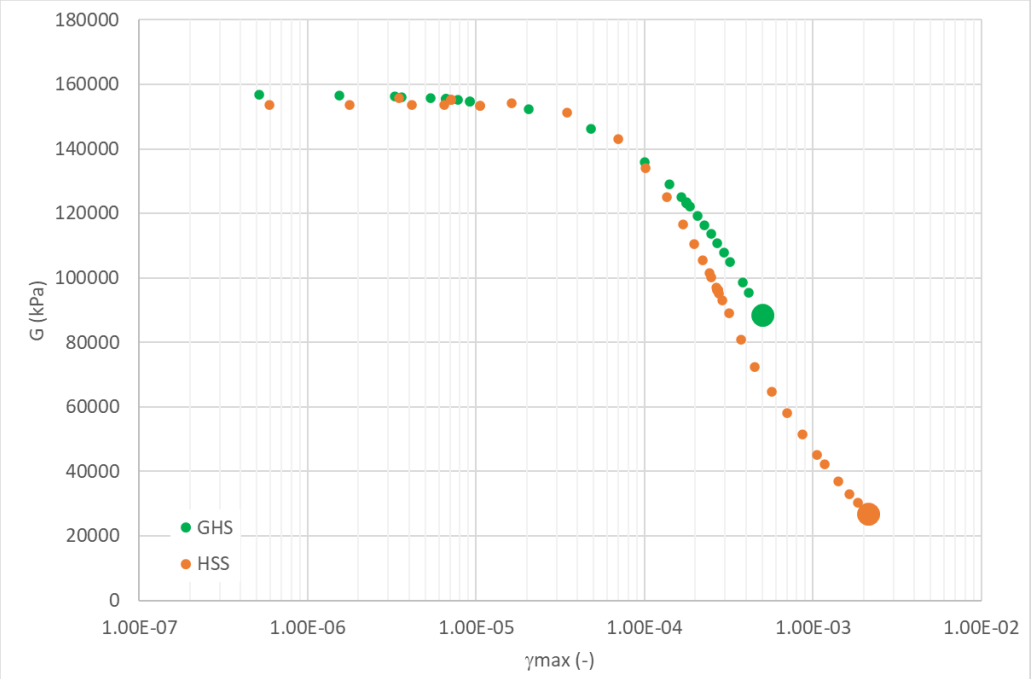

Figure 3.10 Evolution of stiffness (Shear Modulus G) at point P (see Figure 3.9)

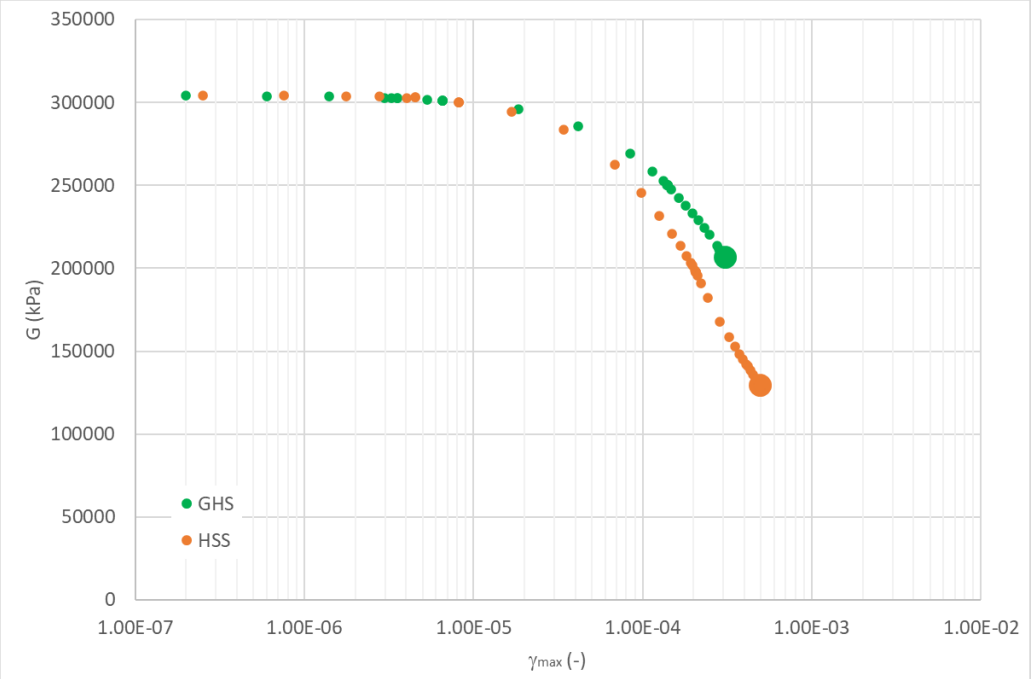

Figure 3.11 Evolution of stiffness (Shear Modulus G) at point Q (see Figure 3.9)

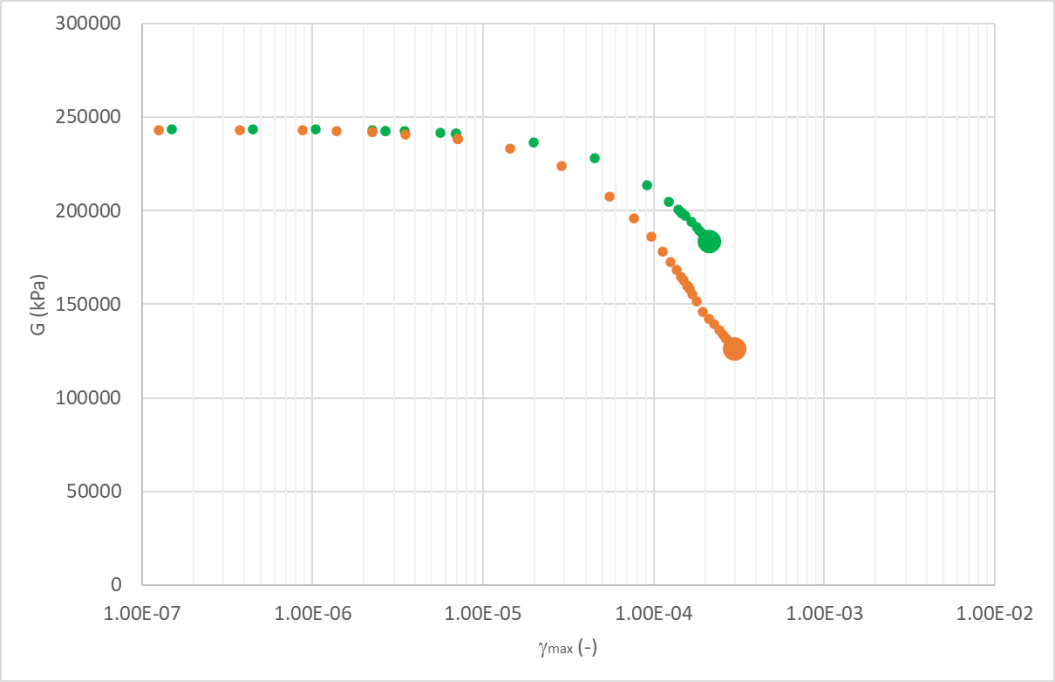

Figure 3.12 Evolution of stiffness (Shear Modulus G) at point R (see Figure 3.9)

Analysis output

Key output of the Plaxis analyses, including vertical and horizontal displacements contour plots, wall horizontal deflections and ground level settlements, are presented in Figure 3.13 to Figure 3.21, for the end of excavation stage.

Figure 3.13 and Figure 3.14 show horizontal displacement contours, respectively, using the Mohr-Coulomb model.

Figure 3.15 and Figure 3.16 show horizontal and vertical displacement contours, respectively, using the HSS model.

Figure 3.17 and Figure 3.18 show horizontal and vertical displacement contours, respectively, using the GHS model.

Ground movement values are presented in metres in all contour plots. Positive u_x (horizontal displacements) values refer to displacements in the left to right direction.

Positive u_y (vertical displacements) values refer to heave displacements. Negative u_y values refer to settlements.

The contour plots indicate maximum ground movements in proximity of the retaining wall, reducing moving away from it. The reduction is relatively gradual in the Mohr-Coulomb model, while a more rapid decrease is observed in the HSS and GHS models, which predict more concentrated displacements in the zone immediately behind the wall, both in the horizontal and the vertical directions.

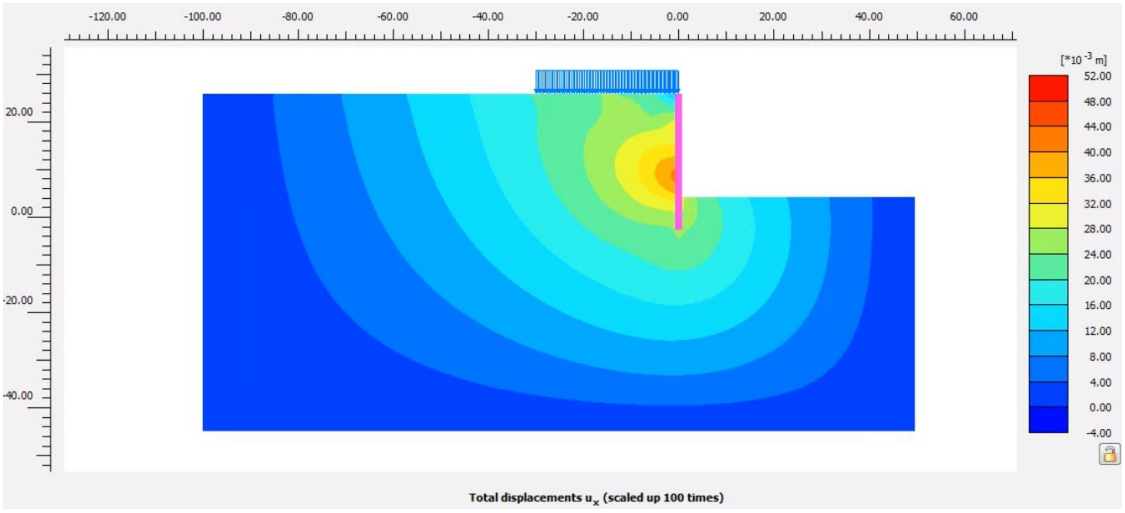

Figure 3.13 Horizontal displacement contours (Mohr-Coulomb model)

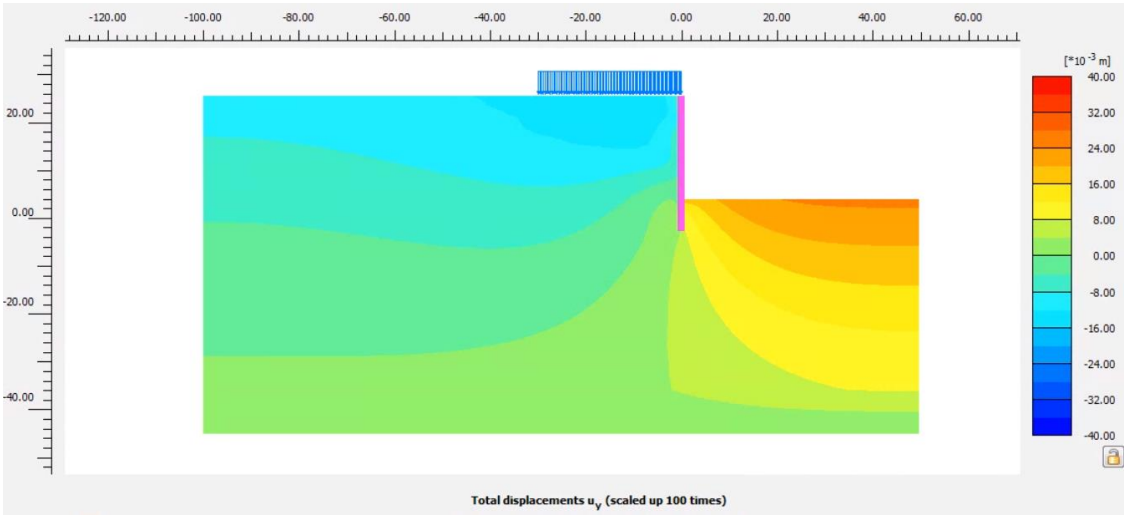

Figure 3.14 Vertical displacement contours (Mohr-Coulomb model)

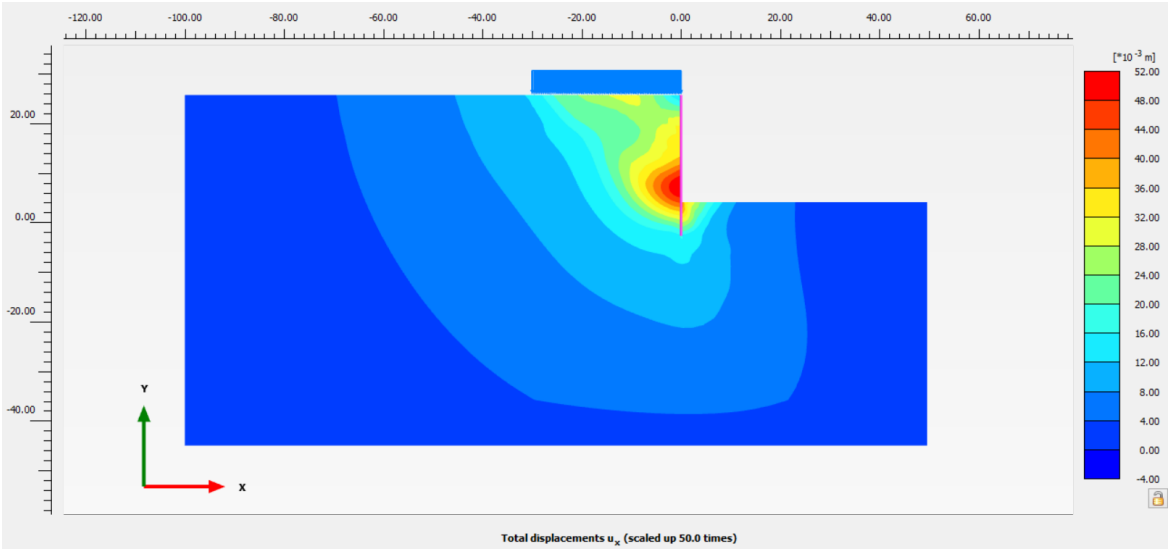

Figure 3.15 Horizontal displacement contours (HSS model)

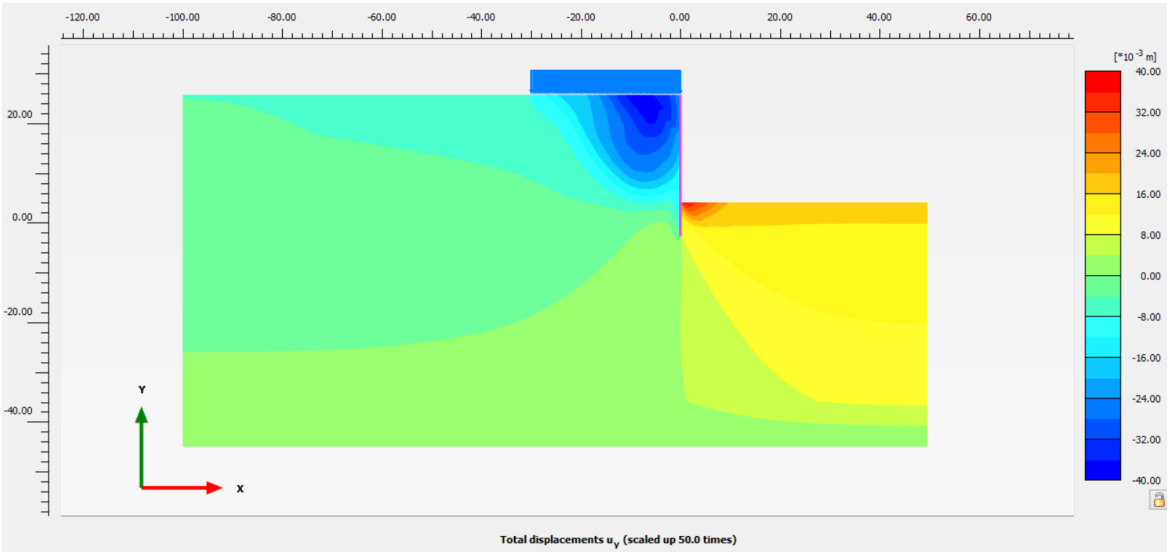

//

Figure 3.16 Vertical displacement contours (HSS model)

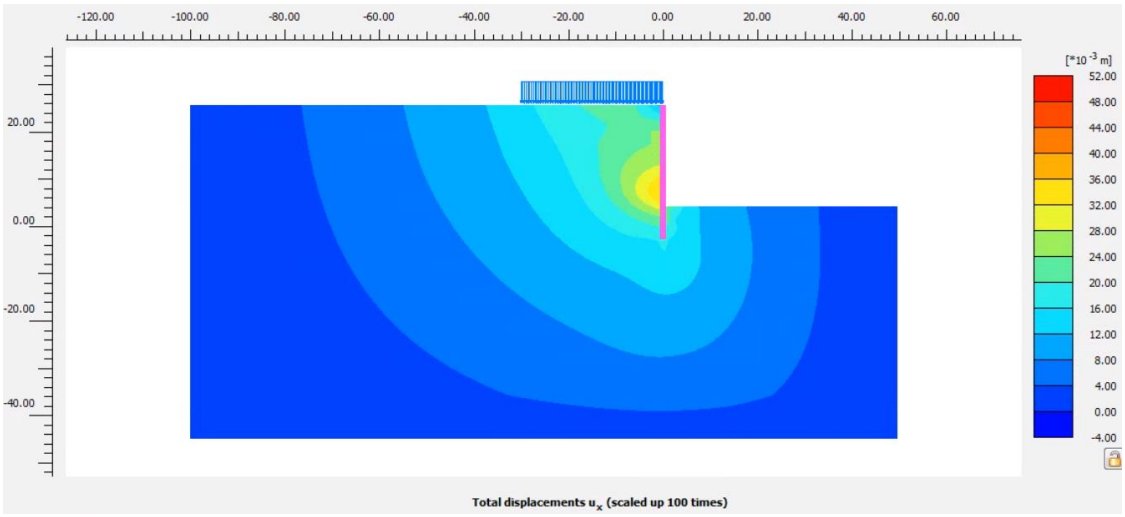

Figure 3.17 Horizontal displacement contours (GHS model)

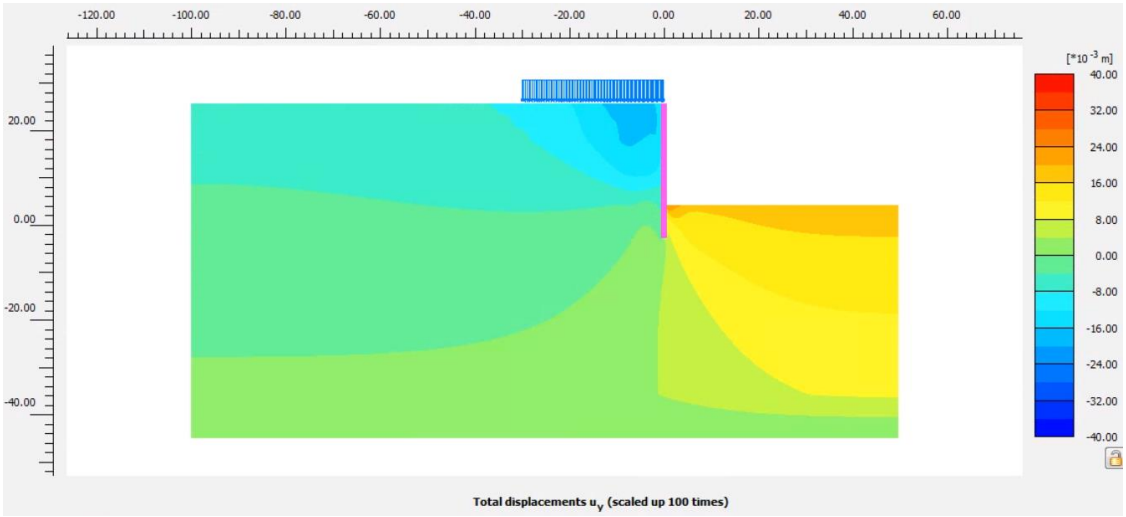

Figure 3.18 Vertical displacement contours (GHS model)

Figure 3.19 shows the wall horizontal deflection profiles for the three analysis cases considered, namely using the Mohr-Coulomb, HSS and GHS models.

Figure 3.20 and Figure 3.21 show curves of horizontal and vertical ground movements (at ground level) at varying distances from the wall. Negative distance values indicate increasing distances from the wall. Positive horizontal ground displacement values refer to movements towards the excavation. Negative vertical ground movements refer to settlements.

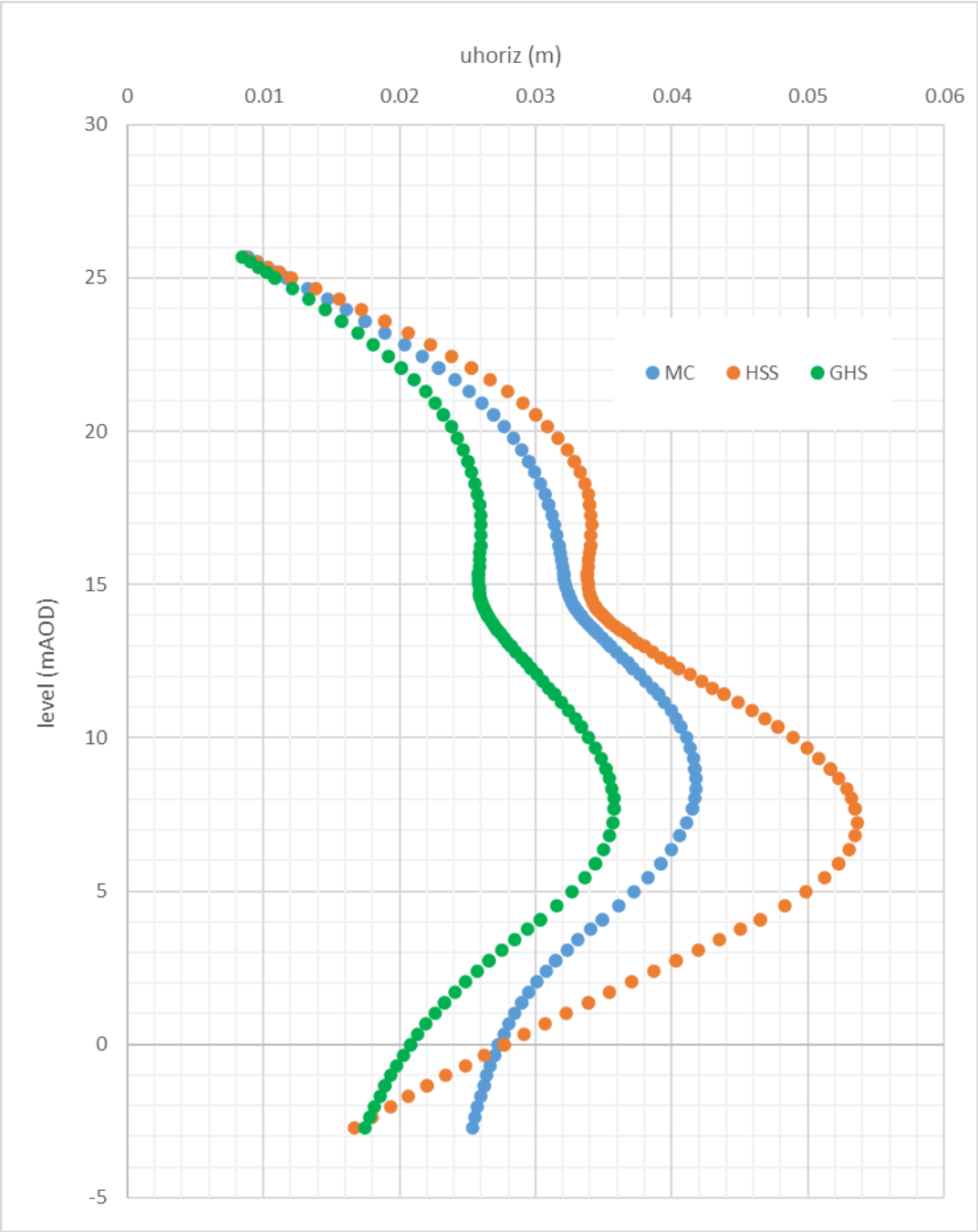

Figure 3.19 Comparison of horizontal wall deflections

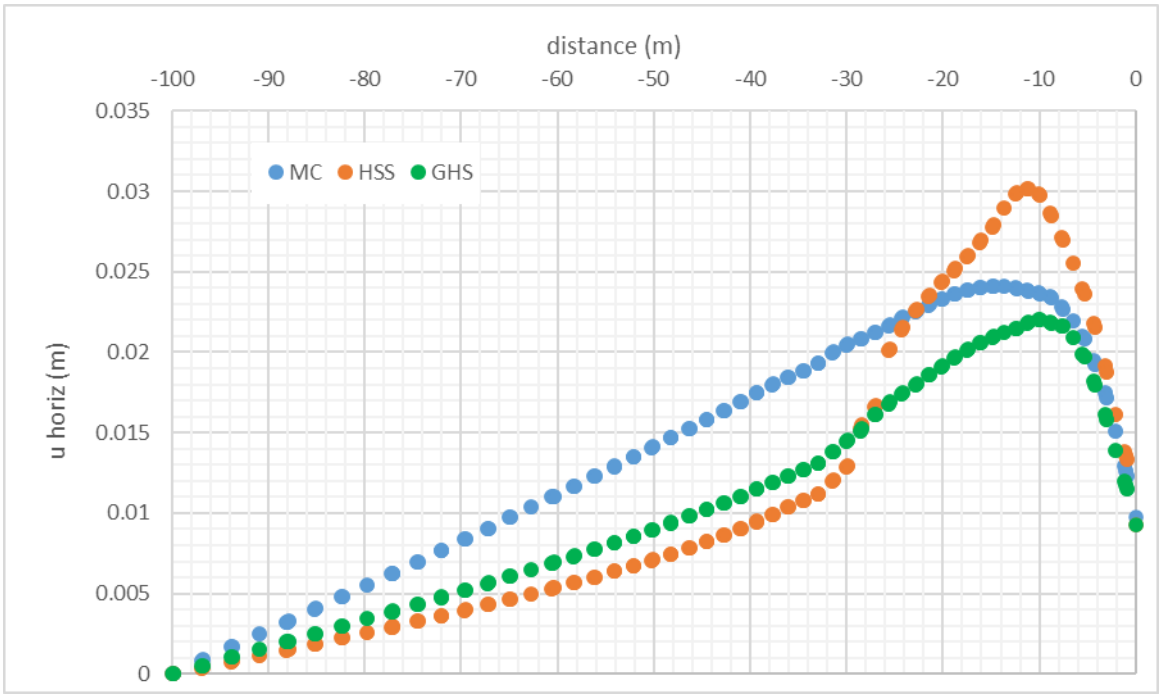

Figure 3.20 Comparison of horizontal ground movements at varying distances from the wall

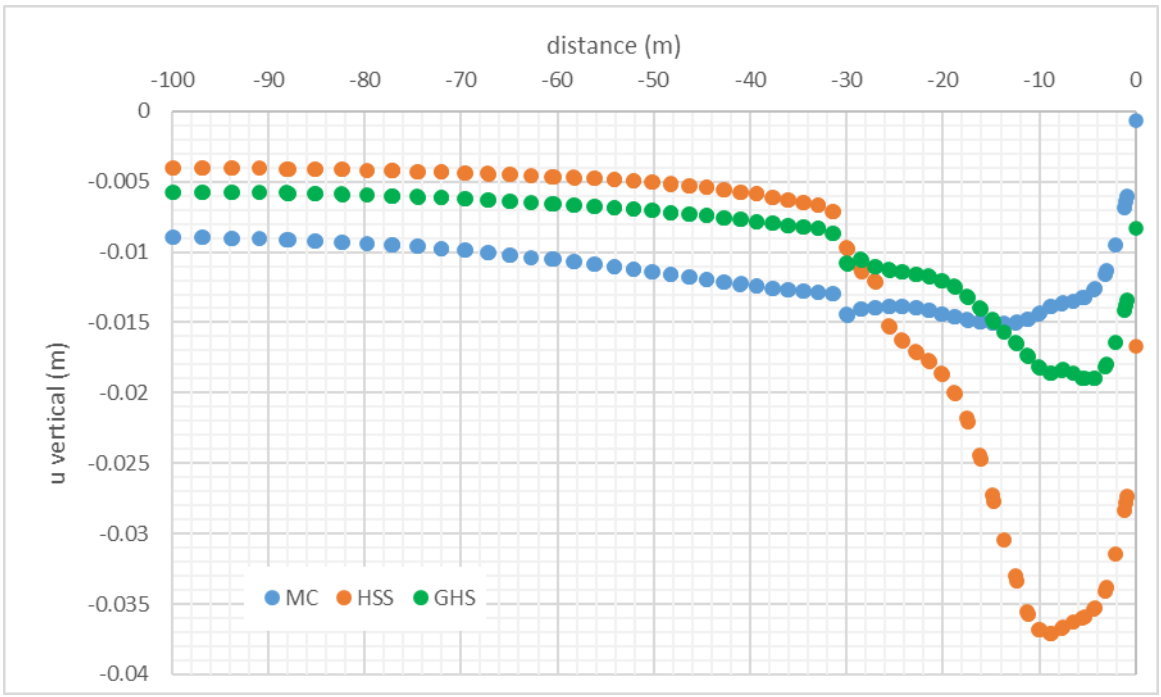

Figure 3.21 Comparison of ground settlements at varying distances from the wall

A comparison of predicted bending moment distributions at the end of the excavation is presented in Figure 3.22.

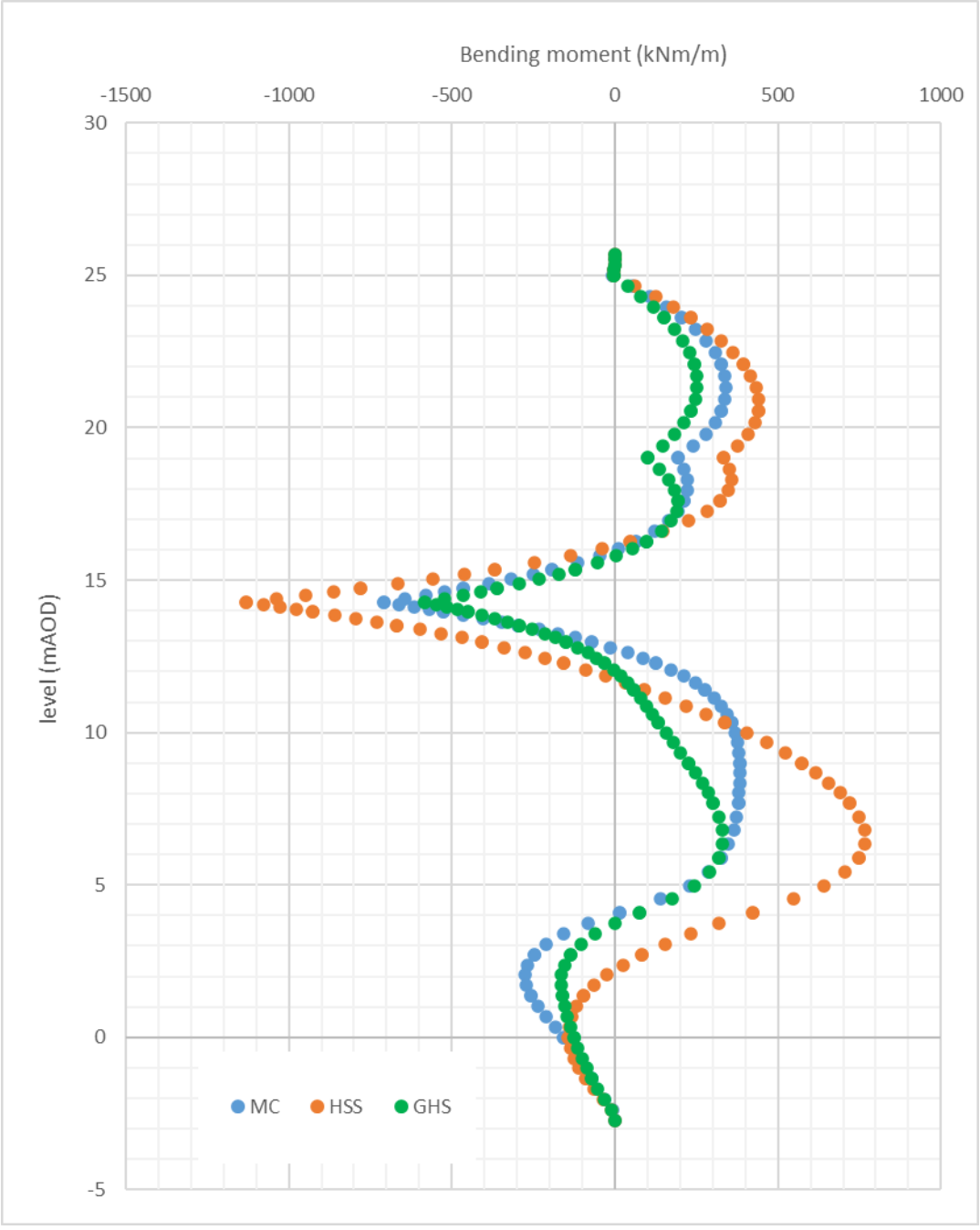

Figure 3.22 Comparison of wall bending moments

Comparing the diagrams presented above, representative of the various analyses carried out, a series of considerations can be made, as follows:

- The Mohr-Coulomb model provides a predicted wall deflection profile broadly in line with the small strain GHS prediction, as indicated in Figure 3.19. The Mohr-Coulomb model tends to over predict the wall deflections in the wall toe region, compared to the GHS model.

- As shown in Figure 3.19, the wall deflections predicted by the HSS model are larger than the other two models. This is a consequence of the model's stiffness formulation, which is significantly affected by the variations in the minimum principal effective stress (σ_3').

- Compared to the HSS and GHS models, the Mohr-Coulomb model appears to predict relatively uniform settlements in the zone behind the retaining wall, extending to a great distance from the wall, as shown in Figure 3.21. On the contrary, the small strain models predict more pronounced settlements in the zone immediately behind the wall, with a relatively rapid reduction moving away from the wall. In line with the wall deflections pattern, the HSS model settlements are greater than the other two models.

  The uniform nature of the predicted settlements from the Mohr-Coulomb model results in limited differential settlements in the zone behind the retaining wall (see Figure 3.21) and would therefore potentially underestimate the impact/damage induced to any building or utility/element of infrastructure, present in the area surrounding the site.

- With regards to horizontal ground movements at ground level (see Figure 3.20), the models show an increase in displacements in the zone from 0 to approximately 10m distance from the wall, as a result of the early installation of the ground level slab/prop. Beyond this zone, the Mohr-Coulomb model shows a uniform reduction of horizontal movements moving away from the wall, while the HSS and GHS models indicate a

more rapid reduction of horizontal ground movements in the zone between 10m and 30m away from the wall, and a gentler reduction beyond 30m.

The rapid reduction in horizontal movements in the 10m to 30m zone predicted by the small strain models (HSS and GHS) results in higher ground tensile strains and, in turn, in more onerous impact/damage to any building or utility/element of infrastructure, located in this zone, oriented in a direction perpendicular to the basement wall (in plan). The opposite (i.e. more onerous conditions predicted using the Mohr-Coulomb model) would apply for the zone beyond 30m distance from the wall.

- In terms of wall bending moments, significantly higher values are predicted by the HSS model, compared to both the GHS and Mohr-Coulomb models. The profile predicted by the GHS model shows values slightly lower than the Mohr-Coulomb ones, indicating that an optimised wall structural design would be possible using the GHS model.

3.5.3 Comparison with CIRIA C760 case histories

In the absence of site-specific displacement monitoring data, the predicted wall and ground movements of the selected case study have been compared with several case histories of excavations in similar ground conditions, presented in CIRIA C760.

The CIRIA C760 data sets are based on data collated from Clough and O'Rourke (1990), Carder (1995) and Carder et al (1997), for surface movements arising from excavation in front of bored pile, diaphragm and sheet pile walls embedded in stiff clays.

The CIRIA C760 data is presented in terms of the high and low support stiffness categories, as defined by Carder (1995). High stiffness systems refer to top-down construction, or schemes with temporary props installed before permanent props at high level. Low stiffness systems refer to cantilever walls, or walls with temporary props of low stiffness or installed at low level.

The diagrams in Figure 3.24 and Figure 3.25 show a superposition of the ground movement curves estimated as part of the numerical simulations carried out and the CIRIA C760 case histories data. The graphs present horizontal (Figure 3.24) or vertical (Figure 3.25) ground movements shown as a percentage of the maximum excavation depth, against horizontal distance from the wall, normalised with the excavation depth (distance from the wall and maximum excavation depth are shown in Figure 3.23).

The reader should refer to CIRIA C760 Appendix A6 for details in relation to the individual cases histories included.

The following considerations can be made:

- The Mohr-Coulomb model output indicates relatively large ground movements, both horizontal and vertical, at significant distances from the wall, compared to the CIRIA C760 case histories. This is particularly evident for the settlement profile (Figure 3.25), which shows predictions well in excess of the monitoring data at distances beyond the excavation depth ($d/H>1$, where d is the horizontal distance from the wall and H is the excavation depth). As previously mentioned, this may result in underprediction of the differential settlements, and associated impact/damage, induced to any building or utility/element of infrastructure, present in the area surrounding the site.

- The HSS model curves indicate larger ground movements in proximity to the wall, particularly in the region $0<d/H<1$, compared to the high stiffness case histories data. This is particularly evident for the settlement profile (Figure 3.25). This would likely result in significantly onerous prediction of impact to any building or utility/element of infrastructure present in close proximity to the site, particularly if oriented in a direction perpendicular to the basement wall (in plan).

- As previously mentioned, the GHS model predictions indicate lower settlements at a significant distance from the wall, compared to the Mohr-

Coulomb output. The GHS data also shows lower ground movements (both horizontal and vertical) compared to the HSS model output, in close proximity to the wall ($0<d/H<1$). When compared to the CIRIA C760 data, the GHS predictions appear to provide slightly conservative predictions, reasonably close the high stiffness wall data (see CIRIA C760 Appendix A6 for details of the individual case histories – the proposed scheme and top-down construction sequence falls within the high stiffness walls category, as defined by Carder, 1995).

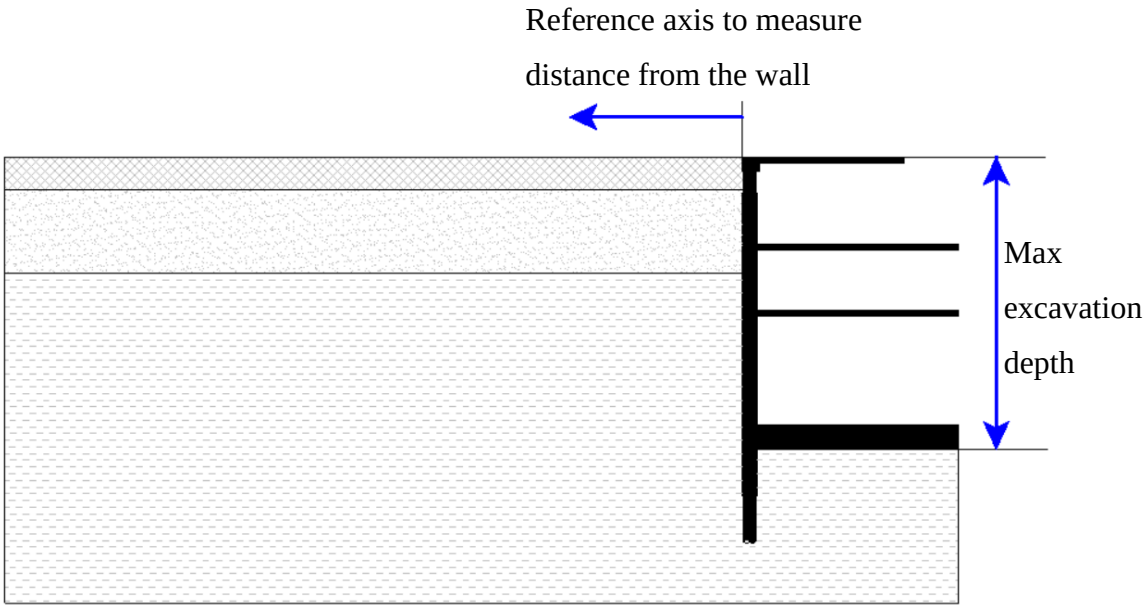

Figure 3.23 Definition of Maximum excavation depth and Distance from the wall

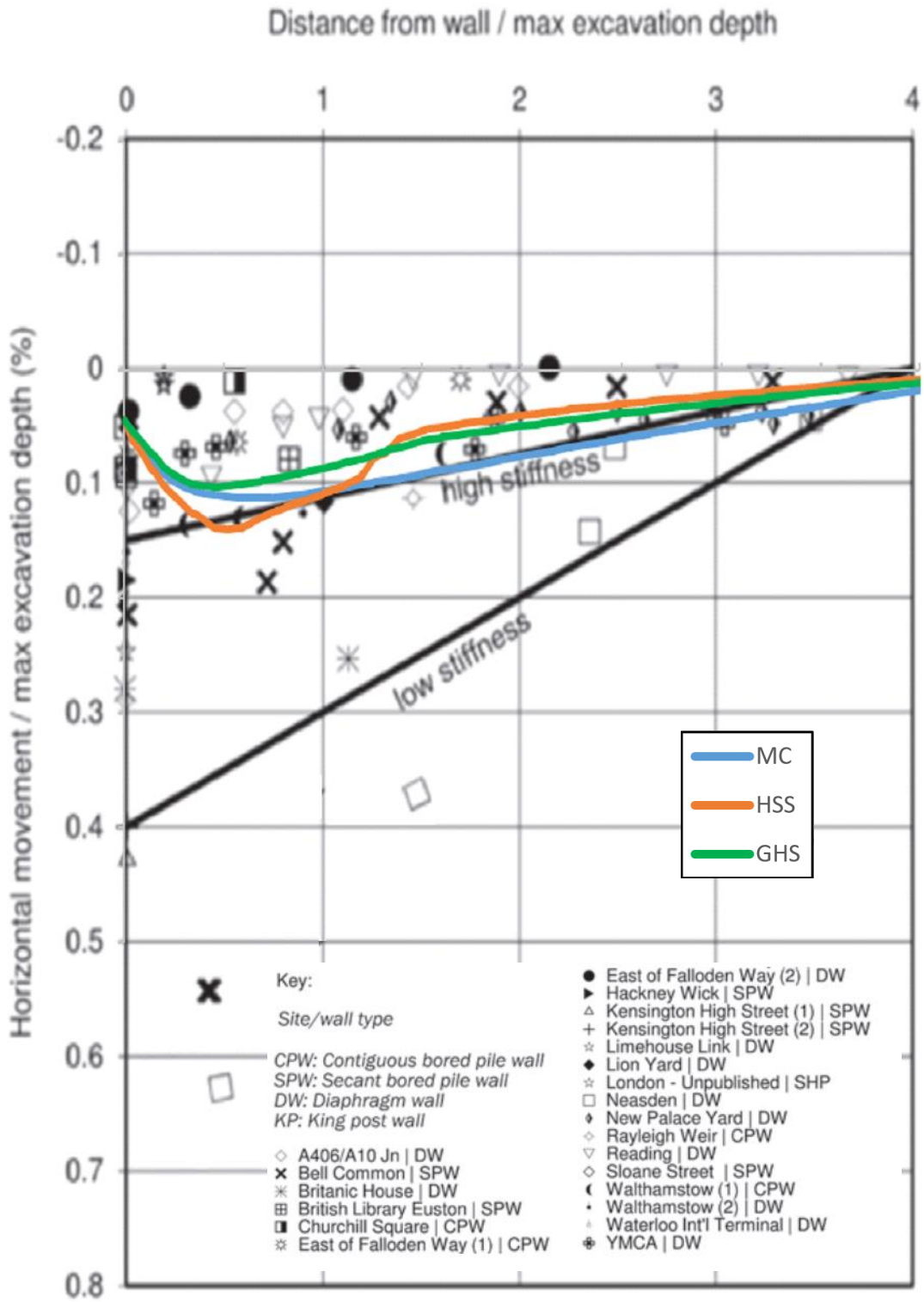

Figure 3.24 Normalised horizontal ground movements at varying normalised distances from the wall (comparison with CIRIA C760 case histories)

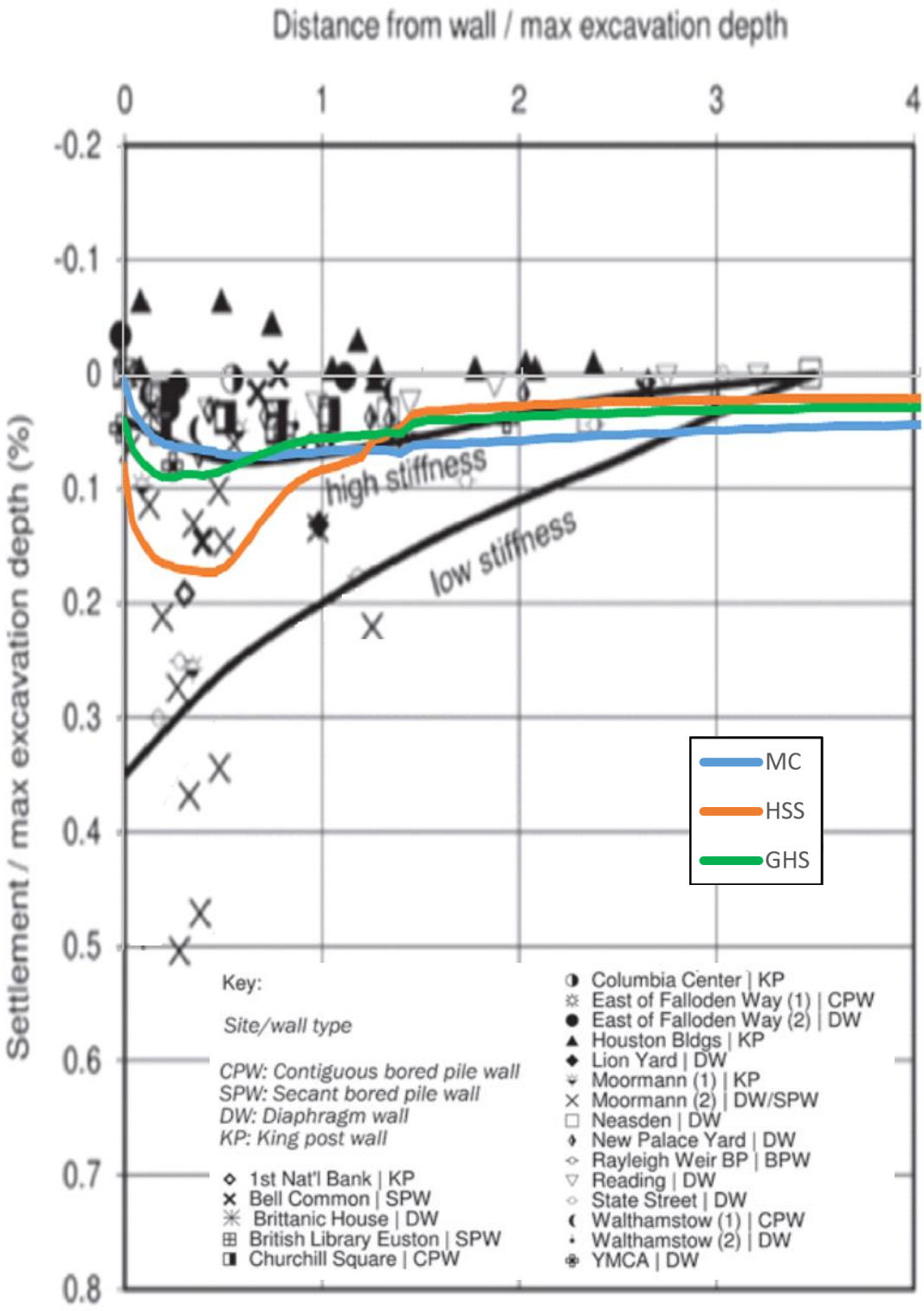

Figure 3.25 Normalised settlements at varying normalised distances from the wall (comparison with CIRIA C760 case histories)

3.5.4 Summary of findings

Based on the findings presented in the previous sections, comparing analyses using different constitutive models with case histories from excavations in similar ground conditions, it is concluded that, although the commonly adopted Mohr-Coulomb model may provide a relatively reasonable prediction of wall deflections, it is considered inadequate for the prediction of ground movements in the zone surrounding the excavation. The use of a model able to capture the progressive stiffness degradation behaviour with increasing strains is considered essential for this purpose.

However, it is important to note that the Plaxis readily available HSS model may result in relatively poor ground movement predictions, in view of the particular stress dependency formulation of the stiffness parameters. The ground movements predicted using the HSS model would likely result in an overestimation of the impact/damage to any building or utility/element of infrastructure present in close proximity to the site, particularly if oriented in a direction perpendicular to the basement wall (in plan).

The findings indicate that the use of a model in which the stiffness is controlled by the mean effective stress (p') and the pre-consolidation stress (p_c) would provide more reasonable wall and ground movements predictions.

In view of the above considerations, it is concluded that the GHS model provides better ground movement predictions than the Mohr-Coulomb and HSS models. The GHS output appears slightly conservative, when compared to the CIRIA C760 data, and is considered suitable to inform impact assessments for third party assets located in proximity to the excavation.

3.6. Conclusions

A Central London excavation case history has been considered. The project comprises a new 7-storey building with a 3-level basement.

A reinforced concrete secant pile wall will be installed along the basement perimeter and the excavation works will be undertaken in a top-down sequence.

The ground conditions at the site comprise the typical Central London strata sequence, including Made Ground, River Terrace Deposits, London Clay, Lambeth Group, Thanet Sand and Chalk. A site-specific ground investigation has been carried out at the site, including self-boring pressuremeter testing of the London Clay and Lambeth Group strata.

A series of plane strain analyses have been carried out, using Plaxis 2d, in order to evaluate the ground movement field likely to arise as a result of the proposed works. A number of constitutive models have been adopted to simulate the behaviour of the London Clay and Lambeth Group strata, including the widely adopted linear elastic – perfectly plastic Mohr Coulomb model and non-linear models (HSS and GHS) capturing stress and strain dependency of the material stiffness.

The aim of the research is to compare the performance of the various constitutive models examined, with a view of investigating the viability of the non-linear models as a day-to-day tool, in alternative to the standard Mohr Coulomb model, which is still commonly adopted by a large section of the industry for the analysis of deep excavations in London Clay.

Comparisons between the different analyses have focussed on the retaining wall deflections and ground movement field in the zone immediately surrounding the excavation. Key output plots from the Plaxis analyses are presented in Figure 3.13 to Figure 3.21, for the end of excavation stage.

In addition, comparisons of predicted ground movement profiles (at ground level) against a number of case histories from CIRIA C760, have been presented.

Although the commonly adopted Mohr-Coulomb model may provide a reasonable prediction of wall deflections, it is considered inadequate for the prediction of ground movements in the zone surrounding the excavation. The use of a model capturing the progressive stiffness degradation behaviour with increasing strains is considered essential for this purpose. However, it is important to note that the Plaxis readily available HSS model may result in relatively poor ground movement predictions in view of the particular stress dependency formulation of the stiffness parameters. The findings indicate that the use of a model in which the stiffness is controlled by the

mean effective stress (p') and the pre-consolidation stress (p_c) would provide more reasonable results in terms of both wall deflections and overall ground movements.

CHAPTER 4

THREE DIMENSIONAL ASSESSMENT OF AN EXCAVATION IN LONDON CLAY

4.1 Background

In the majority of instances, the design of retaining wall systems is undertaken by means of two dimensional plane strain analysis. This simplifying assumption neglects many of the geometrical and stress field distribution effects associated with the three dimensional shape of the excavation, which may have a significant influence on excavation and earth retention system behaviour. This chapter summarises current industry practice and explores the use of three dimensional numerical modelling simulation in the field of soil-structure interaction. A number of analytical techniques are presented, which have been implemented across a selection of excavation case study examples using three dimensional numerical modelling simulation. The study reveals the significance of a series of mechanisms (including soil arching effects, prop load paths, etc) associated with three dimensional effects in excavations.

Opportunities for retention system design optimisation using three dimensional soil-structure interaction analyses are presented, together with an insight into potential construction related savings and efficiencies. These opportunities include reduction in retaining wall reinforcement or bending moment capacity requirements, reduction in wall embedment requirements and retention system propping/bracing optimisation. The impact of actual construction sequence, in contrast with simplified analytical and simulation assumptions which are frequently adopted, is reviewed in light of data arising from instrumented case studies in the field. The advantages of implementing more representative three dimensional analytical techniques are discussed, alongside common modelling pitfalls. The chapter emphasises the importance of adopting an integrated

geotechnical and structural engineering approach when undertaking earth retention system design.

A 20m deep excavation case study in London Clay (the same analysed in the previous chapter) is considered. Direct comparison between output of two and three dimensional analyses is presented, in order to highlight the influence of three dimensional mechanisms on the retaining system behaviour. For details of the project, construction sequence, ground model at the site and the strata strength and stiffness parameters, the reader should refer to Chapter 3.

4.2 Research objectives

The three dimensional approach allows the consideration of specific soil-structure interaction mechanisms (for example soil arching effects in proximity of excavation corners, propping load paths associated with variable ground levels or uneven excavation sequences) which are ignored in plane strain analyses, commonly adopted in the design practice.

This chapter explores the benefits of three dimensional analysis and the potential value engineering opportunities which can be introduced in retaining wall design and assessment. A corner optimisation strategy is investigated, whereby the wall design is carried out considering different wall zones, at varying distance from excavation corners.

4.3 Three dimensional effects for excavations

Traditionally, excavations have been analysed as plane strain problems, considering a cross-section perpendicular to the retaining wall, for the design of the earth retaining system and for the assessment of wall and ground displacements.

In reality, in many cases, the excavation geometry is such that the plane strain assumption is not strictly applicable, and the performance of retaining systems is strongly affected by the excavation spatial layout.

The impact of excavation corners on the stress distribution in their proximity is indicatively illustrated in Figure 4.1. The horizontal cross-section diagram shows the distribution of principal stresses within the soil behind an excavation corner. The segments directions indicate the principal stresses orientations, and their sizes are indicative of the stress magnitude. The distribution shows a stress arching effect behind the excavation corner, with principal stress components oriented to form an arch-shaped pattern, as highlighted by the yellow arrows.

The mechanism results in a reduction in horizontal earth pressures acting on the retaining wall, moving towards the excavation corner, as indicatively shown by the stress contours in Figure 4.2, in which contours of normal stresses in the horizontal x and y directions are shown.

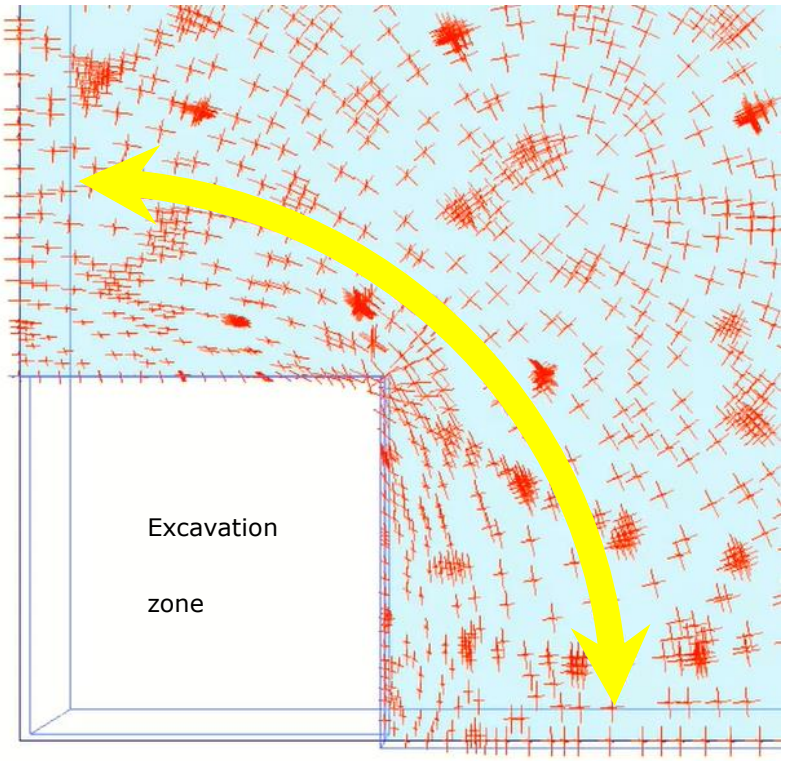

Figure 4.1 Horizontal cross-section showing the distribution of principal stresses within the ground behind an excavation corner

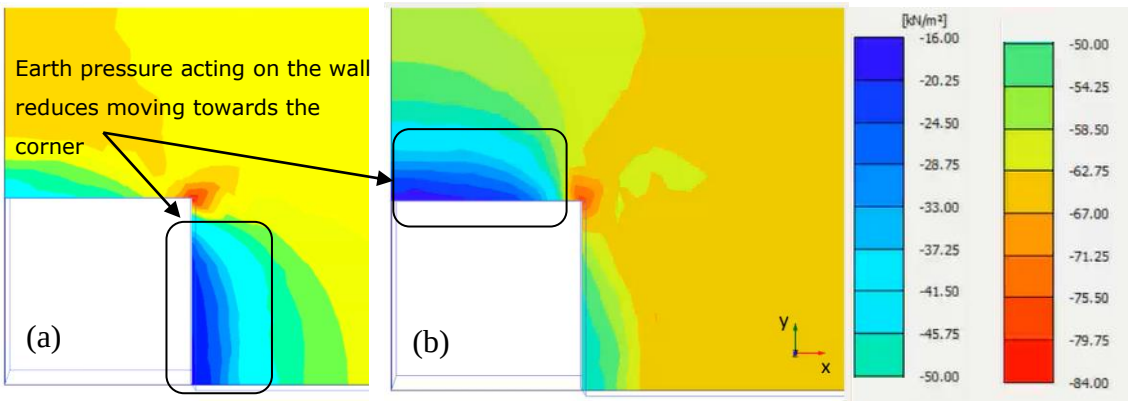

Figure 4.2 Horizontal cross-section showing contours of horizontal stresses within the ground behind an excavation corner, σ_{xx} (a) and σ_{yy} (b), negative values refer to compression

4.4 Previous three dimensional studies on excavations

Numerous authors have discussed the relevance of three dimensional effects for excavations, reviewing monitoring data from case histories or carrying out parametric studies varying geometry, soil properties, type of retaining system, etc.

Ou et al. (1996) introduced the Plane Strain Ratio (PSR) parameter, defined as the ratio of maximum wall deflection at a particular section and maximum wall deflection in plane strain conditions. The PSR is a useful parameter to give a quantitative estimate of three dimensional effects related to excavations. Charts showing the dependence of PSR on excavation geometry (excavation width/depth ratio), distance from excavation corners, wall length in plan, have been produced on the basis of parametric numerical studies by a number of authors (including Ou et al. (1996), Lin et al. (2003)) and a typical example is provided in Figure 4.3. In this figure, the term "primary wall" indicates the wall on which deformations are evaluated, while the term "complementary wall" indicates the transverse wall. The results in Figure 4.3 clearly indicate that the wall deflection considerably decreases when approaching the corner of the excavation and plane strain conditions are approached at a considerable distance from the corner (approximately 30m). Therefore, these results demonstrate that there is a clear scope for increase design efficiency using three dimensional modelling techniques. It is worth

noting that most of these studies are carried out modelling retaining walls using shells with isotropic flexural rigidity.

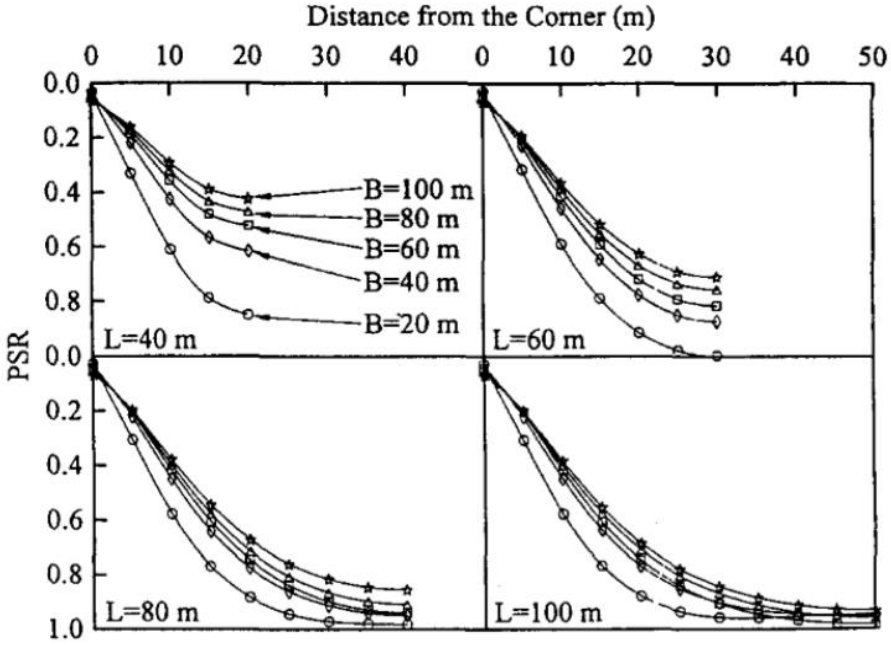

Figure 4.3 Variation of PSR for maximum wall displacement with distance from the corner. L indicates the length of the primary wall while B indicates the length of the complementary wall (after Ou et al. 1996)

Zdravkovic et al. (2005) highlighted the importance of using anisotropic shell elements (with reduced axial and bending stiffness of the wall along its perimeter), in order to avoid the development of unrealistic bending moments about the vertical axis, as shown in Figure 4.4. This consideration is valid when modelling both contiguous/secant piled walls and diaphragm walls. All these types of walls have zero or limited flexural rigidity (*EI*) about the vertical axis. Similar considerations apply to vertical and horizontal in-plane forces in the shell elements, i.e. zero or limited axial rigidity (*EA*) should be adopted in the shell in-plane horizontal direction, to prevent the development of unrealistic horizontal forces. Zdravkovic et al. (2005) also indicate rotational degrees of freedom should be released in the corners of the excavation, to avoid bending moments due to the fixity between adjacent walls.

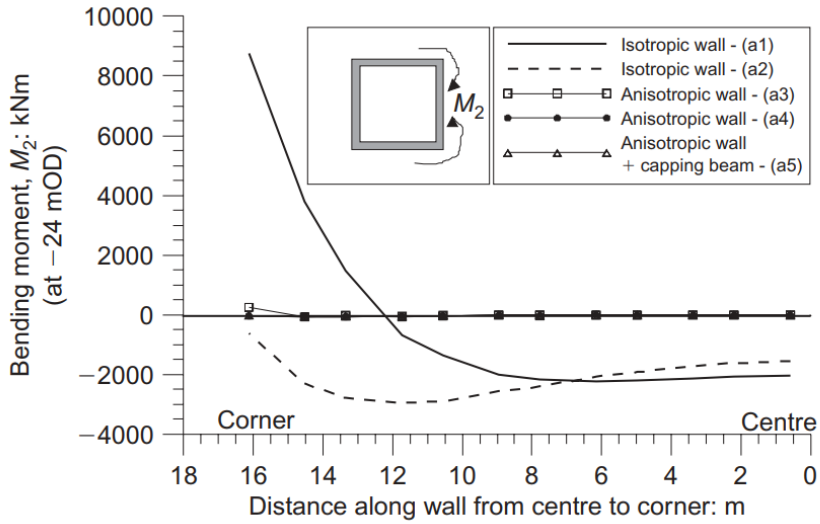

Figure 4.4 Effect of using isotropic or anisotropic shell elements for modelling walls in square excavations (after Zdravkovic et al. (2005))

Lee et al (1998) noted that the corner effect is strongly dependent on the type of soil strata below excavation level. If stiff strata underlie the excavation, the maximum wall deflection is likely to be reached above excavation level and the corner effect may be suppressed if a sufficiently stiff strutting system is used. In this case the adoption of plane strain models may be accurate. If soft soil underlies the excavation, the maximum deflection is likely to take place below the excavation depth and the corner effect may appear more obvious. In this case, the use of three dimensional models may provide more realistic predictions.

An attempt to consider excavation geometry and soil arching effects in retaining wall design is made by the German Geotechnical Society, in their Recommendations on Excavations (1994) publication. Here, with regards to rectangular excavations in granular or stiff cohesive soils, reference is made to two classes of problems, namely i) retaining systems with corners as flexible as the middle sections of the excavation, or ii) retaining systems with stiff corners compared to the middle sections of the excavation. In the two cases, shear forces developing across the flank sides of a sliding wedge (i) or

actual three dimensional sliding wedge (ii) are considered, and reduced pressure distributions are proposed for the design of different sections.

Excavations in urban environments induce ground movement fields that are often associated with damage arising in adjacent structures and infrastructure. Authors have usually focussed on displacement profiles in sections perpendicular to retaining walls and associated damage to structures. Little attention has been given to three dimensional ground displacement fields, and in particular with regards to estimating the distributions of the induced movements in a direction parallel to a retaining wall. Roboski & Finno (2006) emphasised the fact that distortions arising in a direction parallel to an excavation can also produce damage to a structure and proposed a fitting function for the settlements and horizontal movements of the ground along a line parallel to an excavation side.

4.5 Three-dimensional excavations – some modelling aspects

The three dimensional analysis of excavation problems is relevant to geotechnical serviceability, stability and structural design of retaining systems, foundations and other sub-structure elements. The methodology adopted for modelling the retaining wall element is a key ingredient of the soil-structure interaction analysis. Either solid elements (explicit wall) or shell elements can be adopted. Shell elements are adopted in most cases, due to their formulation and ease of definition and use. They directly provide bending moments and shear forces for the retaining wall design. Some selected aspects and pitfalls to be considered when using shell elements are listed below.

- The zero physical thickness of the shell elements representing the wall prevents the development of beneficial moments due to the vertical shear stresses acting on the wall. In view of this, the model may overestimate wall deflection and bending moment profiles.

- Piled walls (secant or contiguous), diaphragm walls and sheet pile walls are made up of elements (pile, panels, sheets) that provide flexural rigidity about the

horizontal axis lying in the wall plane. In general, they have zero or limited flexural rigidity about the vertical axis. On the other hand, shell elements are generally formulated as two dimensional elements that can bend in two directions and twist. In order to reproduce the retaining wall behaviour, they have to be assigned anisotropic properties, i.e. $EI_{xx} >> EI_{yy}$ (where the subscript indicates the bending axis, as shown in Figure 4.5 for a piled wall).

- Due to the thin shell formulation, Poisson's ratio should be set to zero to avoid the development of bending moments about the horizontal axis due to curvature about the vertical axis.

- Rotational degree of freedom between shells should be released at wall corners.

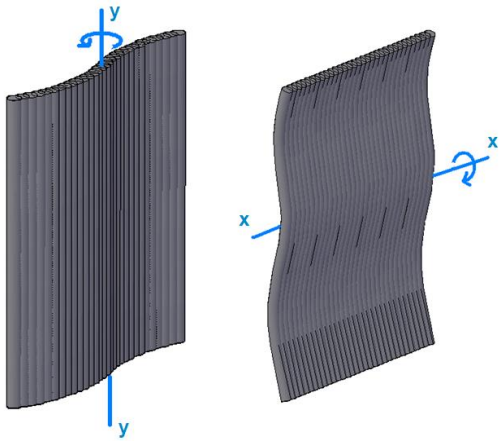

Figure 4.5 Piled wall bending mechanisms

Although more accurate in some cases, modelling retaining walls using solid elements can be relatively laborious. Wall bending moments and shear forces, for example, have to be evaluated from stress distributions or from multiple differentiations of deflection profiles.

Elements capable of providing bending capacity about the vertical axis, such as capping beams or waling beams, should be modelled accordingly. If the wall is modelled using shell elements, shell properties should be modified locally to adequately model these elements. In some cases, the presence of capping/waling beams can significantly

improve the performance of retaining systems. Obviously, three dimensional modelling is very relevant for their design. For example, Figure 4.6 shows the distribution of bending moments in a capping beam, significantly influenced by the position of the temporary props.

Temporary props are often adopted to provide restrain to retaining walls and they have to be included in the finite element staged construction sequence. They can be modelled using node springs or node-to-node spring elements (beams pinned at each end). The latter should be adopted in cases where non-symmetric force distributions are present (variable ground level, irregular excavation sequence, unbalanced propping arrangement, etc).

Modelling the correct excavation sequence is important, as this can affect the excavation behaviour. Contractor involvement from the early stages of a project and presence of designers throughout construction is essential.

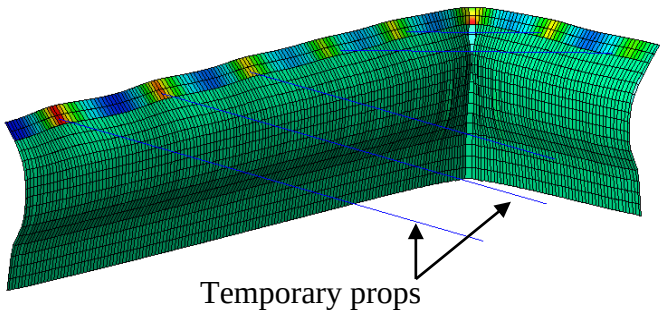

Figure 4.6 Indicative bending moment contour plot for the design of the capping beam

4.6 Holistic substructure analysis

Consideration of key element of the sub-structure (cores and stiff shear walls, slabs, etc) within soil-structure interaction modelling is important to understand the holistic performance of the basement structure and to aid the design of these structural elements. Due to the interaction between different sub-structure elements, the retaining wall cannot be treated as an individual/single element but its performance within the whole substructure should be considered.

This aspect becomes particularly relevant in cases where there is a force imbalance between different sides of an excavation. This can be due to lack of symmetry in earth pressure distributions across opposite sides of an excavation, particular temporary propping arrangement or irregular layout of stiff sub-structure elements such as cores. Some examples are given below.

A case study of an excavation within a chalk slope is presented in Figure 4.7. A photograph of the site is shown in Figure 4.7a and a view of a three dimensional finite element model in Figure 4.7b. In the permanent condition stage, the sub-structure model includes retaining walls, basement slabs and central cores. The model was not only used for the wall design, but also to aid the design of slabs, subject to in plane forces, cores, subject to bending to provide part of the earth pressure balance reaction, and raft foundation.

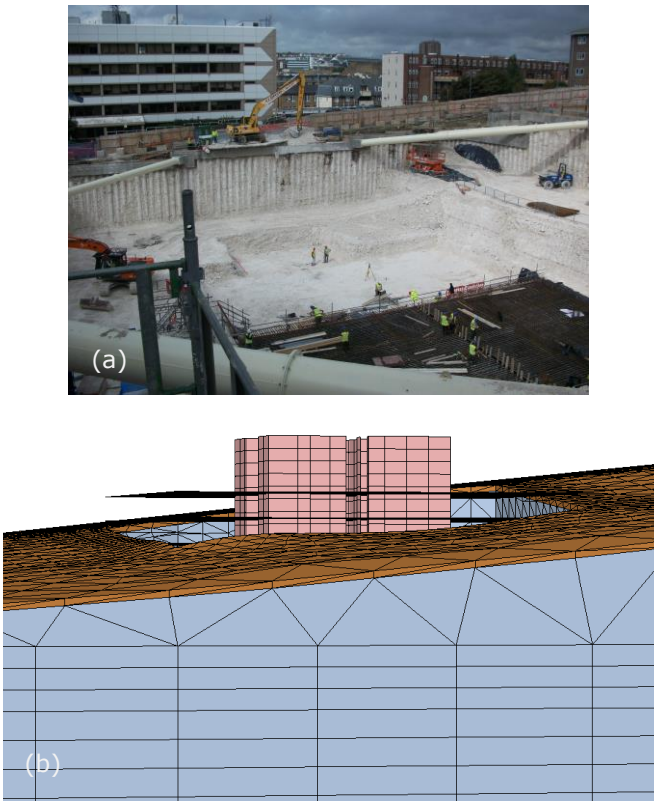

Figure 4.7 Excavation in sloping chalk (max 20m depth)

Figure 4.8 shows an excavation in Central London, in which the depth varies from 13m to 6m across two opposite sides of the basement. Figure 4.8a shows a photo of the site during the excavation works. Figure 4.8b shows indicative (exaggerated) ground movement vectors, evaluated in a plane strain analysis simulating the excavation process. Consideration of both opposing walls and modelling the temporary propping explicitly is fundamental in this case, to assess the soil displacement field behind the lower wall, where railway tracks may be affected.

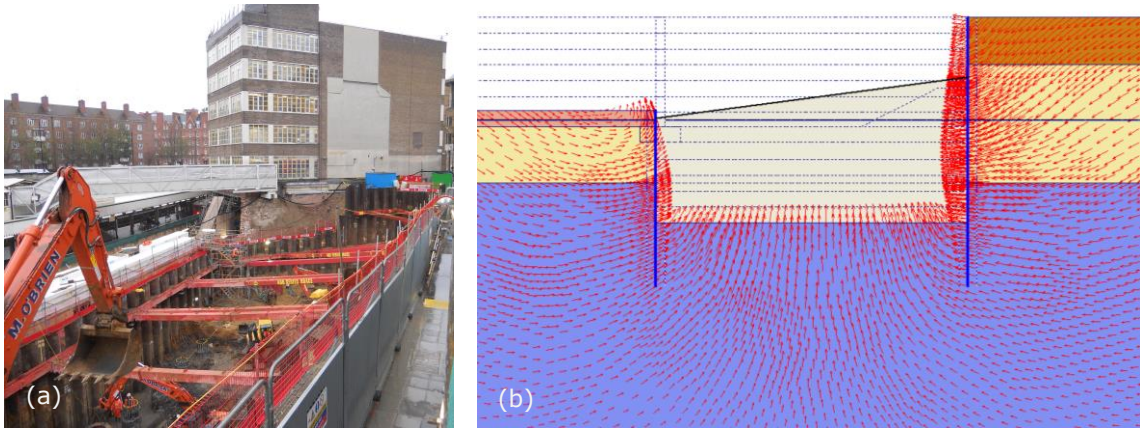

Figure 4.8 "Unbalanced" excavation in central London (max 13m depth)

The example in Figure 4.9 is an excavation in Central London. Figure 4.9a shows a photograph of a zone of the excavation, Figure 4.9b show the temporary prop arrangement for the same zone and Figure 4.9c presents a view of a local three dimensional finite element model. In this case, although the ground level is relatively constant, the particular temporary propping arrangement, the excavation plan layout (relatively narrow basement, very long in the east – west direction, with associated pronounced arching in the soil behind the west side) and the excavation sequence, induced an imbalance in earth pressure, which caused the top of the west wall to move backwards in the initial excavation phases, as schematically shown by the dashed blue line in Figure 4.9b (plan view). It is worth highlighting that the use of localised springs to model temporary props would have produced misleading results, since it would not have captured the interaction between the different sides of the excavation, observed in reality.

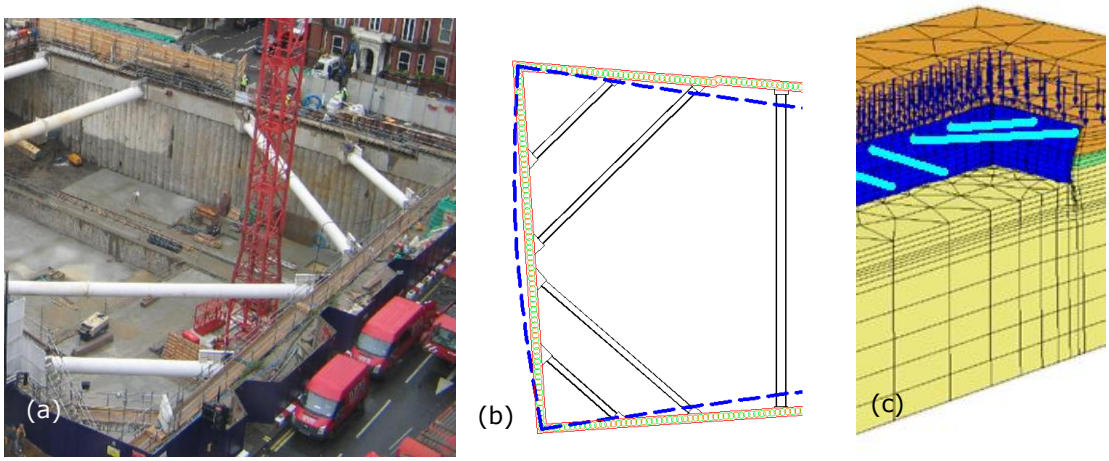

Figure 4.9 Central London excavation –temporary propping arrangement (max 13m depth)

4.7 Retaining wall corner optimisation technique

As mentioned earlier, three dimensional soil-structure interaction simulation can be adopted to optimise the design of retaining walls. For many excavations, wall deflections and associated bending moments tend to reduce when approaching excavation corners. For example, Figure 4.10 shows the distribution of bending moments in a top-propped piled wall, following the excavation. The particular model shown is representative of a quarter of a rectangular excavation. In view of the particular bending moment distribution, a Corner Optimisation Technique (COT) can be implemented to refine the wall design. For example, for piled walls, a number of optimisation strategies can be applied in proximity of corners, for the sake of a more efficient and cost-effective wall design, as follows:

- Increase pile spacing
- Reduce pile diameter
- Reduce reinforcement

In the last years, the author has gained confidence in the implementation of such techniques in practice, in various ground conditions. The third option listed above has proven more practical and has been implemented for the Central London excavation

project previously presented (Figure 4.9). Bending moment reduction of up to 30% compared to plane strain conditions (see Figure 4.10) resulted in substantial savings in steel reinforcement quantities.

The COT can also be implemented for the evaluation of the required wall embedment, shortening the wall in proximity of corners. Depending on the design standard or code of practice adopted, the ultimate limit state calculation may require the adoption of factored strength parameters in the three dimensional simulation.

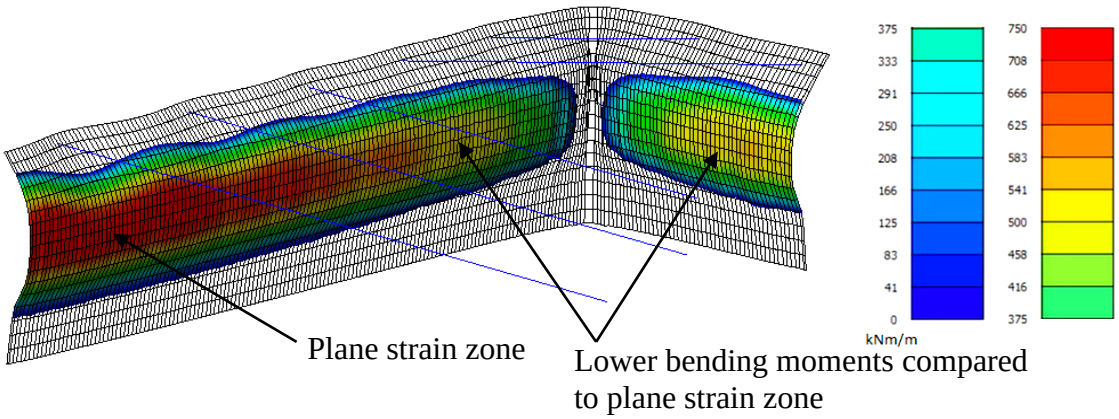

Figure 4.10 Indicative bending moment distribution along wall

4.8 London Clay excavation project

4.8.1 Three dimensional analysis

Three dimensional analyses have been carried out for the excavation case study described in chapter 3, using the commercial software Plaxis 3d. The scheme comprises an approximately 20m deep rectangular excavation, 100m x 65m in plan. The reader should refer to Chapter 3 for details of the scheme and excavation sequence. With regards to ground model assumptions, the London Clay and Lambeth Group strata have been modelled using the Generalised Hardening Soil (GHS) constitutive model, while all other strata have been modelled using the Mohr-Coulomb constitutive model. Specific input parameters for all strata are presented in Chapter 3. A view of the Plaxis 3d model is presented in Figure 4.11.

A sensitivity study similar to the one presented in Chapter 3, regarding mesh refinement, has been undertaken for the three dimensional model. A suitable mesh, comprising approximately 200,000 elements, has been adopted, taking into account both accuracy of the output and analysis running time (approximately 5 hours on a computer with Intel Xeon X5667 3.07GHz dual processor and 48GB of RAM, using the GHS model).

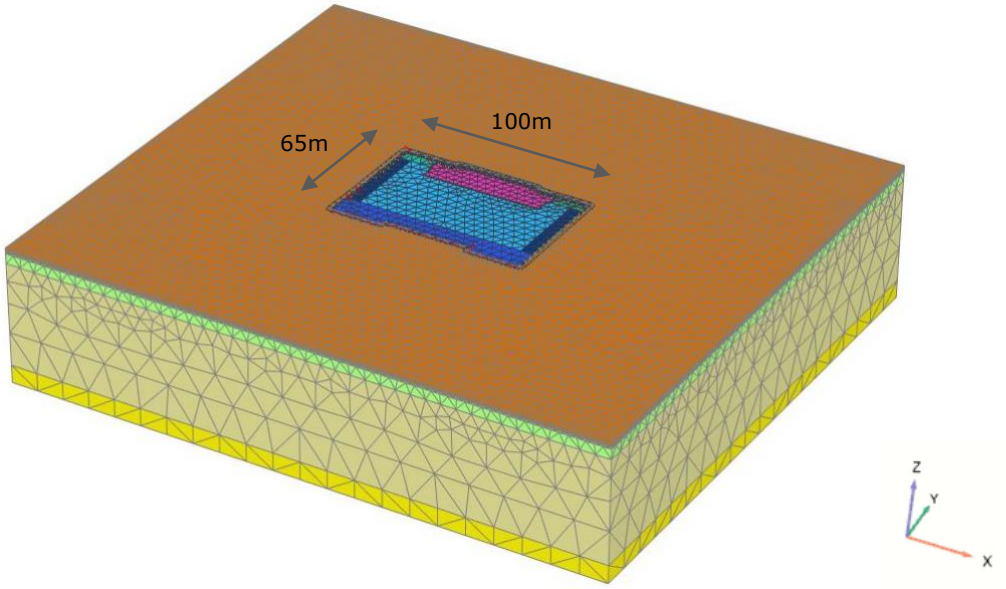

Figure 4.11 View of the Plaxis 3d model

The excavation sequence involves the use of a combination of portions of permanent slabs and temporary steel props, to provide support to the piled retaining walls. Permanent slabs construction is then completed prior to the removal of temporary props. The assumed temporary propping arrangements for ground floor and basement B2 levels are indicatively presented in Figure 4.12 and Figure 4.13, respectively. The complex slab and temporary prop arrangements highlight the difficulty in evaluating equivalent spring stiffnesses to adopt in plane strain analyses. The spring stiffness adopted in the two dimensional analyses carried out have been conservatively evaluated by the contractor working on the project (PJ Carey Ltd, 2019), considering the behaviour of the slabs at mid span.

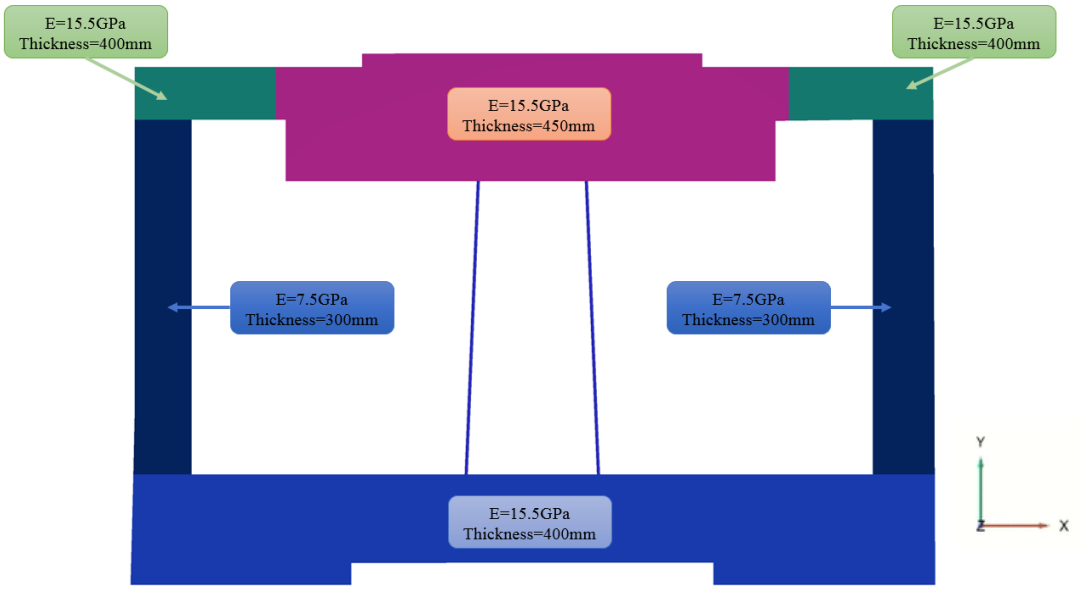

Figure 4.12 Ground floor slab/temporary propping properties (plan view)

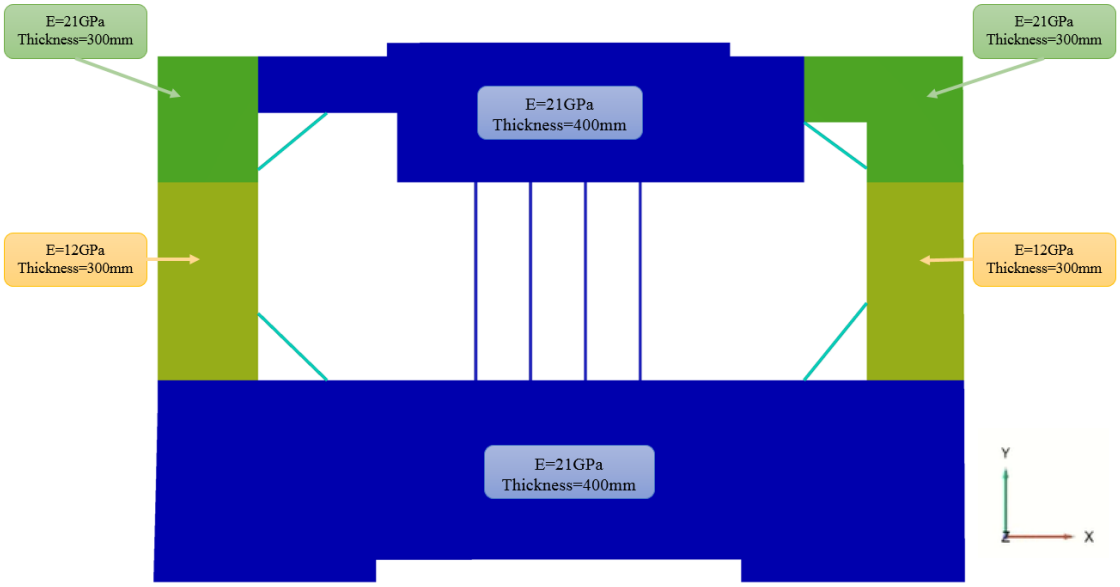

Figure 4.13 B2 slab/temporary propping properties (plan view)

Anisotropic behaviour has been assumed for the retaining wall plates, as described in the previous sections of this chapter, simulating the negligible flexural rigidity of the piled wall about the vertical axis. Pinned connections have been assumed between the slabs and the walls. An indicative three dimensional view of the basement structure is shown in Figure 4.14.

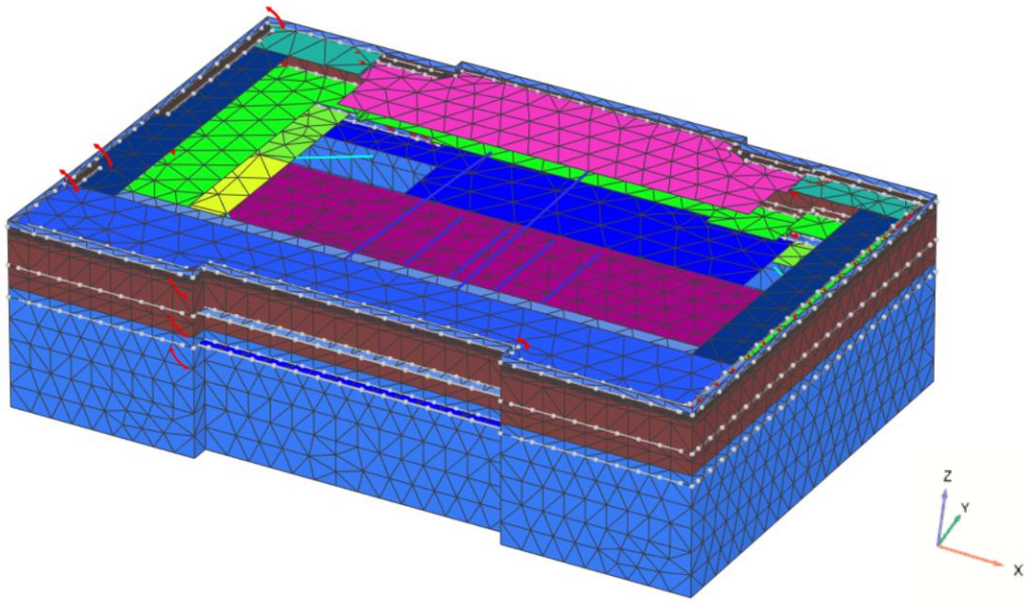

Figure 4.14 Basement box sub-structure modelled in Plaxis 3d

Idealised construction stages have been modelled, in line with the two dimensional assessment presented in Chapter 3.

Key output of the analysis, including ground movements and wall deflections following completion of the excavation works, is presented in Figure 4.15 to Figure 4.18. Greenfield ground movement distributions are often used to assess the potential impact on third party assets, including neighbouring buildings, the positions of which are indicatively shown in pink in the figures.

Figure 4.15 and Figure 4.16 show horizontal movements in the x and y directions. The contours clearly indicate concentration of ground movements in the zones immediately behind the retaining walls, with maximum values in the wall mid span zone and values

progressively reducing approaching the excavation corners. The values progressively dissipate moving away from the walls, reaching negligible values at a distance of approximately 50m from the two short sides of the excavation and 75m from the two long sides.

Figure 4.17 shows vertical ground movements. Following a similar pattern to the horizontal ground movement components, settlements are concentrated in the zones immediately behind the retaining walls, with maximum values typically occurring at wall mid span, with the exception of the wall long side shown in the lower part of the plot. In this case, higher settlements are predicted in the zone beside the wall mid span, as a result of the particular temporary propping/slab arrangement.

Figure 4.18 shows contours of wall horizontal deflections. Also in this case, maximum wall deflections generally tend to reduce moving from the mid span zones towards to corners. The mechanism is less evident for the long excavation side in the lower part of the image, for the reason explained above in relation to ground settlements.

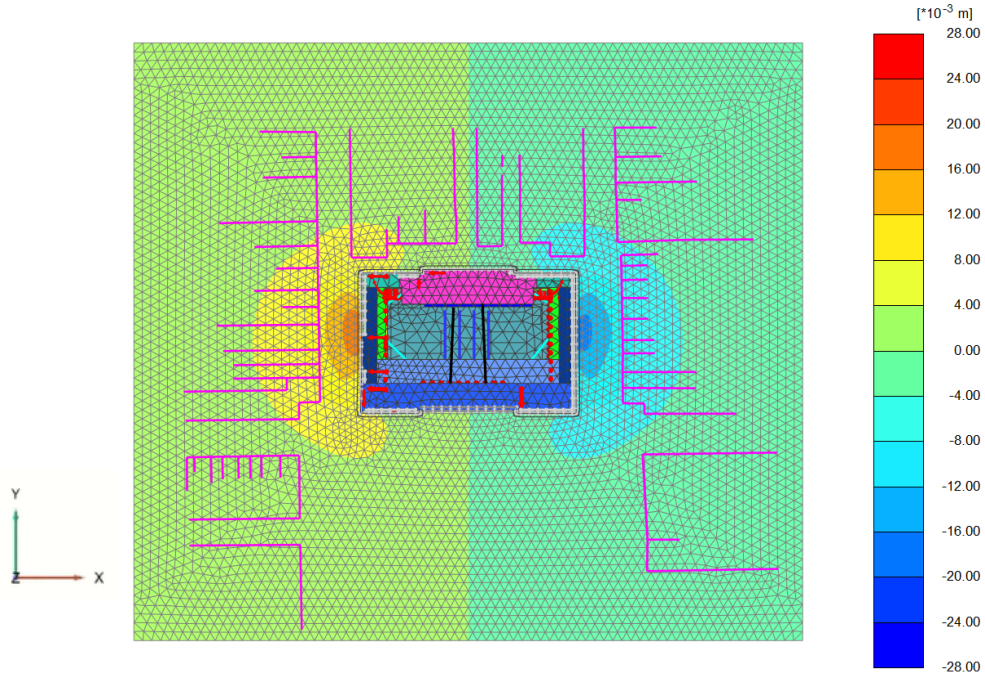

Figure 4.15 Plaxis 3d output: u_x ground movement contour plot - end of excavation

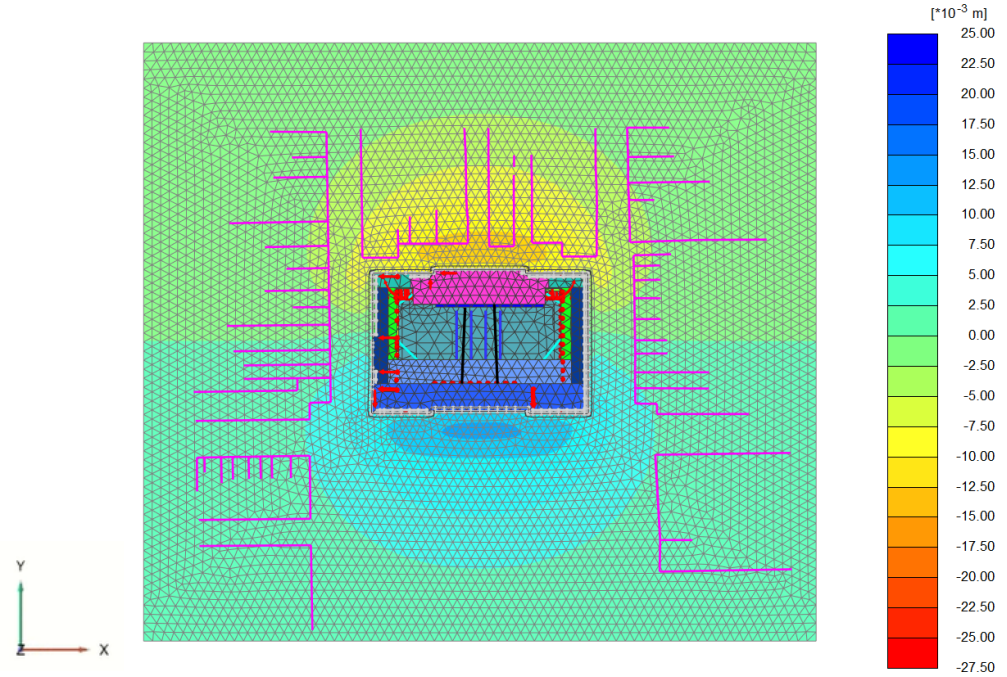

Figure 4.16 Plaxis 3d output: u_y ground movement contour plot - end of excavation

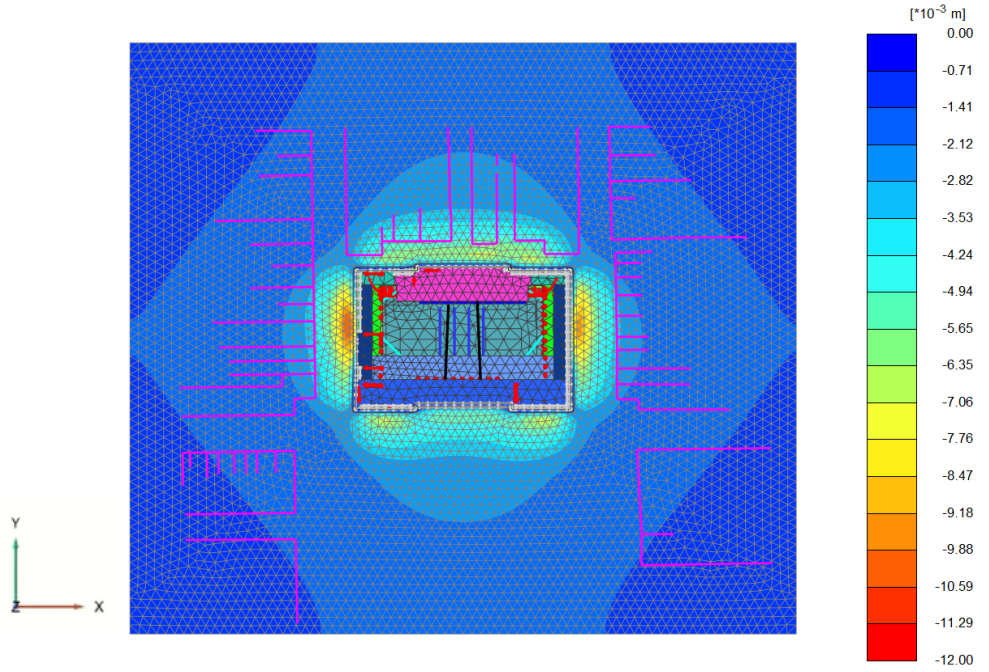

Figure 4.17 Plaxis 3D output: u_z (vertical) ground movement contour plot - end of excavation (negative values refer to settlements)

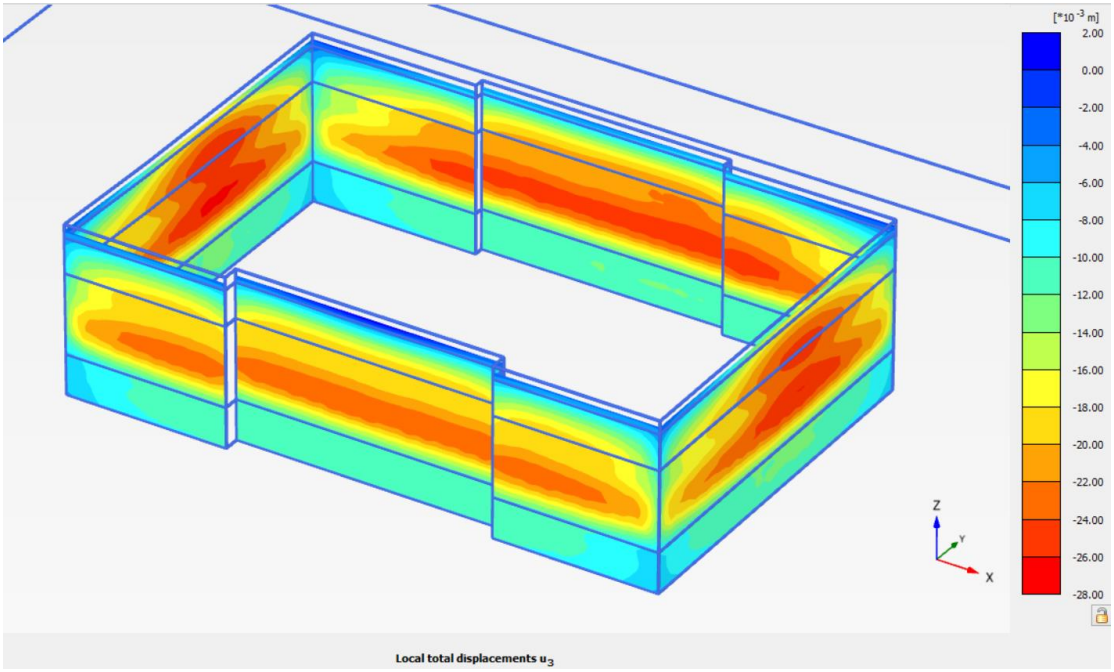

Figure 4.18 Plaxis 3D output: wall horizontal deflections

4.9 Comparison with two dimensional analysis

Figure 4.22 presents a comparison of the wall deflection profiles between the two dimensional analysis and a number of wall cross-sections from the three dimensional analysis. The cross-sections locations are shown in Figure 4.19.

Results from the Plaxis 3d analysis clearly indicate the three dimensional wall deformation mechanism, with wall deflections reducing when moving towards an excavation corner. In general, wall deflections predicted from the Plaxis 3d analysis are lower than the 2d analysis. A relatively significant difference in deflections is particularly evident in the lower part of the wall, indicating that three dimensional effects, associated with stress distributions, are also important on the wall passive side, below excavation level.

The contour plots presented in Figure 4.15 to Figure 4.18 indicate a reduction in horizontal and vertical ground movement, moving from the centre of the excavation sides towards the corners. In view of the plane strain assumption, it is not possible to

capture these mechanisms from the two dimensional analysis. Simplified empirical methods (for example the one proposed by Fuentes & Devriendt, 2010) would have to be implemented to allow the evaluation of three dimensional ground movement fields, based on the plane strain analysis output. While the adoption of these methods can be very useful during preliminary design stages or for relatively simple excavation problems, explicit three dimensional analyses allows a more accurate assessment of complex excavation geometries and temporary/permanent wall propping arrangements.

Figure 4.20 and Figure 4.21 show distributions of PSR (Ou et al., 1996) with varying distance from the excavation corner (top left corner in Figure 4.19). The Plaxis analysis curves are compared with the distributions presented by Ou et al. (1996) (see Figure 4.3), for representative primary and complementary/transverse wall lengths (L and B, respectively).

The Plaxis analysis results indicate a much less pronounced reduction of wall deflections in proximity of the excavation corner, compared to the findings of Ou et al. (1996). This may be related to the fact that isotropic behaviour may have been assumed for the walls as part of the study by Ou et al. (1996). As previously mentioned in this chapter, this assumption is not appropriate to simulate the behaviour of a piled wall as it may artificially enhance the three dimensional "box" effect associated with the excavation plan shape and aspect ratio.

The diagrams also indicate that, in the Plaxis analysis, plane strain conditions (PSR=1) are not reached in the central part of the walls (50m and 32.5m distances from the corner in Figure 4.20 and Figure 4.21, respectively). This is particularly evident for the long wall (Figure 4.20). The inconsistency with the findings of Ou et al. (1996) may be related to the shallower excavation depth (16m) and the different ground conditions (normally consolidated deposits) considered in the latter study.

A comparison of bending moment distributions between the two and three dimensional analyses is shown in Figure 4.23. Approximately 15% to 60% lower values are predicted for the various cross-sections examined in the three dimensional analysis. The reduction is particularly evident at the B2 slab position (approximate level 14mAOD), as a result of the lower slab propping reaction predicted in the three dimensional analysis.

Stress distributions within the soil surrounding the excavation, from the three dimensional analysis, are presented in Figure 4.24 and Figure 4.25, at a level of 15mAOD (i.e. approximately 11m below ground level) within the London Clay stratum. The plots show contours of normal stresses in the x and y horizontal directions. They clearly indicate the impact of the excavation plan shape on the stress distributions, with stress relaxation taking place within semi-circle-shaped zones behind the excavation sides.

As a result of this mechanism, the soil zone mobilised behind the retaining wall (which can be considered similar to an active wedge, involved in the development of active pressures acting on the wall – Coulomb, 1776) varies in size, moving from the central zone of the excavation sides, towards the corners. Indicative shapes of these mobilised soil zones can be visualised plotting incremental displacement contour lines passing through the wall toe. These plots are shown in Figure 4.26 for sections 1 and B (see Figure 4.19 for cross-sections locations), and compared with the results of the two dimensional analysis. A reduction in size of these mobilised soil volumes is observed when going from a two dimensional analysis to the mid-span and corner cross-sections of the three dimensional analysis.

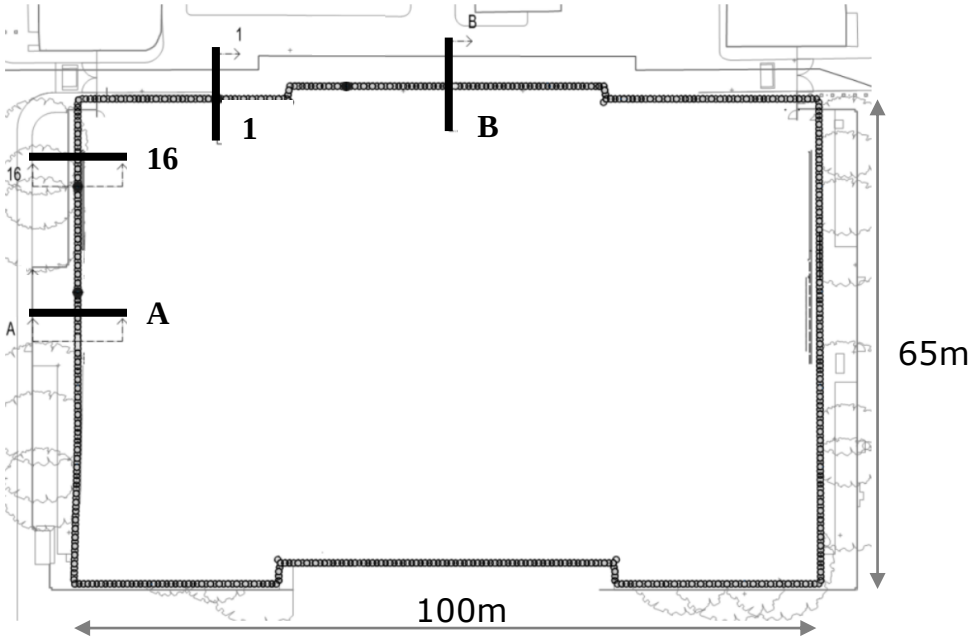

Figure 4.19 Selected cross-sections locations

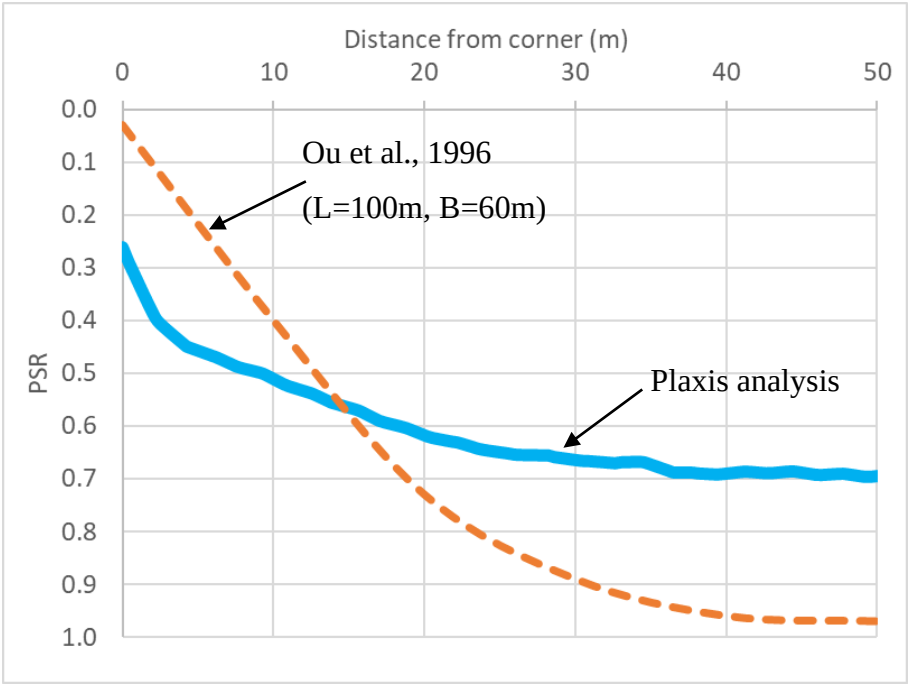

Figure 4.20 Variation of Plane Strain Ratio (PSR – Ou et al. 1996) for maximum wall displacement with distance from the corner (100m wall) – comparison of Plaxis analysis output and data from Ou et al., 1996

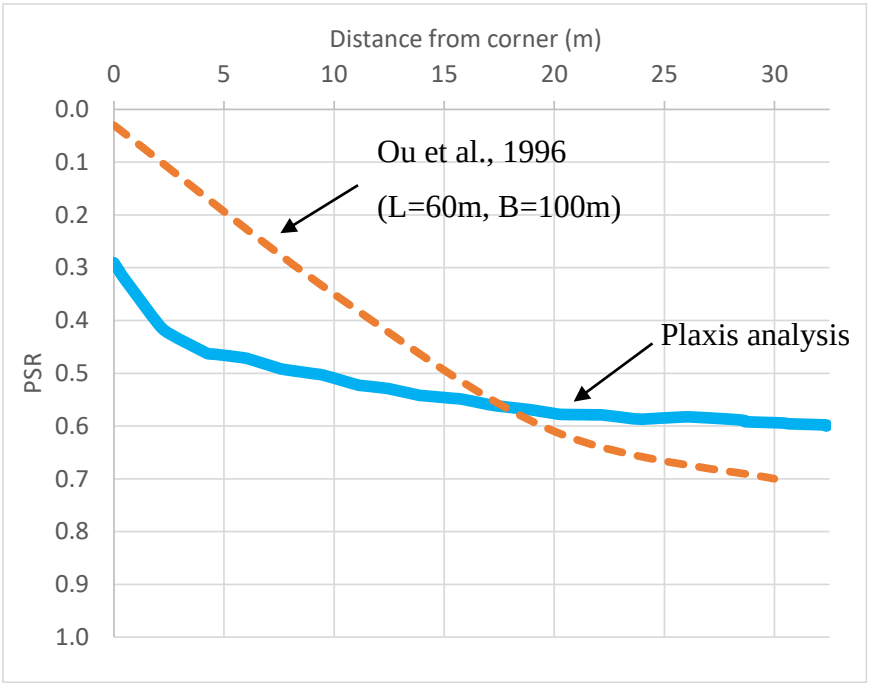

Figure 4.21 Variation of Plane Strain Ratio (PSR – Ou et al. 1996) for maximum wall displacement with distance from the corner (65m wall) – comparison of Plaxis analysis output and data from Ou et al., 1996

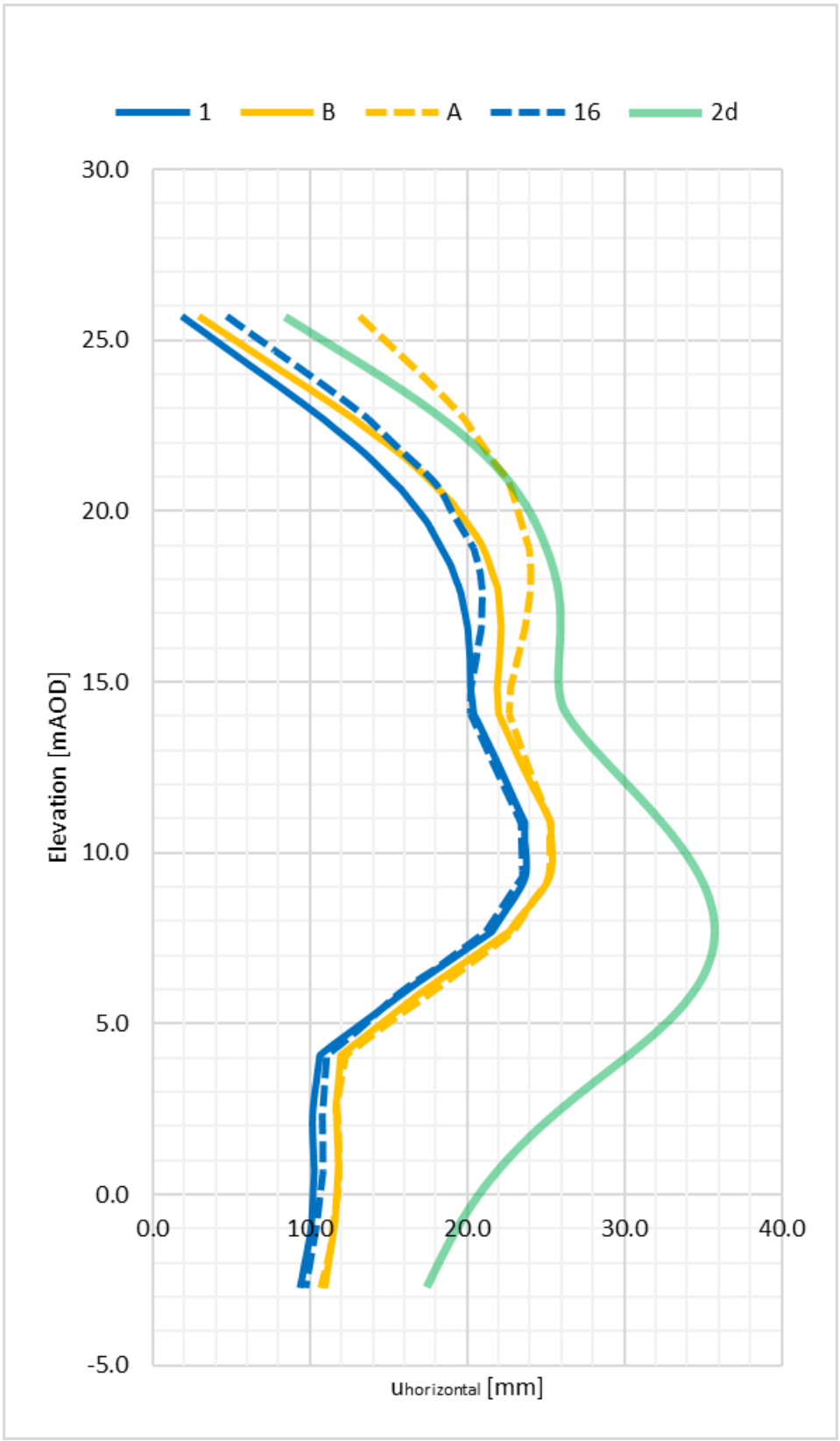

Figure 4.22 Comparison between Plaxis 2d and 3d wall deflections

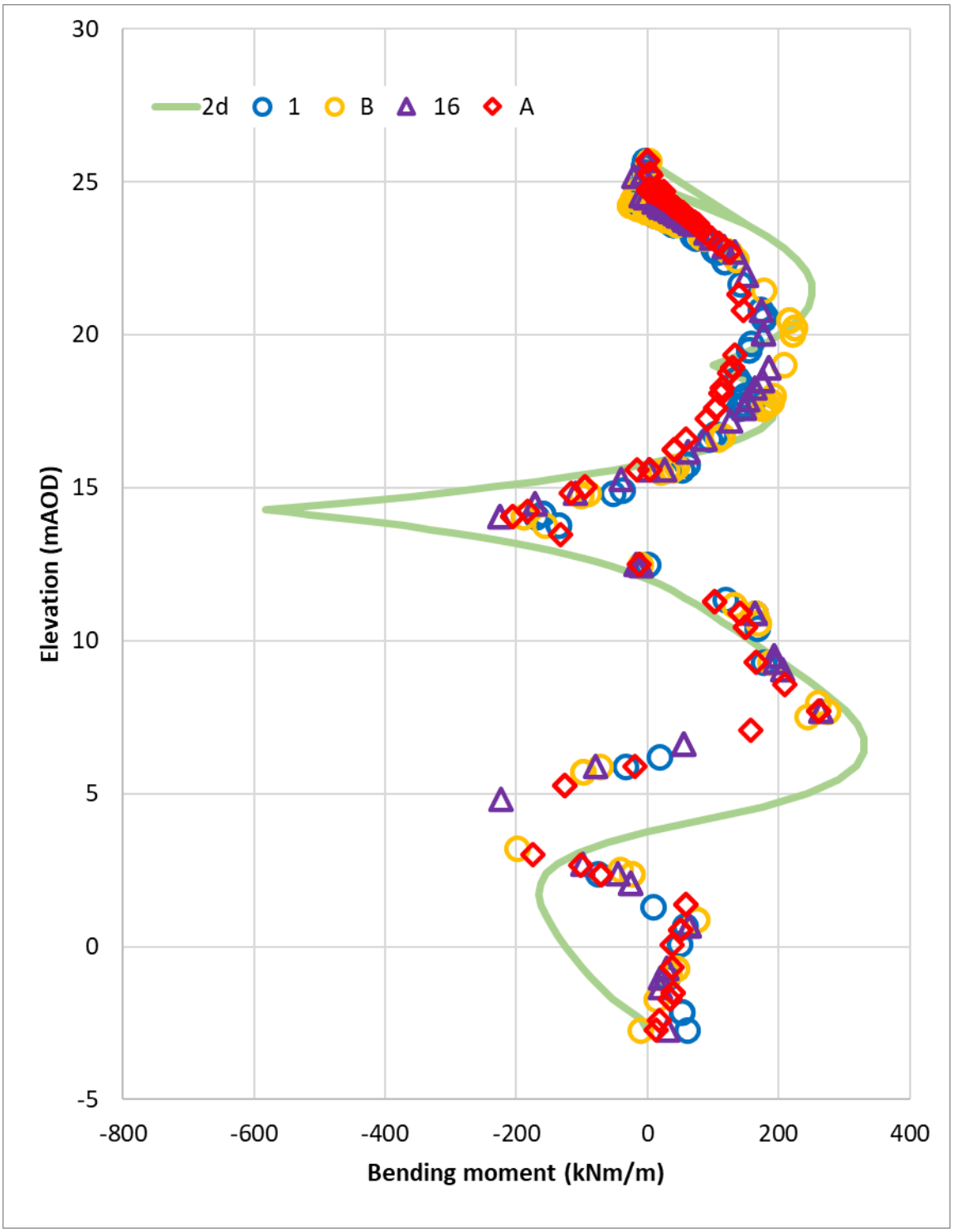

Figure 4.23 Comparison between Plaxis 2d and 3d wall bending moments

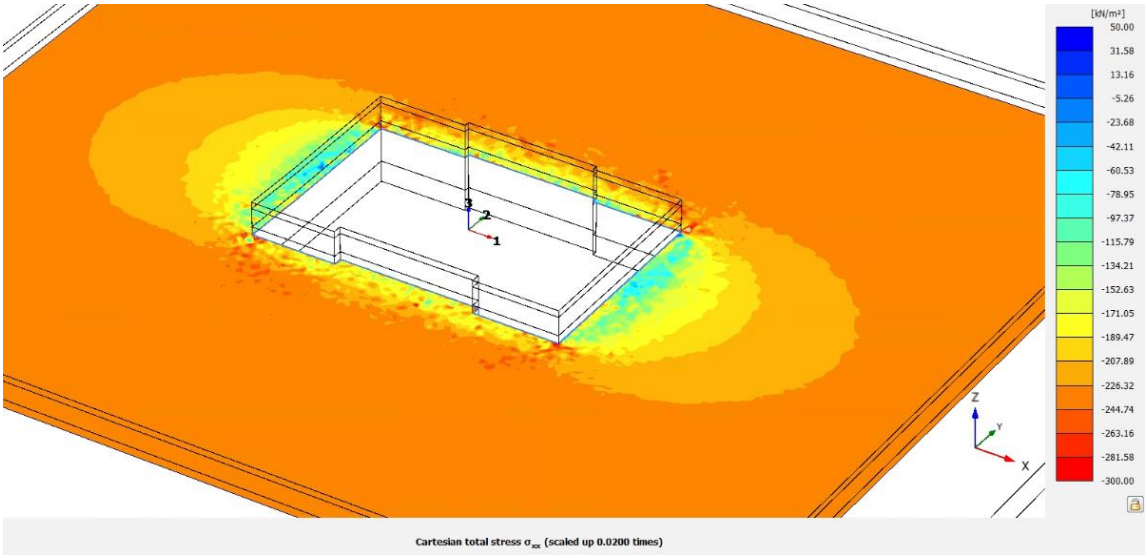

Figure 4.24 Total normal stress distribution (in the x direction) on a plane at 15mAOD – negative values refer to compressive stresses

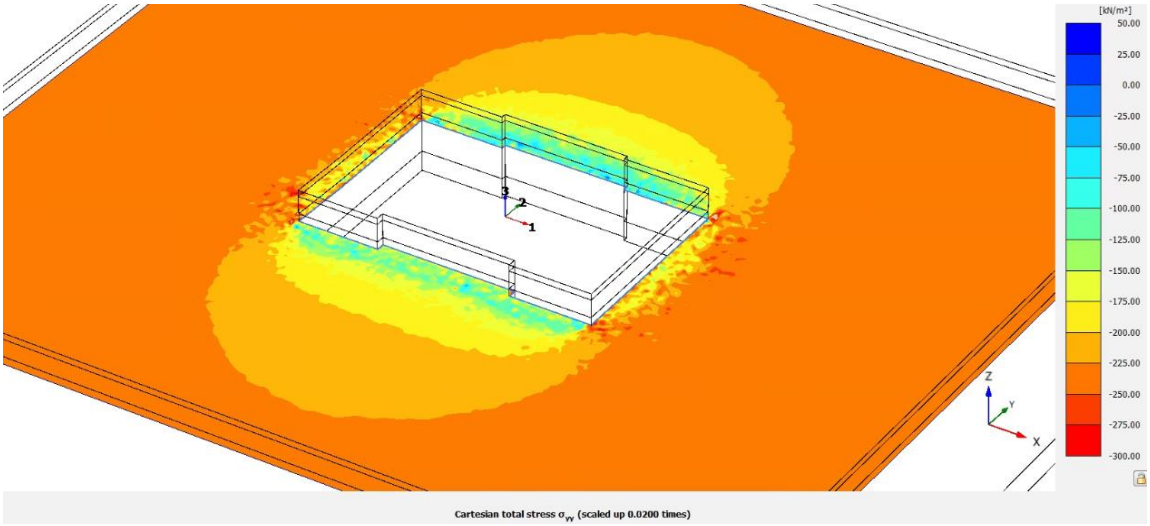

Figure 4.25 Total normal stress distribution (in the y direction) on a plane at 15mAOD – negative values refer to compressive stresses

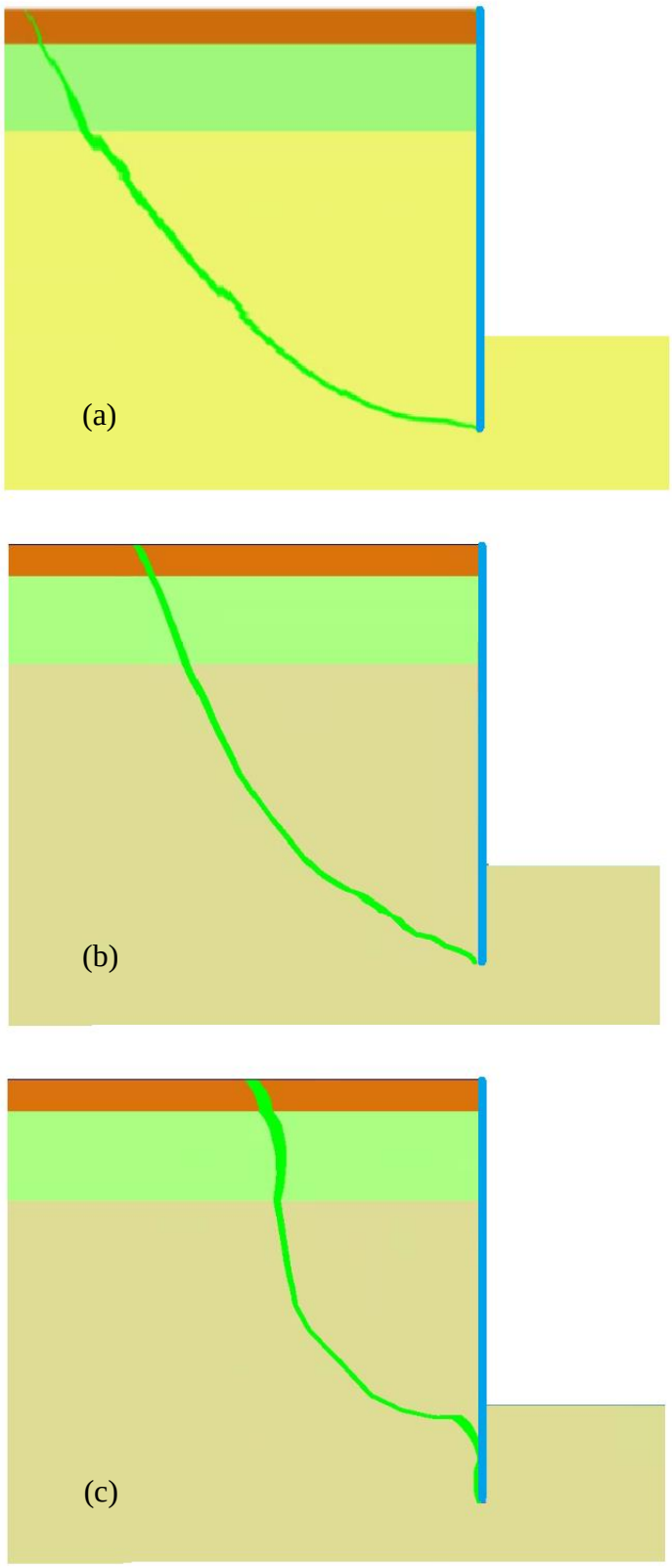

Figure 4.26 Comparison of mobilised soil zones between Plaxis 2d (a) and Plaxis 3d at cross-section B (b) and cross-section 1 (c) (see Figure 4.19 for cross-sections locations)

4.10 Comparison with published data

In terms of predicted ground movement distribution behind the wall, Figure 4.27 and Figure 4.28 show a superposition of the ground movement curves estimated from two and three dimensional analyses, and the CIRIA C760 case histories data. The graphs present horizontal (Figure 4.27) or vertical (Figure 4.28) ground movements shown as a percentage of the excavation depth, against horizontal distance from the wall, normalised with the excavation depth.

The ground movements predicted from the three dimensional analysis are generally smaller compared to the two dimensional one. The three dimensional predictions also show a more rapid reduction of ground movements, moving away from the wall.

When compared with the CIRIA C760 case histories, while the two dimensional predictions envelope most of the empirical data, the results of the three dimensional analysis appear to broadly average the data. It is worth noting that the particular excavation analysed comprises a significantly stiff earth retaining system and construction sequence (i.e. top-down), while most of the CIRIA C760 data refers to case histories from 1970s to 1990s, which often comprise less stiff retaining systems.

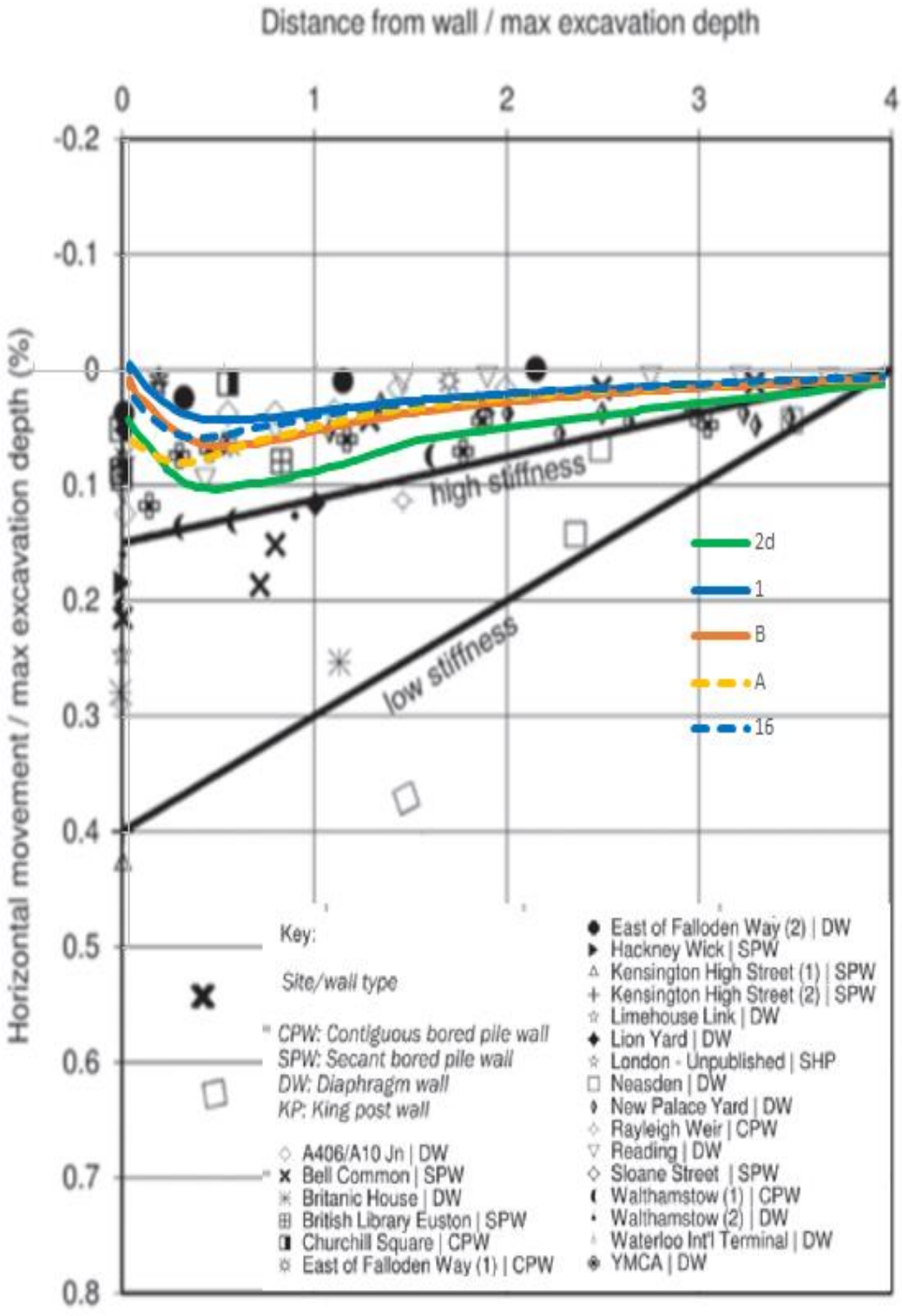

Figure 4.27 Normalised horizontal ground movements at varying normalised distances from the wall (comparison with CIRIA C760 case histories)

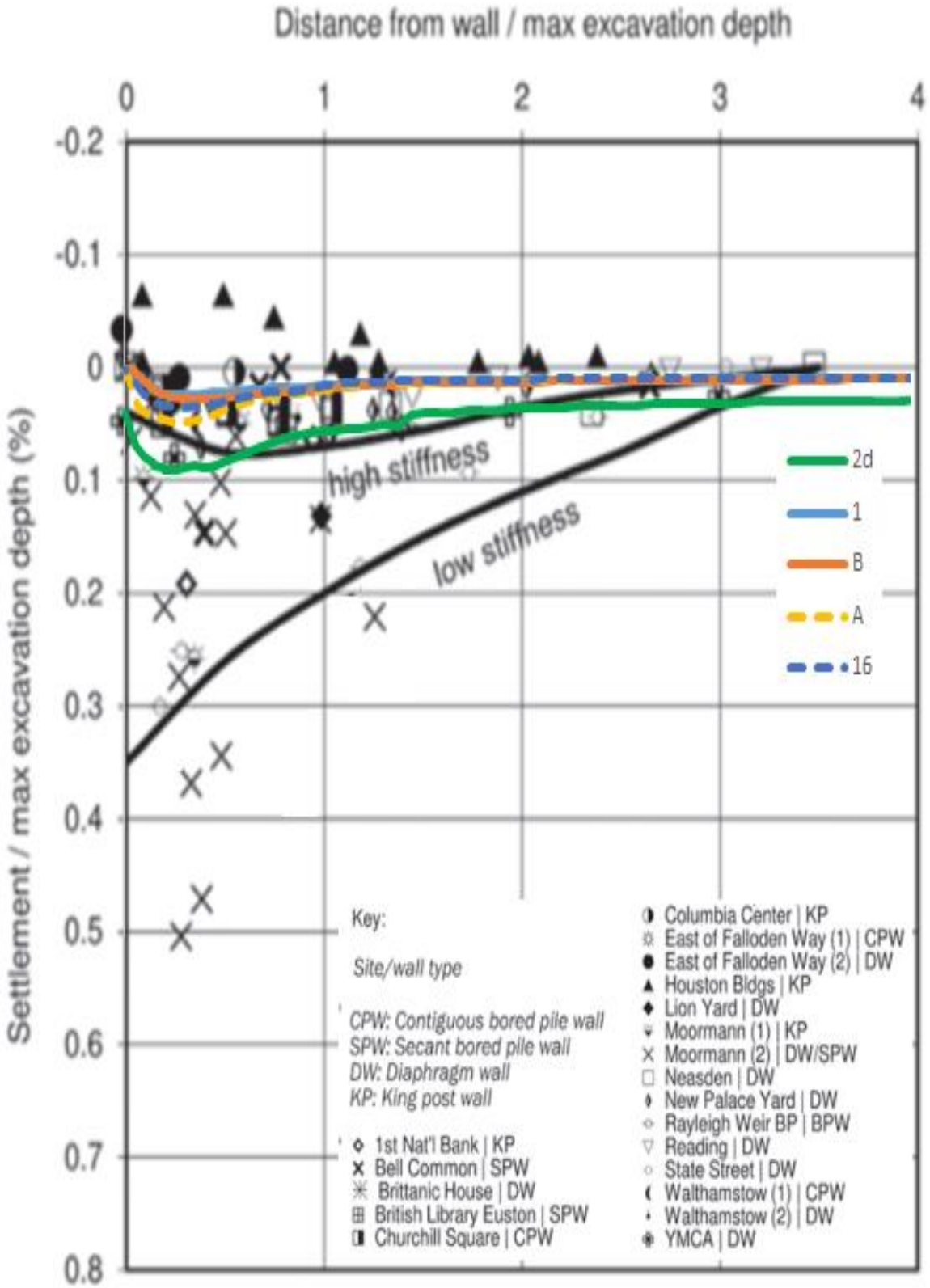

Figure 4.28 Normalised settlements at varying normalised distances from the wall (comparison with CIRIA C760 case histories)

4.11 Conclusions

Traditionally excavations are studied as plane strain problems, analysing a cross-section to assess retaining system performance and ground movement field and for the design of retaining walls, propping systems, etc.

This chapter highlights the impact of the actual excavation geometry and the associated three dimensional stress fields on the excavation performance. Soil stresses arching mechanisms developing behind excavation corners (corner effects) often result in a reduction in horizontal earth pressures acting on retaining walls in these zones.

The use of three dimensional soil-structure interaction simulation allows to capture these mechanisms, with significant benefits in terms of more accurate ground movement predictions and value engineering opportunities for retaining wall design.

In addition, the explicit consideration of the main basement structural elements (retaining wall, slabs, cores and foundations), is important in order to assess the holistic sub-structure behaviour and for the design of these elements.

Modelling assumptions are very important especially when using shell elements to model retaining walls. In particular, due to the two dimensional formulation of shells, anisotropic flexural rigidity must be set in order to reproduce actual retaining wall behaviour.

Following a review of three dimensional soil arching/corner effects, a Corner Optimisation Technique (COT) has been proposed, allowing the optimisation of retaining wall design. With reference to a piled retaining wall, the approach would consider the following value engineering strategies, in proximity of excavation corners:

- Increase pile spacing
- Reduce pile diameter
- Reduce reinforcement

The COT has been implemented by the author on a number of projects, resulting in substantial material savings, i.e. reduction in wall reinforcement of up to 30% (compared to plane strain) and reduction in wall embedment requirements, approaching excavation corners.

The analysis of a 20m deep excavation in London Clay has been presented. The results clearly indicate the three dimensional wall deformation mechanism, with wall deflections reducing moving towards an excavation corner. Capturing these mechanisms is considered essential when undertaking impact assessments on nearby structures, utilities or elements of infrastructure. The findings can also be used to inform value engineering exercises for the retaining systems and overall substructure.

CHAPTER 5

STABILITY AND SERVICEABILITY ASPECTS OF AN EXCAVATIO IN BOSTON BLUE CLAY

5.1 Background

This chapter focusses on selected aspects related to a deep excavation case history in Boston, USA. The author has been directly involved in the various phases of the project, from concept/feasibility to detailed design of the retaining walls and raft foundation.

A number of facets of the behaviour of the Boston Blue Clay (BBC) are examined, ranging from the evaluation of the stress-strain behaviour of the material to excavation stability and performance/serviceability aspects.

The following sections start with a description of the proposed project and key challenges involved. A detailed assessment of the ground model at the site is then presented, alongside considerations related to the BBC undrained shear strength, small strain stiffness and stiffness – strain degradation behaviour, based on advanced laboratory and in situ testing carried out at the site. The chapter subsequently focusses on aspects related to the stability of the proposed excavation, which is often a primary concern when working in these ground conditions. Considerations related to the behaviour of the excavation, in terms of time dependent heave of the excavation base, are then presented.

5.2 Research Objectives

The study presented in this chapter follows the author's working experience on the Harvard Allston Science Complex (HASC) project. The main aims of the research presented are related to the following aspects:

- Experimental investigation of the strength (section 5.4.2) and stiffness properties (sections 5.4.3, 5.4.4 and 5.4.5) of the BBC by means of advanced testing.
- Assessment of the relevance of strength anisotropy and three dimensional collapse mechanisms in base stability calculations/analyses (section 5.5).
- Observed time dependent performance of the excavation base (section 5.6).

Laboratory tests have been performed using the conventional triaxial cell and direct simple shear apparatus, following selection of suitable specimens aided by X-ray scanning of the core samples.

The in situ testing presented comprise seismic piezocone and self-boring pressuremeter testing. In particular, with regard to the latter, the author is not aware of the existence of data from this testing technique, from previous case histories in BBC.

The investigation has mainly focussed on evaluating the undrained shear strength and stiffness properties of the BBC. The main objectives of the experimental investigation are summarised below:

1) Laboratory testing:
   - Explore and evaluate the BBC undrained shear strength anisotropy and compare the findings with available testing data from the literature.
   - Explore aspects of the BBC behaviour related to its sensitivity and structure.
2) In situ testing:
   - Review small strain stiffness data and compare it with testing data from other sites in Boston.
   - Explore the relationship of the BBC small strain stiffness and parameters such as void ratio, stress state and over-consolidation ratio.

- Explore the BBC stiffness degradation with strain, based on data from self-boring pressuremeter testing.

Based on the evaluated undrained shear strength properties, a series of calculations and analyses have been carried out to evaluate the factor of safety with respect to base stability failure mechanism. The findings have been reviewed, in order to investigate a suitable choice of parameters for this type of assessment.

A parametric study has been carried out, in order to assess the influence of the excavation aspect ratio (excavation plan size in relation to its depth) on the three dimensional collapse mechanism and associated factors of safety.

The last part of the study focusses on the observed time dependent behaviour of the clay beneath the excavation base and explores the suitability of the partially drained (as opposed to undrained) assumption for the design of the raft foundation.

A back-analysis of the retaining walls performance for the HASC project has been undertaken by Elia et al. (2016) and Rouainia et al. (2017). The study of the retaining wall serviceability behaviour is outside the scope of the study presented herein.

5.3 HASC project

The HASC site is located in the western part of Boston, on the southern side of the Western Avenue, as shown in Figure 5.1. The site occupies a broadly square area, of approximately 150m x 150m.

The proposed HASC scheme comprises four 6 to 8-storey buildings, with a common 15 to 17m deep basement, which covers the entire site footprint. An indicative view of the proposed development is presented in Figure 5.2. Significant areas of the site, between the proposed buildings, do not have any superstructure above ground level, and are therefore characterised by relatively limited loading acting on the foundation.

The temporary earth retention system comprises diaphragm walls with four levels of ground anchors. An internal permanent reinforced concrete wall is then constructed along the basement perimeter, to form the permanent retaining wall. This internal wall is restrained by the basement permanent slabs, at various levels.

A 1.5m thick raft foundation is proposed, with a permanent underdrainage system installed beneath the raft, to prevent groundwater uplift pressure build up. The underdrainage system comprises a compacted granular layer, with a network of slotted drainage pipes leading to a number of sumps located across the basement footprint.

Due to the relatively limited building loading, in comparison with the unloading associated with the excavation works, a general ground heaving mechanism is anticipated as a result of the proposed works.

Figure 5.1 HASC site location

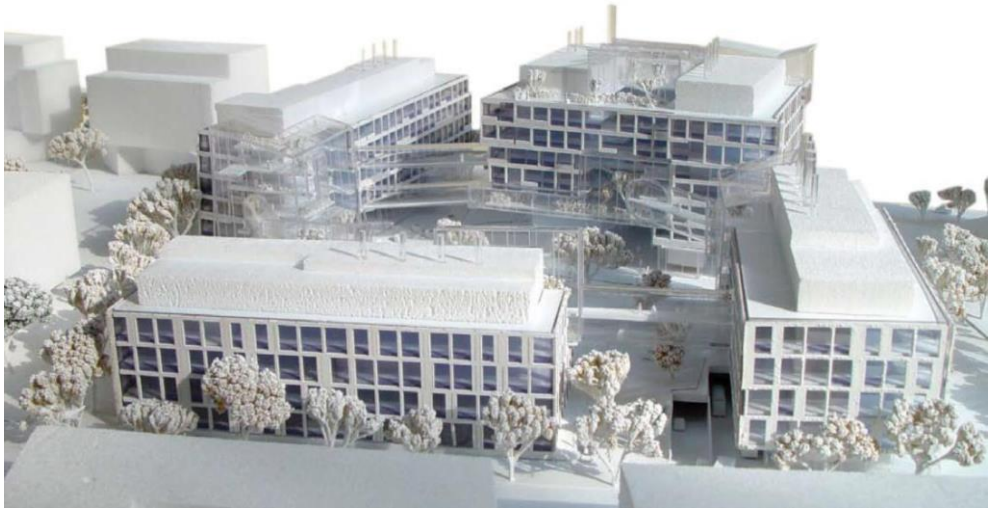

Figure 5.2 Indicative view of the proposed HASC scheme

Figure 5.3 Aerial view of the site during the basement excavation works

Figure 5.4 View of the site during basement excavation and construction

5.4 Ground conditions

5.4.1 General

Ground conditions at the HASC site typically comprise 1m of Made Ground overlying alluvial deposits, mainly comprising medium dense sands and gravels to an approximate depth of 5m below ground level. The BBC underlies the sands and gravels with an overall thickness ranging from 25m to 35m. The BBC, in turn, is underlain by a thin layer of predominantly cohesionless Glacial Till, with bedrock (Cambridge Argillite) at a depth of approximately 34 to 45m below ground level.

Vibrating wire piezometer data indicated a generally hydrostatic pore water pressure distribution, throughout the various strata, with a groundwater table typically located at 1.5m to 3m below ground level, within the sands and gravels.

The BBC is a marine illitic clay present throughout the Boston area. It is a relatively recent deposit (approximately 13000 years old, Kenney, 1964) generally characterised by low plasticity (Liquid Limit and Plasticity Index in the ranges 24 – 48% and 13 –

29%, respectively). The stratum comprises, in the upper part, a relatively stiff crust, over-consolidated due to historical fluctuations of the groundwater table and post sedimentation ageing phenomena. The graphs in Figure 5.5 give an overview of the properties of the BBC deposit. Atterberg limits and in situ moisture content values are shown in Figure 5.5a. Figure 5.5b indicates the OCR profile with depth. Figure 5.5c indicates the coefficient of earth pressure at rest (k_0) variation with depth. The material's direct simple shear undrained shear strength profile is presented in Figure 5.5d.

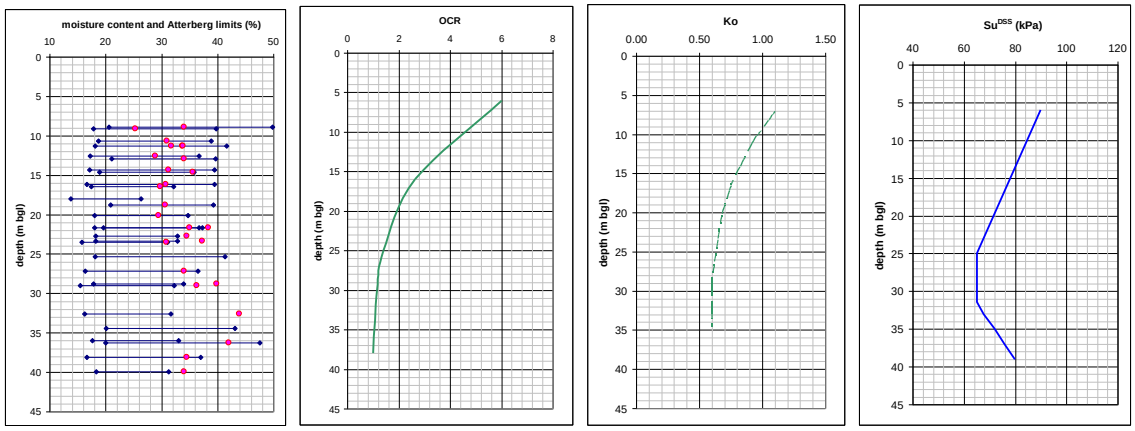

(a) (b) (c) (d)

Figure 5.5 Overview of the BBC properties

5.4.2 BBC undrained shear strength

The undrained shear strength of a clay is a parameter commonly used in simple total stress calculations, to evaluate the stability conditions of a geotechnical system. For stability assessments, it is important that the appropriate undrained shear strength profile, associated with a particular relevant shearing mode, is adopted, depending on the anticipated loading path that the soil will experience.

Common laboratory testing techniques for assessing the shear strength include undrained triaxial tests (compression and extension) and direct simple shear (DSS) tests. An

isotropic or anisotropic (K_0) consolidation stage may be undertaken prior to shearing the sample (consolidated undrained testing).

The in situ structure and stress history of a clay deposit play an important role in the decision making process for the soil testing strategy.

Consolidation techniques and undrained shear strength testing

Two testing procedures can be adopted, which mainly differ in the manner of carrying out the reconsolidation stage, as schematically presented in Figure 5.6. They are the classic *Recompression* and the *SHANSEP* (*Stress History And Normalised Soil Engineering Properties*) techniques.

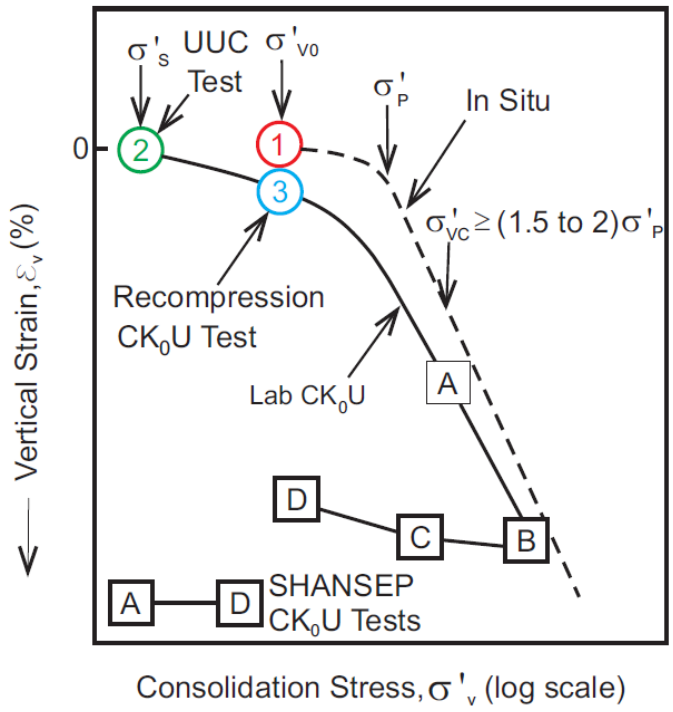

Figure 5.6 *Recompression* and *SHANSEP* consolidation procedure for laboratory testing (after Ladd (1991))

In the *Recompression* procedure (Bjerrum, 1973) the following testing stages are carried out:

- Consolidation of the sample to its in situ stress level.
- Testing the sample following a particular mode of shearing (triaxial or DSS, for example).

The method assumes that the reduction in water content associated with the sampling and reconsolidation process is negligible, so that the sample tested has roughly the same void ratio (and therefore strength) as in situ.

The *SHANSEP* procedure (Ladd & Foot, 1974), is based on the experimental evidence that, for many clays, the undrained shear strength for a particular shearing mode is related to the stress history of the material. The method is applicable for soils that exhibit normalised behaviour and it is indeed founded on the observation of existence of normalised soil parameters. The following testing stages are followed:

- Consolidation of the sample to a stress level beyond the pre-consolidation pressure (i.e. the maximum stress the sample has ever experienced in situ).
- Sample unloading to define a specific over-consolidation ratio (*OCR*).
- Testing the sample following a particular mode of shearing (triaxial or DSS, for example).

The undrained shear strength evaluated is normalised, using the pre-shearing vertical effective stress (S_u/σ'_v). The method is based on the existence of a relationship between S_u/σ'_v and the *OCR* for a given shearing mode.

$$\frac{S_u}{\sigma_v'} = S \cdot (OCR)^m \qquad (5.1)$$

where $S=S_u/\sigma_v'$ for normally consolidated soil and m is a strength increase exponent, usually 0.8±0.1 (Sheahan (1991)). A graphical representation of the relationship for a number of different clays is presented in Figure 5.7 (Ladd et al. (1977)) with reference to DSS testing.

The application of *SHANSEP* data for design purposes is founded on an accurate knowledge of the stress history (*OCR* profile) of the clay deposit. High quality consolidation testing data is required.

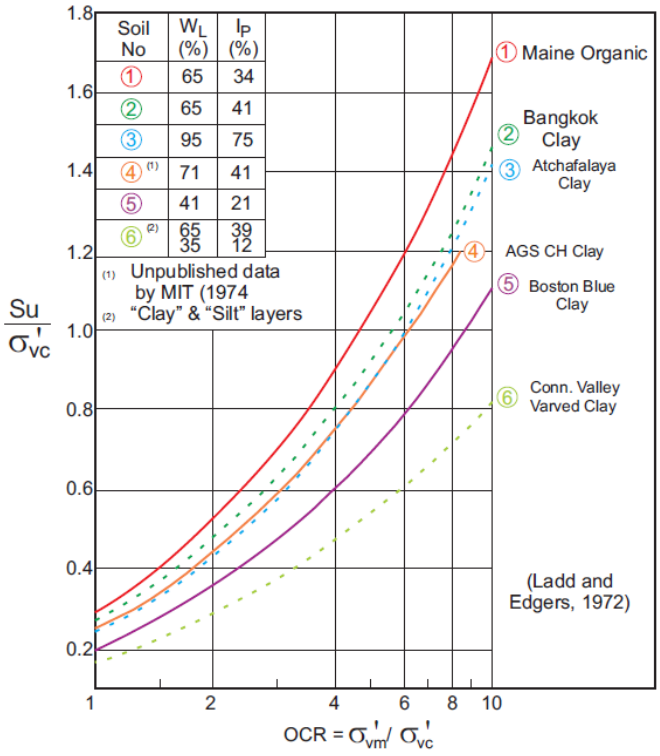

Figure 5.7 Typical SHANSEP test program results (after Ladd et al. (1977))

The *SHANSEP* technique aims to overcome sampling disturbance and associated reduced void ratio when reconsolidating the sample to its in situ stress. Ladd & Foot (1974) noted that "…*since changes in void ratio associated with soil swelling are much smaller than those associated with virgin compression, over-consolidated soils will always plot below the virgin compression line…".* This phenomenon is particularly evident for normally consolidated soils (see schematic representation in Figure 5.8, after Ladd & Foot (1974)).

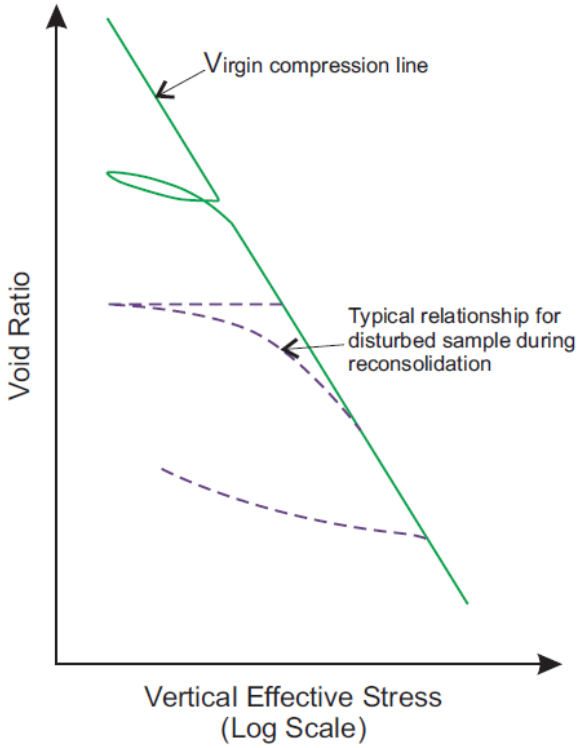

Figure 5.8 Idealised plot showing effect of sample disturbance (after Ladd & Foot (1974))

BBC structure

Burland (1990) examined the relationship between the properties of naturally sedimented clays and one-dimensionally consolidated reconstituted clays, the latter being a clay that has been thoroughly mixed at a water content equal to or greater than the liquid limit (w_L). The author introduced the concept of void index (I_v), defined as follows:

$$I_v = \frac{e - e^*_{100}}{e^*_{100} - e^*_{1000}} \tag{5.2}$$

where e^*_{100} and e^*_{1000} are the void ratios of the reconstituted material at a vertical effective stress of 100 and 1000kPa, respectively.

Burland (1990) defined the intrinsic compression line (ICL), a compression line representing the behaviour of many normally consolidated reconstituted clays with a wide range of liquid limits. The ICL is plotted in Figure 5.9 in a σ'_v-I_v space.

The framework also defines a sedimentation compression line (SCL), representing the in situ stress state of a large range of normally consolidated natural sedimentary clays having sensitivities in the range 2–9 (Cotecchia & Chandler, 2000). The difference between ICL and SCL is due to the difference in structure of reconstituted and natural clays, the latter having in general a more opened structure. The framework introduced by Cotecchia & Chandler (2000) indicates that the sedimentation compression curve for a clay deposit should be related to the particular clay sensitivity (see Figure 5.9).

The SCL is plotted in Figure 5.10 as an indicative curve. This SCL does not necessarily coincide with the sedimentation compression curve (SC) for the natural BBC at the site examined here.

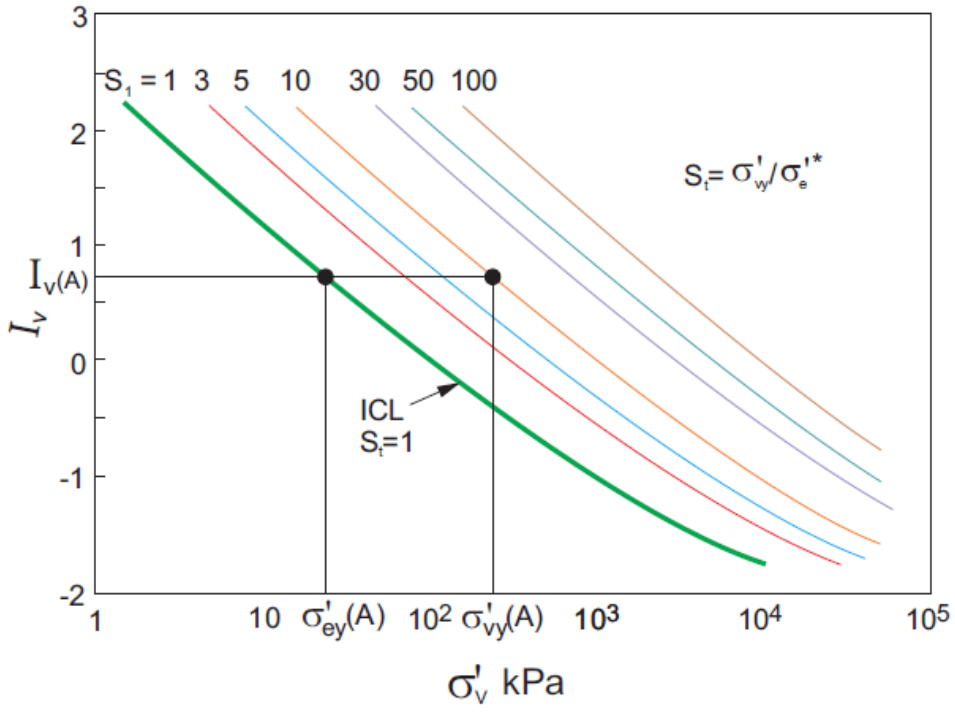

Figure 5.9 Sedimentation compression curves in the idealized sensitivity framework (after Cotecchia & Chandler, 2000)

Using the correlations provided by Burland (1990) and adopting an average liquid limit ($w_L=36.8\%$), it was possible to estimate the constants of intrinsic compressibility (Terzaghi (1925)), $e^*_{100}=0.73$ and $C^*_c=0.223$. Using the same procedure, Santagata & Kang (2007) obtained $e^*_{100}=0.853$ and $C^*_c=0.282$ for resedimented BBC. Skempton (1944) provided measured values of the constants, obtained through oedometer tests on reconstituted BBC, $e^*_{100}=0.80$ and $C^*_c=0.21$.

The in situ stress state of a number of samples is plotted in the I_v-σ'_v space in Figure 5.10. Indicative points from Sheahan (2005) and Santagata & Kang (2007) are also plotted for comparison. The BBC in situ stress state points lie well above the SCL, demonstrating a degree of structure which characterises the natural BBC.

An indicative range within which the SC line for the BBC at the examined site would fall, is presented in Figure 5.10.

Constant rate of strain consolidation (CRSC) test loading curves are plotted in Figure 5.11 (normally consolidated BBC) and Figure 5.12 (over-consolidated BBC) together with ICL and SCL, in e-σ'_v space. The indicative range of possible SC curves is also included in both of the figures.

In Figure 5.11, the in situ stress states for the two samples are also shown, indicating a substantial agreement between in situ stress level and yield stress for the normally consolidated BBC. This indicates that the yield stress ratio ($YSR=\sigma'_{vy}/\sigma'_{vo}$ - Burland, 1990) is in the same order of the OCR. This is consistent with the consolidation curves presented by Sheahan (2005) for deep BBC.

The curves in Figure 5.11 indicate a reduction in stiffness after reaching the yield condition. The reduction is particularly abrupt for the top curve. This is related to the high void ratio (i.e. more open structure) that the sample has in its in situ condition. After the initial post-yield reduction in stiffness (more or less abrupt), the curves fall more gently towards the SCL, however are still relatively far from crossing it. Progressive convergence towards the ICL is anticipated, were stress levels to continue increasing.

The over-consolidated samples in Figure 5.12 show a more gradual fall in stiffness at yielding. This may be due to the fact that the lower void ratio of the over-consolidated clay makes it inherently less susceptible to the sharper drop in stiffness observed with the normally consolidated material. The majority of the curves in Figure 5.12 show yielding before the SC min curve is reached. A similar pattern of behaviour was found by Sheahan (2005). This behaviour may be attributed to differences in deposition conditions (i.e. different SC curves) between different BBC zones, although the clay deposit is expected to have a common consolidation history (Kenney (1964)).

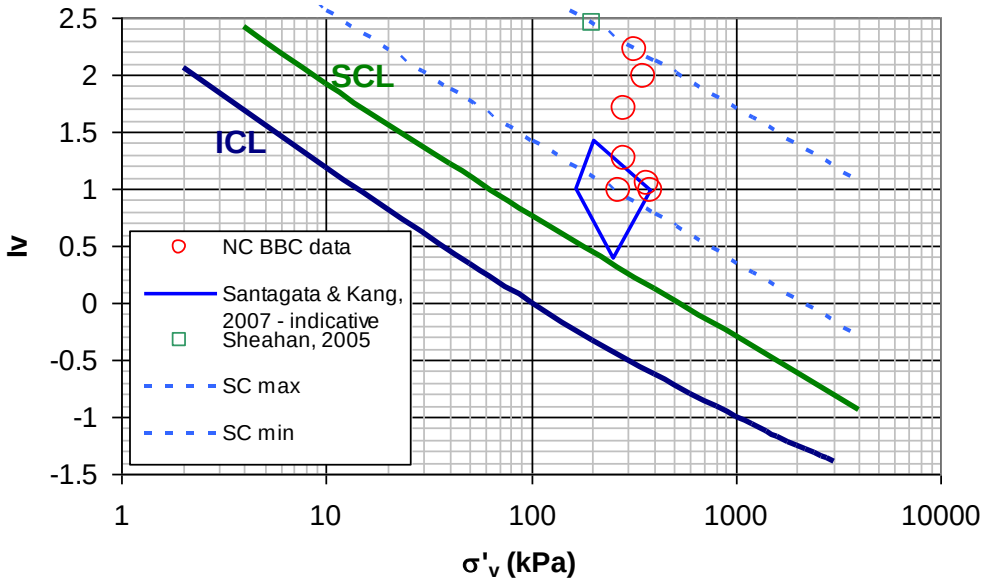

Figure 5.10 In situ conditions for natural NC BBC

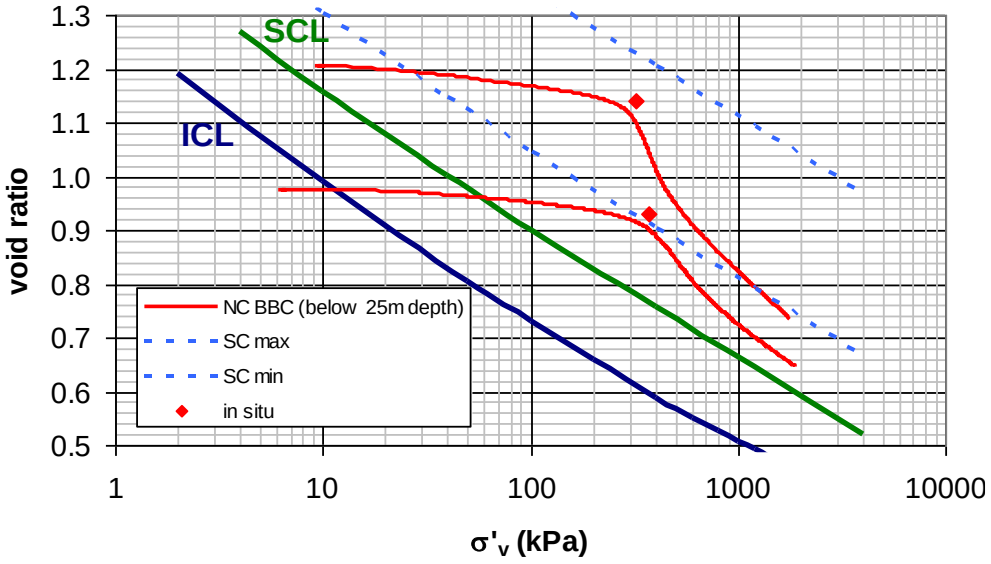

Figure 5.11 Results from CRSC tests on natural NC BBC

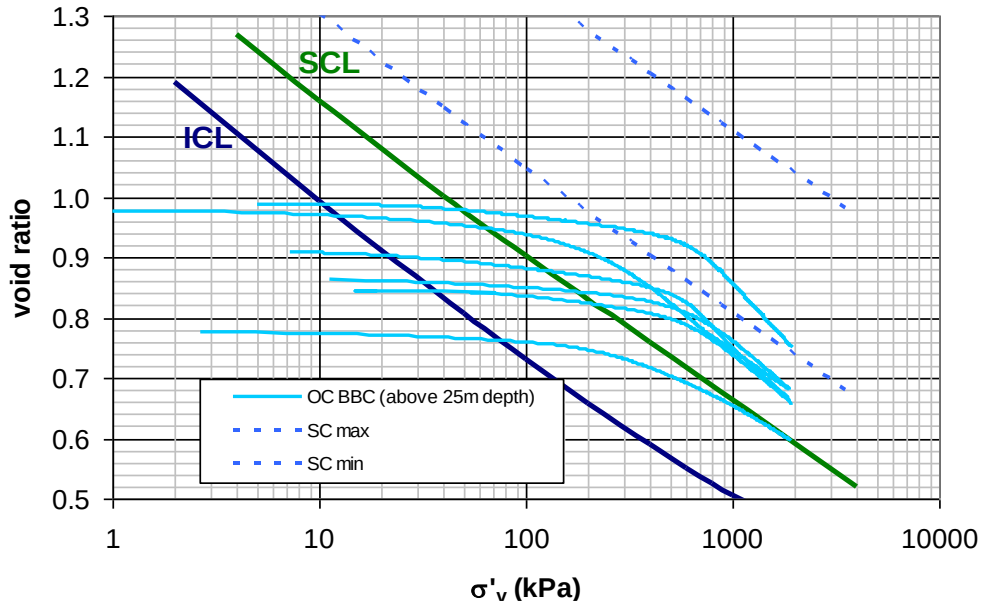

Figure 5.12 Results from CRSC tests on natural OC BBC

Use of the SHANSEP procedure

Burland (1990) investigated the behaviour of a North Sea clay deposit (Troll field site), characterised by the presence of two layers for which the different deposition conditions and associated material structures have a significant effect on the in situ stress state and mechanical properties. On the basis of the material response in one dimensional compression, Burland indicates that, for normally consolidated clays for which the in situ stress state lies on or above the SCL, the *SHANSEP* test procedure alters the structure of the clay and therefore underestimates both the peak strength and the brittleness of the clay. In contrast, the *SHANSEP* procedure provides a reasonable normalised pattern of the behaviour for the natural material (for a clay which lies in relative proximity to the ICL). In this case, the structure is not significantly changed during the initial consolidation.

Other authors have explored the applicability of the *SHANSEP* procedure from a more qualitative perspective.

Sheahan (1991) indicates that the *SHANSEP* technique is only applicable for uniform cohesive soils that have been mechanically over-consolidated, or are truly normally consolidated and exhibit behaviour that can be normalised by pre-shear consolidation stresses. The technique is not intended to be used in cemented, highly sensitive clays, or in a drying crust of a soil deposit.

Ladd & De Groot (2003) and Santagata & Germaine (2005) indicate that the *Recompression* technique can result in an unsafe evaluation of undrained shear strength of normally consolidated clays, and is generally more appropriate for over-consolidated clays. The *SHANSEP* technique generally produces relatively conservative undrained shear strength estimates and results which are particularly appropriate for normally consolidated clays. The latter procedure is not particularly appropriate for weathered over-consolidated clay crusts, which are not mechanically over-consolidated through loading/unloading.

According to Seah & Lai (2003), the *SHANSEP* technique can be applied to fairly uniform clay deposits, while the *Recompression* technique is more appropriate with

highly structured, brittle clays, such as high sensitivity clays, cemented cohesive soils, weathered clay crusts and heavily over-consolidated deposits.

SHANSEP testing on Boston Blue Clay

As previously mentioned, the BBC stratum at the HASC site is characterised at the top by a relatively stiff crust, over-consolidated due to historical fluctuations of the groundwater table. The stress history of the BBC deposit was investigated by performing a suite of CRSC tests on high quality undisturbed samples. The CRSC testing curves are presented in Figure 5.13. Figure 5.14 shows the evaluated OCR profile with depth.

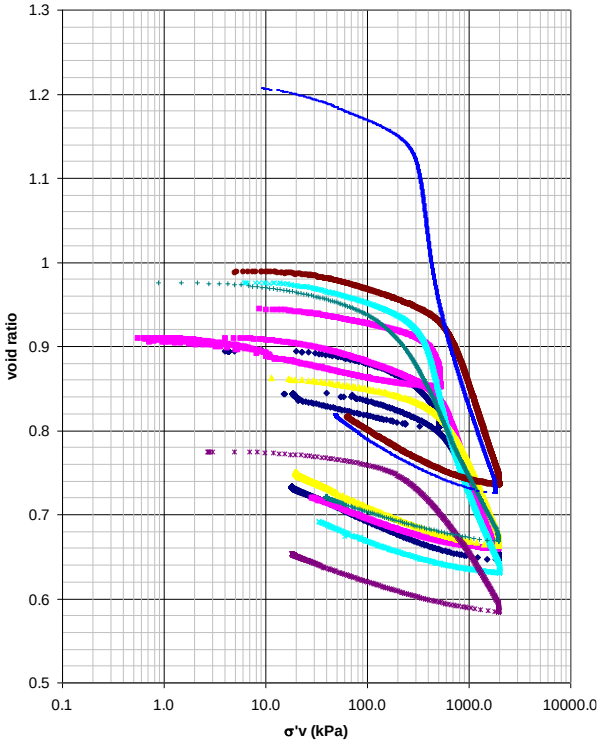

Figure 5.13 CRSC testing on a number of BBC samples

Although the data presented in Figure 5.10 indicates a relatively high sensitivity for the BBC, the one-dimensional consolidation curves (Figure 5.11 and Figure 5.12) show that

even at relatively high stress levels (1.5MPa, equal to the upper bound of the *SHANSEP* consolidation stresses used) the stress state remains quite far from the ICL. Therefore the change in structure associated with the *SHANSEP* reconsolidation phase is likely to be relatively limited and will produce conservative estimates of the peak strength.

Furthermore, although the *SHANSEP* method does not appear particularly appropriate to investigate the stress-strain behaviour of the BBC, it has been widely used in the past to assess the undrained shear strength of this clay and should provide slightly conservative estimates of S_u, particularly for the normally consolidated material. In this specific case study, the *SHANSEP* method has been adopted, in order to avoid the potential overestimation of the strength associated with the classic *Recompression* technique.

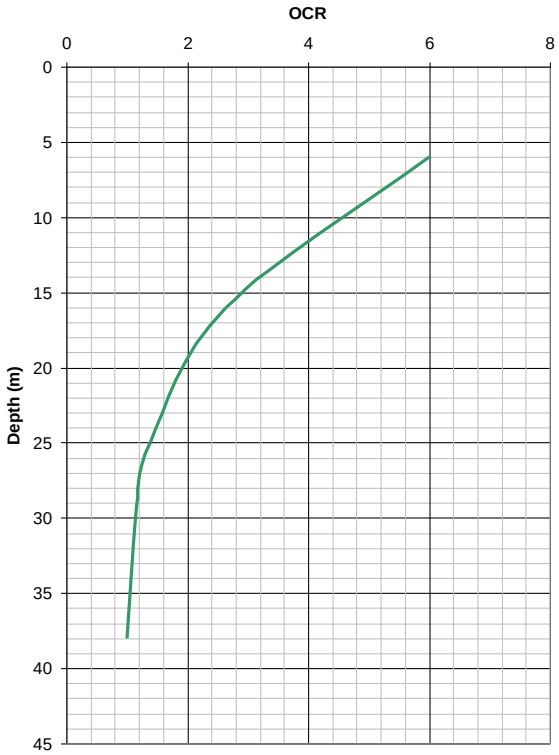

Figure 5.14 Indicative BBC OCR profile with depth

Anisotropically (K_0) and isotropically consolidated *SHANSEP* triaxial extension (TE), triaxial compression (TC) and direct simple shear (DSS) tests were carried out on undisturbed BBC samples to investigate the undrained shear strength of the material.

Fixed piston tube samples were subjected to x-ray radiography to assess the sample quality and to assist in the selection of the samples to be tested. Figure 5.15 shows one of the radiography images, clearly indicating thin laminations within the material. The laminations lay on sub-horizontal planes also in close proximity to the sampling casing, denoting the high quality samples retrieved.

The samples were consolidated to 10% axial strain and then the stress was held for 24 hours to allow for some secondary compression.

Normalised undrained shear strength data are presented in Table 5.1 for different modes of shearing and various OCRs (TC and TE data at OCR>1 are extrapolated using the DSS increments as reference).

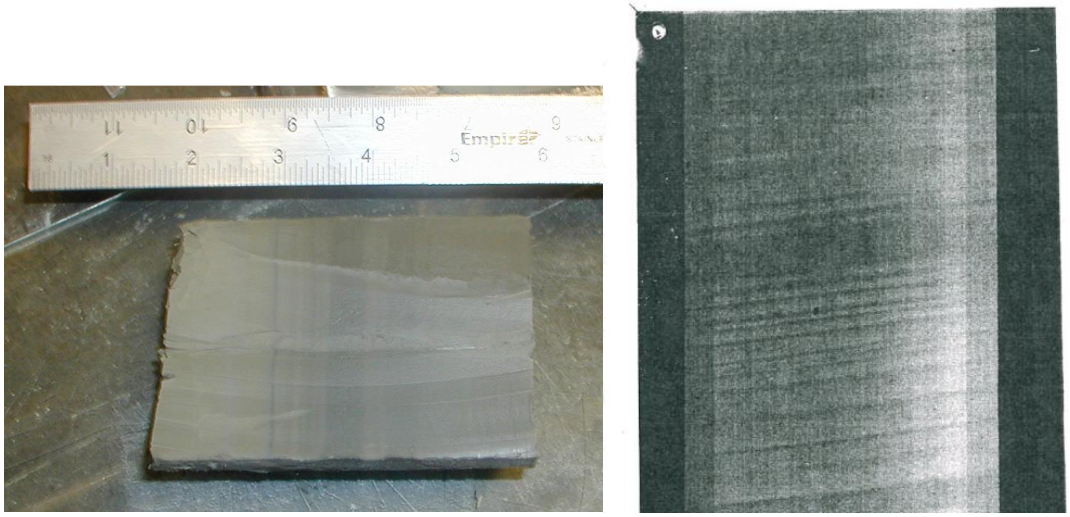

Figure 5.15 X-ray radiography image from one of the BBC samples

Table 5.1 S_u/σ'_v for range of OCR

OCR	S_u/σ'_v		
	DSS	TC	TE
1	0.2	0.27	0.15
1.5	0.27	0.36[1]	0.20[1]
2	0.35	0.47[1]	0.26[1]
4	0.65	0.88[1]	0.49[1]

Notes:

[1] extrapolated

The normalised DSS undrained shear strength data are compared with data from Ladd et al. (1999) in Figure 5.16. The red square symbols indicate data points from the present study (the value for OCR=1 is the average of a number of tests). Note that Ladd et al. (1999) separated the over-consolidated crust data (Upper Clay) from the normally consolidated material (Lower Clay) data.

The values from the present study lay slightly above the Ladd et al. (1999) data. Note that the values for OCR=1.5, 2 and 4 are from material sampled at approximately 20m depth, in the lightly over-consolidated zone.

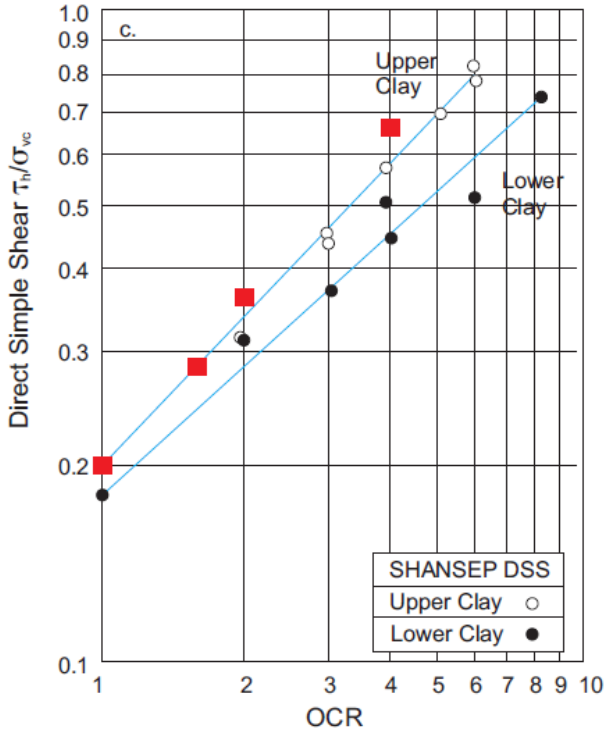

Figure 5.16 Comparison with Ladd et al. (1999) data

In the present study, soil stiffness at various strain levels has been measured by means of instrumented DSS and triaxial testing on undisturbed samples of BBC. Normalised soil stiffness values (E_u/σ'_v) evaluated with the *SHANSEP* DSS testing are presented in Figure 5.17. The data points do not seem to follow a specific pattern with varying OCR, indicating the inappropriateness of the *SHANSEP* testing technique for assessing the BBC stress-strain behaviour (Ladd et al. (1999)).

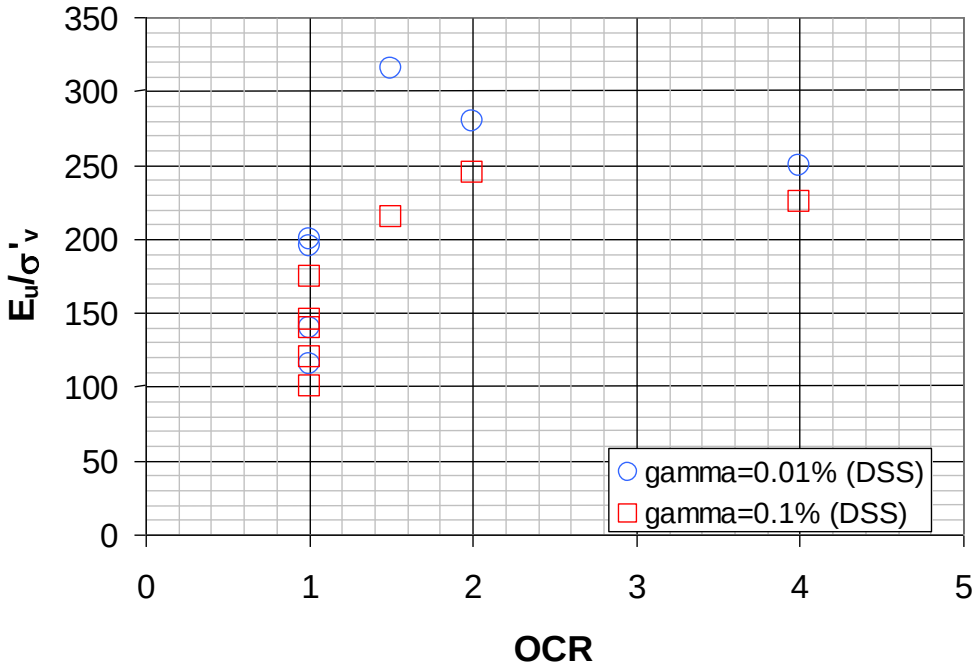

Figure 5.17 Normalised undrained Young's Modulus as function of the OCR

Figure 5.19, Figure 5.20 and Figure 5.22 present the stress-strain curves obtained from the triaxial (TC & TE) and DSS tests. Stress paths are plotted in Figure 5.18 and Figure 5.21 (σ'_{vc}: pre-shear consolidation stress; σ'_{vm}: maximum consolidation stress applied in the laboratory). Significant strain softening behaviour is observed at high strain levels in the TC and DSS tests. Following Burland (1990) considerations, the brittleness in the material behaviour is likely to be smoothed and the peak strength underestimated.

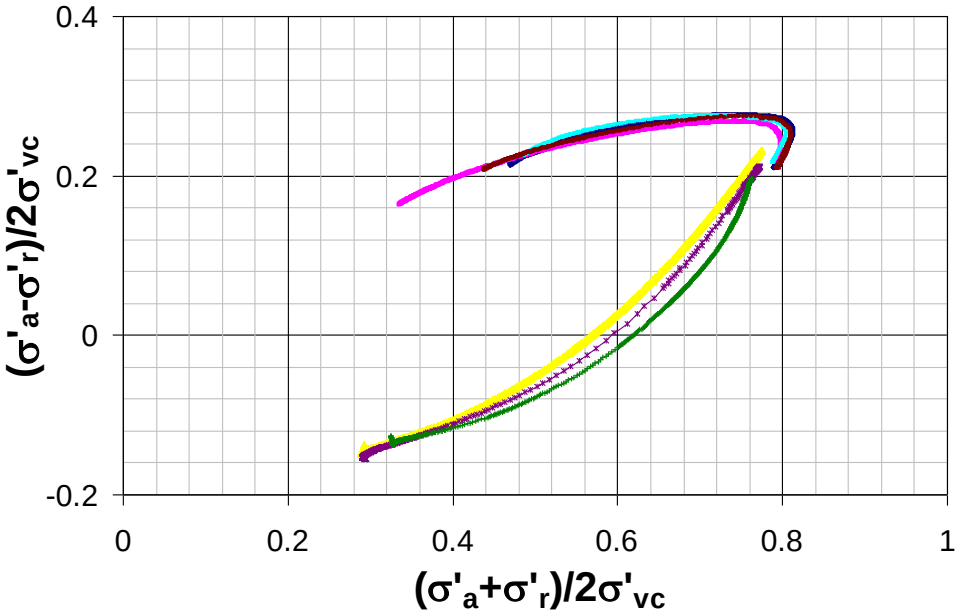

Figure 5.18 K0 consolidated (SHANSEP, OCR=1) undrained triaxial (TC & TE) tests

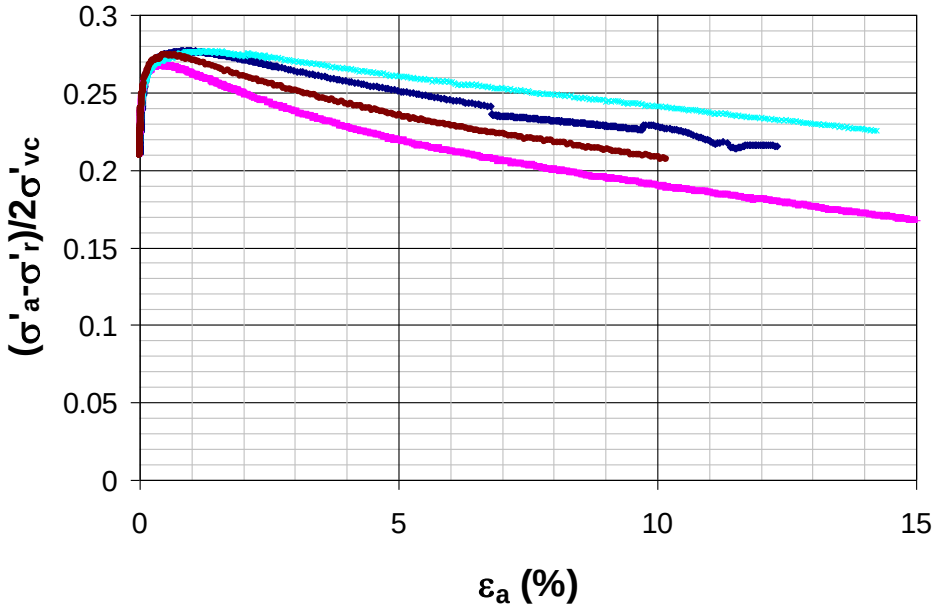

Figure 5.19 TC tests

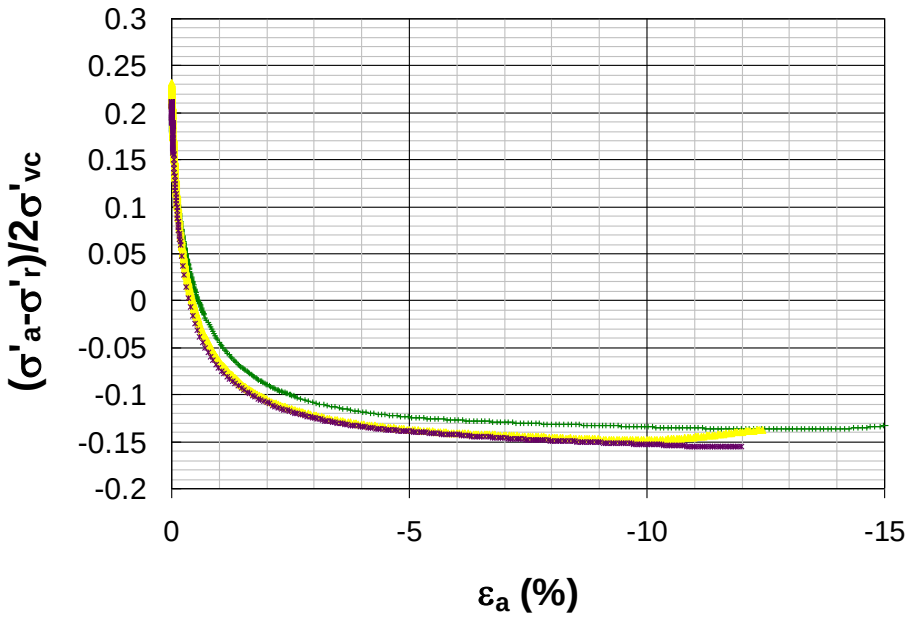

Figure 5.20 TE tests

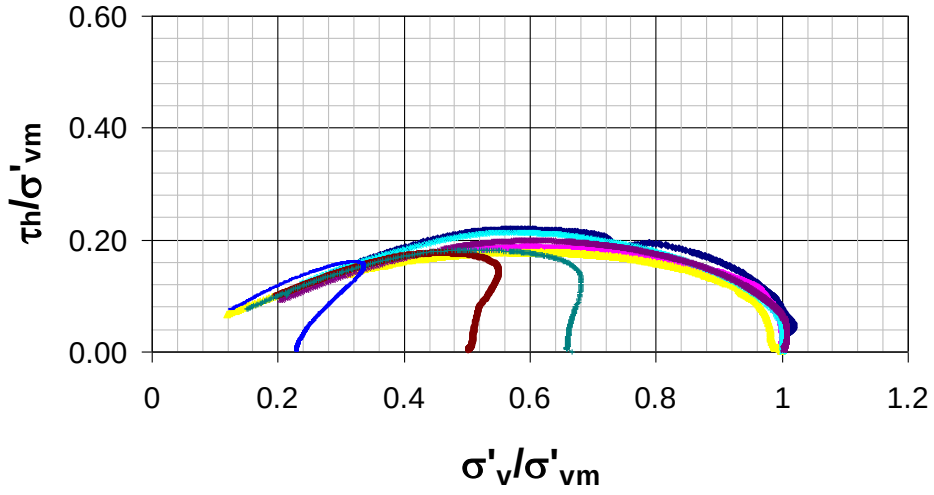

Figure 5.21 Isotropically consolidated (SHANSEP, various OCRs) undrained DSS tests

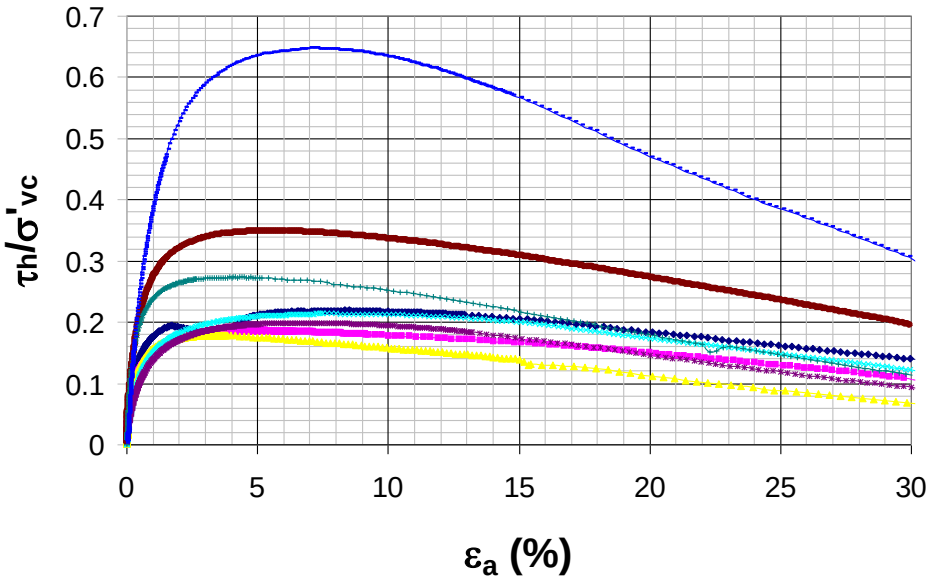

Figure 5.22 DSS tests

Comparison with in situ testing

In situ testing was undertaken to characterise the undrained shear strength profile of the BBC stratum, namely Field Vane (FV) and Cone Penetration (CPTu) tests.

The undrained shear strength is calculated from the FV torque readings using the following relationship:

$$S_u = \frac{6M}{7\pi D^3} \qquad (5.3)$$

where: M is the torque at failure and D is the diameter of the vane. The FV undrained shear strength values were corrected taking into account average liquid limit (LL) and an estimate of the over-consolidation ratio (OCR) with depth using the formula given by Larsson and Ahnberg (2005). The correction factor varied with depth between 0.83 and 1.06 with a mean of 0.95.

The undrained shear strength is computed from the CPTu cone tip resistance test data using the following relationship:

$$S_u = \frac{q_t - \sigma_v}{N_k} \tag{5.4}$$

where: q_t is the corrected cone resistance, σ_v is the total in situ stress and N_k is the cone factor. The derivation of the N_k value is critical and careful judgment is required in its selection. N_k values, varying between 12.07 and 15.36 as function of OCR, are determined to represent DSS shearing, using the procedure established by Mesri (2001).

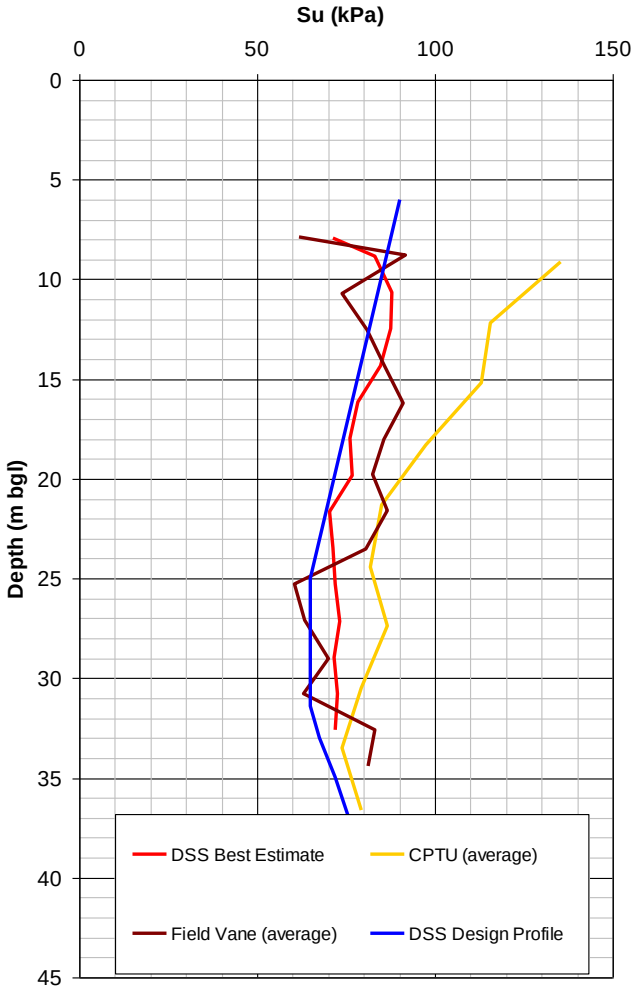

Figure 5.23 BBC Su (Direct Simple Shear (DSS) equivalent) profile with depth

The average S_u profiles from FV tests and CPTu are presented in Figure 5.23, together with the undrained shear strength profile evaluated in the laboratory using the *SHANSEP* technique. The DSS design line adopted is also shown.

The CPTu strengths are remarkably higher than the DSS *SHANSEP* data, particularly in the upper BBC crust zone. The FV data show a good agreement. This is in contrast with the data presented by Ladd & Foot (1974) for MIT-MDPW embankment test section site, for which the FV data were closer to a Plane Strain Passive (PSP, 2d extension) mode of failure.

The range of results from the suite of undrained shear strength laboratory testing is compared with in situ testing results. This comparison confirms a general agreement between *SHANSEP* DSS and Field Vane test data.

In terms of stiffness, a comparison between laboratory stiffness data and data from a series of in situ self-boring pressuremeter tests is presented in Figure 5.24. The substantially softer behaviour exhibited by the *SHANSEP* laboratory testing data is evident.

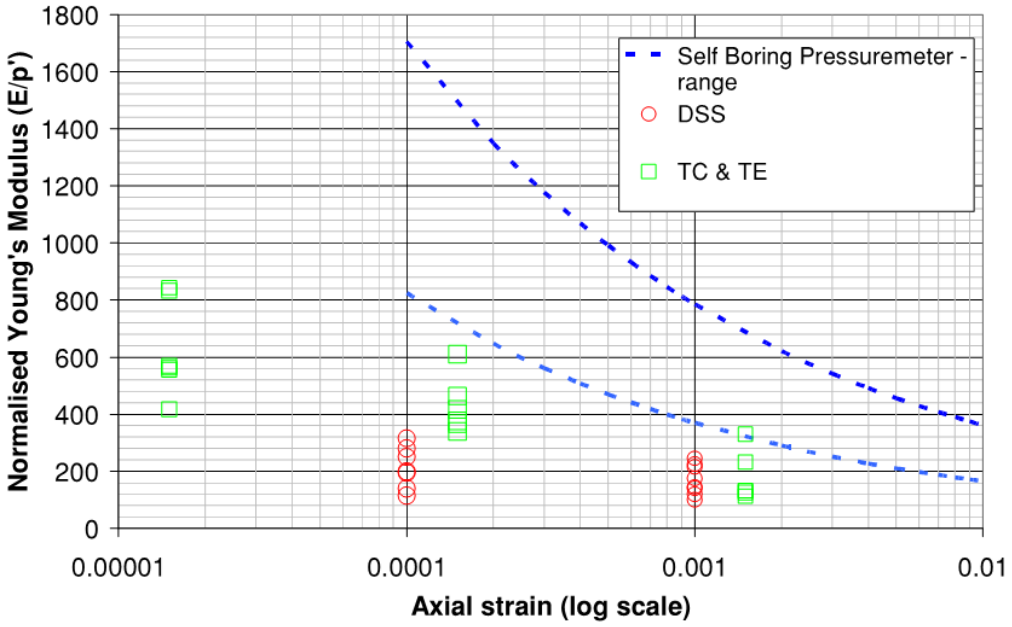

Figure 5.24 Stiffness comparison between SHANSEP tests and in situ self-boring pressuremeter tests

5.4.3 BBC stiffness within the small strain range

The high stiffness of soils at small strain levels is an important soil property which has implications in both dynamic and most static geotechnical problems, including excavations. Soils are renowned for their highly non-linear behaviour. However, at very small strain levels, of the order of 0.0001%, their behaviour can be assumed to fall with good approximation within linear elasticity. The small strain shear modulus (G_0) of natural BBC at the HASC site has been investigated with in situ seismic cone penetration testing. In this section, measured shear wave velocity profiles are compared with other three case studies from sites in Boston presented in the literature. The effect of a number of soil properties on G_0 is investigated and the importance of explicitly considering the void ratio in the G_0 formulation is discussed.

General

The stiffness at very small strains (G_0) is a relevant soil property in the prediction of the performance of geotechnical systems. This parameter, in combination with a suitable stiffness-strain degradation profile, is of particular relevance for analysing the behaviour of multi-supported retaining systems. Typical soil strain ranges for excavations and other geotechnical problems are indicated in Figure 5.25 (Atkinson 2000).

Experimental evaluations of G_0 are often based on laboratory or in situ measurement of the velocity of shear waves propagating through the soil.

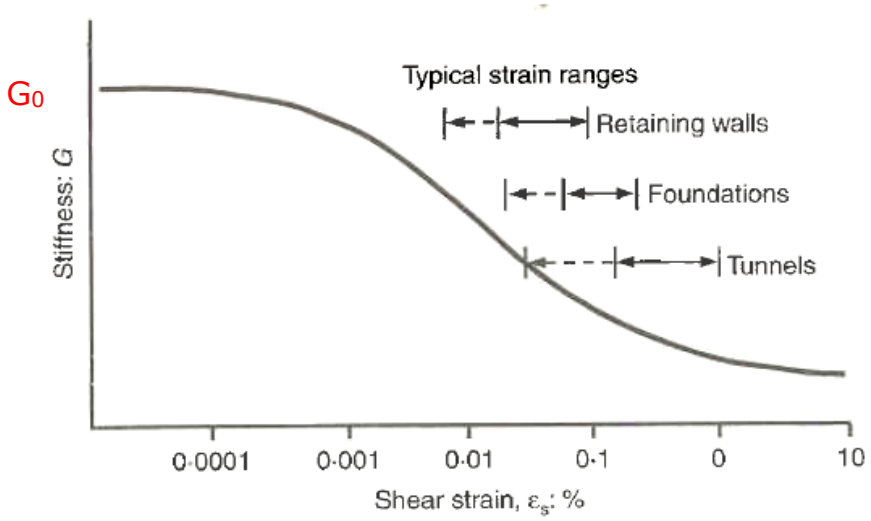

Figure 5.25 Characteristic stiffness-strain behaviour of soil with typical strain ranges for engineering systems (after Atkinson 2000)

Experimental evaluations of G_0 are often based on laboratory or in situ measurement of the velocity of shear waves propagating through the soil. Laboratory static measurements of G_0 can also be obtained by instrumenting the testing apparatus with small strain measurement devices.

Many researchers have investigated the effect of a number of factors on the clay small strain stiffness. These factors include stress state, void ratio, over-consolidation ratio (*OCR*), material structure, etc. A series of different formulations have been proposed to evaluate G_0.

Early work done by Hardin & Black (1968) pointed out the dependence of G_0 on soil structure, void ratio (e), current stress state (i.e. mean effective stress, p') and OCR, through a relationship of the type

$$G_o = S \cdot OCR^K \cdot f(e) \cdot p'^n \qquad (5.5)$$

where $f(e)$ is a function of void ratio, n and K are two constants and S is a term related to soil structure. The relationship can be normalised introducing a reference pressure as shown by Benz (2007).

More recent work by Viggiani & Atkinson (1995) indicated that the three parameters void ratio, stress and *OCR* are interdependent. Thus only two of these parameters are required to evaluate the small strain stiffness of soils (equations (5.6) and (5.7) below).

$$G_o = S \cdot OCR^K \cdot p'^n \tag{5.6}$$

$$G_o = S \cdot f(e) \cdot p'^n \tag{5.7}$$

A number of researchers (including Tatsuoka & Shibuya 1992, Jamiolkovski et al. 1995) indicated that the mechanical over-consolidation has a negligible influence on G_0.

The existence of a unique relationship between stress state and void ratio at each given *OCR* is confirmed by experimental evidence for reconstituted clays. For natural clays in their in situ conditions, this consideration may not be strictly applicable. For example for structured (as defined by Mitchell 1976 and Burland 1990) deposits, *OCR* cannot take into account the structure varying along the profile and ideally the structure parameter (*S*) should vary with depth. The adoption of a function of void ratio in the G_0 formulation (equation (5.7)) appears more appropriate. In fact, this parameter is influenced by the clay fabric (arrangement of particles) which may vary along a soil profile due to variable deposition conditions, not an unusual feature for many clay deposits (Burland 1990).

Experimental evidence shows that the shear wave velocity (directly linked to G_0) is independent of the normal stress in the direction perpendicular to the plane defined by wave propagation and polarisation directions (Poesler 1979). Therefore if *i*, *j* and *k* are three Cartesian axes, G_0ij is independent of σ'_k and can be expressed by the more general expression (Jamiolkovski et al. 1995)

$$G_{oij} = \frac{S_{ij} \cdot f(e) \cdot (\sigma'_i \, \sigma'_j)^{nij}}{p_r^{\,2nij-1}} \quad \text{where} \qquad f(e) = e^{mij} \tag{5.8}$$

where p_r is a reference stress (1kPa).

In situ measurements of v_s

Seismic cone penetration tests (SCPT) were undertaken at three locations to measure shear wave velocity (v_s) profile with depth, from which the small strain shear stiffness G_0 was calculated using the relationship

$$G_o = \rho \cdot v_s^2 \tag{5.9}$$

where ρ is the soil density. The seismic signals were recorded using a geophone mounted in the cone and an up-hole digital oscilloscope. A sledge hammer hit against a beam was used for the seismic source. Normal reaction for the beam was provided by the dead weight of the rig placed upon the beam. A schematic of the shear wave testing configuration is shown in Figure 5.26.

The measured shear wave velocity values generally ranged between 210m/s and 330m/s.

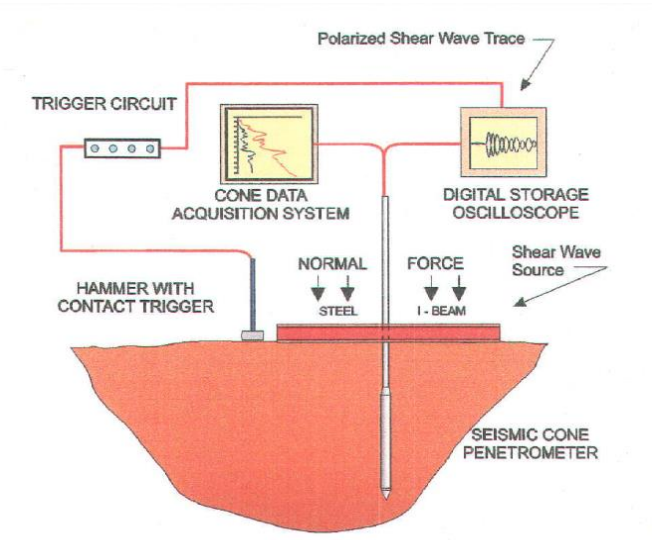

Figure 5.26 Scheme of seismic CPT configuration

Santagata (2007) presents shear wave velocity profiles for three sites in Boston (site locations are shown in Figure 5.27). Two of the sites (East Boston and South Boston)

were part of the Central Artery Tunnel (CA-T) project, while the third is at the Massachusetts Institute of Technology (MIT) Campus. Details of the seismic CPT testing procedures adopted for the MIT Campus and CA-T South and East Boston sites are presented by Santagata & Kang (2007).

Santagata & Kang (2007) found that values of v_s obtained from in situ testing at the three sites mentioned are approximately 50% larger than laboratory measurements using instrumented triaxial tests on resedimented BBC (RBBC).

The G_0 profiles at the three sites are presented in Figure 5.28, in comparison to the HASC data. The profiles for the three sites are rather consistent between them and show values lower than those observed at the HASC site in the over-consolidated crust. Similar values are observed below 30m depth.

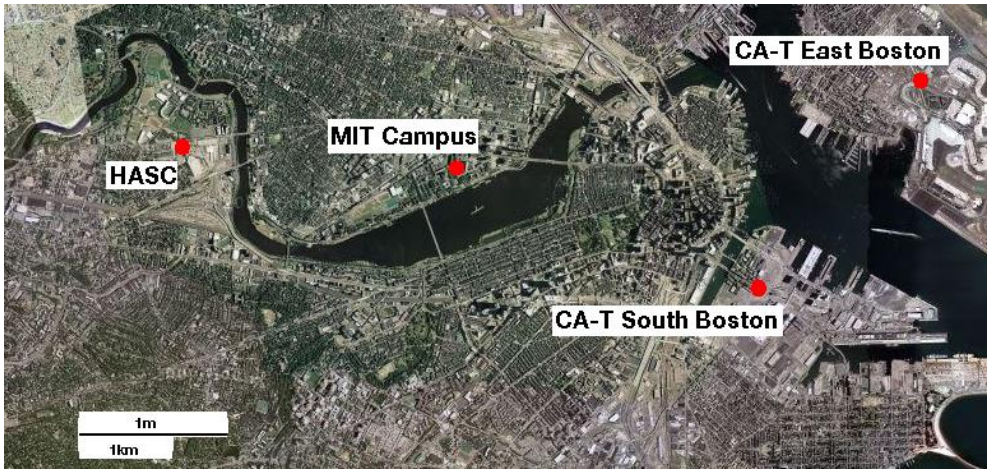

Figure 5.27 Site locations

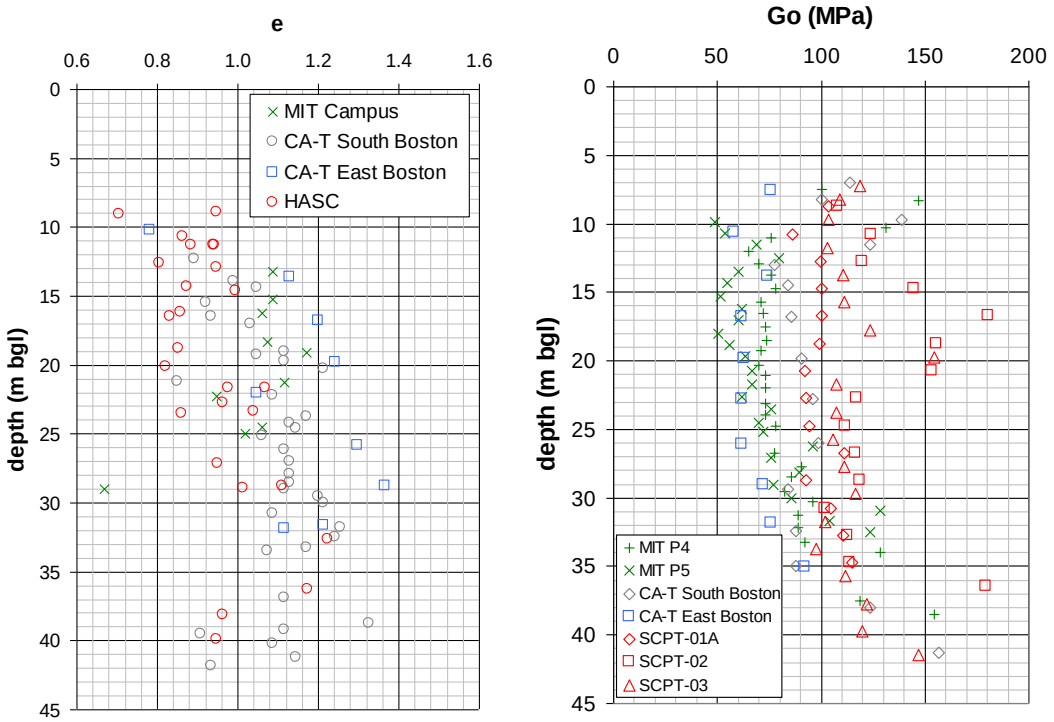

(a) (b)

Figure 5.28 Void ratio (e) and G_0 profiles

Interpretation of the G_0 profiles

The formulation proposed by Jamiolkovski et al. 1995 (equation (5.8)) is adopted to interpret the in situ G_0 profiles, determined using measured v_s data (equation (5.9)).

Cross-anisotropy is a widely accepted assumption to account for the directional variation of mechanical properties of natural soil deposits. The small strain stiffness (G_0) measured using the seismic CPT testing can therefore be indicated as G_{0vh}, where v and h represent the vertical and horizontal directions. The subscripts v and h are omitted in the following sections.

Data from laboratory triaxial tests, instrumented with particular small strain measurement devices (Santagata et al. 2005) are used to evaluate the material constants which appear in equations (5.8) and (5.9).

The parameters m and n have been evaluated through a curve fitting exercise (Nash et al. 2008) using the extensive collection of data presented by Santagata et al. 2005, based on instrumented triaxial tests on RBBC (only $d\varepsilon/dt=0.1\%/h$ rate of testing data were used). This was possible due to the consistent structure properties of the RBBC, in which "post sedimentation structure" (Cotecchia & Chandler 2000) and associated chemical/aging processes have not played a significant role. Figure 5.29 show the parameter evaluation graphs. $m=-1.6$ and $n=0.28$ result from the curve fitting procedure. S equal to 2750 was adopted in the curve fitting procedure.

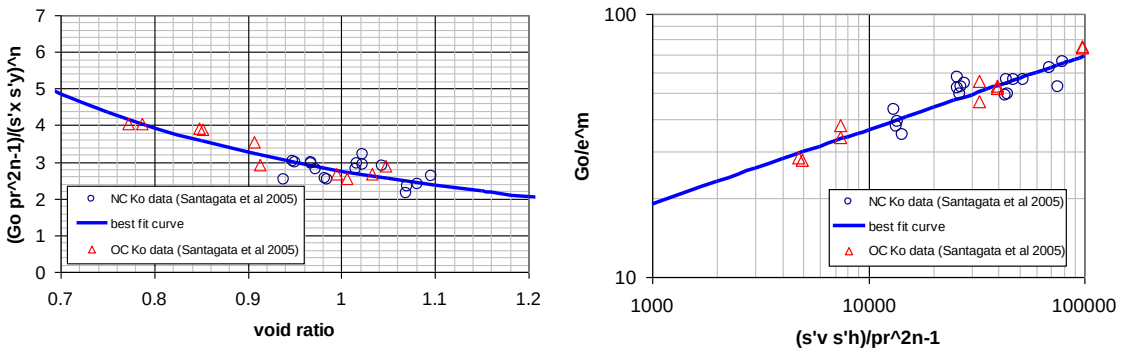

(a) (b)

Figure 5.29 G_0 normalisation (curve fitting)

Equation (5.8) has been used to interpret the G_0 profiles for the different sites. In the absence of laboratory measurements of shear wave velocity on natural BBC samples, ad hoc values of the structure parameter S have been adopted for the various sites in order to best represent the in situ v_s profiles. The S values adopted are presented in Table 5.2. The difference between the in situ S ($S_{in\ situ}$) and the S value used to interpret the RBBC laboratory data (S_{RBBC}) used previously (Santagata et al. 2005) should depend mainly on post sedimentation processes which affect the clay structure.

Table 5.2 S values adopted

MIT Campus	4500
South Boston	5500
East Boston	5000
HASC	5500

The void ratio data from the four sites are compared in Figure 5.28. The following considerations can be made:

- The HASC void ratio profile shows lower values than the other sites over the top portion of the deposit (i.e. above 30m depth)
- The East Boston void ratio profile shows higher values than the other sites above 30m depth

The calculated G_0 profiles at the four different sites are compared with the experimental data in Figure 5.30. The void ratio based formulation gives relatively good estimates of the G_0 profiles for the various sites (with the exception of the normally consolidated zone at the MIT Campus, where G_0 is overestimated).

In view of the expected similar age of the deposits at the four sites, it seems reasonable that the S values fall in a rather narrow range, assuming that clay mineralogy and other factors responsible for the development of a post-sedimentation structure are consistent at the various sites. As shown in Table 5.2, the S values adopted to best reproduce the in situ G_0 profile are rather consistent for the four sites.

The fact that the HASC G_0 profile is higher than the other sites in the crust and similar in the normally consolidated zone appears to indicate the significant effect of the void ratio on the small strain stiffness. As discussed previously, for the HASC site the void ratio profile (Figure 5.28) indicates a less open fabric in the top part of the deposit when

compared to the other three sites. Conversely, the high void ratios measured for the BBC at the East Boston site, are corresponded by a G_0 profile generally lower than the other sites. The following relationship may be adopted to define the G_0 profile in BBC, if the void ratio and effective stress profiles with depth are known.

$$G_{ovh} = 4500 \div 5500 \cdot e^{-1.6} \cdot (\sigma'_v \sigma'_h)^{0.28} \tag{5.10}$$

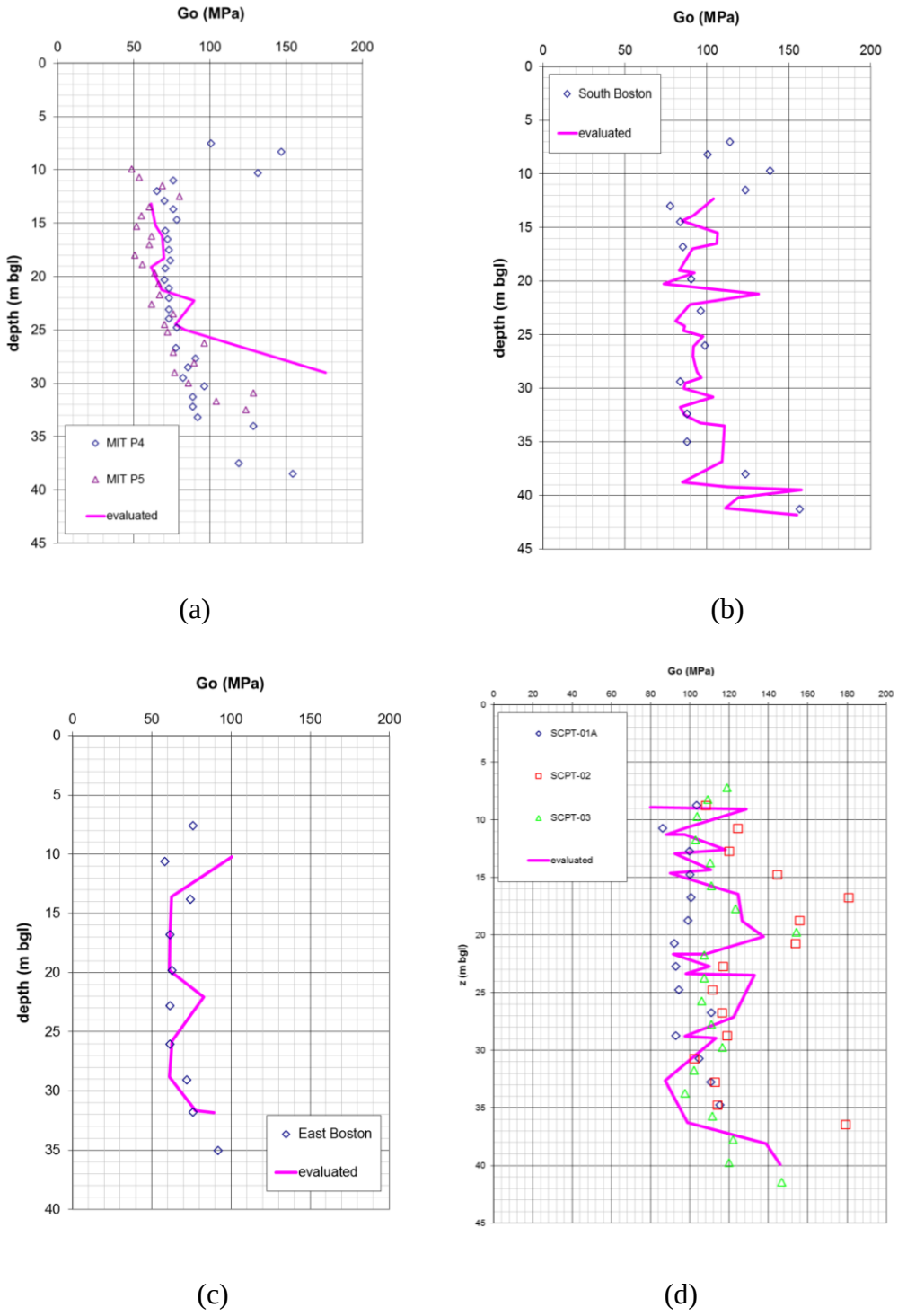

Figure 5.30 Comparison of G_0 calculated and experimental

Discussion

The small strain stiffness profile of the BBC at the HASC site was evaluated using shear wave velocity (v_s) from seismic CPT. When compared with other three sites in Boston the profile shows higher values above 30m depth and then is generally in line with them in the normally consolidated (or lightly over-consolidated) zone. The dependence of G_0 on stress level and void ratio has been investigated. The constants characterising the stress and void ratio dependency are determined on the basis of resedimented Boston Blue Clay data from Santagata et al. 2005. The parameter S accounting for the clay structure is selected in order to have a best possible representation of the field G_0 data. The S values adopted to represent the in situ G_0 profiles for the different sites are greater than the values used to interpret the resedimented BBC data, indicating the effect of the post-sedimentation phenomena on G_0.

On the basis of the data examined from the four sites, a general formulation is proposed to evaluate G_0 profiles in BBC.

$$G_{ovh} = 4500 \div 5500 \cdot e^{-1.6} \cdot (\sigma'_v \sigma'_h)^{0.28} \tag{5.11}$$

5.4.4 BBC stiffness

The decay in soil stiffness with strain is a well known phenomenon and its consideration in boundary value problems is in many cases essential for the prediction of the performance of geotechnical systems. In situ self-boring pressuremeter testing (SBPT) can provide useful data to characterise the stress-strain behaviour of soil. This section presents a series of pressuremeter tests in BBC, carried out at a deep excavation site. Stiffness-strain curves are evaluated within the context of non-linear elastic perfectly plastic soil behaviour. The non-linear elasticity is characterised by a power law relationship describing the stiffness decay with strain.

General

SBPT in BBC was carried out as part of an extensive site investigation at the HASC excavation site. This section focuses on the BBC stiffness degradation with strain along the particular stress path imposed by this testing technique. These curves are particularly useful when used to model the clay behaviour in soil-structure interaction analyses.

In the following sections, after presenting a brief summary of the ground conditions at the HASC site, the SBPT data are presented and the attention is focused on the soil stiffness-strain behaviour. Interpretation of the pressuremeter data is undertaken assuming a power law type correlation to describe the stiffness decay with strain.

Stiffness from pressuremeter testing at the HASC site

A series of SBPT were undertaken at the HASC excavation site, with the aim of capturing the soil stiffness degradation as function of increasing strain levels. The tests were carried out at numerous depths along two verticals B105 and B106. The cavity pressure vs radial displacement (average of the six arms) curves are presented in Figure 5.31 and Figure 5.32.

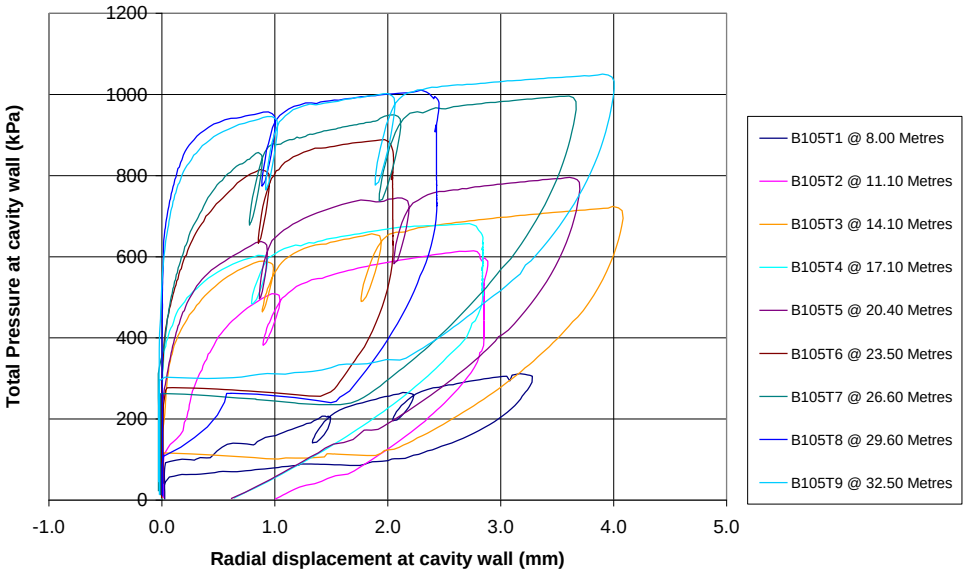

Figure 5.31 B105 vertical, SBPT data

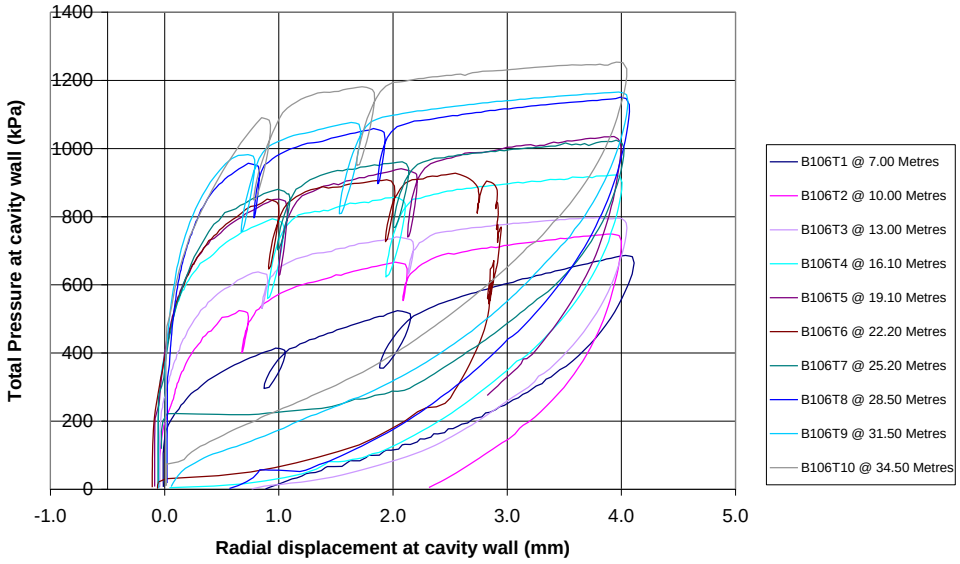

Figure 5.32 B106 vertical, SBPT data

The pressuremeter test is capable of evaluating the stress-strain behaviour of a soil. A number of soil properties can be gathered from the test, including in situ horizontal

stress, undrained shear strength, soil stiffness, etc. The study presented focusses on the clay stiffness and its degradation with strain level.

Interpretation of pressuremeter testing in saturated clay is usually carried out introducing a series of assumptions. These include undrained conditions, with associated no volumetric strain, and plane strain cylindrical cavity expansion. Jardine (1990, 1992) presented a number of routes that can be followed to evaluate the soil strain-secant stiffness (ε_s-G_s) curve from cavity pressure-cavity strain data. One option is to adopt particular expressions to fit the test data and derive analytically closed form expressions of the soil stiffness degradation curves. Various studies of the cavity expansion problem have been carried out, based on particular strain-stiffness relationships.

Bolton & Whittle (1999) and Whittle (1999) analysed the undrained expansion of a cylindrical cavity assuming a non-linear elastic perfectly plastic soil behaviour. The non-linear elasticity was defined using a power law (Gunn, 1992) to relate stress and strain.

$$\tau = \alpha \cdot \gamma^{\beta} \tag{5.12}$$

Bolton & Whittle derived the following expression for the shear modulus

$$G_s = \eta\beta \cdot \gamma_c^{\beta-1} \tag{5.13}$$

where γ_c is the shear strain at the cavity wall. The constants η and β can be easily evaluated as intercept and angular coefficient of the straight line fitting cavity pressure-shear strain data for the reloading part of an unload-reload loop, with both axes plotted using logarithmic scales.

The Bolton & Whittle approach was adopted to interpret the HASC pressuremeter data. The strain-stiffness power law curves are presented in Figure 5.33, Figure 5.34 and Figure 5.35, for various depths of the BBC profile: above 15m, between 15m and 25m, below 25m depth respectively.

Reasonably consistent curves for the two site positions (B105 and B106) are shown below 25m depth. A generally stiffer behaviour is indicated by the B106 data above

25m depth. In general, the stiffness values are higher than the *SHANSEP* laboratory testing stiffnesses, as previously shown (Figure 5.24).

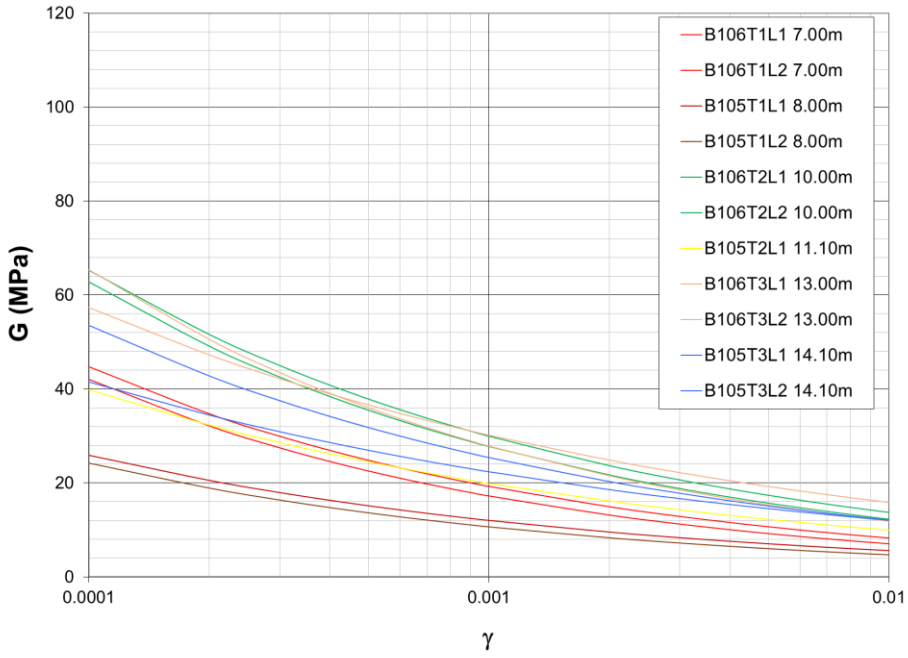

Figure 5.33 Stiffness decay curves above 15m depth

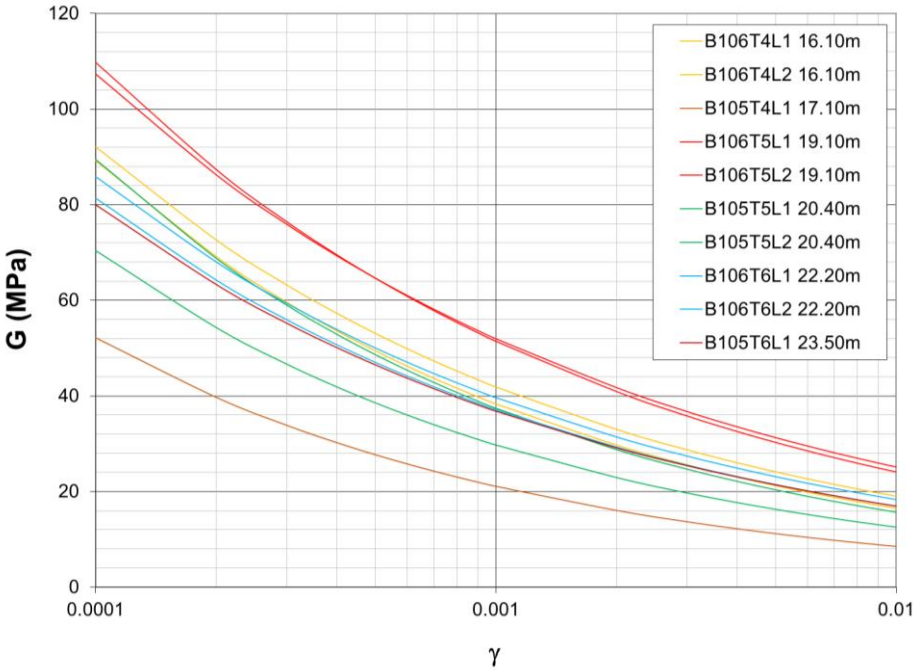

Figure 5.34 Stiffness decay curves between 15m and 25m depth

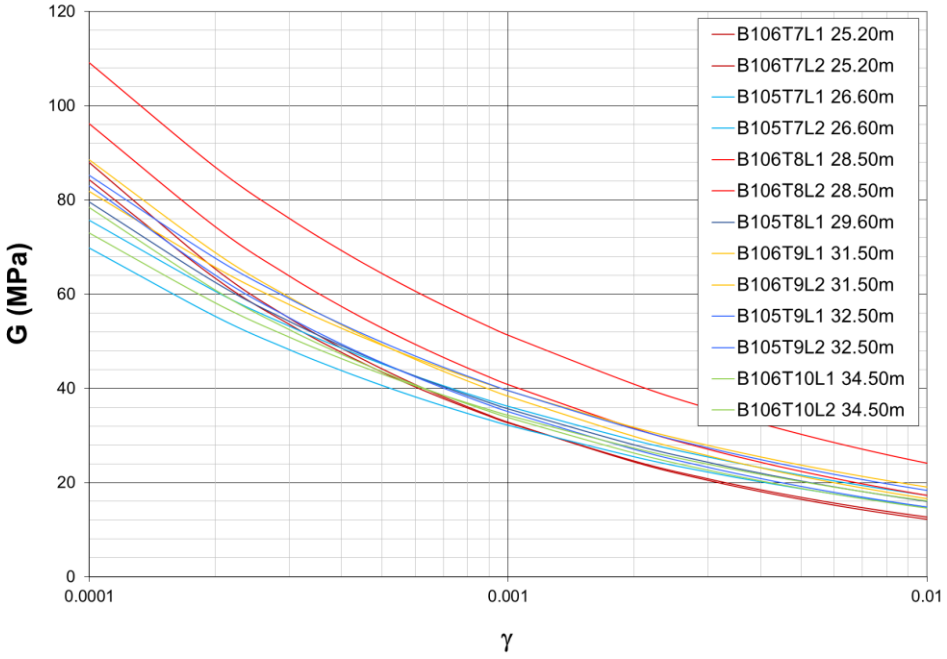

Figure 5.35 Stiffness decay curves below 25m depth

Profiles of stiffness with depth at different strain levels are shown in Figure 5.36. All the profiles seem to indicate a gradual increase in stiffness with depth above 20m depth. The various stiffnesses then appear to drop slightly and become roughly constant with depth.

A rather different shape characterised the G_0 distribution with depth evaluated using seismic CPT profiles, previously shown in Figure 5.28.

The concept of cross-anisotropy is considered here. In the following the subscripts *h* and *v* indicate the horizontal and vertical directions respectively. The stiffness values evaluated with the pressuremeter is G_{hh}, while the small strain stiffness from seismic CPT is a G_{0vh}. The dependence of G_{0vh} on a number of soil parameters, such as void ratio, over-consolidation, stress level, etc, has been explored in the previous section, obtaining the following relationship

$$G_{ovh} = 5500 \cdot e^{-1.6} \cdot (\sigma'_v \, \sigma'_h)^{0.28} \qquad (5.14)$$

If a similar relationship is assumed to apply to the G_{hh} data, a constant ($a(\gamma)$) has to be included to account for the different strain levels.

$$G_{hh}(\gamma) = a(\gamma) \cdot 5500 \cdot e^{-1.6} \cdot \sigma'_h{}^{2x0.28} \tag{5.15}$$

$G(\gamma)$ profiles calculated using this relationship are plotted in Figure 5.37. Ad hoc values of $a(\gamma)S$ were assumed in order to have the closest match with the experimental data.

The agreement with the measured data is poor above approximately 20m depth for B105 and above 15m depth for B106. Better agreement is shown below these depths. Two possible justifications for this finding are presented below.

Variation in stiffness degradation curve

Different stiffness degradation curves may be applicable at different depths. Let γ_x indicate the strain level at which the soil shear modulus is reduced to a given percentage (100x) of the small strain value (G_0). γ_x depends on a number of factors, such as soil plasticity, void ratio, stress level, etc. Some indications on the factors affecting $\gamma_{0.7}$ (strain at which $G=70\%$ of G_0) are given by Benz (2007). The variation of γ_x with depth (for a given x) may be responsible for the stiffness overestimation using equation (5.15) at the HASC site. γ_x may be lower in the upper part of the BBC stratum and therefore induce lower stiffness at each given strain, as schematically indicated in Figure 5.38. This would imply that equation (5.15) is not directly applicable to interpret non-small strain stiffness data (i.e. lower than G_0).

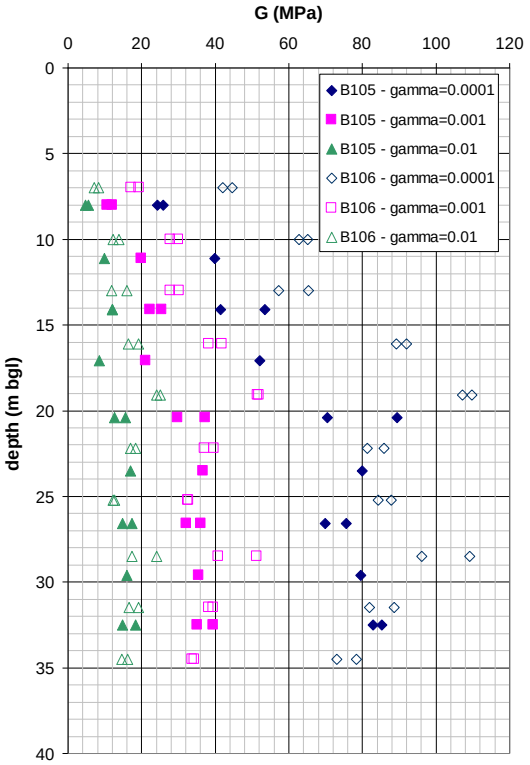

Figure 5.36 Stiffness profiles at different strain levels

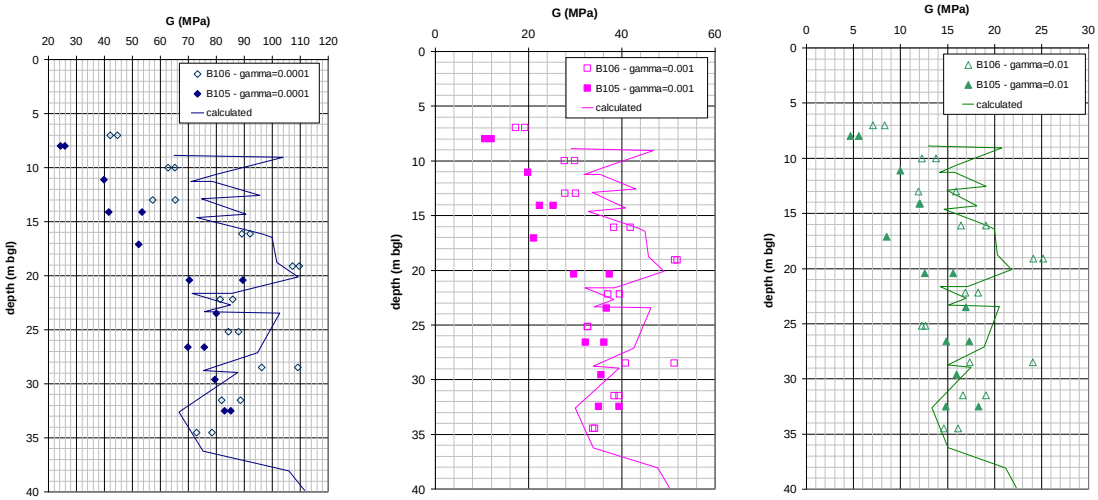

(a) (b) (c)

Figure 5.37 Stiffness profiles interpretation

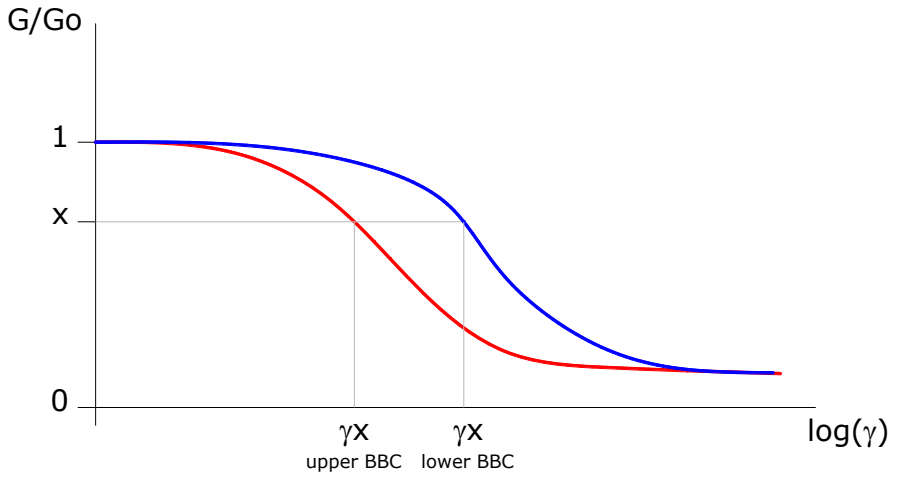

Figure 5.38 Idealised possible stiffness decay behaviour

Clay destructuration

Another explanation is based on the potential disturbance induced in the clay by the first loading phase of the test. The degree of structure modification produced by this initial loading may be significant in a sensitive deposit and may induce a degradation of its mechanical properties. The destructuration process would be more evident in the upper over-consolidated BBC crust (lower stiffness) than in the normally consolidated lower part of the deposit.

Discussion

The BBC stiffness data from self-boring pressuremeter testing at an excavation site are presented. The raw data interpretation was carried out using the approach proposed by Bolton & Whittle (1999) and Whittle (1999), based on a power law stress-strain relationship. The stiffness values evaluated are much higher than the ones measured in the laboratory with *SHANSEP* instrumented triaxial and direct simple shear tests, at the same strain levels. The stiffness profiles at different strain levels show a relatively different shape when compared to G_0 profiles from seismic CPT. A tentative of

interpretation of the pressuremeter G_{hh} data using the G_0 formulation previously obtained (section 5.4.3) proves inappropriate in the top 15-20m of depth. Two possible explanations are proposed. The first one assumes that the finding may be related to the varying shape of the strain-stiffness curve with depth. Values of γ_x, strain at which the shear modulus G is equal to $100x\%$ of G_0 may be lower in the upper part of the BBC stratum, as shown indicatively in Figure 5.38. A second justification considers the clay structure modification induced by the first loading phase of the test. This destructuration would be more significant in the upper over-consolidated BBC crust than in the lower normally consolidated part of the deposit. The observed behaviour is possibly due to a combination of the two phenomena proposed.

5.4.5 BBC compressibility and permeability

Compressibility

The compressibility characteristics of the BBC were evaluated from the results of the CRSC tests. Sample loading, unloading and in some instances reloading paths have been investigated. The test results in terms of void ratio (e) and vertical effective stress (σ_v') are presented in Figure 5.39 in semi logarithmic space.

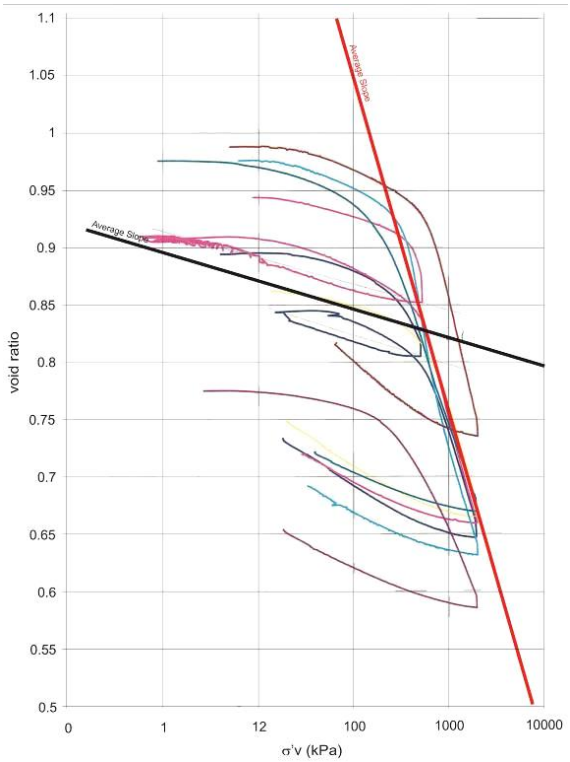

Figure 5.39 Example constant rate of strain consolidation test results for BBC.

The slopes of the curves presented in Figure 5.39 provide estimates of compressibility parameters λ^* and κ^* for given ranges of void ratio (e). The two parameters characterise the stress dependent soil stiffness within the elastic domain (κ^*) and when plastic strains are concerned (λ^*).

Note that λ^* and κ^* are defined in terms of volumetric strain and are related to the original Cam Clay parameters as follows:

$$\lambda^* = \lambda / (1 + e) \tag{5.16}$$

$$\kappa^* = \kappa / (1 + e) \tag{5.17}$$

The evaluated compressibility parameters have been used in the numerical analyses presented herein to assess and back-analyse the time dependent performance of the

excavation. $\lambda^*=0.072$ and $\kappa^*=0.018$ have been evaluated for a void ratio $e=0.8$ as a best estimate benchmark for the analytical study presented in the following sections.

Permeability

The permeability (k) of the BBC has been evaluated by means of both insitu and laboratory testing. A range of isotropic values of k have been assessed from self-boring pressuremeter, cone penetration and CRSC laboratory tests.

The data from the various tests indicates permeability values ranging between $1x10^{-10}m/s$ and $3x10^{-9}m/s$. For the purposes of the numerical analyses undertaken and presented in the following sections, a permeability of $k=1x10^{-9}m/s$ has been adopted for the numerical analyses presented in the following sections.

5.5 Excavation stability aspects

Deep excavations in normally consolidated clay are notoriously challenging in terms of soil mechanics and engineering behaviour. The prime concerns relate to the stability assessment and the difficulty in evaluating excavation performance under serviceability conditions.

This section focuses on the stability aspects of the HASC deep excavation in marine clay.

The excavation concerned is up to 17m in depth and approximately 150m x 150m in plan. The retention system comprises a reinforced concrete diaphragm wall supported by four levels of grouted ground anchors. The excavation is set in an urban environment and is surrounded by existing buildings and infrastructure. The author aims to emphasise the importance of characterising the marine clay mechanical properties, which dominate the stability and behaviour of the excavation concerned.

Various methods for assessing the base and global stability of the excavation were reviewed as part of this study. A selection of these limit equilibrium based methods are detailed and compared. Results from the more traditional limit equilibrium analyses have been compared with simple plane strain finite element assessments. The section focusses on the significance of undrained shear strength anisotropy of the marine clay and understanding of stress paths in relation to in situ and laboratory testing, in view of the excavation stability mechanisms.

5.5.1 Approach to Stability Assessment

In general, the behaviour of soils is studied in terms of effective stresses. However, particularly when stability analyses are carried out, a total stress approach is often adopted. In principle, both the total and effective stress approaches to assess the stability conditions of a geotechnical problem yield representative analytical results, provided that the following conditions are satisfied:

- Effective stress approach: the soil strength parameters and the pore water pressure fields have to be known. Throughout the soil mass, pore water pressures comprise two components, a permanent part due to the presence of hydrostatic or steady seepage conditions and a component related to the loading/shearing of the soil (excess pore water pressures induced by relatively rapid loading of the clay). The latter part of the pore pressure is more difficult to estimate, since it is dependent on the soil properties and the particular stress path.

- Total stress approach: the soil strength has to be known in the various zones of the soil mass. It is common practice to carry out total stress analyses when the loading conditions and soil characteristics are such that undrained conditions can be assumed. This approach is often adopted because of the difficulties in evaluating the excess pore water pressures generated in a low permeability soil during relatively rapid loading. This is particularly significant in the instance of soft clays, for which plastic strains are expected to occur from the initial stages of a loading process. However, as detailed above, the reliability of the total stress approach

requires the adoption of appropriate undrained shear strength values. In general, the undrained shear strength of a soil is stress path dependent. Therefore in this type of analytical approach, each point of the soil mass should be characterised using a strength which is appropriate for the expected stress path that the point will experience.

For the excavation problem considered, undrained conditions are assumed for the marine clay stratum and the excavation stability assessment is carried out in terms of total stresses, considering a Tresca failure criterion. In view of this type of analytical approach, the ground investigation tests (in particular the laboratory tests) described in the previous sections, have placed significant emphasis on the determination of the undrained shear strength of the material under different loading conditions.

5.5.2 Excavation stability

Short term (total stress) excavation stability conditions often govern the design of multi-supported retaining systems for deep excavations in clay. The system stability is considered to be of prime concern with normally consolidated deposits. The assessment of both base and global stability is required for appropriate selection of factors of safety. The most commonly adopted techniques to assess excavation stability are based on the limit equilibrium approach and the finite element method. The undrained shear strength anisotropy of clay can significantly affect the stability conditions of geotechnical systems such as embankments, slopes and excavations. In general, different shearing modes related to the principal stress orientation, can be assumed for the various zones surrounding a retaining wall, as shown in Figure 5.40. Consequently, an appropriate range of strengths should be adopted for each of these zones. In Figure 5.40 the symbols PSA (Plane Strain Active) and PSP (Plane Strain Passive) indicate that compression and extension plane strain tests are representative of the strength in zones where the shearing of the soil takes place at 45° to the horizontal. Undrained shear strength from DSS tests are more representative of zones where the soil is sheared along the horizontal and vertical directions. Part of the laboratory testing regime included a series of triaxial tests that were carried out on marine clay samples. It is worth noting that an approximation is

introduced when considering the equivalence between PSA and TC (compression) and PSP and TE (extension) strengths, applicable to the zones shown in Figure 5.40.

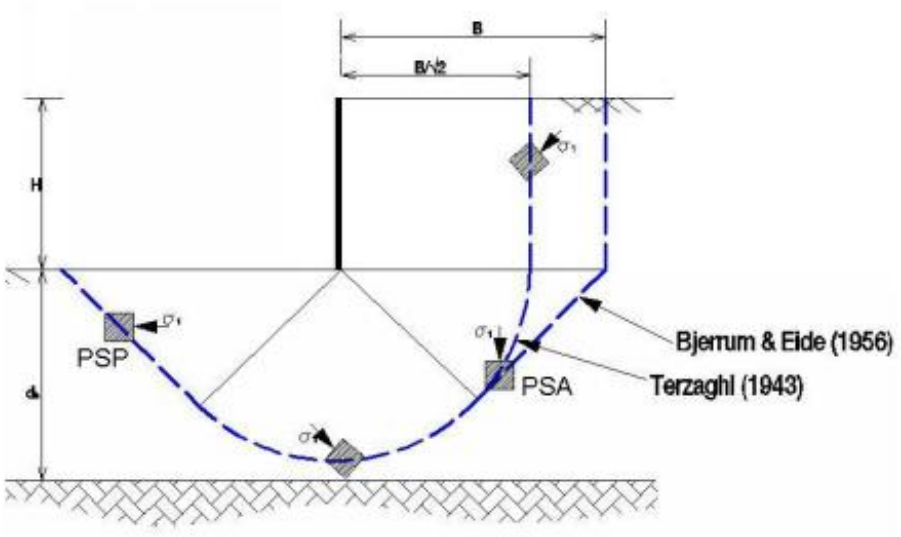

Figure 5.40 Direction of principal stress and associated strength for an indicative plane strain excavation

The complications introduced by undrained shear strength anisotropy may be overcome by adopting an isotropic strength profile related to a DSS failure mechanism. This simplification (O'Rourke 1993 and Osman & Bolton 2006) is based on the fact that the DSS undrained shear strength is approximately equivalent to the average of the PSA and PSP strengths, and that the zones where PSA and PSP strengths should apply have roughly the same zone of influence. This simplification is adopted for the limit equilibrium analyses and some of the finite element analyses described in the following sections.

Limit Equilibrium Approach

Limit equilibrium methods are based on the assumption of a given failure surface. The stability limit condition is governed by the violation of the soil failure criterion along this given failure surface. The simple approach involves exclusively equilibrium

considerations, with no attempt to take into account stress distribution inside the sliding mass.

Global stability is assessed using techniques widely adopted for slope stability problems. The sliding soil mass, bounded by a circular or non-circular failure surface, is divided into a number of slices. Several assumptions regarding the inter-slice forces are introduced (Bishop 1955, Morgenstern & Price 1965).

Base stability calculations are usually carried out considering failure mechanisms proposed for example by Terzaghi (1943) or Bjerrum & Eide (1956). The limitations of these methods range from the arbitrary assumption of an imposed failure surface to the assumption of an interslice force distribution (for the slope stability methods). In the study presented here, the General Limit Equilibrium (GLE) method (Fredlund & Krahn 1977, Spencer 1967) is adopted, using the software Slope/W for the global stability assessment. The methods proposed by Terzaghi (1943), Bjerrum & Eide (1956) and Eide et al. (1972) are adopted for the base stability evaluation. In the base stability methods, a weighted average (along the failure surface) of the soil strength is considered. The factors of safety (FoS) resulting from the different limit equilibrium methods are presented in Table 5.3. The shapes of the failure surfaces for the global (minimum FoS) and base stability (Terzaghi 1943) are shown in Figure 5.43.

Finite Element Approach

Numerical models using the finite element method can be adopted to assess excavation stability. The usual approach for this assessment is based on factoring the soil strength until failure is achieved. In the present study two plane strain models have been analysed using the software Plaxis. In both of the models the granular strata (Made Ground Fill, Sand and Glacial Till) are modelled using a linear elastic – perfectly plastic (Mohr-Coulomb) constitutive model. The strength parameters for these granular materials were evaluated using SPT, CPT and SBPT data. Angles of shearing resistance (ϕ') of 30° and 35° were adopted for the made ground fill and sands and gravels, respectively. In the first model the marine clay is modelled using a linear elastic –

perfectly plastic (Mohr-Coulomb) material constitutive model and adopting the DSS undrained shear strength profile (isotropic). In this case, the FoS was evaluated by carrying out a strength reduction stage in the analysis. In the second model, the NGI ani2 material constitutive model was adopted for the marine clay (Andresen & Jostad 2002). As presented in Chapter 2, this is a total stress material model that takes into account the strength and stiffness anisotropy of a normally consolidated (or slightly over-consolidated) clay. The NGI ani2 model requires the input of three normalised undrained shear strength parameters, related to the three modes of shearing discussed previously (DSS, PSA and PSP). Convenient strength normalising parameters (S_{norm}) could be the DSS undrained shear strength (S_{uDSS}) or the effective vertical stress (σ'_v). The normalised undrained shear strength can then be set as a function of depth. The model also requires the input of three strain levels at which these principal stress orientation dependent strengths are achieved. The excavation stability conditions were assessed by adopting suitable undrained shear strength profiles adopted for the three modes of failure (the S_{uDSS} profile adopted is shown in Figure 5.23, the compression and extension profiles have been evaluated factoring the S_{uDSS} by 1.35 and 0.7, respectively) and factoring the undrained shear strength manually. The FoS=1 condition was assumed when numerical convergence was not achieved in the last excavation stage. The FoS resulting from the finite element approach are presented in Table 5.3 together with the limit equilibrium results.

The principal stress directions (σ_1 and σ_3), evaluated using the NGI ani2 constitutive model, are presented in Figure 5.41. The cross-shaped symbols indicate the stress directions and the size of the cross segments is proportional to the stress magnitude. As previously highlighted, the orientation of the principal stresses can be associated with laboratory testing modes of failure, namely compression (maximum principal stress direction vertical), extension (horizontal) and direct simple shear (diagonal, 45°). A contour plot showing the maximum principal stress inclination angle, with respect to the vertical direction, is presented in Figure 5.42. Relevant shearing mechanisms are indicated along the evaluated failure surface. The mechanisms broadly resemble the idealised ones indicated in Figure 5.40.

A comparison between the failure surface shapes, evaluated using global (minimum FoS) and base stability (Terzaghi 1943) calculations and finite element analysis (NGI ani2 model) is shown in Figure 5.43.

Table 5.3 Factors of safety summary

Analytical Approach		Method of Analysis	FoS
Limit Equilibrium	Base Stability	Terzaghi	1.61
		Bjerrum & Eide	1.41
		Terzaghi (modified)	1.79
		Eide et al.	1.45
	Global Stability	Slope/W [GLE]	1.43
Finite Element Solution		Plaxis [Mohr- Coulomb (SuDSS)]	1.42
		Plaxis [NGI ani2]	1.45

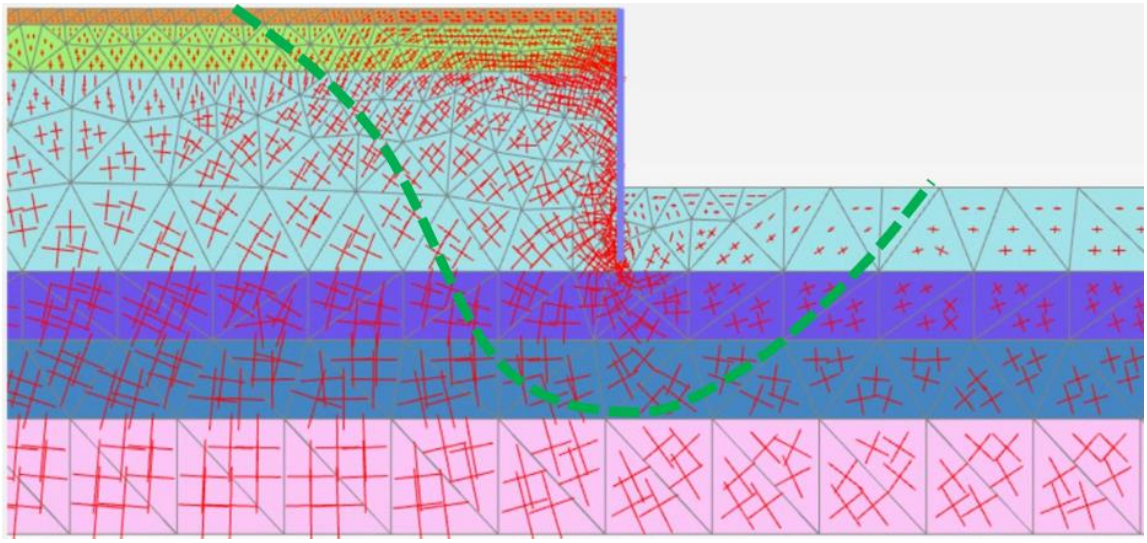

Figure 5.41 Principal stress directions (σ_1 and σ_3) indicated by cross-shaped symbols – the size of the cross segments is proportional to the stress magnitude

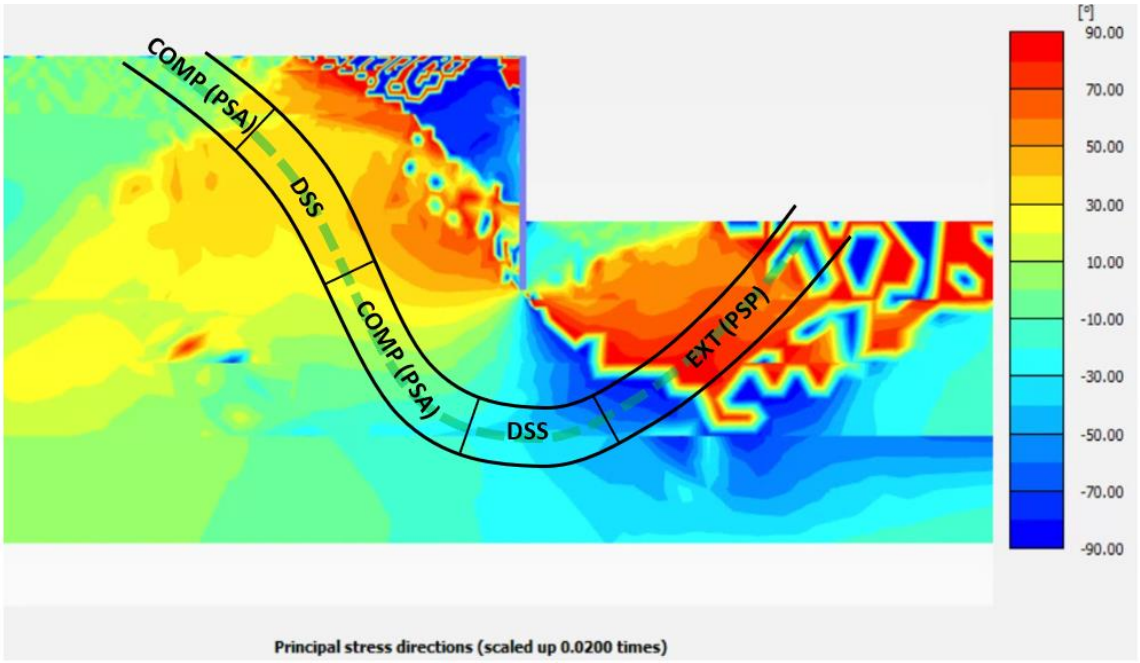

Figure 5.42 Contour plot showing inclination of maximum principal stress with respect to the vertical direction – relevant shearing mechanisms are indicated along the estimated failure surface

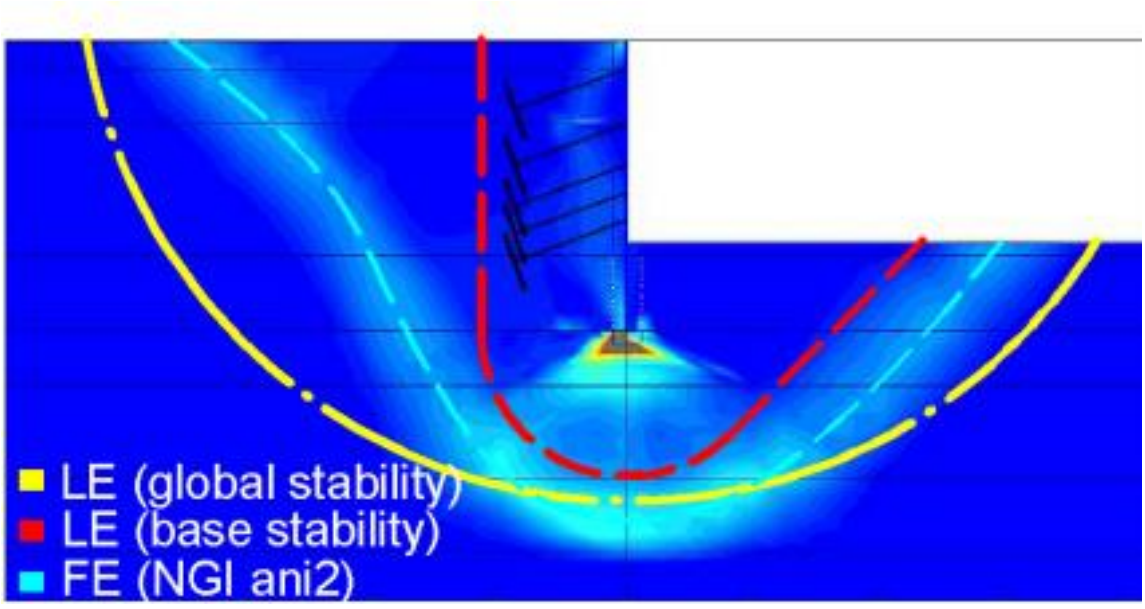

Figure 5.43 Comparison between limit equilibrium and finite element indicative failure mechanisms

5.5.3 Excavation stability – three dimensional effects

The excavation stability assessment presented in the previous section is based on the assumption of plane strain conditions, adopting two dimensional finite element or limit equilibrium analyses/calculations. In general, the assumption is appropriate for excavations with large dimensions in plan, compared to the excavation depth, in which corner effects (as presented in Chapter 3) are limited to localised zones in proximity to excavation corners.

This section explores the impact of the excavation geometry and associated three dimensional effects on the excavation stability conditions.

A parametric study has been carried out, using the software Plaxis 3d, simulating the stability conditions of excavations of varying plan dimensions. The HASC ground model and excavation depth have been considered. The BBC has been modelled using a linear elastic – perfectly plastic (Mohr-Coulomb) constitutive model, with a DSS undrained shear strength profile.

Square excavations have been considered, ranging from 50m x 50m to 350m x 350m plan dimensions. A quarter of the geometry has been modelled in Plaxis, taking advantage of the symmetry conditions. The aim is to evaluate the impact of the excavation size on the excavation collapse mechanism and associated FoS.

In a similar manner to the two dimensional analyses previously presented, FoS have been estimated by carrying out a strength reduction stage in the analyses.

The findings of the study are summarised below:

- As the excavation aspect ratio (excavation side length to depth ratio – *L/H*, see Figure 5.44) increases, the estimated FoS tends to go towards the plane strain analysis value (FoS=1.42), presented in the previous section.

- Contours of incremental resultant displacements, in the last calculation step before the strength reduction stage (i.e. excavation to formation level stage), are presented in Figure 5.45, at a depth of 13m below ground level, for aspect ratios

L/H of 10 and 3. A relatively significant difference in incremental displacement values is observed between the corner zone and the central part of the excavation side, away from the corner, for the *L/H=10* case. Conversely, a broadly axisymmetric contour pattern (with symmetry axis at the excavation centre) is shown for the *L/H=3* case. The plots

- Exaggerated deformation plots and phase displacement contour plots (representative of the strength reduction stage) are presented in Figure 5.46 and Figure 5.47, respectively. The plots are representative of excavations with aspect ratios *L/H* of 10 and 3. The diagrams indicate the failure mechanism, which involves the zone in proximity of the retaining walls for the wider excavation (*L/H=10*) and reaches the excavation centre for the smaller excavation (*L/H=3*).

- For relatively large excavations, the failure mechanism takes place mainly along the excavation sides, away from the corner zones. As the excavation aspect ratio reduces, the failure mechanism tends to capture the entire retaining wall, including the corner zones. This is indicatively shown in Figure 5.48a (*L/H=10*) and Figure 5.48b (*L/H=3*) where incremental displacement contour surfaces give an indication of the slip surface and failure mechanism.

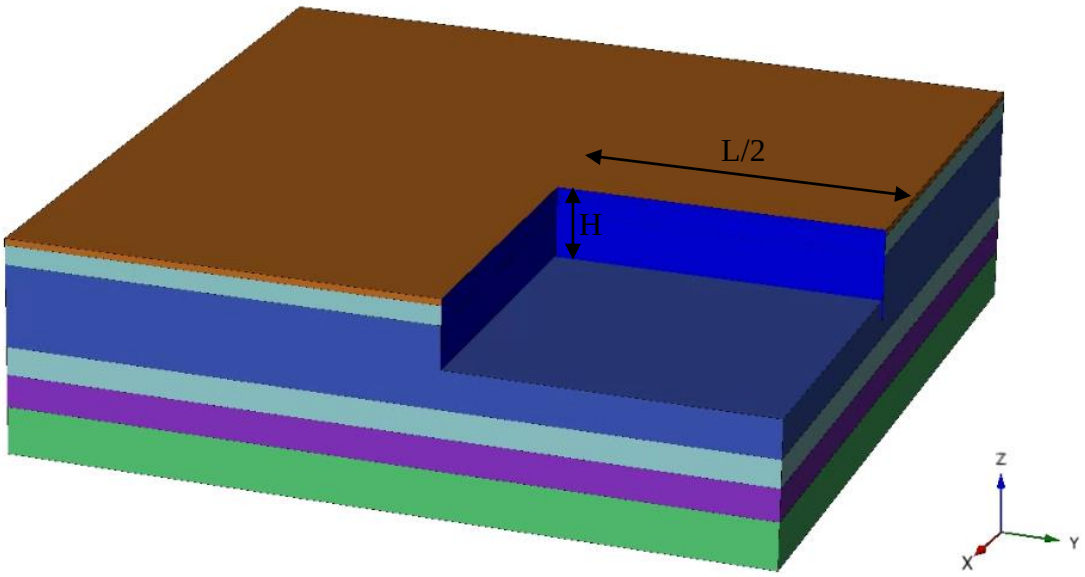

Figure 5.44 View of one of the Plaxis 3d models, comprising a quarter of a square excavation

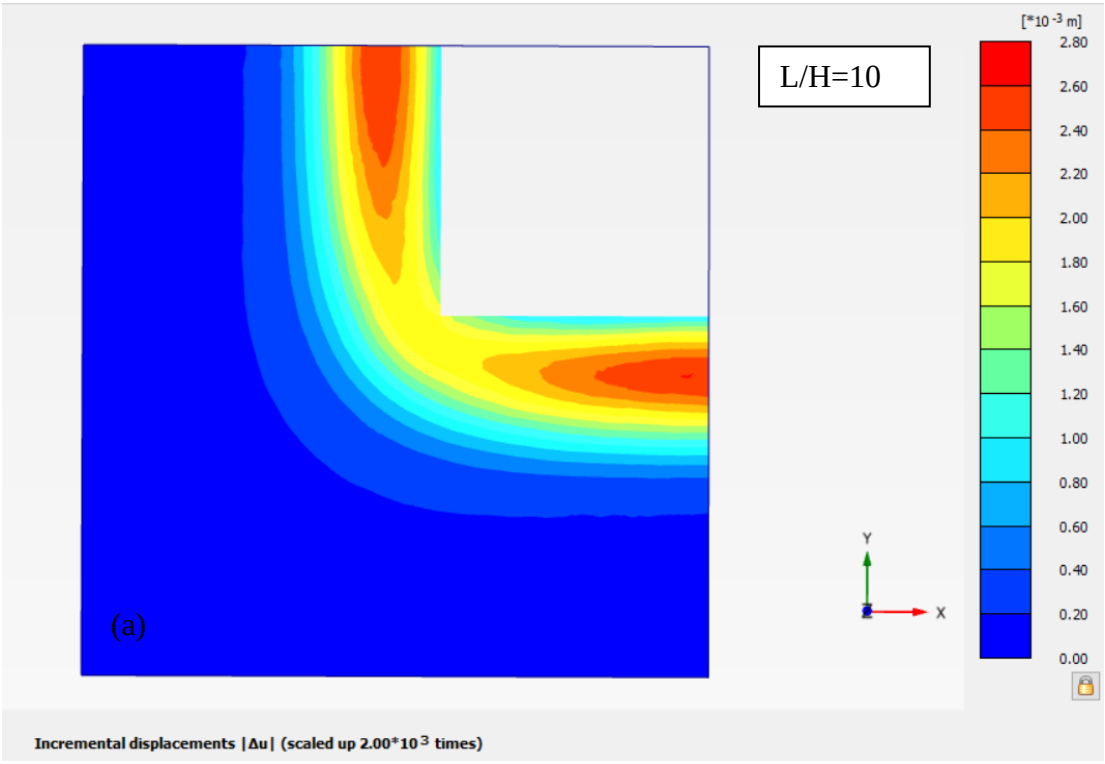

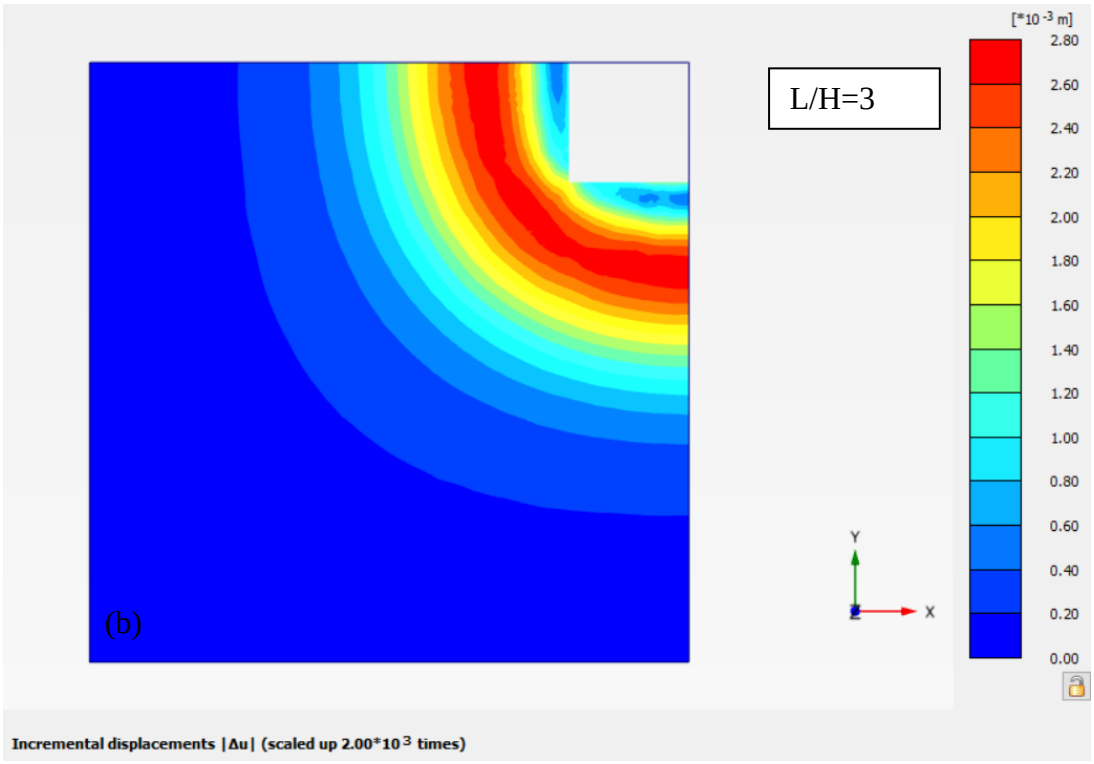

Figure 5.45 Contour plot of incremental resultant displacements in last calculation step before strength reduction (i.e. excavation to formation level stage) for L/H=10 (a) and L/H=3 (b)

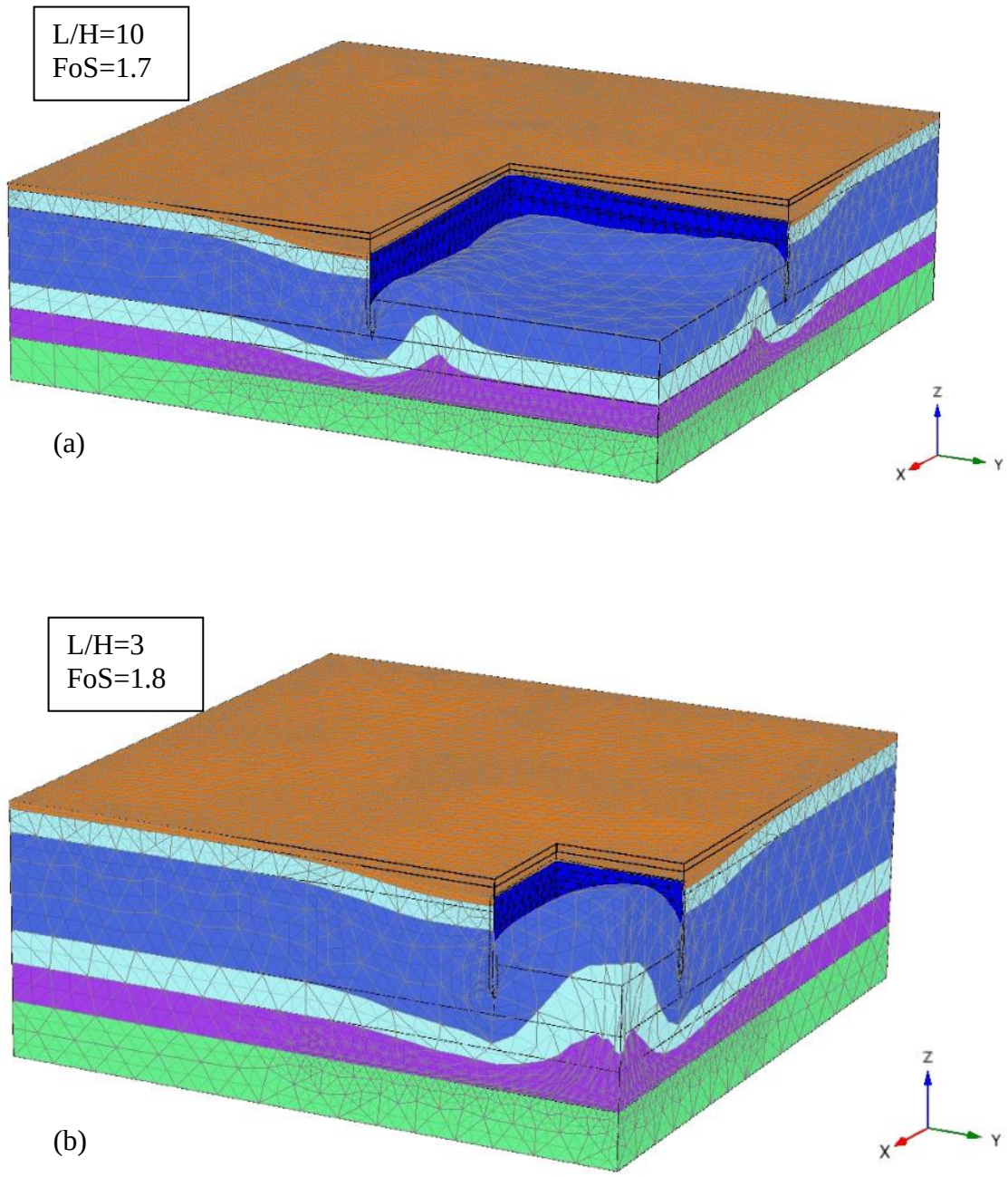

Figure 5.46 Exaggerated deformation plots (representative of the strength reduction stage) for *L/H=10* (a) and *L/H=3* (b)

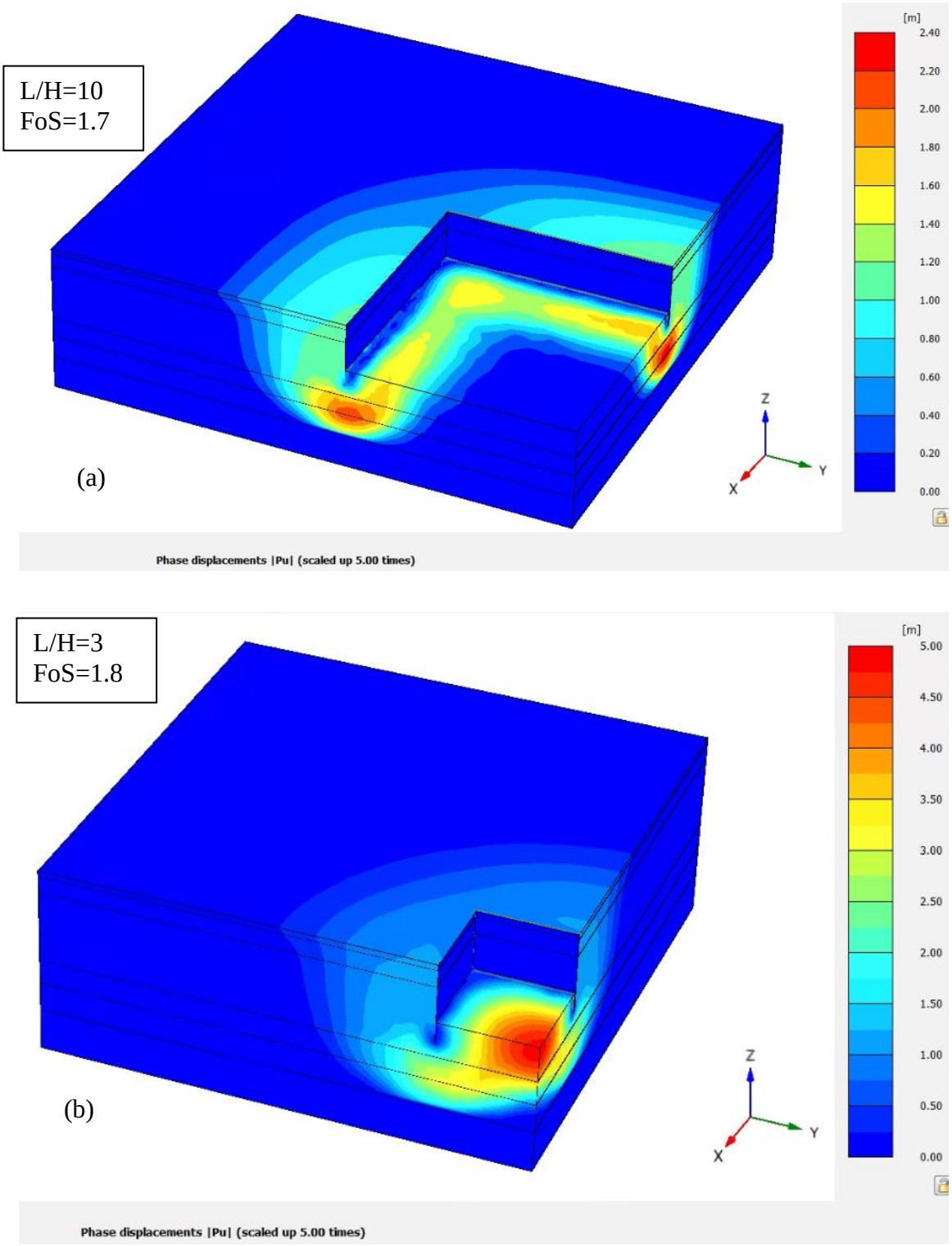

Figure 5.47 Phase displacement contour plots (representative of the strength reduction stage) for *L/H=10* (a) and *L/H=3* (b)

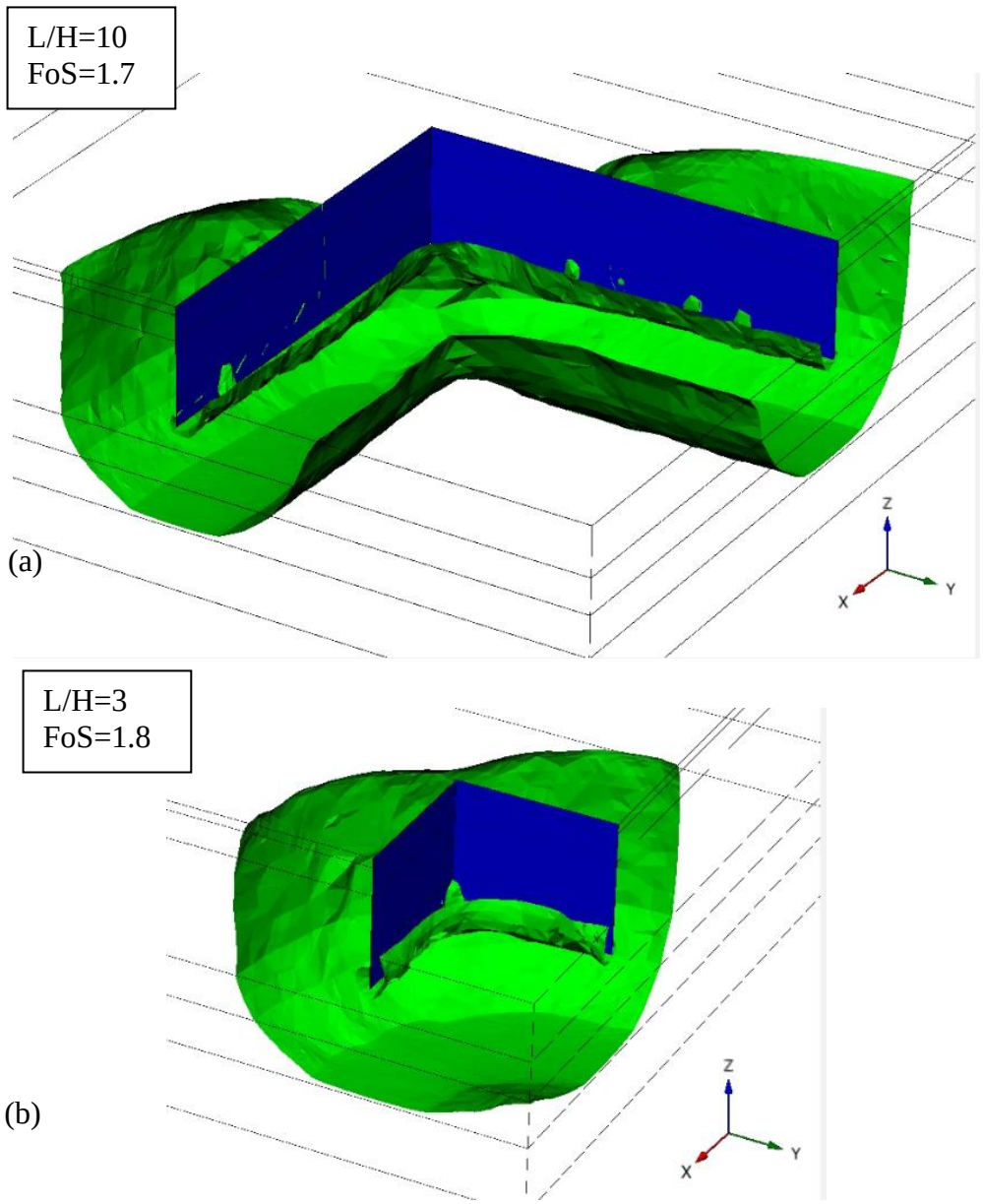

Figure 5.48 Indicative incremental displacement contour surfaces indicating the failure mechanism geometry for *L/H=10* (a) and *L/H=3* (b)

A diagram showing the variation of FoS with the excavation aspect ratio (L/H), for the specific ground model and excavation depth considered, is presented in Figure 5.49. The findings indicate that the three dimensional assessment would lead to a relatively

significant improvement in terms of estimated FoS, for excavations with relatively small plan size compared to their depth (approximately 25% increase in FoS for excavations with aspect ratio <3).

Figure 5.49 Diagram showing the variation of FoS with the excavation aspect ratio (plan size to excavation depth ratio)

5.5.4 Discussion

The undrained stability of the up to 17m deep HASC excavation has been analysed. The author highlights the need for reliable undrained shear strength data from in situ and laboratory testing, to inform total stress analyses. The stability assessment has been carried out by adopting selected classic limit equilibrium methods and by performing simple finite element analyses. The different limit equilibrium methods show some variability in FoS, ranging from 1.41 using Bjerrum & Eide (1956) to 1.79 using modified Terzaghi (1943), which takes into account the embedded wall length. It is interesting that the more conservative limit equilibrium methods (Bjerrum & Eide 1956 and Eide et al. 1972) give FoS in line with the global stability and finite element

approaches for the excavation concerned. Both of the Terzaghi methods (with and without wall embedment) result in less safe estimates. The failure surface indicated by the strength reduction procedure is very similar in both of the finite element models analysed (modelling the marine clay as a Mohr-Coulomb material or using the NGI ani2 material model). An indicative shear strain contour plot at failure is shown in Figure 5.43, which indicates the failure mode. Indicative slip surfaces related to the base stability and global stability mechanisms are also presented for comparison. The finite element failure mode develops along a surface positioned between the base failure and a global failure surfaces. The FoS obtained in the two finite element analyses are similar, 1.42 using Mohr-Coulomb and 1.45 using NGI ani2 material models for the clay. The results demonstrate that, for the case study concerned, the DSS undrained shear strength profile can be adopted for excavation stability assessments using limit equilibrium or finite element methods, assuming isotropic behaviour for the material.

A parametric study has been carried out using three dimensional analysis, considering square excavations of varying plan sizes. The findings are summarised in Figure 5.49. A relatively significant enhancement in estimated FoS is achieved by explicitly considering the three dimensional excavation collapse mechanism, for excavations with relatively small plan size compared to their depth (approximately 25% increase in FoS for excavations with aspect ratio <3, compared to plane strain conditions).

It is worth mentioning that, as indicated in the following section focussing on the time dependent behaviour of the BBC, the actual behaviour of the clay stratum if affected by partial dissipation of excess pore water pressures taking place during the excavation period. This results in partially drained conditions, indicating that the undrained assumption made as part of the stability assessment presented, may not be accurate. It is therefore considered that total stress stability calculations should be based on conservative undrained shear strength parameters. Such analyses should be carried out as a preliminary means of assessing the excavation stability and should be accompanied by coupled effective stress analyses, capable of capturing the partially drained nature of the BBC behaviour.

5.6 Observed time dependent behaviour of the excavation base

Excavations in saturated clayey soils generate negative excess pore water pressures in the soil below the excavation base. Time dependent dissipation of these excess pore water pressures and associated ground heave often govern the design of ground bearing foundation rafts and potential requirement for tension piles. The estimation of time and movement dependent soil heave pressure acting at the underside of a raft is a complex soil-structure interaction problem which should also account for loading stages associated with the substructure construction works. Simplifications are often introduced and conservative assumptions are usually made for the foundation design and performance assessment under serviceability conditions. This section focuses on selected extensometer and vibrating wire piezometer monitoring data for the HASC site. Long term (post-excavation) groundwater conditions are influenced by the presence of an underdrainage system beneath the raft foundation. The time dependent excess pore water pressure generation, dissipation and associated ground movement throughout the excavation and basement construction sequence are simulated using finite element analyses. A comparison of computed and measured pore water pressures and ground movement with time is presented. The appropriateness of using Cam Clay type models for this type of soil under the particular loading condition is discussed. The potential benefits of undertaking time dependent simulation of the construction process for the design of the basement raft foundation are investigated.

5.6.1 General

This section investigates the measured time dependent behaviour of the BBC at the HASC excavation site.

A raft foundation system is adopted in view of the relatively small superstructure loading from the 6 to 8 storey buildings. The overall mass balance of the system is governed by a net unloading condition whereby the removal of overburden is not matched by the subsequently imposed building loading. An underdrainage system is adopted to relieve the raft foundation from otherwise significant water uplift pressures.

An extensive real-time monitoring system has enabled the author to review the measured time dependent behaviour of the BBC during basement construction. Upon excavation, negative excess pore water pressures are generated within the BBC which dissipate with time, leading to swelling of the material. If the swelling process is confined or restricted by any means, such as construction of a basement or foundation system prior to the dissipation of the negative excess pore water pressures, time and movement dependent heave pressures may need to be considered in the design of such elements. This can lead to complex soil-structure interaction scenarios and a requirement for advanced numerical modelling analyses.

Traditionally, based on engineering judgement and engineering experience within a given cohesive stratum, simplified design techniques have been adopted to assess the effects of heave on substructure elements. Heave pressure can be conservatively modelled, assuming the substructure is effectively wished into place. This can often lead to significant over-conservatism in terms of foundation and substructure design. Alternatively, a proportion of the heave pressure can be adopted in design or it can be neglected, based on some form of analytical evaluation of excess pore water dissipation or engineering judgement.

This section focusses on analysing a particular section of the excavation, by comparing the measured piezometric response with corresponding heave data from extensometers throughout the basement excavation and construction process. Finite element analyses are presented which demonstrate the effects of heave pressures in substructure design for this particular case study.

5.6.2 Measured time dependent behaviour of the excavation

As part of the comprehensive monitoring programme, real-time data collection from inclinometers (30), piezometers (7), extensometers (6) and numerous total station monitoring points were reviewed and analysed throughout the basement excavation and construction sequence.

In order to review the time dependent behaviour of the excavation, this section focuses on selected extensometer and piezometer monitoring data. Extensometer and groundwater head data for a representative cross section of the excavation are presented in Figure 5.50. The change in groundwater head (i.e. the generation of negative excess pore water pressures), as excavation progresses, is recorded by three vibrating wire piezometers located at different depths within the excavation. The associated ground heave movement within the BBC stratum is recorded by a vertical string of magnetic extensometers located in close proximity to the piezometers (as presented in the indicative cross section in Figure 5.50). Excavation progress with time is also schematically illustrated in Figure 5.50.

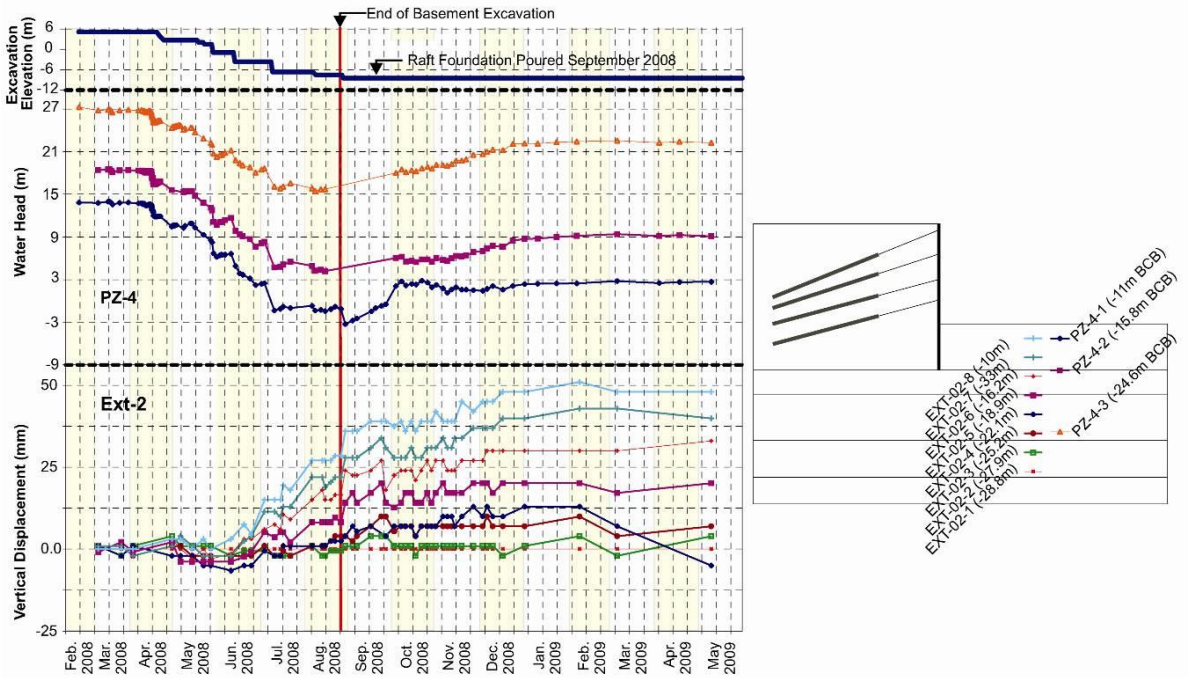

Figure 5.50 Measured time dependent response from vibrating wire piezometers (PZ4) and extensometers (Ext-2) for selected excavation cross section.

By reviewing the groundwater head data in detail, in addition to the negative excess pore water pressure generation during excavation stages, the effects of partial drainage can be noticed. Upon completion of a given stage of excavation, a rise in groundwater head

(i.e. partial dissipation of excess pore water pressures) can be observed, prior to undertaking the following stage of excavation.

The end of excavation and completion of raft foundation construction are indicated in the plots in Figure 5.50. In view of the underdrainage system installed, it is clear that groundwater heads do not tend to go towards the previous hydrostatic condition, prior to excavation commencement. The excess pore water pressures dissipate so that the groundwater heads go towards a new steady state seepage equilibrium. This is shown indicatively in the output from finite element seepage analyses presented in Figure 5.51. The long term groundwater seepage conditions are modelled by imposing zero pressure head at excavation formation level, preventing groundwater flow through the symmetry boundary (right edge of the model in Figure 5.51) and imposing a groundwater head based on the initial groundwater table along the left and base boundaries of the model (ref. Figure 5.51).

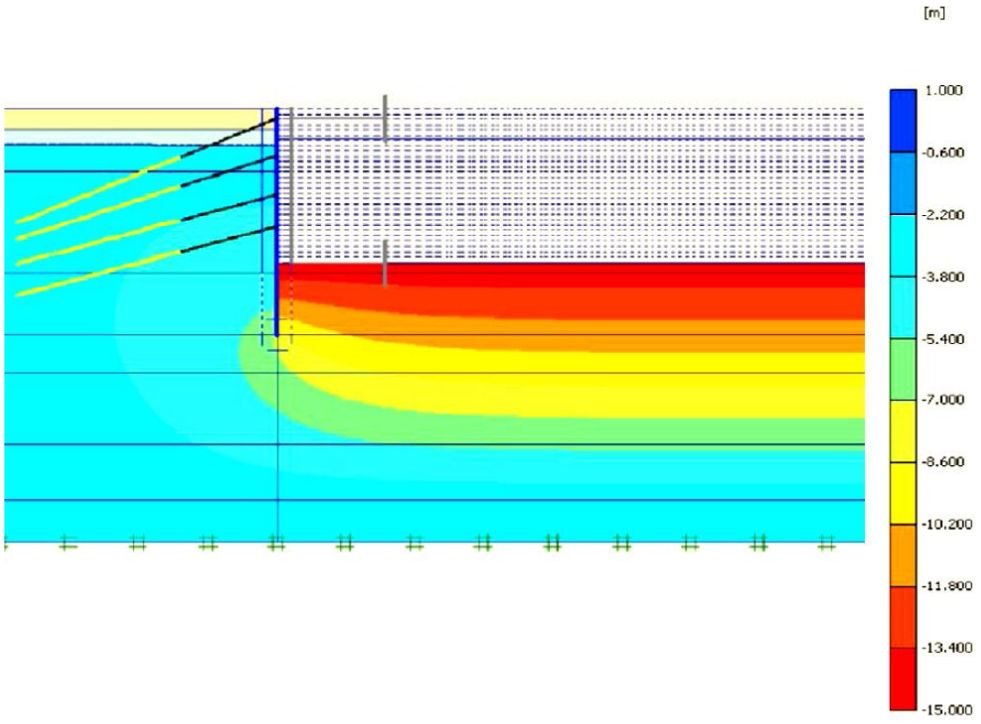

Figure 5.51 Indicative contour plot of long term steady state seepage groundwater heads (in mBCB – Boston City Base) with operational underdrainage system.

5.6.3 Time dependent soil-structure interaction simulation

A number of plane strain finite element models have been analysed, simulating the basement construction sequence for the particular example cross section of the excavation discussed previously. The aim of the finite element analyses was to simulate and back-analyse the measured time dependent behaviour of the BBC and to assess the effects of partial drainage on the substructure design.

Coupled mechanical/flow finite element analyses were undertaken simulating the actual recorded construction sequence. The idealised construction sequence in plane strain and associated simplifying assumptions in the finite element models are as follows:

- The excavation is carried out by removing approximately 3m soil layers at each stage, each lasting approximately 28 days (total excavation duration of approximately 130 days). This is analysed in a coupled manner as described above.
- The prestressed ground anchors are installed between excavation stages.
- The substructure loading is simulated using a representative uniformly distributed load, applied gradually over a period of 250 days.
- Complete excess pore water pressure dissipation is then allowed to achieve long term conditions.
- The installation of an underdrainage layer underneath the raft is modelled by imposing the long term steady state groundwater seepage condition, towards which the pore pressure field tends to during the consolidation process.

The time dependent dissipation of negative excess pore water pressure and associated swelling mechanism are evaluated and compared with the measured data for the given example excavation cross section.

In terms of constitutive assumptions, the Soft Soil model available in Plaxis has been used for the BBC layer, whilst a linear elastic – perfectly plastic Mohr-Coulomb model has been used for the Made Ground, Sand and Glacial Till strata.

As presented in Chapter 2, the Soft Soil model is based on the Modified Cam Clay model (Muir Wood, 1990). However, the stress states are limited within a Mohr Coulomb failure locus. By adopting this criterion, potentially unrealistic high deviatoric stresses at low mean stress levels are avoided.

15 node triangular iso-parametric elements have been adopted to discretise the geometry. Retaining wall and raft foundation structures have been modelled using 5-node plate elements, with appropriate axial and flexural rigidities. The four anchor levels have been modelled using node-to-node anchors over the free length and geogrid elements over the bonded length.

A series of parametric finite element models have been analysed varying the stiffness and permeability properties of the BBC.

Best estimate geotechnical parameters are adopted for the "base" model. The compressibility and permeability parameters evaluated above were adopted in the base model. The BBC stiffness and permeability were subsequently adjusted and varied in an attempt to back-analyse the time dependent measurements from the piezometers and extensometers.

Compressibility and permeability parameters evaluated as part of the comprehensive ground investigation carried out are presented in the previous sections. Table 5.4 summarises the compressibility and permeability parameters adopted for the BBC in three selected parametric finite element analyses undertaken.

Table 5.4 BBC Compressibility and permeability parameter summary from selected parametric finite element analyses

Model	λ^*	κ^*	k (m/s)
base	0.072	0.018	$1x10^{-9}$
P	0.072	0.018	$7x10^{-9}$
S	0.028	0.004	$1x10^{-9}$

In models "P" and "S" the BBC permeability and compressibility parameters are adjusted respectively in order to simulate and reproduce the excess pore water pressure generation and dissipation as measured by the vibrating wire piezometers.

The comparison of computed and measured pore water pressures and heave displacements along the instrumented profiles are presented in Figure 5.52 to Figure 5.57 for the different models.

Figure 5.52, Figure 5.54 and Figure 5.56 compare the time dependent predicted pore water pressures with the values measured at the three depths shown in Figure 5.50 (PZ-4-1 at -11mBCB, PZ-4-2 at -15.8mBCB and PZ-4-3 at -24.6mBCB).

Figure 5.53, Figure 5.55 and Figure 5.57 present a comparison of predicted (blue curves) and measured (red curves) heave ground movements. The measured data refers to points located at varying depths, between -10mBCB and -28.8mBCB, indicated in Figure 5.50 (EXT-02-1 to EXT-02-8).

The results from the base model over-predict the excess pore water pressures generated during the excavation process (Figure 5.52). In addition, Figure 5.53 shows a significant over-prediction of heave displacements within the BBC, clearly indicating that the best estimate stiffness parameters adopted are not able to capture the mass behaviour of the stratum.

In model P the permeability of the BBC has been set to $k=7x10^{-9}$ *m/s* in order to obtain a reasonable representation of the pore water pressure profiles with time (Figure 5.54). The corresponding heave displacements are once again over-predicted to an even greater extent than in the base model (Figure 5.55). A maximum heave displacement approaching 210mm is evaluated.

A reasonable agreement between simulation and piezometer and extensometer monitoring data (Figure 5.56 and Figure 5.57 respectively) is obtained with model S. The model S back-analysis was undertaken by increasing the BBC stiffness as presented in Table 5.4. In general, some discrepancies can be associated with the simplifying assumptions adopted for the excavation and loading sequence. Additionally, although

the cross section analysed is representative of a plane strain condition, the three dimensional nature of the excavation and construction sequence has been idealised.

Time dependent dissipation of these excess pore water pressures and associated ground heave often govern the design raft foundation systems. As mentioned, the estimation of time and movement dependent uplift soil pressure acting at the underside of a raft is a complex soil-structure interaction problem. Excavation (unloading) and substructure construction (reloading) stages should be considered by means of a coupled assessment.

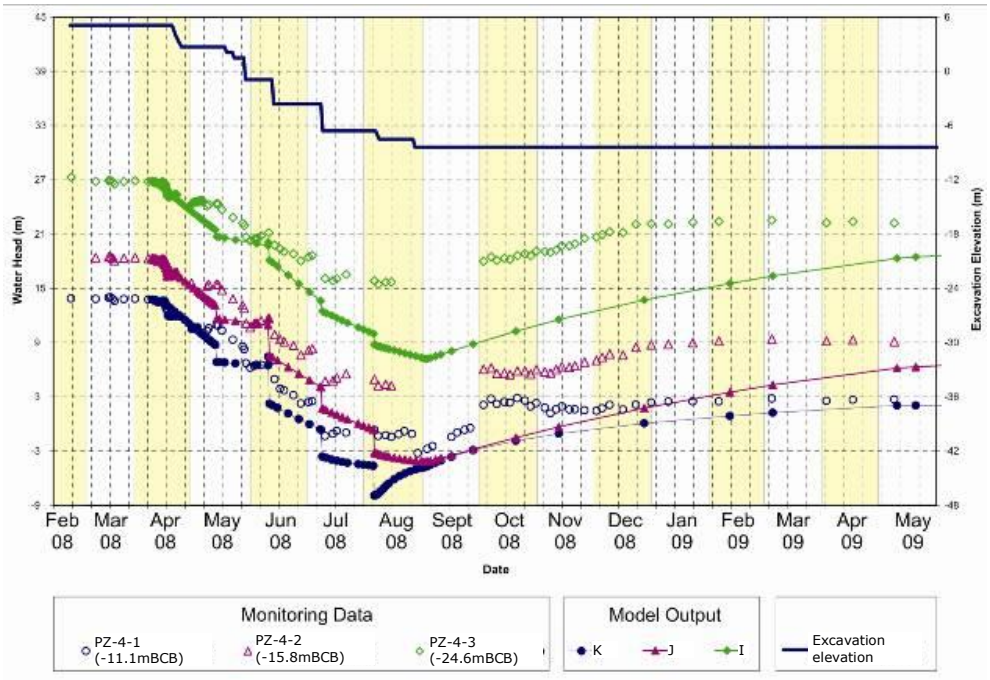

Figure 5.52 Base model – piezometer data

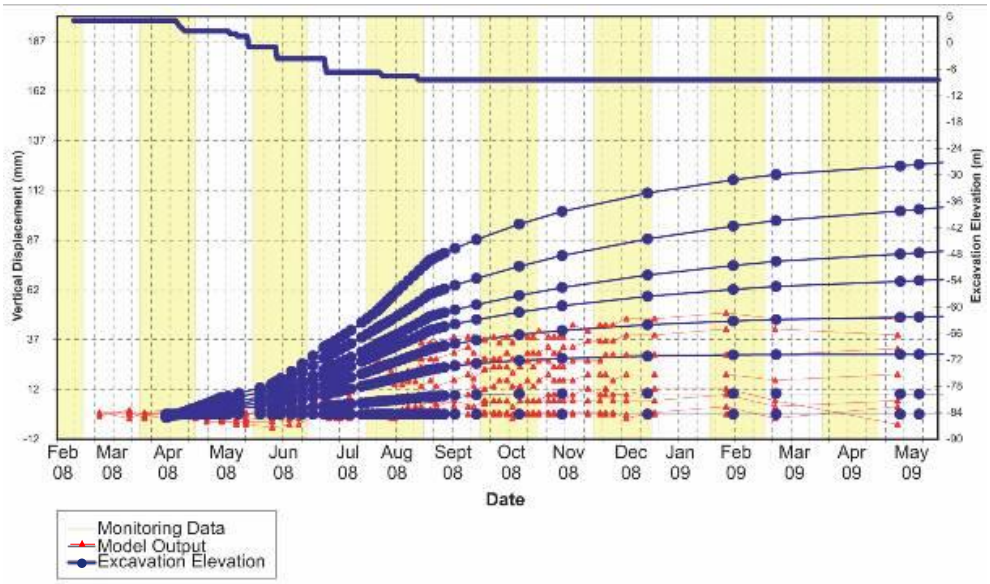

Figure 5.53 Base model – extensometer data

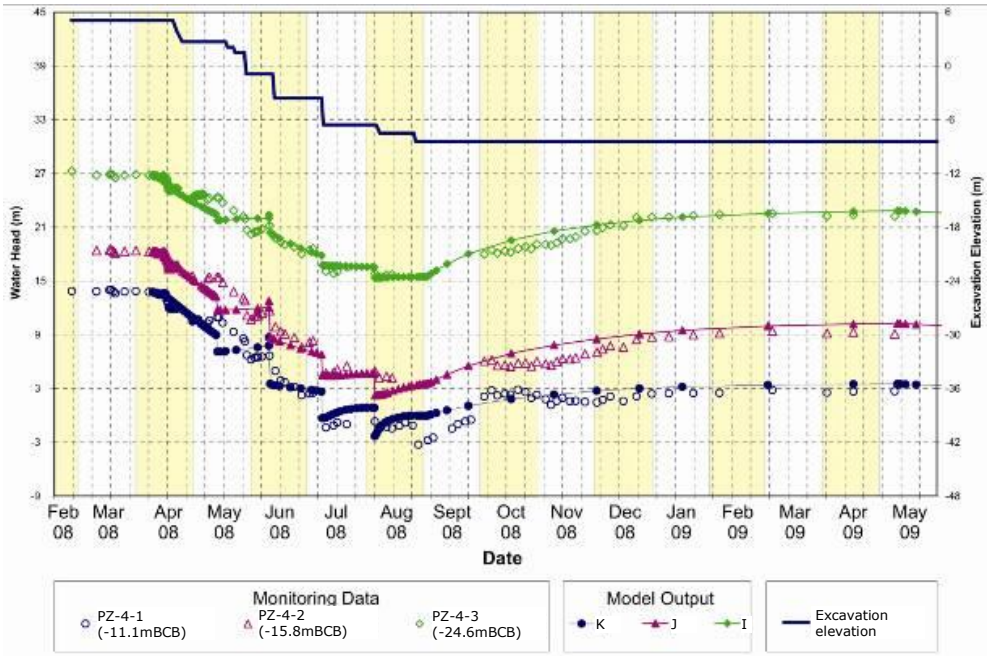

Figure 5.54 Model P – piezometer data

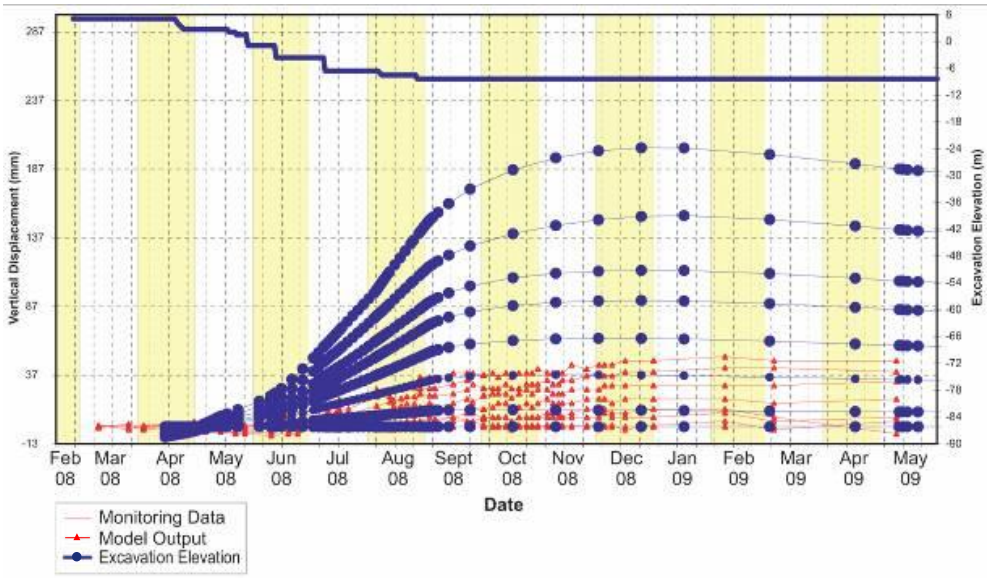

Figure 5.55 Model P – extensometer data

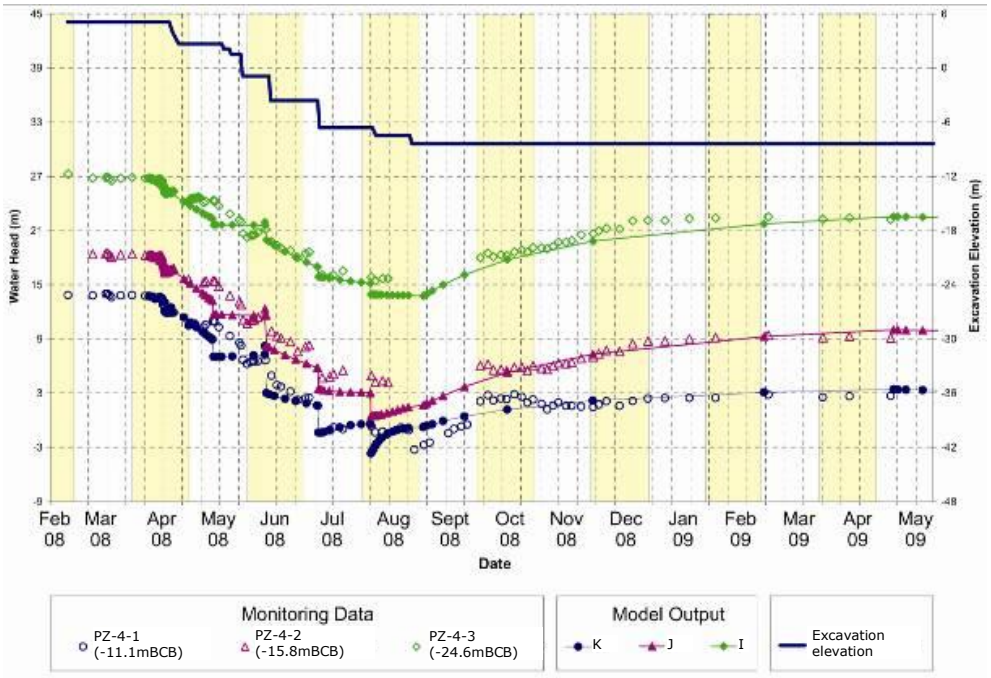

Figure 5.56 Model S – piezometer data

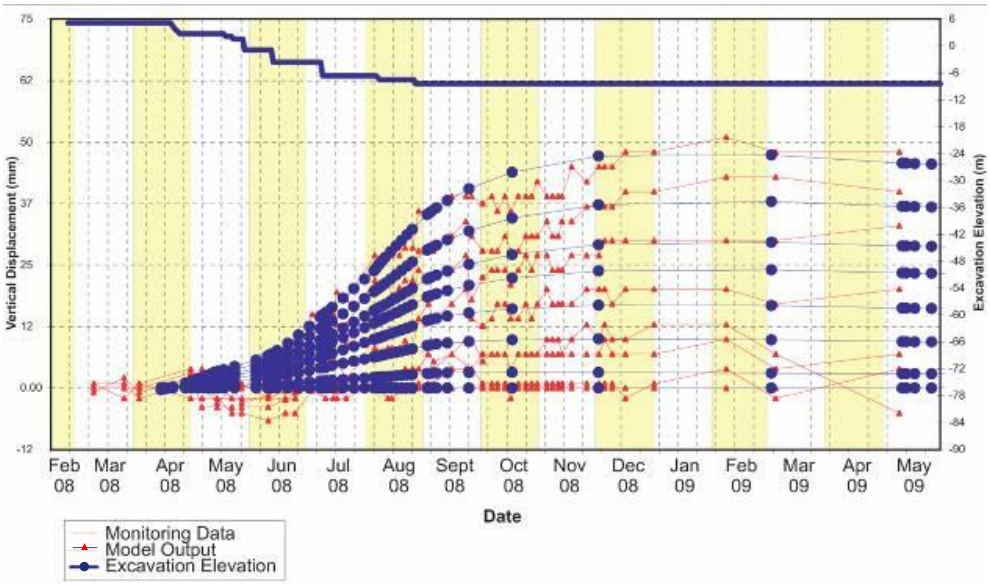

Figure 5.57 Model S – extensometer data

It is evident, from the monitoring data and the numerical simulations, that the assumption of undrained behaviour for the BBC stratum, often considered during the excavation works, may not be accurate. Relatively rapid dissipation of excess pore water pressures takes place throughout the excavation period and can have a significant impact on the behaviour of a geotechnical system.

Ideally, partially drained conditions should be considered in the assessment of both stability and performance of an excavation in these ground conditions. These aspects should be reviewed and addressed on a case by case basis, even in the instance of clays with relatively low global permeability.

5.6.4 Basement raft foundation performance assessment

As discussed previously, simplifying hypotheses are often introduced and conservative assumptions are usually made when designing basement rafts. It is common practice to design basement raft foundations in clays considering the maximum uplift heave pressure, equal to the weight of the excavated soil, acting underneath the raft. The partial

dissipation of excess pore water pressures taking place during the excavation process is often neglected and pure undrained conditions are assumed for periods of up to 6 to 12 months. As mentioned above, these assumptions should be reviewed and addressed on a case by case basis, even in the instance of clays with relatively low global permeability.

One further finite element analysis (model S*) has been undertaken modelling the excavation and loading process in an instantaneous manner and assuming fully undrained conditions. Full dissipation of excess pore water pressures is subsequently permitted. The basement raft bending moments from model S and model S* are compared. Figure 5.58 presents model S* bending moments as a percentage of the corresponding output from model S. This particular comparison demonstrates the degree of potential over-conservatism introduced in the basement raft design when adopting extreme assumptions (such as the wishing a basement into place whilst assuming fully undrained conditions).

The results presented in this section are indicative and a full three dimensional model and actual loading condition should be analysed to appropriately evaluate the raft performance and overall design requirements.

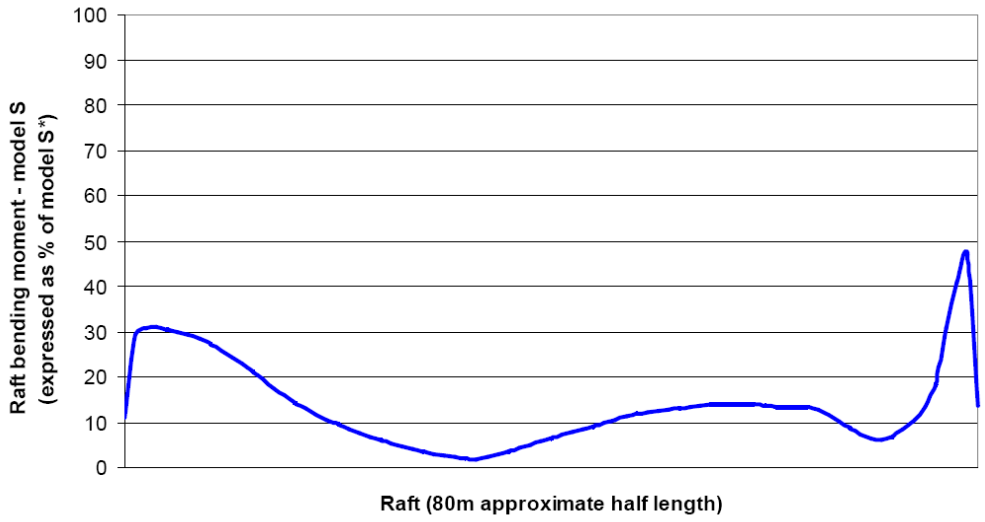

Figure 5.58 Raft bending moment (model S expressed as % of model S*)

5.6.5 Discussion

Selected piezometer and extensometer data from the HASC excavation site have been presented and discussed in terms of time dependent performance. Analysis of the monitoring data highlights the generation of negative excess pore water pressures during excavation and the partial drainage/dissipation during continued excavation and basement construction. The significance of excess pore water pressure changes due to consolidation, occurring during the excavation, has been discussed. The assumption of pure undrained conditions for significant excavation/construction events is not strictly applicable. A coupled time dependent analysis approach is considered more appropriate. This coupled approach enables a more representative assessment of the excavation and basement raft foundation behaviour and performance.

A parametric study has been undertaken using finite element analyses. The BBC layer has been modelled using the Soft Soil model (Plaxis manual), a Cam Clay type model. A stiffness greater than that evaluated from constant rate of strain consolidation test data was required to achieve a reasonable agreement between computed and measured data.

Accounting for the appropriate construction sequence and carrying out a time dependent coupled simulation of the excavation can lead to potentially significant optimisation of basement raft designs and a more sensible assessment of foundation system performance.

5.7 Conclusions

A detailed study has been undertaken for a 15m to 17m deep excavation case history (HASC) in normally consolidated Boston Blue Clay.

A number of aspects of the project have been investigated, as summarised in the following.

5.7.1 Boston Blue Clay behaviour

Undrained shear strength

Two laboratory reconsolidation procedures, namely *Recompression* and *SHANSEP* have been reviewed. Although the *SHANSEP* method does not appear particularly appropriate to investigate the stress-strain behaviour of the Boston Blue Clay, it has been widely used in the past to assess the undrained shear strength of this clay and should provide slightly conservative estimates of S_u, particularly for the normally consolidated material.

The range of results from the suite of undrained shear strength laboratory testing has been compared with in situ testing results. This comparison confirms a general agreement between *SHANSEP Direct Simple Shear* and *Field Vane* test data.

Stiffness

The small strain stiffness profile of the Boston Blue Clay at the HASC site was evaluated using shear wave velocity (v_s) from seismic CPT. Data also from other three sites in Boston has been used to evaluate the following general formulation to estimate G_0 profiles in Boston Blue Clay.

$$G_{ovh} = 4500 \div 5500 \cdot e^{-1.6} \cdot (\sigma'_v \sigma'_h)^{0.28} \qquad (5.18)$$

Stiffness values at varying strain levels from self-boring pressuremeter testing have been reviewed. A tentative of interpretation of the pressuremeter data using the above G_0 formulation has proven inappropriate in the top 15-20m of depth. Two potential justifications have been proposed, based on i) varying shape of the strain-stiffness curve with depth or ii) possible destructuration following the initial loading stage of the test.

5.7.2 Excavation stability

The undrained stability of the excavation has been analysed. The author highlights the need for reliable in situ and laboratory testing undrained shear strength data, to inform total stress analyses. The stability assessment has been carried out by adopting selected classic limit equilibrium methods and by performing simple finite element analyses.

The different limit equilibrium methods show some variability in *FoS*, ranging from 1.41 using Bjerrum & Eide (1956) to 1.79 using modified Terzaghi (1943) which takes into account the embedded wall length. It is interesting that the more conservative limit equilibrium methods (Bjerrum & Eide 1956 and Eide et al. 1972) give *FoS* in line with the global stability and finite element approaches for the excavation concerned. Both of the Terzaghi methods (with and without wall embedment) result in less safe estimates.

The failure surface indicated by the strength reduction procedure is very similar in both of the finite element models analysed (modelling the marine clay as a Mohr Coulomb material or using the *NGI ani2* material model). The finite element failure mode develops along a surface positioned between the base failure and a global failure surfaces. The *FoS* obtained in the two finite element analyses are similar, 1.42 using Mohr-Coulomb and 1.45 using NGI ani2 material models for the clay.

The results demonstrate that, for the case study concerned, the *DSS* undrained shear strength profile can be adopted for excavation stability assessments using limit equilibrium or finite element methods, assuming isotropic behaviour for the material.

A parametric study has been carried out using three dimensional analysis, considering square excavations of varying plan sizes. A relatively significant enhancement in estimated FoS is achieved by explicitly considering the three dimensional excavation collapse mechanism, for excavations with relatively small plan size compared to their depth (approximately 25% increase in FoS for excavations with aspect ratio <3, compared to plane strain conditions).

It is worth mentioning that the actual behaviour of the clay stratum if affected by partial dissipation of excess pore water pressures taking place during the excavation period.

This results in partially drained conditions, indicating that the undrained assumption made as part of the stability assessment discussed above, may not be accurate. It is therefore considered that total stress stability calculations should be based on conservative undrained shear strength parameters. Such analyses should be carried out as a preliminary means of assessing the excavation stability and should be accompanied by coupled effective stress analyses, capable of capturing the partially drained nature of the Boston Blue Clay behaviour.

5.7.3 Excavation base time dependent behaviour

Selected piezometer and extensometer data from the HASC excavation site have been presented and discussed in terms of time dependent performance. Review of the monitoring data highlights the generation of negative excess pore water pressures during excavation and the partial drainage/dissipation during continued excavation and basement construction. The assumption of pure undrained conditions for significant excavation/construction events is not strictly applicable. A coupled time dependent analysis approach is considered more appropriate. This coupled approach enables a more representative assessment of the excavation and basement raft foundation behaviour and performance.

A parametric study has been undertaken using finite element analyses, modelling the Boston Blue Clay behaviour using the Soft Soil model.

Accounting for the appropriate construction sequence and carrying out a time dependent coupled simulation of the excavation can lead to potentially significant optimisation of basement raft designs and a more sensible assessment of foundation system performance.

CHAPTER 6

CONCLUSIONS

6.1 General

The study presented in dissertation encompasses a number of topics related to the stability and performance assessment of excavations in normally consolidated and over-consolidated clayey deposits. Following a review of a series of commonly available constitutive models, the study focusses on two excavation case studies, namely a 20m excavation in London Clay and a 15m to 17m deep excavation in Boston Blue Clay. A summary of the key findings of the research carried out is presented in the following sections.

6.2 Constitutive models review

A number of elasto-plastic constitutive models, available in Plaxis either as standard or user defined models, have been examined and their key features have been reviewed.

The models include the Soft Soil model, the Hardening Soil model family (including the standard Hardening Soil model, the small strain stiffness version and the generalised version) and the total stress NGI ani2 model.

Key features of the models have been explored in detail. Although the general features of these models are presented in the Plaxis software manual, details of their formulation, in relation to elastic properties, yield surface, plastic potential and hardening rules, are often not provided to the user. The study focusses on these aspects of the models' formulation, and provides information which, in the author's view, would be very useful to users of the software.

The suitability of the models for use in routine soil-structure interaction analyses, in lieu of the popular linear elastic – perfectly plastic (Mohr-Coulomb failure criterion), has been investigated with reference to the two case histories considered.

Summary of key contributions/novelty

- Key features of various constitutive models' formulation presented, which are not provided in the Plaxis software manual.

6.3 Excavations in over-consolidated clays

A Central London 20m deep excavation case history has been considered.

A series of plane strain analyses have been carried out, using Plaxis 2d, in order to evaluate the ground movement field likely to arise as a result of the proposed works. A number of constitutive models have been adopted to simulate the behaviour of the London Clay and Lambeth Group strata, including the widely adopted linear elastic – perfectly plastic Mohr Coulomb model and non-linear models (HSS and GHS) capturing stress and strain dependency of the material stiffness.

Comparisons between the different analyses and the CIRIA C760 data set of case histories, have focussed on the retaining wall deflections and ground movement field in the zone immediately surrounding the excavation.

The study shows that, although the commonly adopted Mohr-Coulomb model may provide a reasonable prediction of wall deflections, it is inadequate for the prediction of ground movements in the zone surrounding the excavation. The use of a model capturing the soil stiffness at small strains and the progressive stiffness degradation behaviour with increasing strains is considered essential for this purpose.

However, it is important to note that the Plaxis readily available HSS model may result in relatively poor ground movement predictions in view of the particular stress dependency formulation of the stiffness parameters. The findings indicate that the use of a model in which the stiffness is controlled by the mean effective stress (p') and the pre-consolidation stress (p_c) would provide more reasonable results in terms of both wall deflections and overall ground movements.

Summary of key contributions/novelty

- The use of a model capturing the soil stiffness at small strains and the progressive stiffness degradation behaviour with increasing strains is essential to simulate retaining wall performance and predict excavation induced ground movements in stiff clays.
- The Plaxis HSS model's stiffness stress dependency formulation (based on the minimum principal effective stress, σ'_3) may lead to relatively poor wall and ground movements predictions. The GHS formulation, in which the stiffness is controlled by the mean effective stress (p') and the pre-consolidation stress (p_c) provides more reasonable results in terms of both wall deflections and overall ground movements.

6.4 Three dimensional excavation analysis

The impact of the excavation geometry and the three dimensional stress fields (i.e. arching around excavation corners) on the excavation performance has been reviewed. Soil stresses arching mechanisms developing behind excavation corners (corner effects) often result in a reduction in horizontal earth pressures acting on retaining walls in these zones.

The use of three dimensional soil-structure interaction simulation, including the main basement structural elements (retaining wall, slabs, cores and foundations), is important

in order to assess the holistic sub-structure behaviour and for the design of these elements.

Modelling assumptions are very important especially when using shell elements to model retaining walls. In particular, due to the two dimensional formulation of shells, anisotropic flexural rigidity must be set in order to reproduce actual retaining wall behaviour.

Following a review of three dimensional soil arching/corner effects, a Corner Optimisation Technique (COT) has been proposed, allowing the optimisation of retaining wall design. With reference to a piled retaining wall, the approach would consider the following value engineering strategies, in proximity of excavation corners:

- Increase pile spacing
- Reduce pile diameter
- Reduce reinforcement

The COT has been implemented by the author on a number of projects, resulting in substantial material savings, i.e. reduction in wall reinforcement of up to 30% (compared to plane strain) and reduction in wall embedment requirements, approaching excavation corners.

The analysis of a 20m deep excavation in London Clay has been presented. The results clearly indicate the three dimensional wall deformation mechanism, with wall deflections reducing moving towards an excavation corner. Capturing these mechanisms is considered essential when undertaking impact assessments on nearby structures, utilities or elements of infrastructure. The findings can also be used to inform value engineering exercises for the retaining systems and overall substructure.

Summary of key contributions/novelty

- The study shows that the use of three dimensional soil-structure interaction simulation allows a more accurate assessment of earth pressure distributions, with due account for soil arching effects, and sub-structure behaviour.

- Three dimensional analysis allows a more accurate prediction of ground movement distributions in proximity of excavations, compared to plane strain analysis. The three dimensional approach is particularly useful when undertaking impact assessments on nearby third party assets.

- The development of soil arching mechanisms in proximity of excavation corners, leads to reduced earth pressures acting on retaining walls and, in turn, reduction in wall internal forces. A Corner Optimisation Technique (COT) has been proposed for the optimisation of retaining wall design, which would result in potentially significant material savings.

6.5 Excavations in normally consolidated clays

A detailed study has been undertaken for a 15m to 17m deep excavation case history (HASC) in normally consolidated Boston Blue Clay.

A number of aspects of the project have been investigated, as summarised in the following.

6.5.1 Boston Blue Clay behaviour

Two laboratory reconsolidation procedures, namely *Recompression* and *SHANSEP* have been reviewed. Although the *SHANSEP* method does not appear particularly appropriate to investigate the stress-strain behaviour of the Boston Blue Clay, it has been widely used in the past to assess the undrained shear strength of this clay and should

provide slightly conservative estimates of S_u, particularly for the normally consolidated material.

The stress – strain behaviour of the Boston Blue Clay has been reviewed on the basis of data from seismic CPT and self-boring pressuremeter testing. The following general relationship for the evaluation of G_0 profiles in Boston Blue Clay has been found.

$$G_{ovh} = 4500 \div 5500 \cdot e^{-1.6} \cdot (\sigma'_v \sigma'_h)^{0.28} \quad (6.1)$$

6.5.2 Excavation stability

The excavation stability assessment has been carried out by adopting selected classic limit equilibrium methods and by performing simple finite element analyses.

The results demonstrate that, for the case study concerned, the *DSS* undrained shear strength profile can be adopted for excavation stability assessments using limit equilibrium or finite element methods, assuming isotropic behaviour for the material.

A parametric study has been carried out using three dimensional analysis, considering square excavations of varying plan sizes. The findings indicate that a relatively significant enhancement in estimated FoS is achieved by explicitly considering the three dimensional excavation collapse mechanism, for excavations with relatively small plan size compared to their depth (approximately 25% increase in FoS for excavations with aspect ratio <3, compared to plane strain conditions).

It is worth mentioning that the actual behaviour of the clay stratum if affected by partial dissipation of excess pore water pressures taking place during the excavation period. It is therefore considered that total stress stability calculations should be based on conservative undrained shear strength parameters. Such analyses should be carried out as a preliminary means of assessing the excavation stability and should be accompanied by coupled effective stress analyses, capable of capturing the partially drained nature of the Boston Blue Clay behaviour.

6.5.3 Excavation base time dependent behaviour

Review of piezometer and extensometer monitoring data highlights the generation of negative excess pore water pressures during excavation and the partial drainage/dissipation during continued excavation and basement construction. The assumption of pure undrained conditions for significant excavation/construction events is not strictly applicable. A coupled time dependent analysis approach is considered more appropriate. This coupled approach enables a more representative assessment of the excavation and basement raft foundation behaviour and performance.

Accounting for the appropriate construction sequence and carrying out a time dependent coupled simulation of the excavation can lead to potentially significant optimisation of basement raft designs and a more accurate assessment of foundation system performance.

Summary of key contributions/novelty

- Advanced in-situ and laboratory testing data have been interpreted with a view of providing new insights in the behaviour of this material. The author believes that the data and interpretation presented would be extremely useful to designers of deep excavations in the Boston area.
- Stiffness data from self boring pressuremeter testing has been presented, showing the degradation of the Boston Blue Clay stiffness with increasing strains. The author is not aware of the existence of data from this testing technique in this material.
- A formulation for the evaluation of the Boston Blue Clay stiffness at small strains has been proposed, based on the material's void ratio and stress state.
- The use of a *DSS* undrained shear strength profile can be adopted as part of preliminary excavation stability assessments, using limit equilibrium or finite

element methods, assuming isotropic behaviour for the Boston Blue Clay (i.e. ignoring the anisotropic strength properties of the material).

- The explicit consideration of three dimensional collapse mechanisms can lead to a more accurate prediction of the excavation stability FoS. A significant enhancement in estimated FoS has been shown (approximately 25%) for square excavations with aspect ratios (ratio of excavation side length and excavation depth) lower than 3.

- Accounting for the appropriate construction sequence and carrying out a time dependent coupled simulation of the excavation (in lieu of the traditional assumption of undrained behaviour of the Boston Blue Clay) can lead to potentially significant optimisation of basement raft designs and a more accurate assessment of the foundation performance.

6.6 Further research

Some suggestions for further research on the topics examined as part of this study are presented below.

- The excavation analyses presented in this thesis have adopted a number of constitutive models available in Plaxis. Further research may be undertaken simulating the same case studies, using advanced constitutive models which have been developed for clay materials, and have been implemented in Plaxis or other software packages.

- A key assumption of the study is the undrained behaviour of clays. This idealisation is often rather inaccurate.

  Schemes involving increasing excavation depths are being proposed in recent years, in congested urban settings, driven by the need to maximise development space. In turn excavation timescales are extending, and, as a result, clay

consolidation mechanisms may become relevant during excavation/construction period.

Evidence of partial consolidation during basement excavation is shown by some of the monitoring data presented in chapter 5.

Further research may focus on the adoption of time dependent analysis as a standard tool for the design and assessment of excavations in clays.

- The self-boring pressuremeter test data on Boston Blue Clay has indicated relatively low stiffnesses (at various strain levels), potentially due to varying shape of the stiffness degradation curve at different depths or to destructuration of the stratum upper crust, during the initial phase of the pressuremeter loading. Further research may focus on these aspects, trying to clarify the observed behaviour.

6.7 Closure

This thesis focusses on key aspects of the design and performance assessment of excavation schemes in normally consolidated and over-consolidated clays.

The topics presented somehow follow the author's experience on excavation schemes in varying ground conditions and with different design drivers. Two case histories have been considered, namely a 20m deep excavation in London Clay and a 15m to 17m deep excavation in Boston Blue Clay.

The main aim of the research carried out has been to explore the potential benefits of a series of readily available constitutive models for the routine numerical assessment of excavation stability and serviceability conditions.

REFERENCES

ANDRESEN L. & JOSTAD H.P. (2002) - A constitutive model for anisotropic and strain-softening clay. Proc. Num. Mod. Geomech. NUMOG VIII, Rome, Italy 2002.

BENZ T. (2007) - Small-strain stiffness of soils and its numerical consequences. Universität Stuttgart. PhD Thesis.

BISHOP A.W. (1955) - The use of the slip circle in the stability analysis of slopes. Géotechnique.

BJERRUM L. & EIDE O. (1956) - Stability of strutted excavations in clay. Geotechnique.

BOLTON M.D. & WHITTLE R.W. (1999) - A non-linear elastic/perfectly plastic analysis for plane strain undrained expansion tests. Géotechnique 49.

CARDER D. R. (1995) - Ground movements caused by different embedded retaining wall construction techniques, TRL172, Transport Research Laboratory, Crowthorne.

CARDER D. R, MORLEY C. H. & ALDERMAN G. H. (1997) - Behaviour during construction of a propped diaphragm wall founded in London Clay at Aldershot road underpass, TRL239, Transport Research Laboratory, Crowthorne.

CLOUGH G. W. & O'ROURKE T. D. (1990) - Construction induced movements of in situ walls. In: ASCE specialty conference of design and performance of earth remaining structures, Cornell University, Ithaca, New York, USA, 18–21 June 1990.

COULOMB, C. A. (1776) - Essai sur une application des regles des maximis et minimis a quelquels problemesde statique relatifs, a la architecture. Mem. Acad. Roy. Div. Sav., vol. 7.

DUNCAN, J. M. & CHANG, C. Y. (1970) - Nonlinear analysis of stress and strain in soils. Journal of Soil Mechanics & Foundations Div.

EAB (1994) - Empfehlungen des Arbeitskreises Baugruben der Deutschen Gesellschaft fur Geotechnik.

EIDE O., AAS G. & JOSANG T. (1972) - Special application of cast-in-place walls for tunnels in soft clays. Proc. 5th European Conference on Soil mechanics and foundation Engineering. Madrid, Spain.

ELIA G., ROUAINIA M. & PANAYIDES S. (2016) - Finite Element Modelling of a Deep Excavation in Boston Blue Clay. VI Italian Conference of Researchers in Geotechnical Engineering, CNRIG2016.

FASANO, A., NIKOLIC A., COOK J. & SCOTT P. (2009) - Short-term stability of an excavation in marine clay. GeoHalifax 2009.

FINNO R.J., BLACKBURN J.T. & J.F. ROBOSKI (2007) - Three-dimensional effects for supported excavations in clay. Journal of Geotechnical and Geoenvironmental Engineering.

FREDLUND D.G. & KRAHN J. (1977) - Comparison of slope stability methods of analysis. Canadian Geotechnical Journal.

FUENTES & DEVRIENDT (2010) - Ground Movements around Corners of Excavations: Empirical Calculation Method. Journal Of Geotechnical And Geoenvironmental Engineering.

GIBSON, R.E. & ANDERSON, W.F. (1961) - In situ measurement of soil properties with the pressuremeter. Civil Engineering and Public Works Review, Vol. 56, No. 658 May.

GUNN M.J. (1992) - The prediction of surface settlement profiles due to tunnelling. Proc. Wroth Memorial Symposium, July 1992. Thomas Telford, London.

HASHASH Y.M.A. & WHITTLE A.J. (1996) - Ground movement prediction for deep excavation in soft clay. Journal of Geotechnical Engineering.

JARDINE, R.J. (1991) - Discussion on ‘Strain-dependent moduli and pressuremeter tests’. Géotechnique 41, No. 4.

JARDINE, R. J. (1992) - Nonlinear stiffness parameters from undrained pressuremeter tests. Canadian Geotechnical Journal 29.

JARDINE, R.J., POTTS, D.M., FOURIE, A.B. & BURLAND, J.B. (1986) - Studies of the influence of non-linear stress strain characteristics in soil structure interaction. Géotechnique 36.

KENNEY T.C. (1964) - Sea-level movements and the geologic histories of the postglacial marine soils at Boston, Nicolet, Ottawa and Oslo. Géotechnique 14.

LADD C.C. & DE GROOT D.J. (2004) - Recommended practice for soft ground site characterization. Arthur Casagrande Lecture. Cambridge, MA USA.

LADD, C.C. (1991) - Stability evaluation during staged construction (22nd Terzaghi Lecture). J. of Geotech. Eng., 117(4).

LADD, C.C. & DEGROOT, D.J. (2003) - Recommended practice for soft ground site characterization. The Arthur Casagrande Lecture, Proc. of the 12th Panamerican Conf. on Soil Mechanics and Geotechnical Engineering, Boston, MA.

LADD, C.C. & FOOT, R. (1974) - New design procedure for stability of soft clay, Journal of The Geotechnical Engineering, ASCE, Vol. 100, No. GT7.

LADD, C.C., FOOT, R., ISHIHARA K., POULOS H.G. & SHLOSSER F. (1977) - Stress-deformation and strength characteristics. Proc. 9th ICSMFE. Vol. 2, State-of-the-Art-Paper.

LADD, C.C., YOUNG, G.A., KRAEMER, S.R. & BURKE, D.M. (1999) - Engineering properties of Boston Blue Clay from special testing program. Proceedings, Special Geotechnical Testing: Central Artery/Tunnel Project in Boston, Massachusetts, GSP 91, GeoCongress '98.

LARSSON R. & AHNBERG H. (2005) - On the evaluation of undrained shear strength and preconsolidation pressure from common field tests in clay. Canadian Geotechnical Journal.

LEE, YONG, QUAN & CHEE (1998) - Effect of corners in strutted excavations: field monitoring and case histories. Journal of Geotechnical and Geoenvironmental Engineering.

LIN, CHUNG & PHIEN-WEJ (2003) - Quantitative evaluation of corner effect on deformation behaviour of multi-strutted deep excavation in Bangkok subsoil. Journal of the Southeast Asian Geotechnical Socitety.

MESRI G. (2001) - Undrained shear strength of soft clays from push cone penetration test. Géotechnique.

MORGESTERN N.R. & PRICE V.E. (1965) - The analysis of the stability of general slip surfaces. Géotechnique.

MUIR WOOD D. (1990) - Soil behaviour and critical state soil mechanics. Cambridge: Cambridge University Press.

MUIR WOOD, D. (1990) - Strain dependent soil moduli and pressuremeter tests. Géotechnique, 40.

NGI-ANI2 Material Model (2005) - User defined material model for PLAXIS Version 8.5 - User Manual.

NIKOLIC A., FASANO A. & COOK J. (2010) - Undrained shear strength evaluation for natural Boston Blue Clay. London 2010 DFI Conference.

O'ROURKE T.D. (1993) - Base stability and ground movement prediction for excavations in soft clay. Retaining Structures. London: Thomas Telford.

OSMAN A.S. & BOLTON M.D. (2006) - Ground movement predictions for braced excavations in undrained clay. Journal of Geotechnical and Geoenvironmental Engineering.

OU, CHIOU & WU (1996) - Three-dimensional finite element analysis of deep excavations. Journal of Geotechnical Engineering.

OU & SHIAU (1998) - Analysis of the corner effect on excavation behaviours. Canadian Geotechnical Journal.

PETALAS, A. (2013) - The generalized hardening soil model, notes.

PJ CAREY LTD (2019) – Personal communication.

PLAXIS (2018) - Reference Manual.

PLAXIS (2018) - Material Models Manual

ROBOSKI & FINNO (2006) - Distributions of ground movements parallel to deep excavations in clay. Canadian Geotechnical Journal.

ROUAINIA M., ELIA G., PANAYIDES S. & SCOTT P. (2017) - Non-linear finite element prediction of the performance of a deep excavation in Boston Blue Clay. Journal of Geotechnical and Geoenvironmental Engineering.

SANTAGATA M. & GERMAINE J.T. (2005) - Effect of OCR on sampling disturbance of cohesive soils and evaluation of laboratory reconsolidation procedures. Canadian Geotechnical Journal.

SCHANZ T., VERMEER P. A. & BONNIER P. G. (1999) - The hardening-soil model: Formulation and verification. In R. B. J. Brinkgreve, Beyond 2000 in Computational Geotechnics, Balkema, Rotterdam.

SEAH T. H. & LAI K. C. (2003) - Strength and deformation behavior of soft Bangkok Clay - ASTM geotechnical testing journal, ISSN 0149-6115, Nº. 4.

SHEAHAN T.C., (1991) - ScD Thesis - An experimental study of the time-dependent undrained shear behavior of resedimented clay using automated stress path triaxial equipment.

SHEAHAN T.C. (2005) - A soil structure index to predict rate dependence of stress–strain behavior. In: Yamamuro, J.A., Koseki, J. (Eds.), Testing, Modeling and Simulation in Geomechanics, ASCE GSP No. 143.

SIMPSON B, O'RIORDAN N.J. & CROFT D.D (1979), A computer model for the analysis of ground movements in London Clay. Géotechnique 29.

SPENCER E. (1967) - A method of analysis of the stability of embankments assuming parallel interslice forces. Géotechnique.

SU S.F., LIAO H.J. & LIN Y.H. (1998) - Base stability of deep excavation in anisotropic soft clay. Journal of Geotechnical and Geoenvironmental Engineering.

TERZAGHI K. (1925) - Erdbaumechanik auf bodenphysikalischer Grund-lage, Deuticke (Vienna)

WHITTLE R.W (1999) - Using non-linear elasticity to obtain the engineering properties clay - a new solution for the self boring pressuremeter. Ground Engineering, Vol.32, No.5.

ZDRAVKOVIC, POTTS & ST JOHN (2005) - Modelling of a 3d excavation in finite element analysis. Géotechnique.